UNCLASSIFIED

AD NUMBER
AD387292
LIMITATION CHANGES
TO: **Approved for public release; distribution is unlimited.**
FROM: **Distribution authorized to DoD only; Administrative/Operational Use; OCT 1967. Other requests shall be referred to U.S. Army Aviation Materiel Laboratories, Fort Eustis, VA 23604.**
AUTHORITY
ST-A PER USAAMRDL notice 29 Dec 1972

THIS PAGE IS UNCLASSIFIED

UNCLASSIFIED

AD NUMBER
AD387292
CLASSIFICATION CHANGES
TO: **UNCLASSIFIED**
FROM: **CONFIDENTIAL**
AUTHORITY
31 Oct 1979, DoDD 5200.10

THIS PAGE IS UNCLASSIFIED

SECURITY MARKING

The classified or limited status of this report applies to each page, unless otherwise marked.
Separate page printouts MUST be marked accordingly.

CMF-R- 15508

CONFIDENTIAL

AD

(19)

AD 388202

USAAVLABS TECHNICAL REPORT 67-35

SMALL GAS TURBINE ENGINE COMPONENT TECHNOLOGY REGENERATOR DEVELOPMENT (U)

PHASE II, FULL SCALE REGENERATOR FABRICATION AND ENGINE-REGENERATOR TESTING (U)

By

B. R. Lucas

H. J. Selfors

October 1967

U. S. ARMY AVIATION MATERIEL LABORATORIES FORT EUSTIS, VIRGINIA

CONTRACT DA 44-177-AMC-181(T)

PRATT & WHITNEY AIRCRAFT DIVISION
UNITED AIRCRAFT CORPORATION
EAST HARTFORD, CONNECTICUT

Copy [redacted] Copies

CONFIDENTIAL

Disclaimers

The findings in this report are not to be construed as an official Department of the Army position unless so designated by other authorized documents.

When Government drawings, specifications, or other data are used for any purpose other than in connection with a definitely related Government procurement operation, the United States Government thereby incurs no responsibility nor any obligation whatsoever; and the fact that the Government may have formulated, furnished, or in any way supplied the said drawings, specifications, or other data is not to be regarded by implication or otherwise as in any manner licensing the holder or any other person or corporation, or conveying any rights or permission, to manufacture, use, or sell any patented invention that may in any way be related thereto.

Trade names cited in this report do not constitute an official endorsement or approval of the use of such commercial hardware or software.

Disposition Instructions

When this report is no longer needed, Department of the Army organizations will destroy it in accordance with the procedures given in AR 380-5.

CONFIDENTIAL

DEPARTMENT OF THE ARMY
U. S. ARMY AVIATION MATERIEL LABORATORIES
FORT EUSTIS, VIRGINIA 23604

(U) This program was undertaken to demonstrate an advancement in lightweight, compact, high-effectiveness rotary regenerator technology and to demonstrate combined rotary regenerator and experimental T74 engine performance.

(U) The U.S. Army Aviation Materiel Laboratories has reviewed this report and concurs in the findings contained herein. The report is recommended for use in planning future rotary regenerator and regenerative engine programs.

This report is classified CONFIDENTIAL because of the compilation of information. Individual pages are UNCLASSIFIED when separated from the report.

CONFIDENTIAL

CONFIDENTIAL

Task 1M121401D14413
Contract DA 44-177-AMC-181(T)
USAAVLABS Technical Report 67-35
October 1967

SMALL GAS T RBINE ENGINE COMPONENT TECHNOLOGY REGENERATOR DEVELOPMENT (U)

PHASE II, FULL SCALE REGENERATOR FABRICATION AND ENGINE-REGENERATOR TESTING (U)

PWA-3008

by

B. R. Lucas and H. J. Selfors

Prepared by

Pratt & Whitney Aircraft Division
United Aircraft Corporation
East Hartford, Connecticut

for

U. S. ARMY AVIATION MATERIEL LABORATORIES
FORT EUSTIS, VIRGINIA

CONFIDENTIAL

(U) SUMMARY

This report describes the work accomplished during the 20-month Phase II portion of a 32-month program devoted to the advancement of toroidal rotary regenerator technology for small gas turbine engines. As a result of component investigations conducted in Phase I, major improvements in regenerator technology were made and were incorporated into the design of a flightweight high-effectiveness toroidal rotary regenerator which was fabricated and performance tested on a PT6 (T74) engine. The work described herein includes experimental determination of regenerator duct flow distribution; experimental evaluation of regenerator mass losses, system pressure losses, and overall performance in an ideal test loop; and finally the results of performance testing on the PT6 (T74) engine conducted by the subcontractor, United Aircraft of Canada, Ltd.

(U) FOREWORD

The subject of this report is the work performed by Pratt & Whitney Aircraft Division of United Aircraft Corporation, East Hartford, Connecticut on full scale regenerator fabrication and engine-regenerator testing, which is the Phase II portion of the program for small gas turbine engine component technology, regenerator development. The work was performed in accordance with Contract No. DA 44-177-AMC-181(T), Task 1M121401D14413, during the period 7 May 1965 through 31 January 1967. The report was submitted in February 1967 in compliance with part 2, Statement of Work, paragraph c. (4) of the contract schedule.

This report is the second of a series of two reports. The first report, USAAVLABS Technical Report 67-34 (contractor's report PWA-2942), covers Phase I, preliminary component testing and regenerator design, under the same contract.

The technical representattives for the U. S. Army Aviation Materiel Laboratories were Messrs. J. N. White and N. C. Kailos.

(U) CONTENTS

(U) ILLUSTRATIONS

(U) ILLUSTRATIONS (Cont'd)

(U) ILLUSTRATIONS (Cont'd)

(U) ILLUSTRATIONS (Cont'd)

(U) ILLUSTRATIONS (Cont'd)

(U) ILLUSTRATIONS (Cont'd)

(U) ILLUSTRATIONS (Cont'd)

(U) TABLES

(U) SYMBOLS

ϵ	temperature effectiveness, $\epsilon = \Delta T_{actual}/\Delta T_{ideal}$
η	expansion efficiency
G/G_{avg}	local-to-average flow per unit area
N_{Pr}	Prandtl number
N_{Re}	Reynolds number
N_{St}	Stanton number
$\Delta P/P$	pressure loss coefficient
α	flow angle from axial, degrees
A_c	matrix free flow area, ft.^{2}
G	stream mass velocity, lb./ft.^{2}-sec., $G = W/A_c$
N	regenerator rotor speed, revolutions/min.
N_1, N_{GG}	compressor turbine rotor speed (gas generator speed), revolutions/min.
N_2	power turbine rotor speed, revolutions/min.
P	pressure, lb./in.^{2}
P_{T1}	inlet total pressure, lb./in.^{2} abs. (p.s.i.a.)
ΔP	pressure differential, lb./in.^{2}
ΔP_{T-S}	total pressure minus static pressure, lb./in.^{2}
q	dynamic pressure, lb./in.^{2}
SFC	specific fuel consumption, lb./hp.-hr.
T	temperature, °R.

T_{T1}	inlet total temperature, °R.
W	mass flow rate, lb./sec.
$W\sqrt{T}/P$	flow parameter, lb.-(°R.)$^{0.5}$/sec.-p.s.i.a.

In addition, the following symbols are used as subscripts to some of the above symbols.

a	air
f	fuel
c	cold
h	hot
A	actual (measured)
D	determined (calculated)
S	static
T	total

Numerals used as subscripts to symbols (except in the case of N_1 and N_2) refer to the engine stations shown in the diagram below.

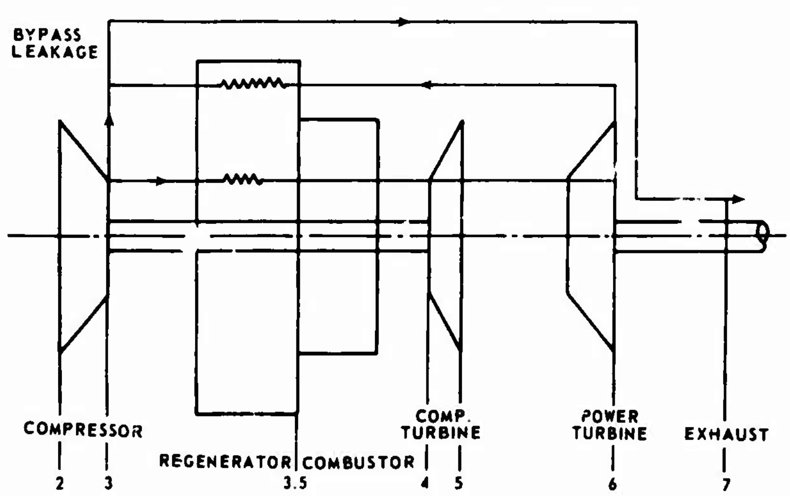

(U) INTRODUCTION

The overall objective of this program was to demonstrate the feasibility of a high-effectiveness, lightweight toroidal regenerator which would be capable of providing a potential reduction in the design-point specific fuel consumption of a PT6B (T74) engine to less than 0.40 pound of fuel per horsepower-hour with a 50-percent reduction in part-load specific fuel consumption relative to that of the simple-cycle engine.

REGENERATOR FABRICATION

In accordance with the requirements of Contract Item 1 of program Phase II, in May 1965 the contractor started the fabrication of two regenerators which had been designed during Phase I. They included a flightweight rotor and semi-flightweight housings and ducts. The test-bed regenerative engine modifications were started by the subcontractor, United Aircraft of Canada, Ltd. (UACL), in May 1965.

No major difficulties were encountered in the fabrication of the regenerator. However, the most difficult and time-consuming operation was the tunnel-ramp grinding in the regenerator housings, which required extremely delicate contour grinding control. Weld shrinkage of the first regenerator housings was resolved by improved machining and heat treatment fixtures. Minor weld shrinkage and warpage of the tie plate lugs required only slight adjustments in fitting the tie plate pins. Fabrication of the turbine exhaust duct and the compressor-discharge-to-regenerator duct was based on results of the duct flow distribution study. This was one of the contractor-sponsored supporting studies and is described in Appendix I. The internal structures of all ducts were a fabrication challenge; a large percentage of the components were handcrafted.

The fabrication of the PT6 engine parts which were modified or redesigned for the regenerative engine was completed without major difficulties. Distortion of some welded sheet metal casings during heat treatment was experienced. This problem was due to insufficient use of locating tooling for this nonproduction assembly; it could be remedied on future assemblies.

The assembly of regenerator No. 1 was started in September 1965 and completed in March 1966. This assembled unit included the following components.

1. 60-mesh, 0.004-inch-wire-diameter matrix packages.
2. Bulkhead piston rings coated with aluminum oxide.
3. One-piece conical carbon inner diameter ring seals.

The assembly of regenerator No. 2 was started in September 1966 and completed in November 1966. It differed from the first unit in the following respects.

1. 80-mesh, 0.004-inch-wire-diameter matrix packages.
2. 10 percent more matrix frontal area and a smaller matrix vee angle.
3. Bulkhead piston rings coated with chrome carbide.

4. Back-to-back segmented package inner diameter seals.

Photographs of major regenerator and engine components are shown in Appendix VI.

REGENERATOR PERFORMANCE TESTS

Contract Item 2a of Phase II required the contractor to conduct performance tests on the toroidal regenerator designed in Phase I.

REGENERATOR NO. 1

After assembly of the regenerator (see Figures 1 through 6) it was prepared for the mass loss test. Blanking plates were installed on the high-pressure section (see Figures 7 and 8) to determine the regenerator mass loss before installation in the performance loop. The mass loss test was performed at 15, 20, and 25 r.p.m. with ambient air to 120 p.s.i.g. in 10-p.s.i.g. increments. No mechanical problems were encountered with the regenerator or its hydraulic drive system during the test. Upon completion of the first test, the regenerator was disassembled and inspected. Since all parts were in good condition, the same parts were reinstalled, and a second mass loss calibration to 80 p.s.i.g. was completed.

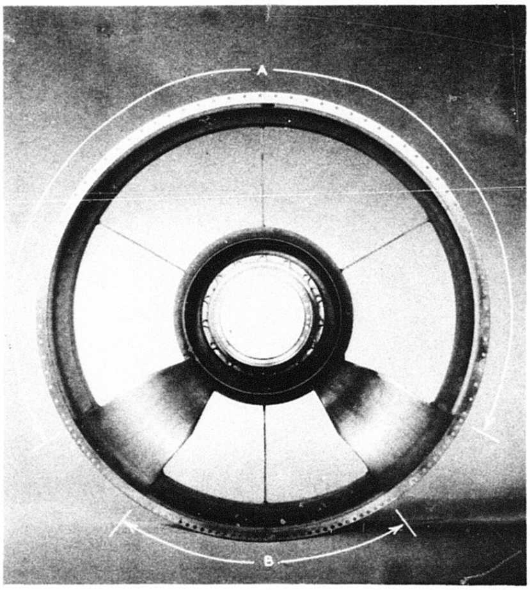

Figure 1. Interior View of Rear Housing: Section A, Low-Pressure Region (Turbine Discharge), and Section B, High-Pressure Region (Compressor Discharge).

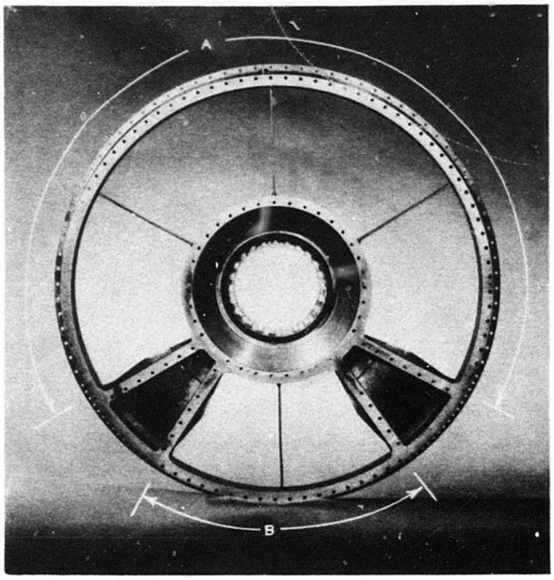

Figure 2. Exterior View of Rear Housing: Section A, Low-Pressure Region (Turbine Discharge), and Section B, High-Pressure Region (Compressor Discharge).

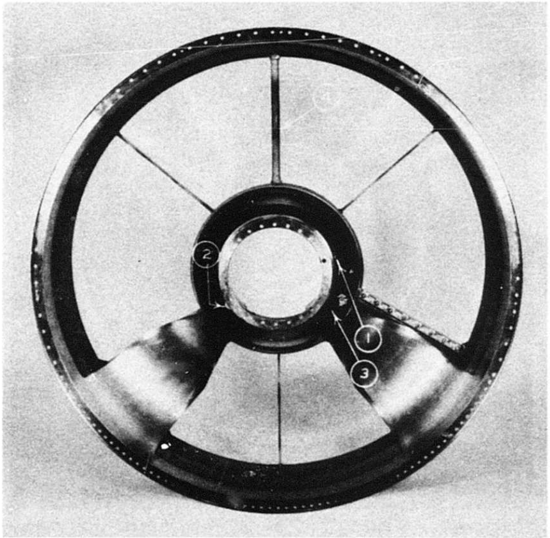

Figure 3. Interior View of Front Housing: (1) Oil Jet, (2) Breather Hole, (3) Drive Shaft Boss, (4) Oil Scavenge Line.

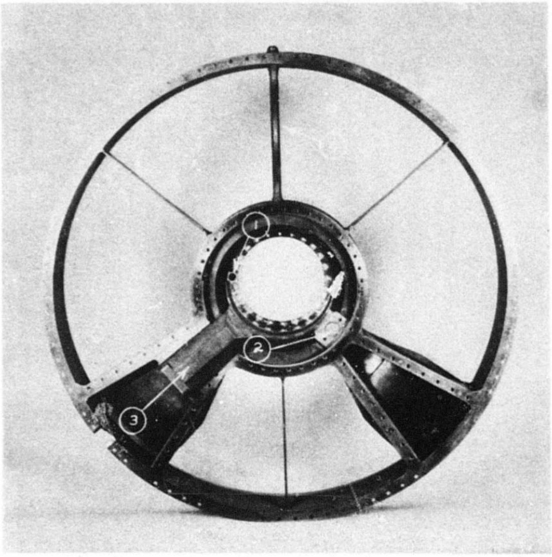

Figure 4. Exterior View of Front Housing: (1) Oil Feed Boss, (2) Breather Connector Boss, (3) Drive Shaft Boss, (4) Oil Scavenge Line.

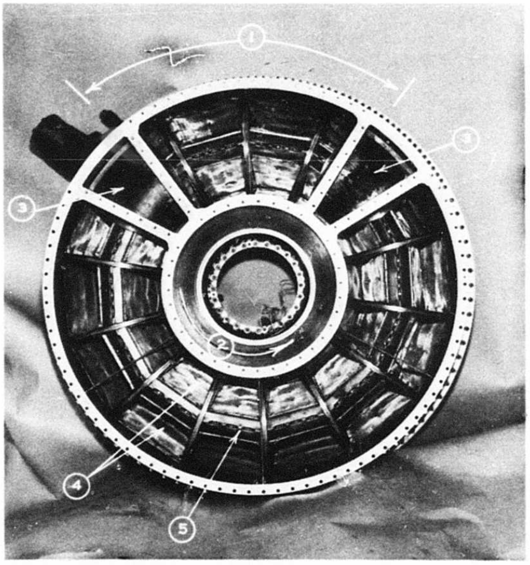

Figure 5. Hot Side (Rear) of Rotary Regenerator: (1) High-Pressure Sector, (2) Direction of Rotation, (3) Sealing Tunnels, (4) Matrix Packages, (5) End Seal.

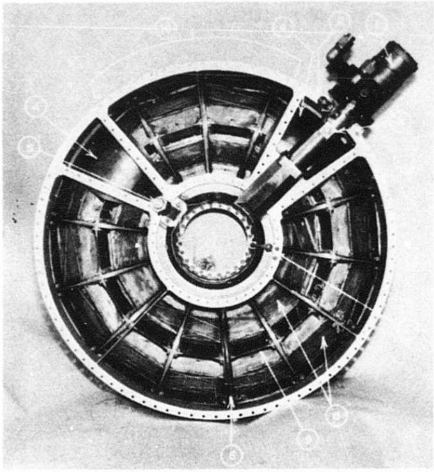

Figure 6. Cold Side (Front) of Rotary Regenerator: (1) Orbit Drive Motor, (2) Magnetic Speed Pickup, (3) Fitting for Drive Bearing Oil Line, (4) Sealing Tunnel, (5) Breather Connector, (6) Scavenge Tube, (7) Fitting for Rig Bearing Oil Line, (8) Matrix Packages, (9) Inner Tie Plate, (10) High-Pressure Area.

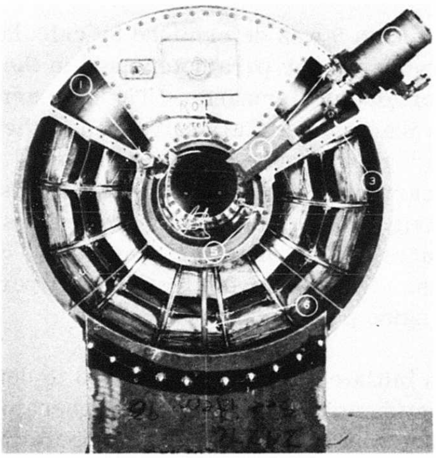

Figure 7. Cold Side (Front) of Rotary Regenerator Assembled for Mass Loss Test: (1) Breather Connector, (2) Orbit Drive Motor, (3) Drive Bearing Oil Fitting, (4) Magnetic Speed Pickup, (5) Rig Bearing Oil Fitting, (6) Oil Scavenge Line.

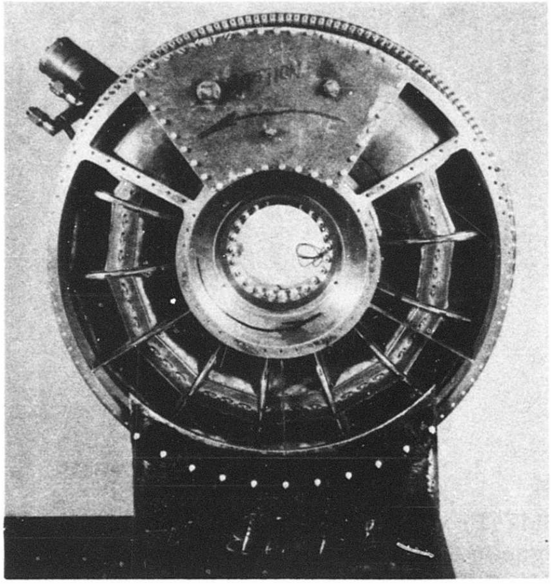

Figure 8. Hot Side (Rear) of Rotary Regenerator Assembled for Mass Loss Test.

The gross carryover in Figure 9 was determined by calculation of the torus void volume. The gross carryover is the parameter used in the regenerator and engine cycle studies to determine performance. The net carryover (Figure 10) is the gross carryover less the volume of air entrapped in the low-pressure area and carried back into the high-pressure section. The total measured flow is a measurement of the net carryover plus the seal leakage, as shown in Figure 11. Correction of the air density from ambient temperature test conditions of 520°R. to regenerator temperatures results in seal leakage of 1.05 percent at 62 p.s.i.g. or design-point conditions. The total mass loss is 3.21 percent, which is the goal required to obtain engine performance.

Performance testing was initiated in early April 1966 to determine effectiveness and pressure loss as functions of mass flow and regenerator speed. This testing was accomplished in a loop which simulates engine operation. The loop is described in the following paragraphs.

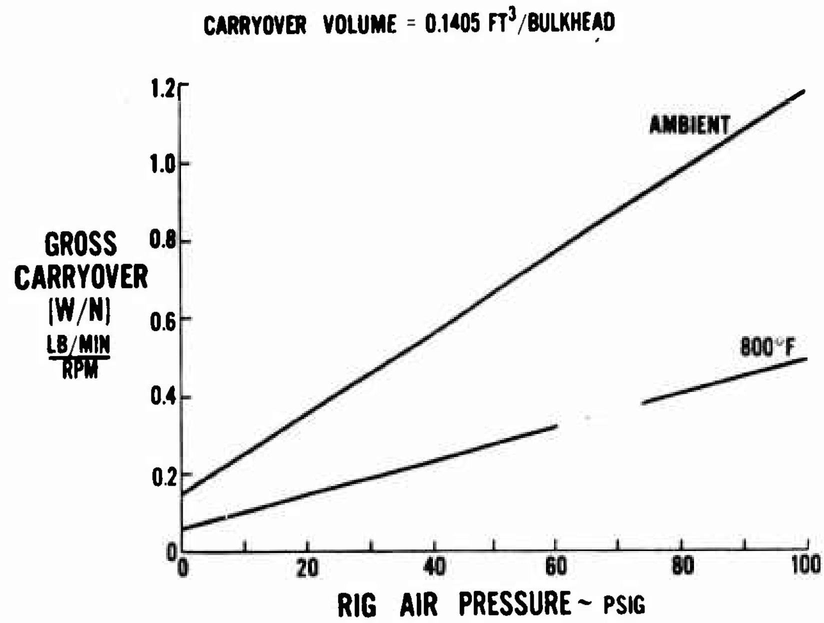

Figure 9. Rotary Regenerator Gross Carryover as a Function of Pressure.

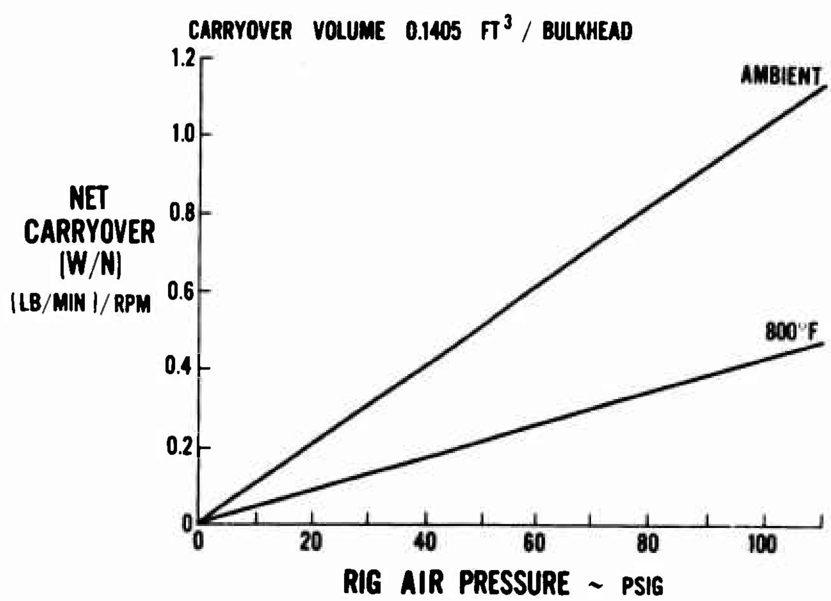

Figure 10. Rotary Regenerator Net Carryover as a Function of Pressure.

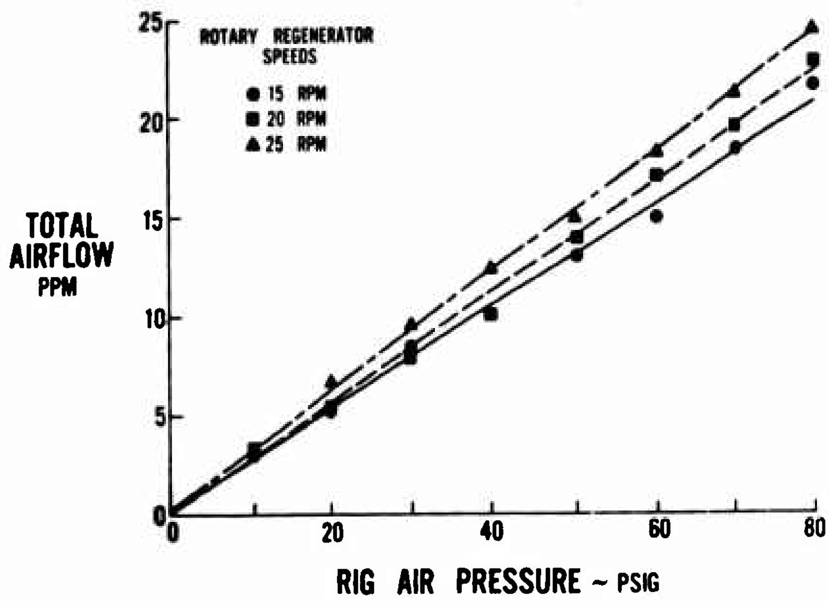

Figure 11. Regenerator No. 1 Measured Net Carryover Plus Seal Leakage (60°F. Test Temperature).

Measured high-pressure air from the compressors is preheated to the engine compressor discharge temperature by means of a primary burner in the main supply line. This heated air is introduced into the regenerator via a flexible pipe (see Figure 12) and a short instrumented pipe section to the compressor discharge duct. An instrumented extension of the compressor discharge duct is used to determine the temperature and pressure of the air entering the regenerator. The air heated by the regenerator then enters the engine regenerator-to-burner duct to an instrumented transition duct to determine effectiveness and pressure loss for the high-pressure sector. This area is instrumented to include the burner duct in the overall pressure loss and also to determine the compressor discharge duct pressure loss at engine conditions.

The high-pressure, high-temperature air is then measured by a downstream orifice (see Figure 13) as a check on leakage and then throttled by a butterfly valve to the turbine discharge pressure level at the regenerator. The air is heated to turbine discharge temperature at the regenerator by a modified engine burner utilizing JP4 fuel in the burner compartment. Directly downstream of the main burner there is a full-flow dummy burner to provide mixing and to maintain a uniform temperature profile entering the regenerator. In addition, in the plenum there are mixing plates, perforated plates, and screening to further improve the flow distribution and temperature profile entering the regenerator through the annular duct.

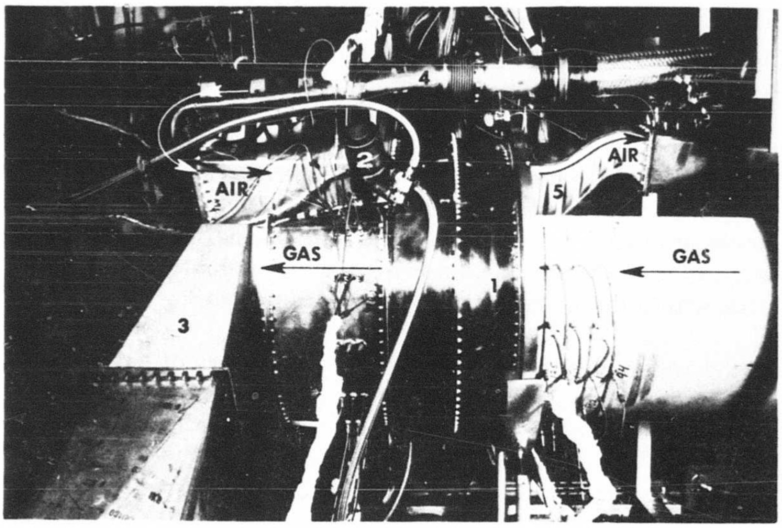

Figure 12. Closeup View of Rotary Regenerator Mounted in Test Loop: (1) Regenerator, (2) Regenerator Drive Motor, (3) Exhaust Duct, (4) Compressor Exit Duct, (5) Regenerator-to-Burner Duct.

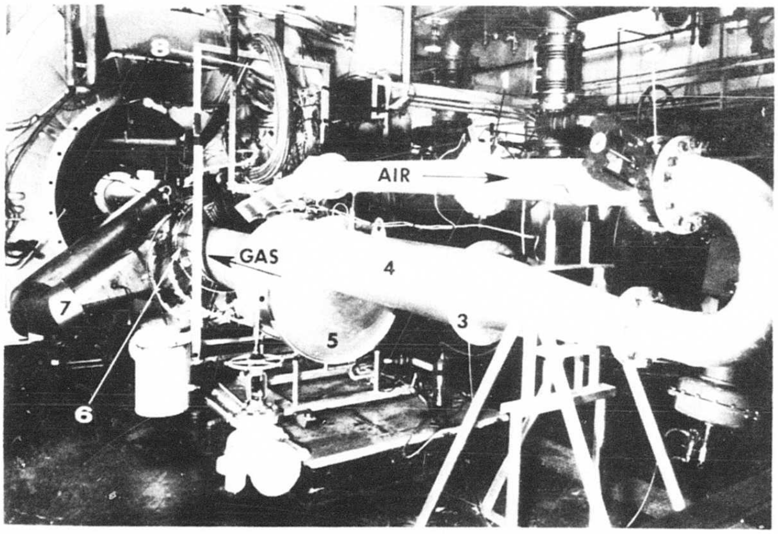

Figure 13. Overall View of Rotary Regenerator Mounted in Test Loop: (1) Orifice Station 4, (2) Butterfly Valve, (3) Mixing Screens, (4) Combustion Section With Dummy Can Downstream for Mixing, (5) Baffled Plenum, (6) Regenerator, (7) Exhaust Duct, (8) Inlet to Regenerator From Heater Burner.

The annular duct is instrumented just upstream of the rig (see Figure 12). The gas passes through the regenerator into another instrumented annular duct and exhausts through the same duct to be used in the engine test.

The performance goal of 85-percent temperature effectiveness was not obtained during the first series of tests. An analysis of the data indicated that there were three major suspect areas which may have caused this reduction in effectiveness. An increase in flow maldistribution at the regenerator inlets, excessive mismatch between the inlet fairing extensions with the matrix blunt ends, or flow maldistribution within the matrix could cause this problem.

Inspection of the regenerator upon completion of 47 hours of hot testing revealed no areas of distress. The piston ring seals were in excellent condition, as were the seal surfaces in the housing. The inner diameter seals revealed good contact surfaces on both the liner and seal plates. The bearing was in excellent condition, with no indication of overheating. The drive gear and pinion had a normal contact pattern. The drive system was exceptionally reliable for the entire test period, with no problem encountered with speed control.

Upon completion of the first performance test, which showed a temperature effectiveness of approximately 78 percent at the design point airflow (see Figure 14), both regenerator inlet ducts were flow checked. This was done to ensure that flow maldistribution at the regenerator inlet was not a cause of the low effectiveness.

The high-pressure inlet duct (which includes the compressor discharge duct and annular instrumentation duct) of the performance loop was flow tested with the regenerator removed. The flow distribution at the high-pressure inlet (Figures 15 through 17) was an improvement over the compressor discharge duct flow distribution observed in a previous test (see Appendix I) and was therefore eliminated as a cause of the low effectiveness. The flow split in each annulus was within a few percent of the required flow split based on the measured screen frontal area of the matrix package.

The low-pressure gas-side inlet to the regenerator was flow tested in the same manner as the high-pressure inlet. The flow distribution of this inlet duct (Figure 18) was within acceptable limits and was therefore eliminated as a cause of the low effectiveness.

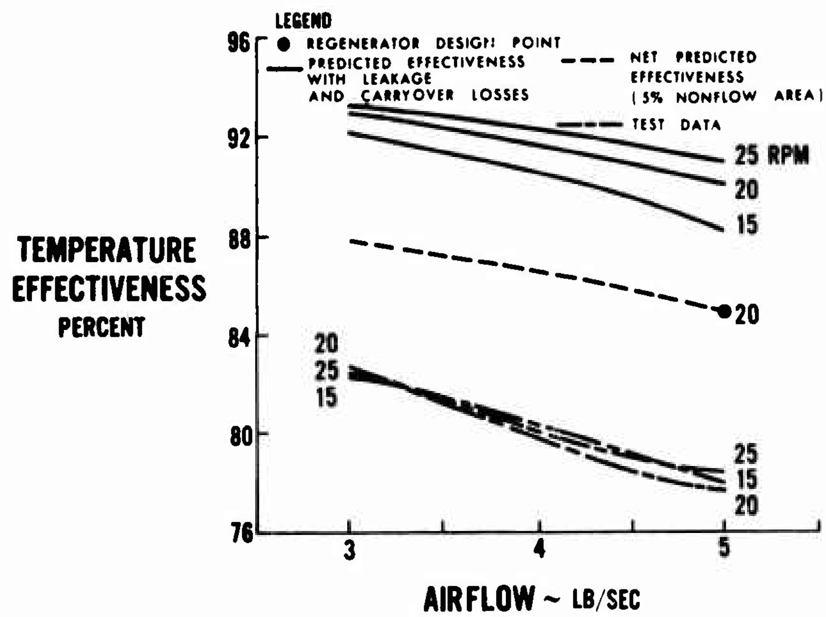

Figure 14. Regenerator No. 1 Performance in Test No. 1.

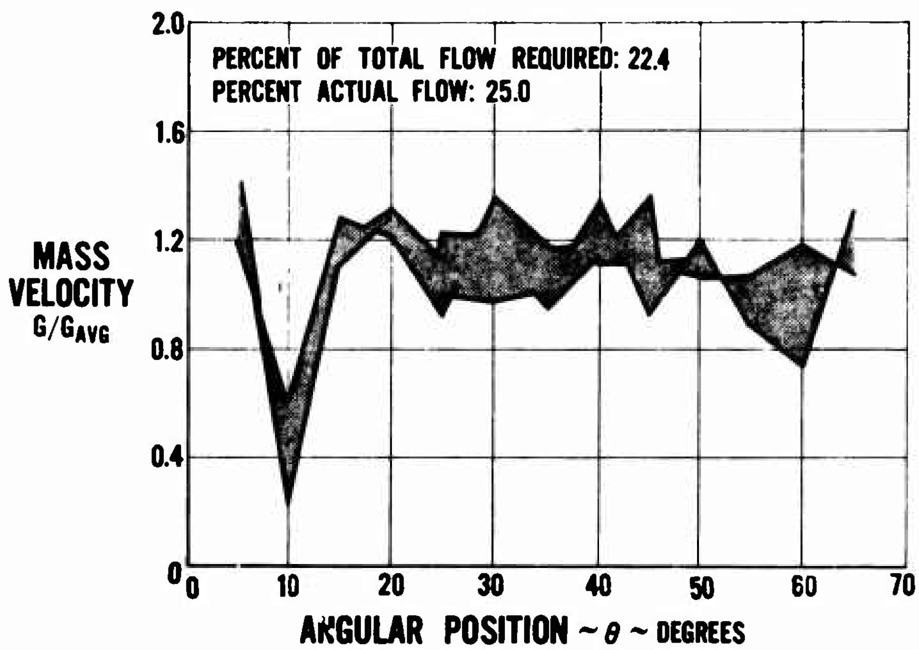

Figure 15. High-Pressure Regenerator Inlet Duct Flow Distribution in Outer Annulus.

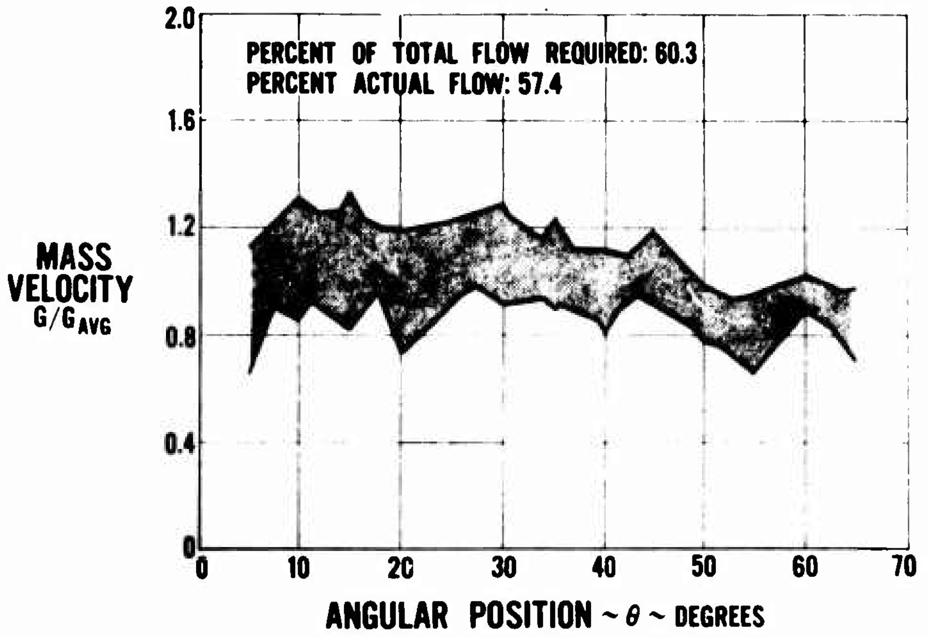

Figure 16. High-Pressure Regenerator Inlet Duct Flow Distribution in Middle Annulus.

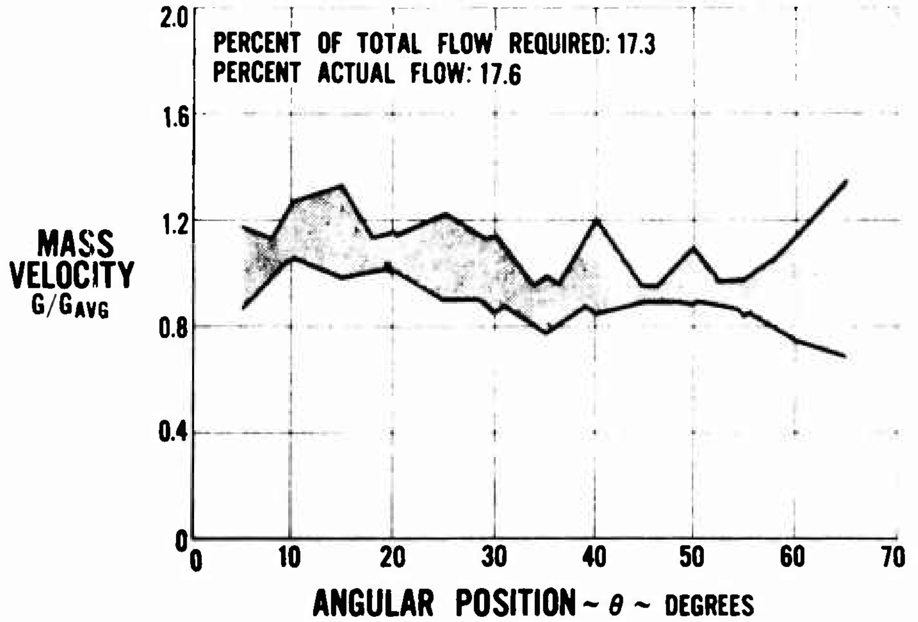

Figure 17. High-Pressure Regenerator Inlet Duct Flow Distribution in Inner Annulus.

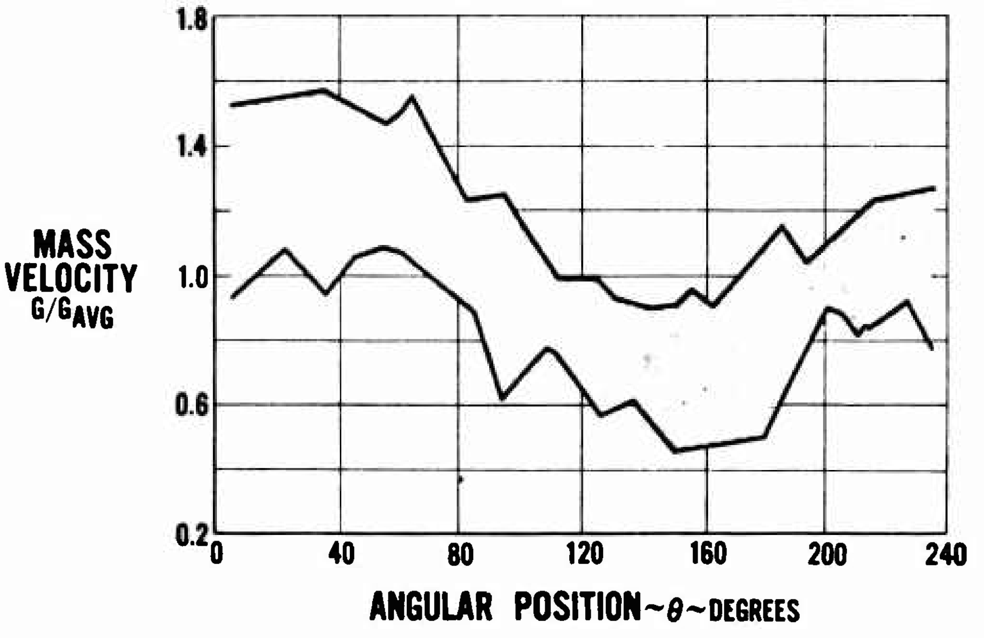

Figure 18. Regenerator Gas-Side Inlet Duct Flow Distribution.

The temperature profiles entering the regenerator were also good. The high-pressure inlet duct had a total temperature variation of approximately 5°F., or 1 percent, and the low-pressure inlet duct had a radial temperature profile of approximately 25°F., or 2 percent, and a maximum circumferential variation of 4 percent. These profiles are sufficiently small to be neglected as a cause of low effectiveness.

The second regenerator performance test was run with the fairing extensions of the high-pressure inlet cut back to the same plane as the flange to agree with the original design, and the bullet nosepiece in the gas side inlet duct was removed. The clearance between the fairing extensions to matrix blunt ends on the high-pressure side was increased from 1/4 inch to 2 inches. This was done since it is geometrically possible, due to mismatch of the arc-shaped fairings with the chord blunt ends of the matrix package, to mask approximately 10 percent of the screen frontal area. The results of this test run at 4 and 5 pounds per second mass flow (Figure 19) show an increase in temperature effectiveness of one percentage point and agreement in slope and spread between the predicted and test curves.

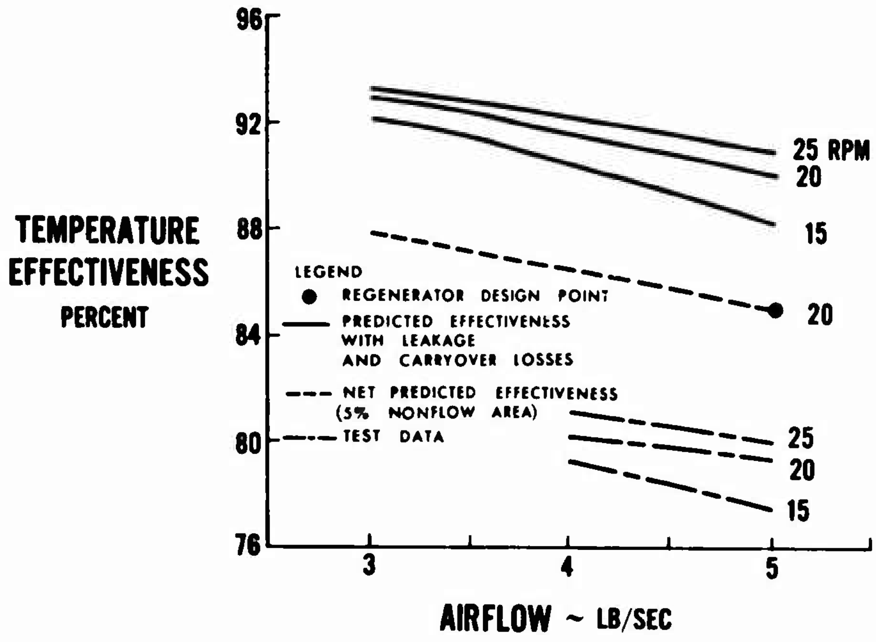

Figure 19. Regenerator No. 1 Performance in Test No. 2.

In the third performance test, the flow splitters in the high-pressure inlet instrumentation duct were removed to form a plenum at the inlet and completely eliminate the effect of fairing mismatch. The mixing splitter in the regenerator-to-burner duct was also removed to simplify evaluation of the data on the high-pressure side. Results of this test run at 4 and 5 pounds per second mass flow increased the temperature effectiveness to 80 percent, as shown in Figure 20.

The pressure loss data shown in Figures 21 and 22 (all three performance tests) indicate that the pressure loss, especially on the low-pressure side, is greater than predicted, but the total pressure loss is within the target loss of 6 percent.

Upon completion of the third performance test, the radial flow profile downstream of the regenerator on the gas side was measured by the hot wire method. Four circumferential locations of the regenerator discharge annular duct were probed at the design-point flow parameter with the regenerator rotation set at 20 r.p.m. Three of the same locations were probed to measure radial temperature distribution. The regenerator was operated at the design-point condition for the temperature probing.

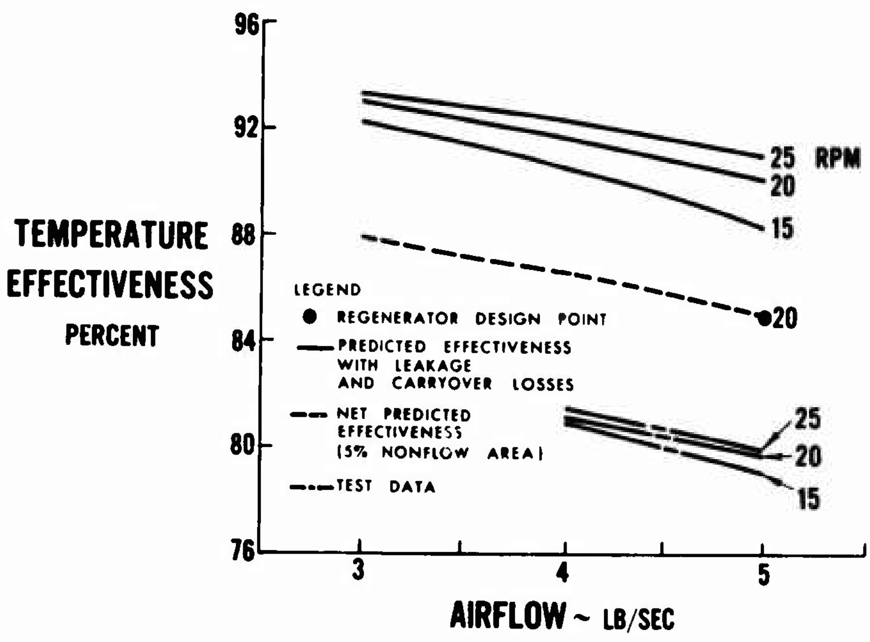

Figure 20. Regenerator No. 1 Performance in Test No. 3.

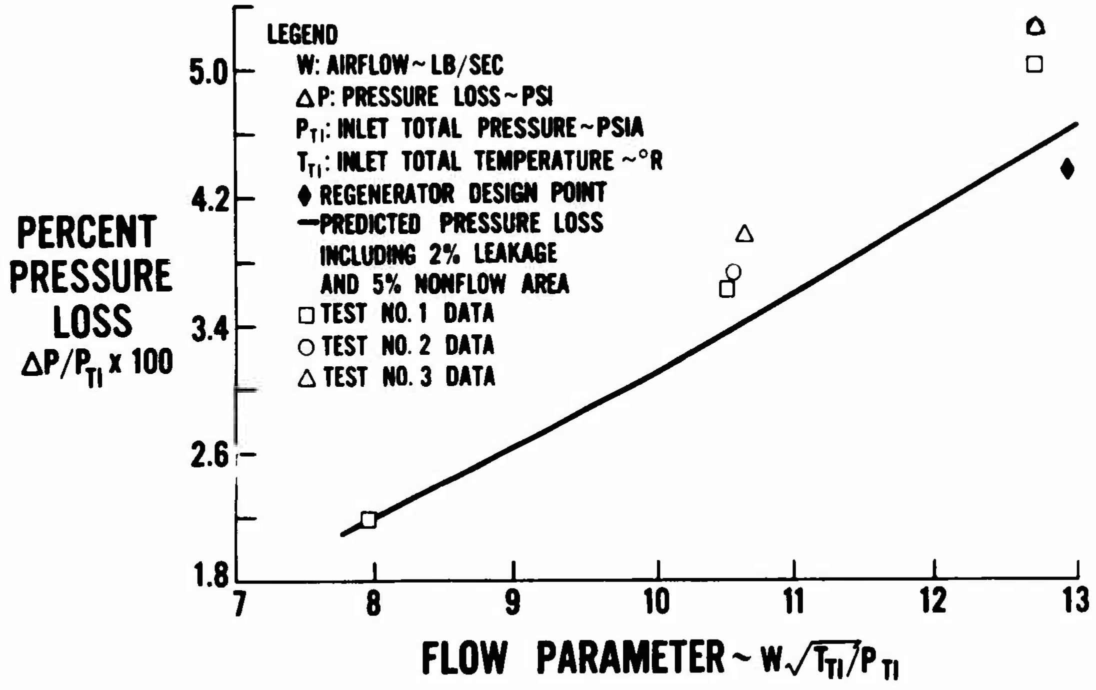

Figure 21. Pressure Loss in Low-Pressure Side for Tests Nos. 1, 2 and 3.

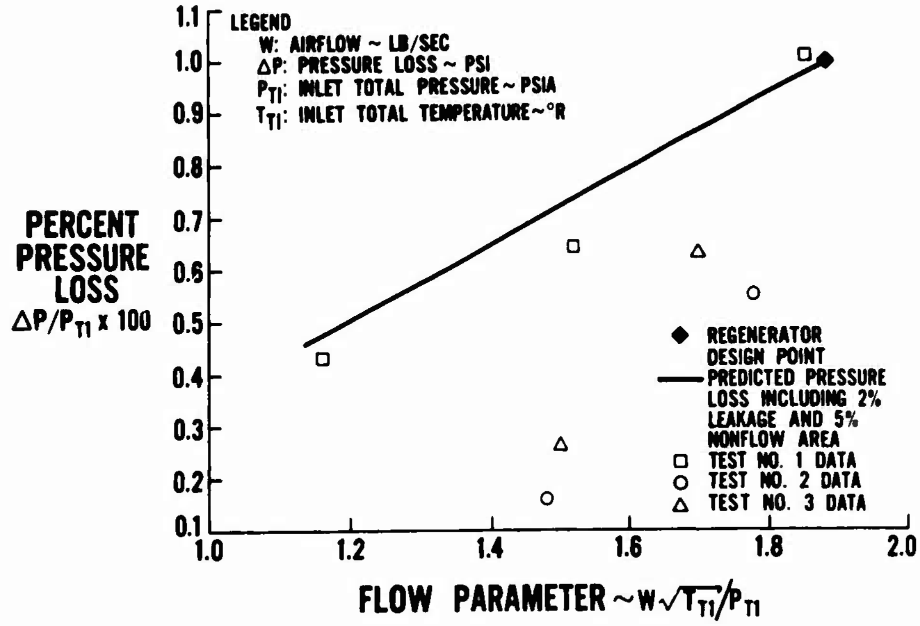

Figure 22. Pressure Loss In High-Pressure Side for Tests Nos. 1, 2,and 3.

The results of this series of tests are shown in Figures 23 and 24. It is noted from these figures that the flow profile downstream of the package is normal. The low-flow regions are in line with the matrix blunt ends, and the high-flow region is in line with the open vee of the matrix package. The radial temperature profile, however, demonstrates that there is a poor flow distribution within the matrix package. The radial temperature profile should be flat for a uniform or equal flow per unit of matrix frontal area. The flow maldistribution and the problem of lower-than-predicted effectiveness were investigated in a single-module heat transfer rig in the supporting study described in detail in Appendix V.

Since minimum targets were met, and to prevent program delay, the regenerator was removed from the performance loop and prepared for engine tests. At this point the regenerator had completed over 120 hours of testing, of which more than 110 hours were hot testing in the performance loop.

The regenerator was in good condition upon completion of the test. Two inner diameter carbon seals were replaced, since they incurred some handling damage. Wear measurements were taken: The maximum wear of 2 mils per 100 hours occurred on the seal against the rotor. The other carbon seal had less than 1 mil of wear.

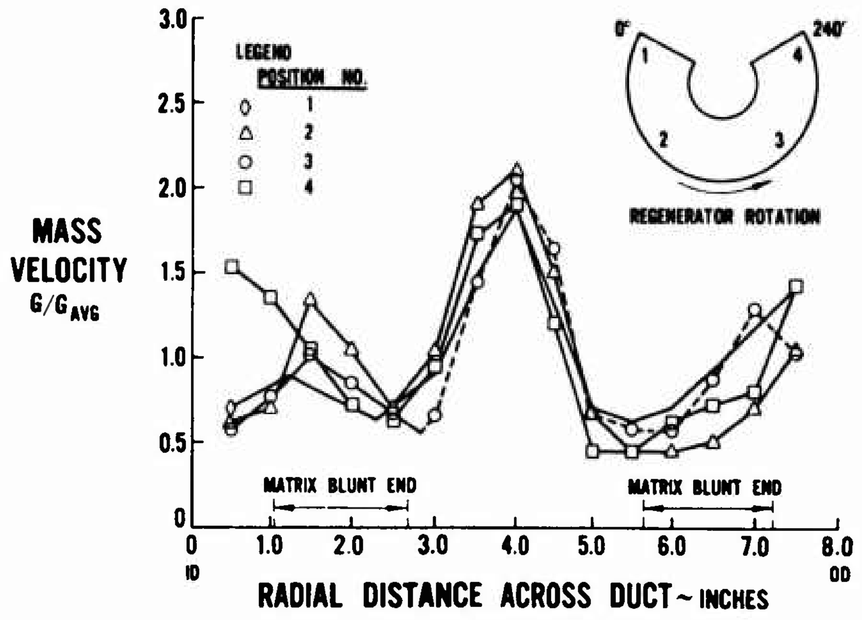

Figure 23. Flow Distribution in Gas Side of Regenerator Discharge Duct.

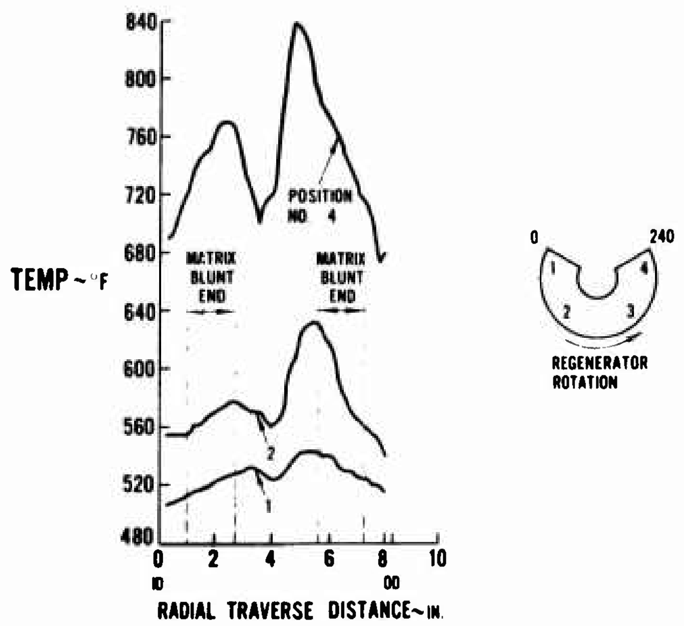

Figure 24. Temperature Distribution in Gas Side of Regenerator Discharge Duct.

In early July 1966 this regenerator, the drive system, and the compressor discharge duct were delivered to United Aircraft of Canada, Ltd. The regenerative T74 engine was assembled and instrumented for performance tests. The complete engine assembly is shown in Figures 139 and 140 of Appendix VI.

REGENERATOR NO. 2

After assembly of regenerator No. 2, it was prepared, in the same fashion as regenerator No. 1, for a mass loss test, which was conducted outside of the performance loop. The mass loss tests were performed statically at 15, 20, and 25 r.p.m. with ambient air supplied in 10-p.s.i.g. increments to 120 p.s.i.g.

The total measured airflow, which is the measurement of net carryover plus the seal leakage, is shown in Figure 25. The ambient air calibration resulted in a somewhat lower mass loss, 3.16 percent, compared with 3.21 percent for regenerator No. 1. Correction of the air density from ambient temperature test conditions of 520°R. to actual regenerator temperatures resulted in a seal leakage of 1.00 percent at 62 p.s.i.g. or design-point conditions.

Prior to conducting the performance tests in November 1966, two major loop improvements were made to provide better air-side discharge temperature data. These were as follows:

1. A mixer was installed in the duct downstream of the regenerator air-side discharge.

2. The air-side discharge duct was insulated to a point downstream of a single thermocouple located a short distance downstream of the mixer.

A static heat-loss test in the insulated duct showed essentially no heat loss. Therefore, the single thermocouple sensed the regenerator hot air discharge temperature as accurately (to within 5°F.) as the several thermocouples used in the previous performance tests.

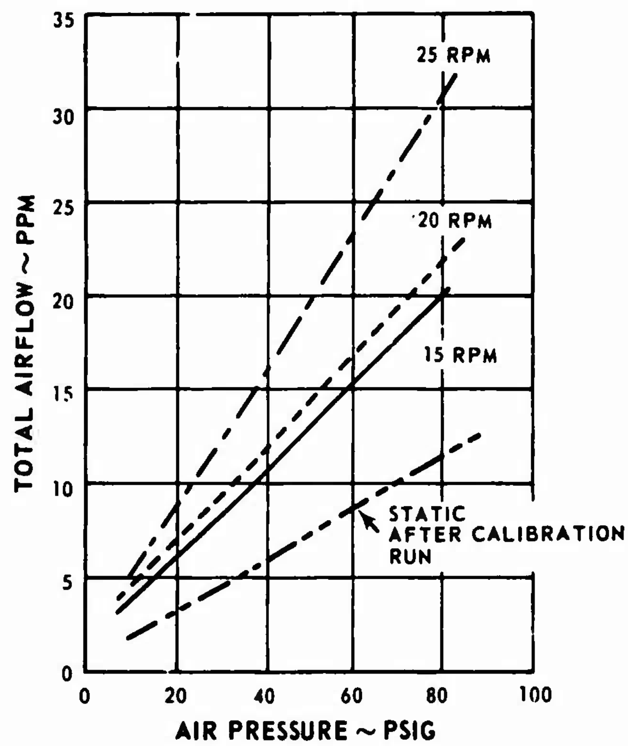

Figure 25. Measured Net Carryover Plus Seal Leakage for Regenerator No. 2 (60°F. Test Temperature).

Performance tests were conducted with airflows of 4.0 and 5.0 pounds per second and at regenerator speeds of 20 and 30 r.p.m. The scope of the test program was limited to the determination of significant change in regenerator performance. Since more confidence was placed in the air-side instrumentation than the gas side, the air-side temperature effectiveness was accepted as the overall regenerator effectiveness. As shown in Figure 26, the effectiveness was about 80.5 percent. The pressure loss for both high- and low-pressure sides of the regenerator was higher than that measured in regenerator No. 1. Essentially, there was no significant difference between the performance of the two regenerators. Thus, although the 80-mesh package had 10 percent more frontal area than the 60-mesh package, the smaller vee angle caused additional flow maldistribution within the matrix, thereby offsetting the area increase.

It is concluded that flow distribution within the matrix package for both designs was not ideal and that this was the single cause for low effectiveness.

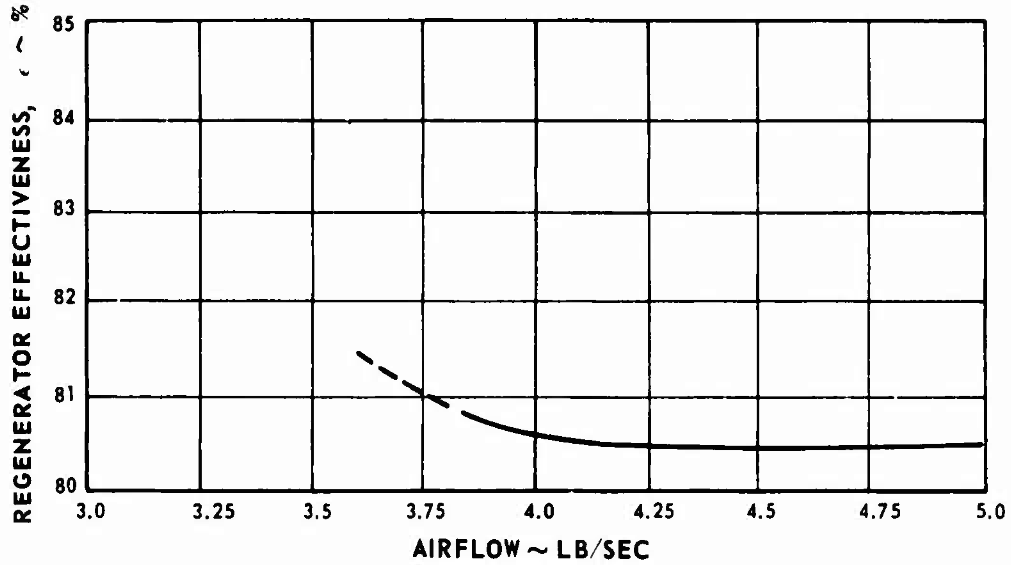

Figure 26. Performance of Regenerator No. 2 at 30 r.p.m.

REGENERATOR ENGINE PERFORMANCE TESTS

Contract Item 2b of Phase II specifies that the regenerator designed in Phase I be tested as part of a full scale regenerative engine, the basic engine to be a modified T74.

DESCRIPTION OF DEMONSTRATOR MODEL

The actual demonstrator (Figure 27) was designated PT6B-XRD, serial number 225. It consisted of the basic model PT6B-9 simple-cycle free-turbine helicopter engine modified to incorporate a rotary regenerator and the associated ducts. The basic engine rotors, gearboxes, and controls were unchanged, but the burner and main sheet metal casings were redesigned to accommodate the regenerator.

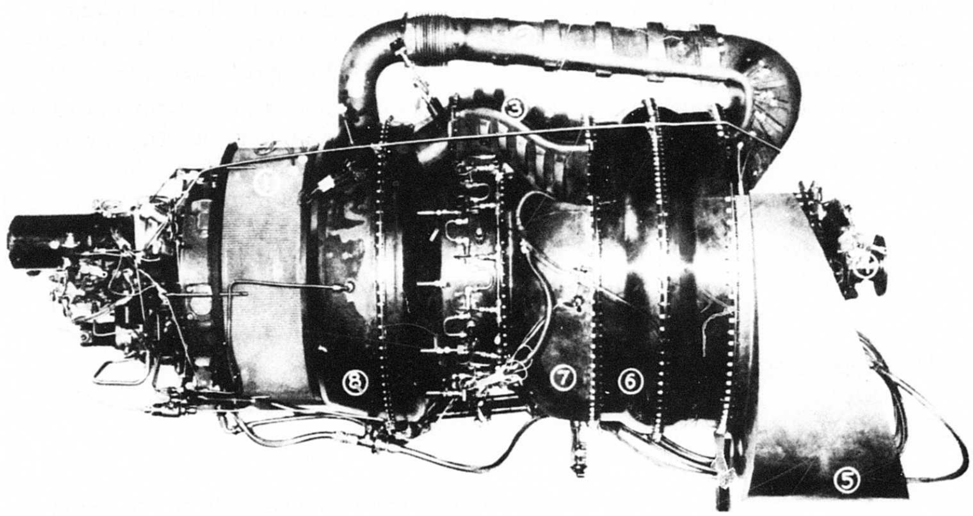

Figure 27. PT6B-XRD Regenerative Engine: (1) Compressor Inlet Screen, (2) Compressor-to-Regenerator Duct, (3) Regenerator-to-Burner Duct, (4) Output Shaft, (5) Stand Exhaust Duct, (6) Rotary Regenerator, (7) Turbine Exhaust Duct, (8) Compressor Scroll Case.

The modified engine consists of an opposed shaft concentric arrangement with a counterrotating free turbine. The standard PT6 compressor (three axial stages and one centrifugal stage) delivers air into a collector scroll via a vaned diffuser. The compressor air is delivered to the regenerator cold segment by a diffusing transfer duct, and, after absorbing heat from the regenerator rotating matrix, it is fed to the burner feed scroll via a duct containing a mixing baffle to ensure even air temperature.

The burner feed scroll delivers air to the burner via radial straightening vanes. The burner consists of a single, reverse-flow, fully annular flame tube with 14 simplex nozzles spraying tangentially into the primary zone. A single-stage compressor turbine is followed by a single-stage power turbine, which delivers power to the output shaft via a high-speed extension shaft and a single-stage epicyclic reduction gear to deliver 6800 r.p.m. maximum output speed. The exhaust gases from the power turbine pass through the hot segment of the regenerator matrix, transferring heat in the process. The cooled gases are then collected in an exhaust duct and ejected sideways through a single port. The accessories gearbox is supported from the annular air intake casting which also forms an integral oil tank. A cylindrical perforated steel intake screen is used, under which the compressor midstage blowoff valve is housed. Three mount points are used, one at each side of the reduction gearbox and one on the underside of the accessories gearbox. The standard PT6B-9 controls are used with the ability to control from either the gas-generator-turbine- or power-turbine-driven governors. The basic engine is self-sufficient in fuel controls, starting system (electric), and oil system, but slave cooling air was used for cooling the fuel nozzles. The regenerator uses independent lubrication and hydraulic drive systems.

AERODYNAMIC DESIGN CRITERIA

General

A maximum of tried and tested aerodynamic components was used in the design of the regenerative engine. The compressor was unchanged from that used in the PT6A-20 production engine. The burner can design was kept as close as possible to that of the PT6. The turbine airfoils were either standard or restaggered versions of airfoils used in the PT6. The exhaust duct design can be developed for use in an actual installation. The design-point conditions through the engine used in the analysis of data are listed below. (The design was actually based on 85-percent regenerator effectiveness, which would have given a specific fuel consumption of 0.395 pound per horsepower-hour.)

Ambient conditions	59°F., sea level static pressure
Compressor airflow	5 lb./sec.
Compressor speed	34,150 r.p.m.
Compressor pressure ratio	5.25
Compressor efficiency	78%
Compressor discharge pressure	77.2 p.s.i.a.
Compressor discharge temperature	462°F.
Regenerator effectiveness	80%
Regenerator air discharge temperature	1101°F.
Gas generator turbine inlet temperature	1900°F.
Gas generator turbine inlet pressure	75.3 p.s.i.a.
Gas generator turbine flow parameter	3.097 lb.-(°R)$^{0.5}$/sec.-p.s.i.a.
Gas generator turbine efficiency	87.2%
Power turbine flow parameter	6.39 lb.-(°R)$^{0.5}$/sec.-p.s.i.a.
Power turbine efficiency	86.5%
Power turbine inlet pressure	33.6 p.s.i.a.
Power turbine inlet temperature	1540°F.
Power turbine exit pressure	16.32 p.s.i.a.
Power turbine exit temperature	1260°F.
Regenerator exhaust temperature	692°F.
Fuel-air ratio	0.0122
Combustion efficiency	98%
Cold-side pressure loss	2.5%
Hot-side pressure loss	9.5%
Regenerator carryover	2%
Regenerator seal leakage	1%
Exhaust nozzle pressure ratio	1.005
Reduction gear efficiency	98%
Shaft power	515.4 hp.
Specific fuel consumption	0.428 lb./hp.-hr.

Compressor

The compressor used was the same as that developed for the PT6A-20 production engine (three axial stages plus one centrifugal stage), with no changes except that the vaned diffuser gases were transferred to a collector scroll via a vaneless diffuser section. At the design match point this compressor is capable of a total-to-total isentropic efficiency of 79.5 percent up to the diffuser outlet.

Compressor Delivery Scroll

The compressor diffuser outlet was modified to incorporate a collector scroll. Instead of turning from radial flow to axial flow in an annular bend and diffusing through a deswirl cascade after leaving the radial diffuser as in the PT6, the flow enters a constant-width radial vaneless space of radius ratio 1.15 at Mach 0.361 and 27.0° from tangential. At the end of this vaneless space the flow enters the tangential collector scroll at Mach 0.278 and 27.4° from tangential and leaves tangentially at Mach 0.249. The scroll itself (Figure 28) is of symmetrical rectangular cross section to simplify manufacturing. To provide a constant static pressure around the periphery of the scroll, the cross-sectional area distribution was defined so that flow diffusion was balanced against friction and secondary bend losses.

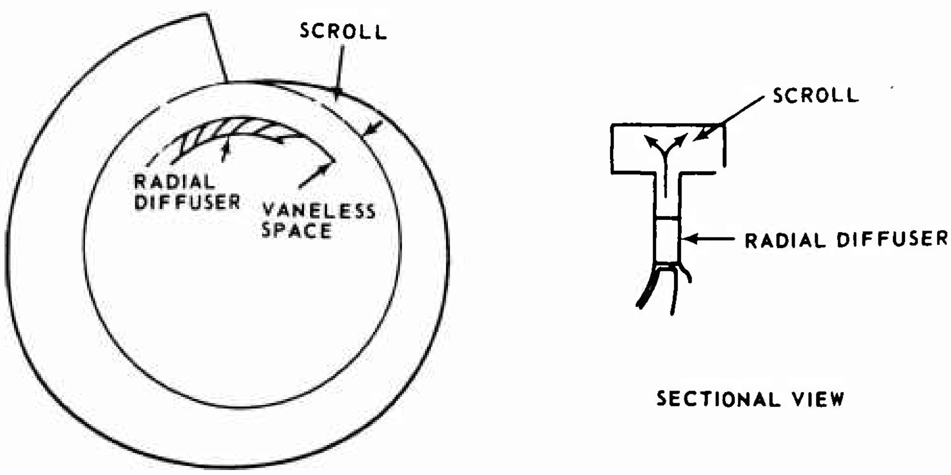

Figure 28. Compressor Delivery Scroll Schematic.

Burner Distributor Scroll

To maintain minimum overall dimensions and path length, the flow approaches the burner scroll axially at Mach 0.088, is divided in two, and turns through 90° to enter the twin scrolls tangentially (see Figure 29). The 90° bends each have two passages with a single splitter vane; structural convenience was the main criterion due to the very low velocity of the flow. To provide a continuous distribution of flow around the burner entrance annulus, the leading edges of the outer bend walls were spaced to direct the correct portion of flow axially into region A (see Figure 29) where this flow is then guided at constant velocity into radial channel B to feed into the burner annulus proper.

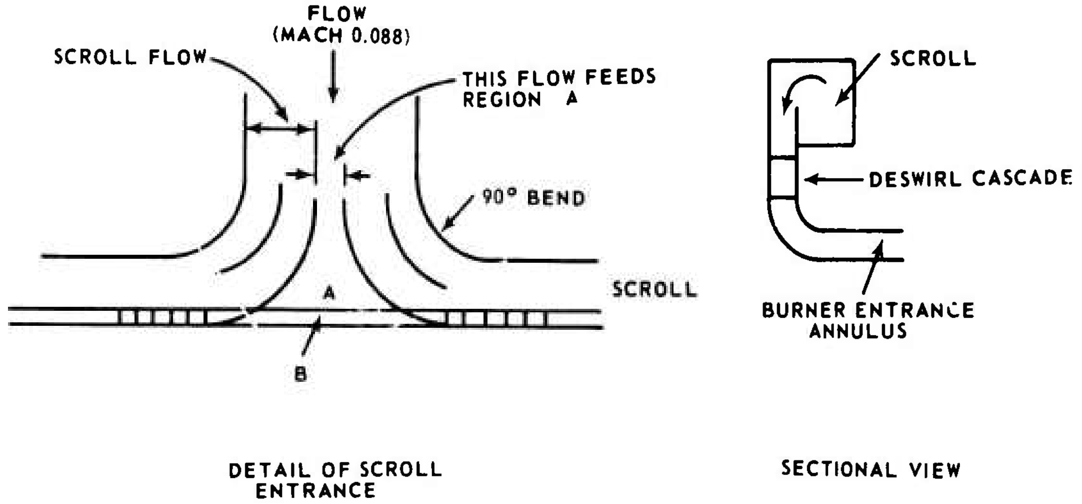

Figure 29. Burner Distributor Scroll Schematic.

For structural convenience,the scrolls were designed as an overhung rectangular section configuration. However, the area distribution was defined to be linear with circumference (constant velocity), since it was felt that the secondary losses in a distributor scroll would be small due to the absence of a driving radial outflow and the friction losses would be small in comparison with secondary losses.

To provide axial flow for the burner, the swirl generated by the scroll was removed in a radial deswirl cascade between the scroll exit and the radial-to-axial bend feeding the burner entrance annulus.

Burner

A contractor-sponsored design and development program for a burner suitable for use on a regenerative engine was conducted prior to full scale engine testing. The design parameters and the results of water model testing and combustion rig testing are given in detail in Appendix III.

Gas Generator Turbine

The turbine initially selected for driving the compressor was that designed for the PT6A-20 engine, which is estimated to give 87 percent efficiency at the design match point. The vanes are integrally cast, the blades are unshrouded, and both vanes and blades are at the nominal stagger angle of the PT6A-20 engine. The mean line temperature and pressure conditions at the design match point of both turbine stages are shown in Figure 30.

Power Turbine

The power turbine initially selected was a restaggered version of that used in the PT6A-20, which has integrally cast vanes and shrouded blades. The vanes were restaggered 3.6° closed and the blades 2° closed from the PT6A-6 nominal stagger angle, and the rotor was run up to 9 percent above the nominal design speed at match point. This is estimated to yield 86.5-percent efficiency.

Exhaust Duct

A single-port sideways-pointing exhaust duct was selected for its potential convenience in typical helicopter, boat, or vehicular installations. This type of exhaust also adapted very well to the dynamometer test cells. The shape was made simple for convenience of manufacture, and the velocity of the gas in the exhaust was made constant at each cross section at a value of 61.5 feet per second so as to provide a uniform static pressure on the downstream side of the regenerator hot section. The final area of 160 square inches at the exhaust port gave a velocity of 120 feet per second.

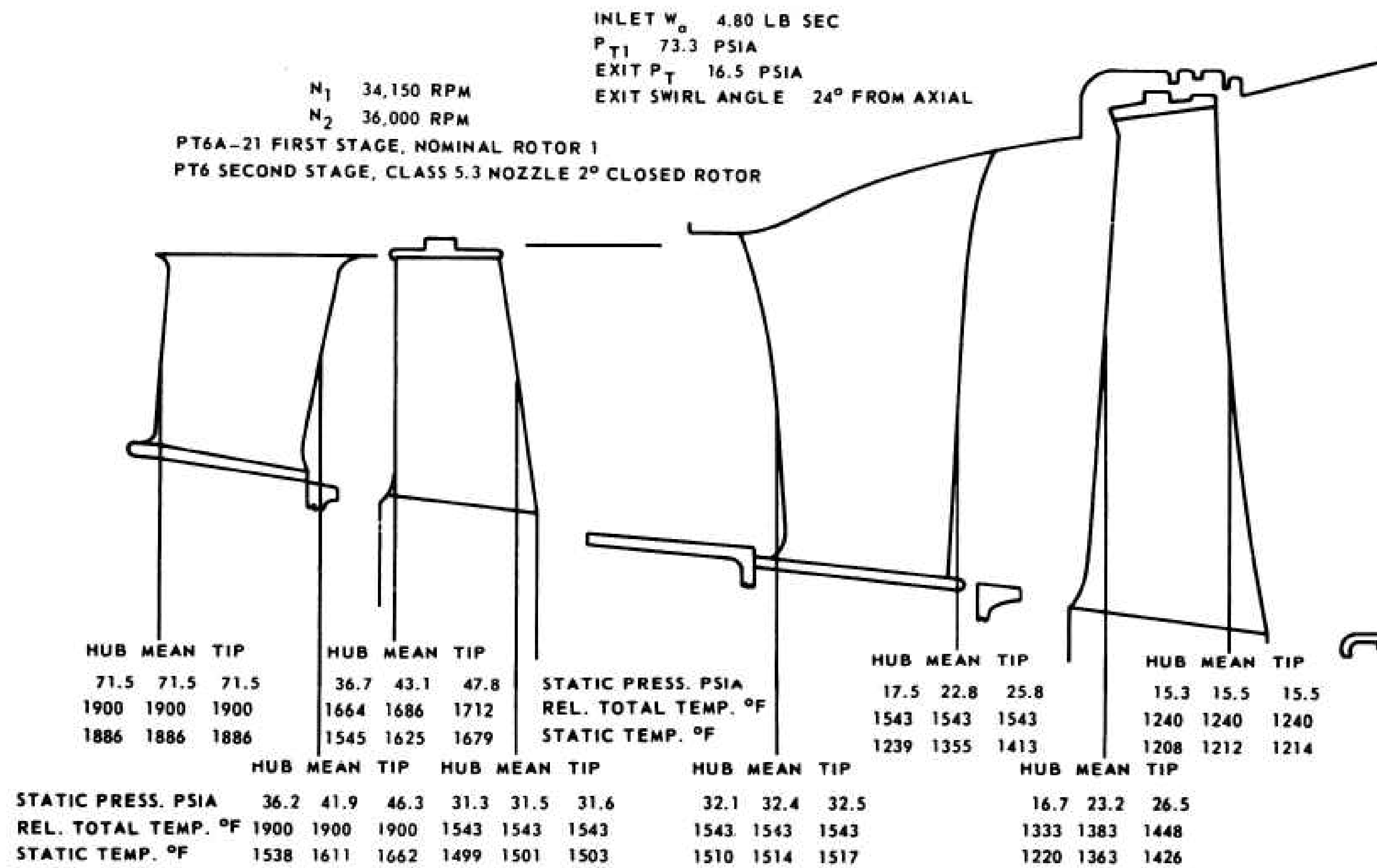

Figure 30. Compressor Turbine Pressure and Temperature Conditions at the Design Match Point.

MECHANICAL DESIGN CRITERIA

General

The underlying philosophy applied to the design was that it must be mechanically reliable and sound. It was designed to run for at least 100 hours to demonstrate the performance goals. The structure was made subject to available stress analysis so as to avoid structural test work, and, although a lightweight design was a goal, it is felt that substantial weight savings could be made with further design refinement and structural testing. The predicted and actual weights are discussed under Test Program, Weights and Deflection Test Results, on page 41.

Structure

The unit is basically a PT6 turboshaft engine adapted to accept the toroidal rotary regenerator which is positioned between the engine power turbine shaft housing and the reduction gearbox. The regenerator carries no structural load and is supported from the duct between the turbines and the regenerator. The standard turboshaft mount system is used; it consists of mounts at three points, one at each side of the gearbox nose case and a steady mount on the underside of the accessories gearbox. The engine structure path lies between these mounts through the inlet case and struts and the gas generator outer case, through struts across the flow path of the turbine-to-regenerator duct, along the extension housing of the high-speed coupling shaft between the power turbine and gearbox housings, and finally through the gearbox rear casing to the nose side mounts. The No. 2 bearing is supported by a cone and cylinder projecting from and welded to the junction of the gas generator and inlet cases. This structure houses the compressor and also provides support for the compressor turbine stator assembly. The power turbine is supported by its own bearing housing from the junction of the turbine-to-regenerator duct support and the high-speed coupling shaft housing. The power turbine stator assembly is held from an extension of the turbine-to-regenerator duct.

Casings and Scrolls

The outer casing of the gas generator section is a structural weldment which extends to accommodate the compressor delivery and burner entry scrolls. This outer case also carries the full compressor delivery pressure, thus relieving the scrolls of any significant loading and leaving them free to act as flow paths for the compressor and regenerator heated air.

The compressor delivery scroll is a square-cross-section weldment attached to the edge of the vaneless diffuser. A transition section at the junction of the diffuser pickup and discharge converts the passage to a circular cross section, which is then swept radially out through the top dead center of the main case. A second bend in this duct outside the case terminates in a forward-facing flange to which the regenerator feed duct is attached.

The burner entry scroll area is separated from the compressor delivery air region by a bulkhead carrying radial straightener vanes. The actual scroll is in two halves fed from a bifurcating inlet on the top dead center of the casing. The forward and outer diameter walls of the scroll are formed by the main casing, and the inner diameter wall is made to decrease the flow area from the inlet point to give constant velocity head and static pressure. The inlet area has turning vanes to feed the two halves, and the air passes from the feed scroll to the burner via the radial straightening vanes on the dividing bulkhead.

Compressor midstage air bleed, oil pipes to and from the No. 2 bearing area, and the standard PT6 fuel nozzle arrangement are incorporated in the casing design, along with a fuel drain valve, instrument bosses, and casing pressure taps for the fuel control unit pneumatic system. The whole is made from stainless steels selected to withstand the maximum operating temperatures and pressures.

Burner

The basic burner is of the reverse-flow fully annular form with 14 simplex fuel nozzles piercing the primary zone outer wall and angled to provide a toroidal flame. The primary zone skin cooling is achieved by holes drilled in the walls feeding into gaps provided by crimped strips welded to the inside of the walls. The dome end of the primary zone is cooled by lapped skins with a blank end through which cooling holes are drilled. Skin cooling for the secondary and tertiary zones is provided by lapped skins with open sides separated by corrugated strips. Secondary mixing air is induced through radial holes on the inner and outer walls. The tertiary mixing flow is inserted via a semicircular section swaged in from the outer wall, through which are drilled downstream-pointing holes. The burner can is connected to an inner and outer duct via slip joints to provide a reversing flow path to the turbines.

Turbines

The design of the turbine area was adapted from the standard PT6A-6 and -21 with a minimum of changes to suit the peculiar requirements of this engine. Both compressor turbine and power turbine have integrally cast vanes and separate blades riveted to the disks in fir-tree root serrations. There is a split point between the stages sealed with a piston ring. Some increase in size of the compressor turbine vane housing was required due to strength reduction at the higher operating temperatures, and some changes to the axial seal clearances were required due to the increased axial expansion of the casings. The cooling airflow path of the standard engine proved adequate for the regenerator version, and compressor delivery air is used for the purpose, being drawn from the area around the compressor delivery scroll.

Controls and Externals

A standard PT6 turboshaft-type control with power-turbine-driven governor is used on this unit driven from the standard pads provided in the gearbox nose case and accessories gearbox. A readjustment of the maximum flow schedule was required because of the lower flow requirements of this engine. As much standard control pipework as possible is used, with the rest made to suit during engine build. The external oil pipelines are flexible hoses connected to special screwed fittings adapted to the engine oil ports.

STRESS DESIGN CRITERIA

General

The main stress effort was focused on the new engine structure, with the turbine area and burner can also receiving attention. The major items in the analysis are listed below:

1. Gas-generator to burner-return-scroll casing.
2. Burner casing.
3. Compressor turbine disk and blades.
4. Effect of 1900°F. turbine inlet temperature on the life of the power turbine disk at overspeed.
5. Effect of reduced cooling air supply, due to lower P_3, on the rim temperatures of the turbine disks.
6. Strength of engine mount pads with increased engine weight.
7. Total engine structure deflections.

The aerodynamic pressures and temperatures used for the stress analysis of the various components were stated previously under Aerodynamic Design Criteria, General, on page 24.

The analyses of the stresses in the engine structure were restricted to those due to symmetrical pressure and thermal loads. The scope of the program did not allow a full assessment of the maneuver load capability of the structure, and thus only a limited analysis was made, mainly of deflections which, it was felt, would be the limiting loading factor.

Casings and Scrolls

Several configurations of the compressor delivery and burner inlet scrolls were considered in the initial stages of the analysis. The final configuration contained the two scrolls in a structural outer casing. This solution allowed a straightforward structural analysis with little sacrifice in weight.

The gas-generator to burner-scroll casing was analyzed under thermal and pressure loading. The limiting factor in the analysis was axial deflection, and stress levels were such that a reasonable margin was left for any additional stresses due to limited maneuver loading. If a complete analysis of the components under all loading conditions were carried out, some weight savings could be obtained.

Burner Casing

Analysis of the burner casing was carried out assuming a maximum skin temperature of 1400°F. The casing end dome was analyzed under the pressure drop and was found to be acceptable in 0.027-inch minimum-thickness*. The stepped cylinders were connected by channel-shaped gap retainers. The shape of these gap retainers was optimized using partial analysis to produce acceptable stresses in the cylinder, weld, and retainer under a 200°F. temperature difference between cylinders. Changes of wall configuration during burner development were monitored to ensure acceptable stresses.

Mount Pads

The PT6B-9 type 3-1-2-restraint 3-point mount system was recommended and used for the regenerator engine. This system provided the best support under vertical, axial, or lateral loading.

---

* Hastelloy X was the selected material.

The maximum allowable vertical mount reactions are listed below.

1. Reduction gearbox (right-hand pad): 3160 pounds.

2. Reduction gearbox (left-hand pad): 2700 pounds.

3. Accessory gearbox (lower pad): 1571 pounds.

4. Engine torque: +434 pounds on the left-hand pad, -434 pounds on the right-hand pad.

5. Maneuver load of 1 g.: 166 pounds on the forward pads, 282 pounds on the accessory pad.

Thus, maximum allowable g. level, governed by accessory gearbox mount pad, is 5.6 g.

Structural Deflection

The maneuver load capability of the regenerative engine is likely to be limited by overall structural deflection rather than local stress levels. The mass distribution, shear force, and bending moments used in the calculation of the structural deflection were based on the estimated weight of 614 pounds.

Considering only the bending stiffness of the various structural components, the maximum vertical deflection under a vertical maneuver loading of 1 g. was calculated to be approximately 0.0175 inch. Actual components are likely to be stiffer than calculated, but shear deflections have not been included. The estimated deflection curve is shown in Figure 31.

The controlling feature for deflections in the regenerative engine should be the allowable relative movements between the power turbine disk and the compressor turbine disk. This movement has been calculated as approximately 0.0065 inch for a vertical loading of 1 g. Seal clearances between the two turbine stages will allow approximately 0.030 inch of radial movement without serious rubs. Thus, the allowable vertical maneuver loading should be restricted to approximately 4 g. if structural stiffening of this engine arrangement is to be avoided.

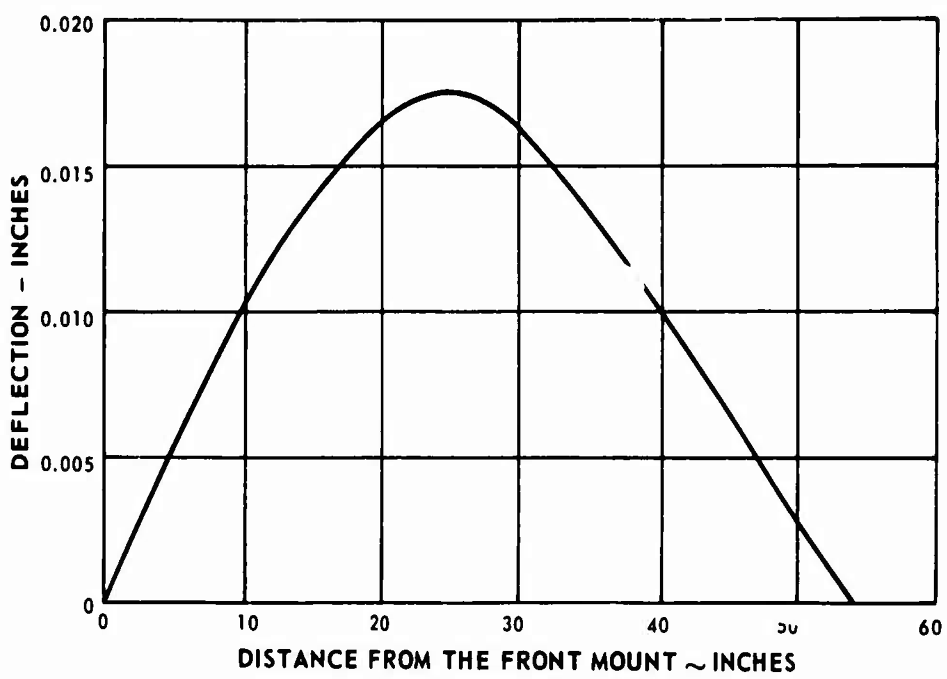

Figure 31. Approximate Structural Deflections of the Regenerator Engine Under 1 g. Vertical Loading.

<u>Gas Generator Turbine</u>

A stress check was carried out on the PT6A-21 gas generator turbine disk and blade assembly for use in the regenerative engine. The results indicate that this is feasible for a limited amount of running time. It was assumed that the gas loads on the first stage turbine blade for the regenerative engine were not sufficiently different from the A-21 gas loads to warrant their calculation. At the worst stress-temperature condition on the blade, the life to 1-percent creep is approximately 50 hours. The minimum lives to 1-percent creep on the A-6 and A-21 blades are 100 hours and 180 hours, respectively. The stress under the shroud of the regenerative engine blade is 10,700 p.s.i.

The A-21 first turbine disk, as used in the regenerative engine, had a burst margin of 3.375 at 34,150 r.p.m.; the burst speed was 52,750 r.p.m.

An investigation was also conducted to determine whether the PT6A-20 standard blades and disk could be utilized in the regenerative engine. Stresses were calculated in the blade airfoils for a turbine inlet temperature of 1900°F. and a shaft speed of 34,150 r.p.m. The minimum number of hours in the airfoil r 1-percent creep at a radius of 3. 50 inches was 22. The corresponding mperature was about 1693°F., with an approximate stress of 23, 650 p. s. i.

wer Turbine

investigation into the possibility of using the existing PT6A-6 power turbine the regenerative engine was carried out. This was done for 1900°F. turbine et temperature, 36, 000 r.p.m., and a 2° closed blade. The results indicate t this proposal was feasible for a limited amount of running time. Maximum ect stress is 63, 800 p. s. i. For the A-6, the maximum direct stress at ᵕᵕ, 000 r. p. m. is 52, 900 p. s. i., but it is 65, 000 p. s. i. at the overspeed case of 36, 000 r. p. m., without any adverse effects being noted. The closing of the blade 2° relative to the nominal A-6 blade does not appreciably affect the stresses and the balancing of the blade.

A vibrations survey indicated that the vibration characteristics of the power turbine blade for the regenerative engine were not expected to differ from those of the PT6A-6. No modes of any severity had been encountered in testing up to 36, 000 r. p. m. on the A-6 engine.

The disk used had the same geometry as the PT6A-6 power turbine disk. The burst margin in the regenerative engine was 2. 42 based on 36, 000 r. p. m. The disk burst speed was then 48, 400 r. p. m.

TEST PROGRAM

Test Features

The unit was mounted on a special test stand to drive a Dynamatic Model 2025-T1 dynamometer via a membrane coupling with control cables, engine feed, and exhaust ducting arranged to suit. Test equipment was as follows:

1. JP4 fuel was supplied with a boost pressure of not less than 5 p. s. i. g.
2. Engine oil conformed to Specification CPW 202 (Esso Turbo Oil 35).
3. Regenerator oil conformed to MIL-L-7808 (Esso Turbo Oil 15) and was fed from an airmotor-pump set supplied with the regenerator.
4. The exhaust stack was designed for this engine with an ejector annulus between the cell stack and the engine exhaust stub.

5. The engine starter was Delco Remy Model X50307 24V and was used with General Electric motor-generator set 5BY202A, rated at 1000 amperes intermittent.

6. Engine fuel manifold cooling was accomplished using 100-p.s.i.g. shop air feeding a collector manifold, which in turn fed each of the 14 nozzles.

7. Regenerator drive was a hydraulic motor using MIL-L-7808 oil driven from a hydraulic pump which was powered by an electric motor.

8. The ignition system was a standard PT6B glow plug powered by a 24-volt d.c. test cell.

Instrumentation

The instrumentation installed at the beginning of the program is shown in Table I.

TABLE I
ORIGINAL INSTRUMENTATION

Measurement	Description	Range
Torque	Dynamometer, engine torquemeter	0 to 120 in. Hg ΔP (0 to 640 ft. -lb.)
Power turbine speed	Tachometer, digital readout	0 to 40,000 r.p.m.
Gas generator speed	Tachometer, digital readout	0 to 40,000 r.p.m.
Fuel flow	2 turbine flowmeters in series, digital readout	0 to 400 lb./hr.
Air inlet temperature	6 thermocouples at intake screen	-40 to +150°F.
Interturbine temp.	Standard engine harness	0 to 2000°F.
Compressor delivery temp.	2 thermocouples in duct to regenerator	0 to 750°F.
Turbine exit temperature	9 thermocouples in outer annulus of turbine exhaust duct	0 to 2000°F.
Burner inlet temperature	4 thermocouples in neck of inlet duct, 6 thermocouples around inlet scroll	0 to 2000°F.
Exhaust duct temp.	4 thermocouples in exhaust duct	0 to 2000°F.
Compressor air mass flow	Calibrated inlet	0 to 60 in. H_2O
Engine inlet pressure	Barometer and test cell depression	0 to 12 in. H_2O
Compressor delivery pressure	1 wall static in duct to regenerator	0 to 100 p.s.i.g.
Burner inlet pressure	1 wall static in neck of inlet duct	0 to 100 p.s.i.g.
Burner case pressure	1 gas generator casing static tap	0 to 100 p.s.i.g.
Turbine exit pressure	3 wall static taps in turbine exhaust duct outer wall, outlet end	0 to 60 in. H_2O
Exhaust plane pressure	Calculated from flow and exit area	-
Oil temperature	Standard thermocouple location	0 to 400°F.
Oil pressure	Standard pressure tap location	0 to 100 p.s.i.g.
Bearing temperature	1 thermocouple in each of No. 2, 3, and 4 bearings	0 to 600°F.
Vibration	4 M & B pickups, 2 on accessories gearbox and 2 on reduction gearbox	0 to 2 kc.
	2 accelerometers, 1 on reduction gearbox and 1 on No. 3 bearing	0 to 20 kc.

As the engine performance program progressed, it became necessary to install additional instrumentation. This supplementary instrumentation is shown in Table II.

TABLE II
SUPPLEMENTARY INSTRUMENTATION

Measurement	Description
Air inlet temp.	6 thermocouples in air intake
Turbine exit temp.	9 thermocouples, 3 in inner turbine exhaust duct annulus, 6 in outer annulus of turbine exhaust duct
Compressor scroll static pressure	1 wall static
Turbine exit pressure	2 wall statics in turbine exhaust duct inner wall discharge end, 8 wall statics in turbine exhaust duct outer wall inlet end
Fuel manifold cooling air pressure	1 static tap

Ratings and Test Schedule

The ratings used for the demonstrator model were as follows:

1. Emergency rating: Conditions achieved at 1900°F. T_{4D} (gas turbine inlet temperature, determined) at a compressor turbine speed (N_1) not more than 34, 500 r. p. m. and a power turbine speed (N_2) of 36, 000 r. p. m.

2. Takeoff rating (T. O.): Conditions achieved at 1840°F. T_{4D} and 35, 000 r. p. m. N_2.

3. Maximum continuous rating (M. C.): Conditions achieved at 1780°F. T_{4D} and 34, 000 r. p. m. N_2.

4. Normal rating (N.R.): Conditions achieved at 1730°F. T_{4D} and 33,000 r.p.m. N_2.

5. Flight idle (F.I.): N_1 approximately 23,000 r.p.m. and N_2 approximately 33,000 r.p.m. (N_2 can drop for handling checks).

6. Ground idle (G.I.): N_1 approximately 21,000 r.p.m. and N_2 approximately 22,000 r.p.m.

The endurance test schedule consisted of 6-hour cycles broken down as shown in Table III.

TABLE III
DEMONSTRATOR ENDURANCE TEST SCHEDULE*

Condition	Rating	Time (hr.:min.)	N_2 (r.p.m.)	Readings
Steady state	N.R.	2:00	33,000	4 sets
Transient**	F.I.	:05	To suit	None
	T.O.	:05	35,000	None
Transient**	G.I.	:05	To suit	None
	T.O.	:01	35,000	None
	F.I.	:05	To suit	None
	T.O.	:01	35,000	None
Steady state	90% N.R.	:40	33,000	3 sets
Steady state	M.C.	:30	34,000	2 sets
Steady state	75% N.R.	:30	33,000	2 sets
Transient	30% N.R.	:10	33,000	1 set
	40% N.R.	:10	33,000	1 set
	50% N.R.	:10	33,000	1 set
	60% N.R.	:10	33,000	1 set
	70% N.R.	:10	33,000	1 set
	80% N.R.	:10	33,000	1 set

*Regenerator speed 20 r.p.m. at all times.
**Repeat 3 times before going on to next condition.

Weights and Deflection Test Results

A breakdown of the predicted weights and actual weights is summarized in Table IV.

TABLE IV
PREDICTED AND ACTUAL WEIGHTS

Item	Predicted Weight (lb.)	Actual Weight (lb.)
Regenerator rotating parts	132.0	143.0
Bearings and seals with inner structure	42.0	39.0
Regenerator housings	72.0	83.8
Regenerator drive less drive motor	9.0	9.0
Subtotal (regenerator)	255.0	274.8
Gearbox extension with drive case	13.0	13.5
Regenerator to burner inlet duct	14.0	14.2
Turbine exhaust duct	36.0	31.3
Compressor exit to regenerator inlet duct	20.0	20.0
Subtotal (engine ducts and gearbox)	83.0	79.0
Subtotal (regenerator plus engine ducts and gearbox)	338.0	353.8
Subcontractor-supplied engine components	279.0	313.32
Total regenerative engine weight	617.0	667.12

The additional regenerator weight is attributed to the matrix packages and the semimachined finished regenerator housings. The actual screen segments were weighed prior to assembly of the screen pack and were found to be 12 pounds heavier than the predicted weight. The tolerances of the commercially available screen resulted in this increase in weight. The additional weight of the regenerator housings is a result of computing the weight using nominal wall thickness, while in the actual parts most of the wall thicknesses are on the high side of the tolerance limits. Some of the excess weight of the UACL-supplied components can be attributed to engine instrumentation and associated bosses.

A study to determine whether other PT6 regenerative engine arrangements are potentially lighter or more compact or offer other advantages over the original test-bed arrangement was conducted. The results of this supporting study are in Appendix II. The outcome of this study is that one possible configuration results in the addition of only 275 pounds to the weight of the basic PT6 engine.

The results of a check on the casing deflections at 1-g. loading are presented in Table V along with the values estimated from the drawings. The complete unit with external plumbing and instrumentation was suspended horizontally by flexible plates from the planes of the reduction gearbox case rear case flange and accessories gearbox diaphragm flange to a stiff support bar. The mean of several readings is indicated in each instance (the readings repeated within 0.001 inch).

TABLE V
ESTIMATED 1-g. CASING DEFLECTIONS AND DEFLECTION TEST RESULTS

Location	Distance From Front Mount Plane (in.)	Estimated Deflection (in.)	Measured Deflection (in.)
Regenerator flange T.D.C.*	12.5	0.012	0.0065
Regenerator rear flange T.D.C. (toward engine intake)	18.0	0.0156	0.0205
Burner case exit flange T.D.C.	30.0	0.016	0.015
Burner case inlet flange T.D.C.	36.0	0.013	0.0075

*Top dead center

On the basis of the deflection test results in Table V, it was concluded that no problem would exist in the turbine seal area.

Résumé of Builds and Tests

Build 1. Performance testing was initiated after the stand systems, and regenerator external systems were checked operationally. The engine started readily, with no apparent defects other than evidence of minor oil leaks. Attempts to accelerate the engine gas generator were prevented by high interstage turbine temperatures and compressor stall. The power turbine speed was kept low initially and then accelerated to the maximum obtainable speed (26, 000 r. p. m.) while maintaining the gas generator speed below that which would produce stall conditions. Removal of instruments from their bosses at the entry to the burner feed scroll to permit compressor bleed-off allowed a somewhat higher gas generator speed but increased interturbine temperature. A hot spot was seen to develop on the exhaust duct between the turbines and regenerator at this stage. The unit was finally uncoupled from the dynamometer, and the power turbine shaft was slowly accelerated to 36, 000 r. p. m. (100-percent speed) to check for critical vibrations. The vibration levels were very low, indicating that this major structural change from the basic PT6 (T74) engine was a satisfactory design for test-bed operation. After 1.47 hours of operation, the engine was removed from the test stand for a compressor rematch and inspection.

Build 2. The engine was reassembled with the following changes.

1. The power turbine nozzle vane throat area was increased by 18 percent (2.2 square inches) to give a cooler match with increased surge margin. The compressor turbine nozzle vane throat area was not changed, since the estimated increase in area required was insignificant.

2. The burner nozzles were flow checked, and two which had flow deviations were corrected.

3. The fuel manifold assembly was changed to incorporate threaded connections in place of the O-ring type which tended to overheat and harden during operation.

4. The gap between the burner feed scroll and the outer casing was closed. This was suspected of having contributed to the hot spot seen on the initial run.

5. Instrumentation improvements were made to provide more reliable temperature and pressure readings throughout the engine.

The engine was mounted on the test stand and performance tests were started. The engine started again readily with low peak starting temperature in the turbine area. The turbine inlet temperature was much lower at idle conditions.

The engine was slowly accelerated up to moderate turbine inlet temperature to obtain performance calibration points and to check for compressor stall problems. The regenerator speed was held steady at 20 r.p.m. with a slight drop in speed at higher engine power settings due to increased seal friction load at higher pressures. On return to ground idle conditions there was an intermittent slight surge noise from the compressor, indicating that it was necessary to rematch slightly farther from the surge point. However, a higher value of gas generator idle speed was chosen to represent more nearly that required for a helicopter engine (needed to sustain the output speed at 100-percent). From this idle power level, handling checks were made to determine the surge margin and effects of the regenerator. Maximum turbine inlet temperature was reached in about 6 seconds with power lever movements of less than 1-second acceleration time. Acceleration times were similar to those found on standard PT6 engines, with little heat sink effect from the regenerator being apparent. Further handling and calibration checks, which were intended to determine the effect of varying regenerator and power turbine speeds, were suspended when symptoms suggested a partial seal failure in the regenerator. Engine calibration was terminated at this point for an investigation of excessive regenerator oil leakage and for a "green-run" teardown and inspection.

All engine and regenerator parts were carefully inspected. All parts were in good condition except for one regenerator inner diameter ring seal which exhibited carbon erosion and breakage (small chips). This seal, which was located in the regenerator hot-side, oil-side position, had accumulated more than 134 hours of operating time, including performance loop testing. Very minor cracks were visible in the turbine exhaust case at junction of flange and skin and at junction of radial struts and skin.

The engine was successfully run in a calibration program (power settings from idle to 380 shaft horsepower) for about 8 hours during this build. The test data results are shown in Figures 32 through 51. Figure 32 shows the predicted T74 regenerative engine performance for an 85-percent-effectiveness regenerator and an 80-percent-effectiveness regenerator and a typical performance curve for a nonregenerative PT6 engine. Engine data at this point in the test program indicated that the regenerator effectiveness was approximately 80 percent, which was in agreement with the results of performance loop tests.

Build 3. The engine was reassembled following the "green run" with the damaged regenerator carbon seal replaced and the engine compressor impeller tip diameter reduced by 0.2 inch to give a cooler match with more surge margin. During subsequent running, engine testing was halted after 24.3 hours of total operation because of regenerator rotational stoppage. During teardown it was found that the safety wire retaining three outer diameter tie-plate pins had broken, permitting movement of the pins and damage to the tie plates, a bulkhead, and a matrix package. The damaged components were replaced, and an improved safety wire procedure was established for the tie-plate pins.

Calibration data were collected for power settings from idle to 395 shaft horsepower. Engine specific fuel consumption showed very little improvement after replacement of the inner diameter regenerator carbon seals and reduction of the compressor impeller tip diameter.

Build 4. Calibration tests were terminated after about 4 hours of operation (28.5 hours total time) because of an oil fire which destroyed one matrix package. Cause of fire was attributed to a failure of the stand-mounted air-driven regenerator oil scavenge pump. This failure caused oil to soak the outer matrix element, which, presumably, was heated to combustion temperature while exposed to the exhaust gases and then ignited when exposed to the compressor air.

Frequently during testing, the inner turbine temperature thermocouple (T_5 designation) failed. Therefore, power turbine inlet temperature was estimated from the turbine exhaust duct temperature (T_6), which was measured in the outer annulus of this duct. This repeated instrumentation failure resulted in the need for thermocouples in the inner annulus of the turbine exhaust case to provide for more accurate measurement of T6 in order that a more accurate determination of turbine inlet temperature may be made. At this stage, it was suspected that engine horsepower was limited because of the maximum power turbine inlet temperature restriction (1900°F.).

Sufficient data were also obtained from the last two unit builds to show that a revision to the engine match would be beneficial. The unit was rebuilt with the following changes:

1. The destroyed matrix package (both inner and outer details) was replaced.

2. The power turbine stator throat area was reduced by 0.5 square inch to improve matching.

3. Additional thermocouples were installed in the inner annulus of the turbine exhaust duct at the regenerator hot-side inlet

Build 5. Endurance and calibration tests were conducted (accumulating 47.1 hours of total operation) until another tie-plate pin failure produced erratic regenerator speed. Whereas the previous pin failures were in the outer tie plate, this failure occurred at the midsection of the inner tie plate. During this 18-hour test period, the maximum power turbine output was 441 shaft horsepower, as limited by the maximum power turbine inlet temperature which was calculated from T_6 temperature measurements.

During teardown, each engine component was inspected in an attempt to find a clue which could explain the power turbine limitations. Under visual examination the power turbine did not exhibit metal discolorations which would be indicative of high gas temperatures. Further investigation suggested that engine growth in this area was larger than predicted, with the result that more cooling air was flowing into this stage, through a single-stage labyrinth, than predicted. This would have the effect of reducing engine shaft horsepower.

The burner section was locally buckled, and one fuel nozzle was clogged. Several small holes and weld cracks were located in the burner section. Some evidence of the clogged nozzle was observed in cool spots located downstream.

The engine was rebuilt with the following repairs and system improvements:

1. The damaged inner tie plate and bulkhead were replaced.
2. A new burner section was installed.
3. Pressure and temperature probes were installed to provide more engine component data.
4. The power turbine hub was replaced with one which had a greater axial length.

Build 6. An endurance test was conducted for 4.5 hours, and about 51.5 hours of total operation were accumulated. Test data indicated that the engine horsepower was still limited, and the additional thermocouples located in the inner annulus of the turbine exhaust duct suggested the presence of a more severe flow maldistribution in this duct than had been expected. At this point, the turbine exhaust duct was removed from the engine for a flow check in a loop which could simulate engine power turbine exit swirl conditions. A report of this supporting study is presented in Appendix IV.

The engine was rebuilt with the following changes for one final performance test:

1. The power turbine nozzle area was increased.

2. A total of 15 T_6 thermocouples were installed in the turbine exhaust duct outer annulus near the regenerator gas side inlet.

3. Additional P_6 static probes were installed.

Build 7. With the significant data obtained from the airflow tests of the turbine exhaust duct, a final engine performance test was conducted. A complete power range calibration was terminated because of erratic regenerator speed. Total engine operation exceeded 56 hours.

Engine performance is shown in Figures 32 through 51.

Final engine teardown indicated that poor compressor efficiency was due to a "dirty" compressor. Erratic regenerator speed was attributed to a failed outer tie-plate pin and corresponding lug. The view of the regenerator in Figure 52 shows greater peeling of the outer matrix package screens than of the inner packages. This tends to substantiate the results of the turbine exhaust duct flow test, which showed more flow in the outer annulus. All tie-plate pin and lug failures are attributed to heavier-than-estimated loadings, again caused by greater flow in the outer annulus than predicted.

The seven builds and the tests run on these builds are summarized in Table VI.

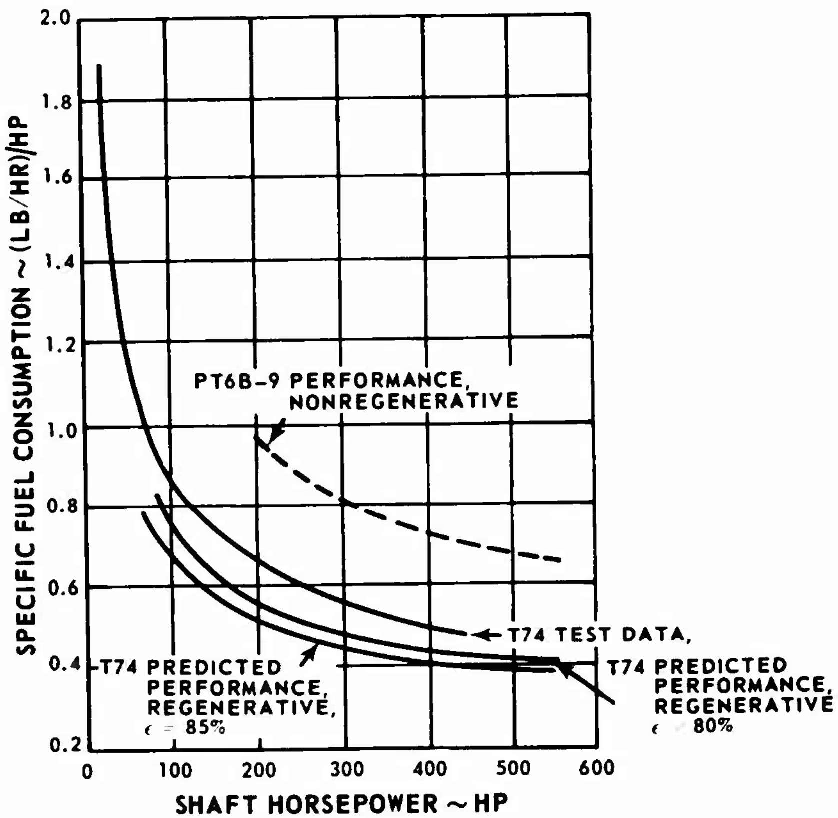

Figure 32. Predicted and Actual Fuel Consumption of Regenerative Engine.

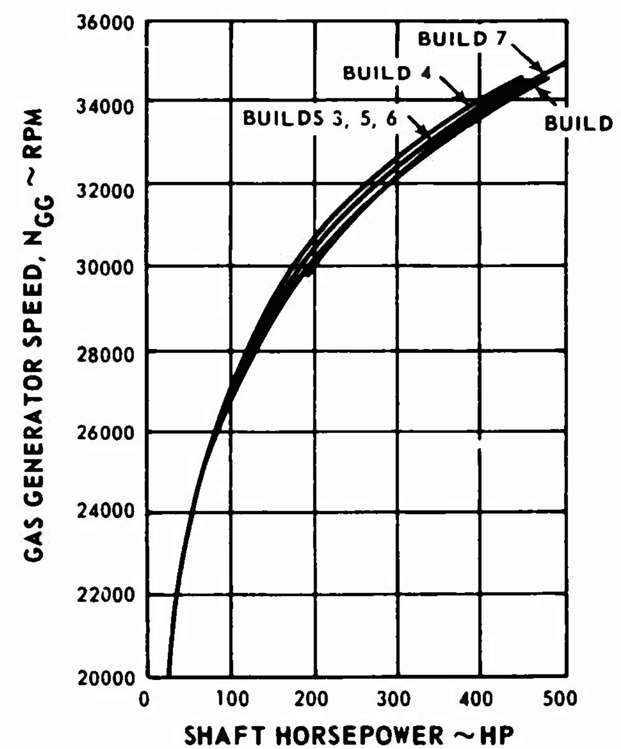

Figure 33. Gas Generator Speed Vs. Shaft Horsepower.

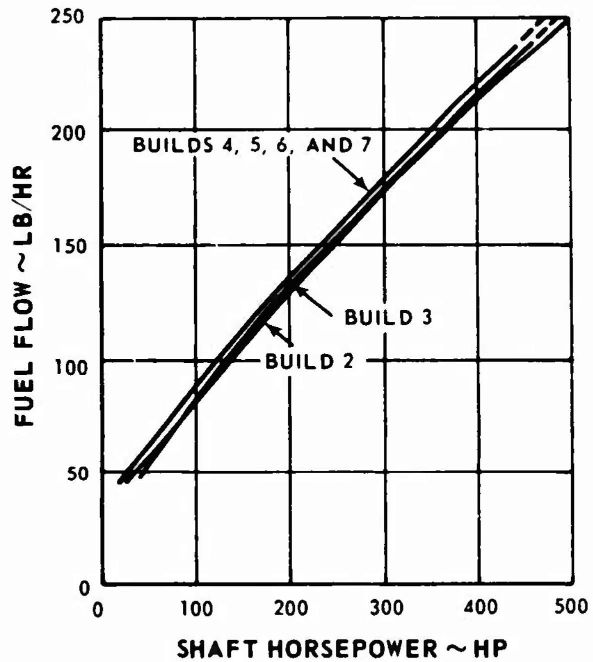

Figure 34. Fuel Flow Vs. Shaft Horsepower.

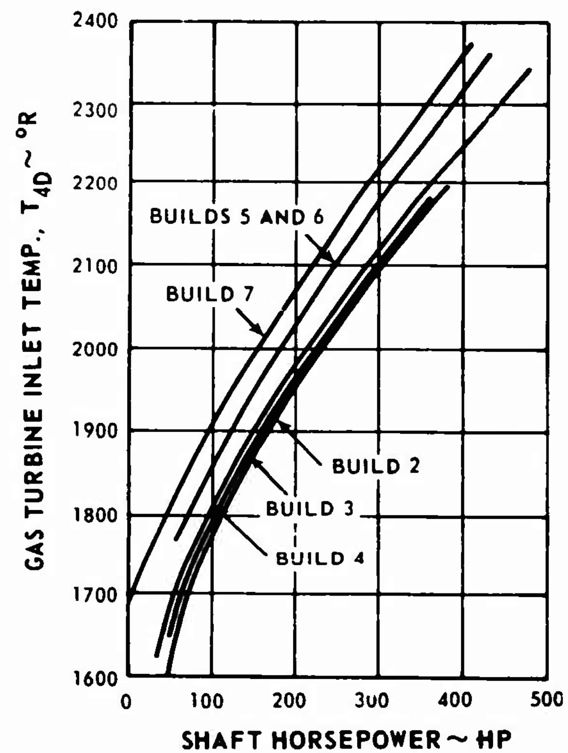

Figure 35. Gas Turbine Inlet Temperature Vs. Shaft Horsepower.

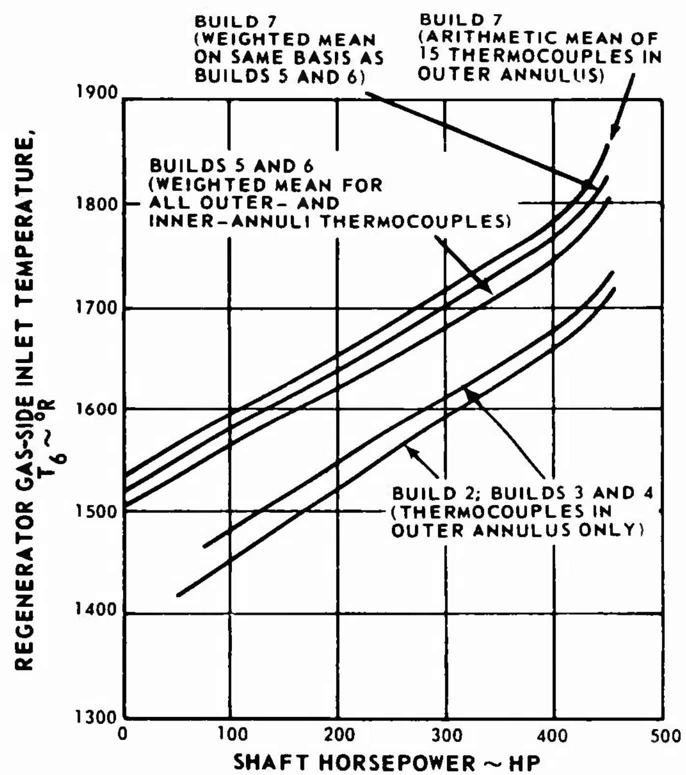

Figure 36. Regenerator Gas-Side Inlet Temperature Vs. Shaft Horsepower.

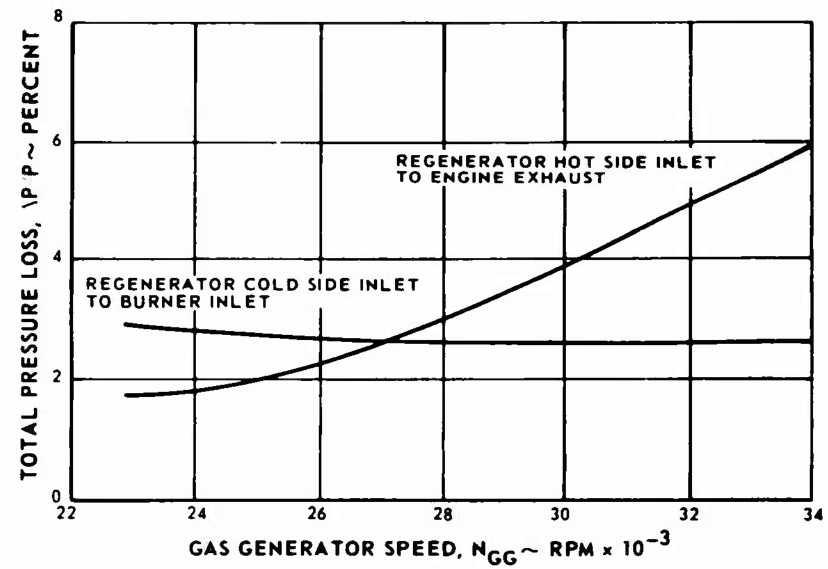

Figure 37. Total Pressure Loss Vs. Gas Generator Speed.

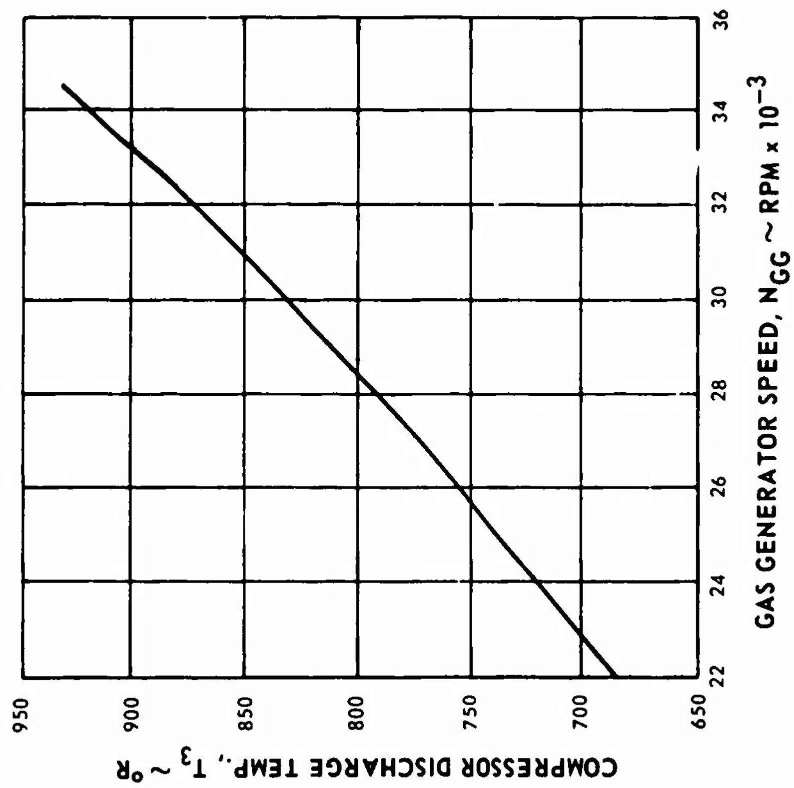

Figure 38. Compressor Discharge Temperature Vs. Gas Generator Speed.

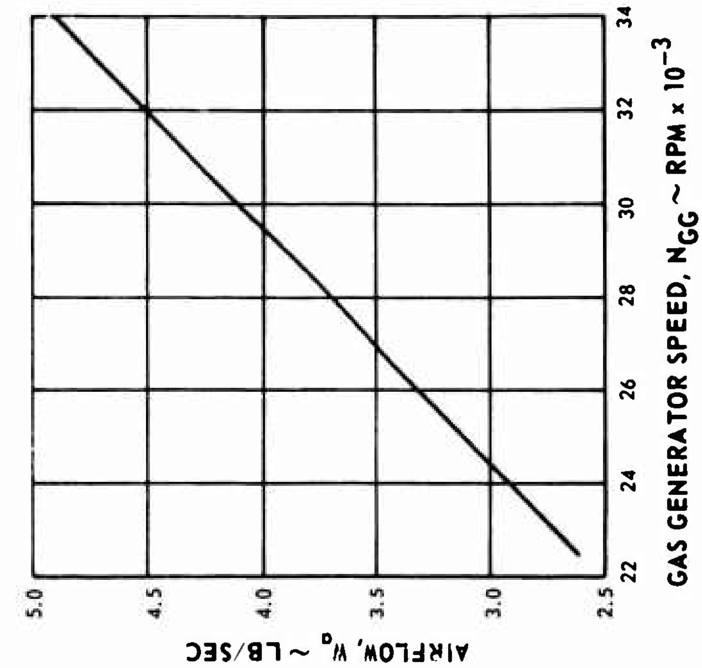

Figure 39. Airflow Vs. Gas Generator Speed.

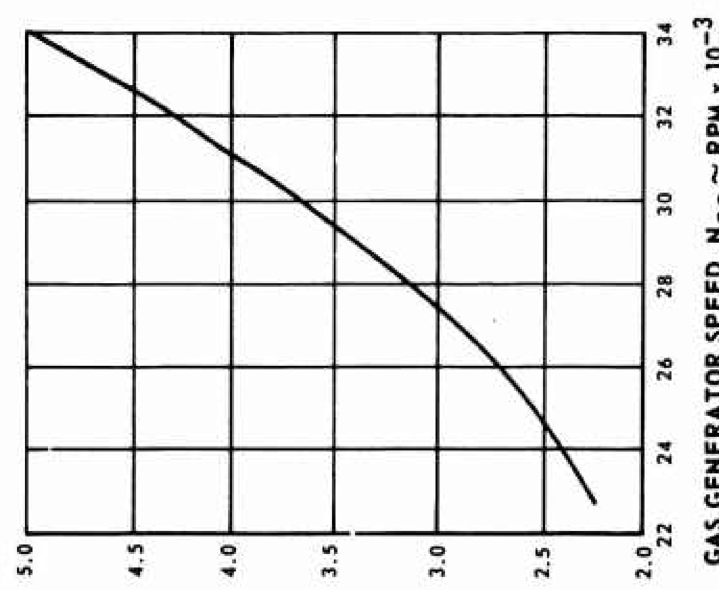

Figure 40. Engine Pressure Ratio Vs. Gas Generator Speed.

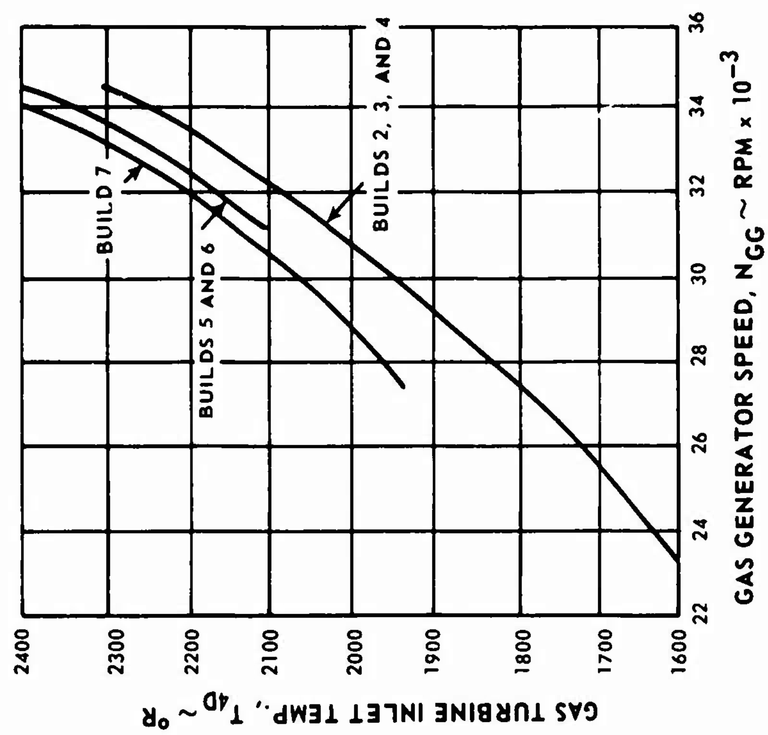

Figure 41. Gas Turbine Inlet Temperature Vs. Gas Generator Speed.

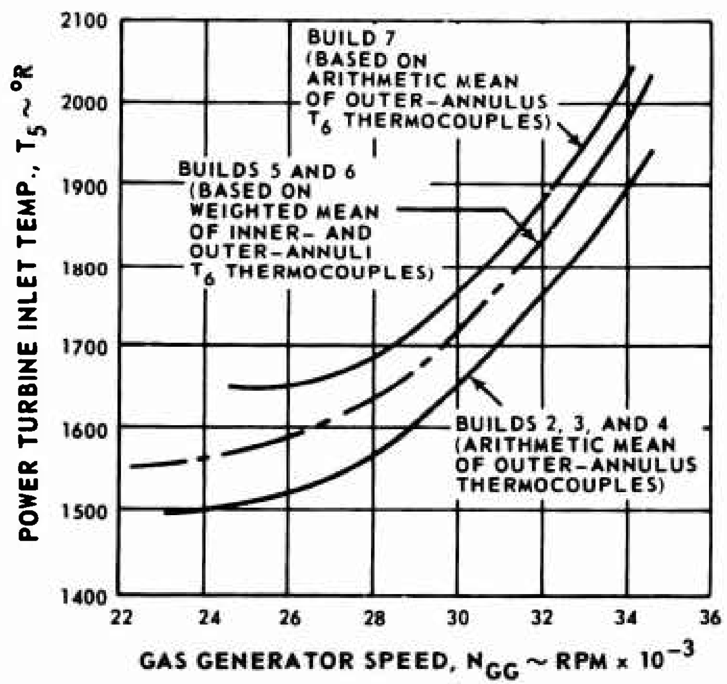

Figure 42. Power Turbine Inlet Temperature Vs. Gas Generator Speed.

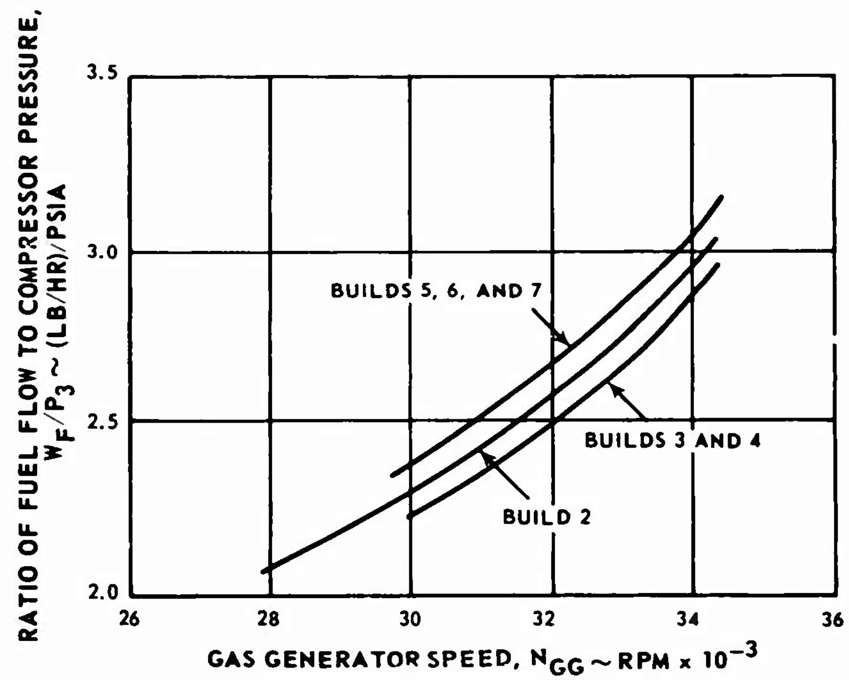

Figure 43. Ratio of Fuel Flow to Compressor Pressure Vs. Gas Generator Speed.

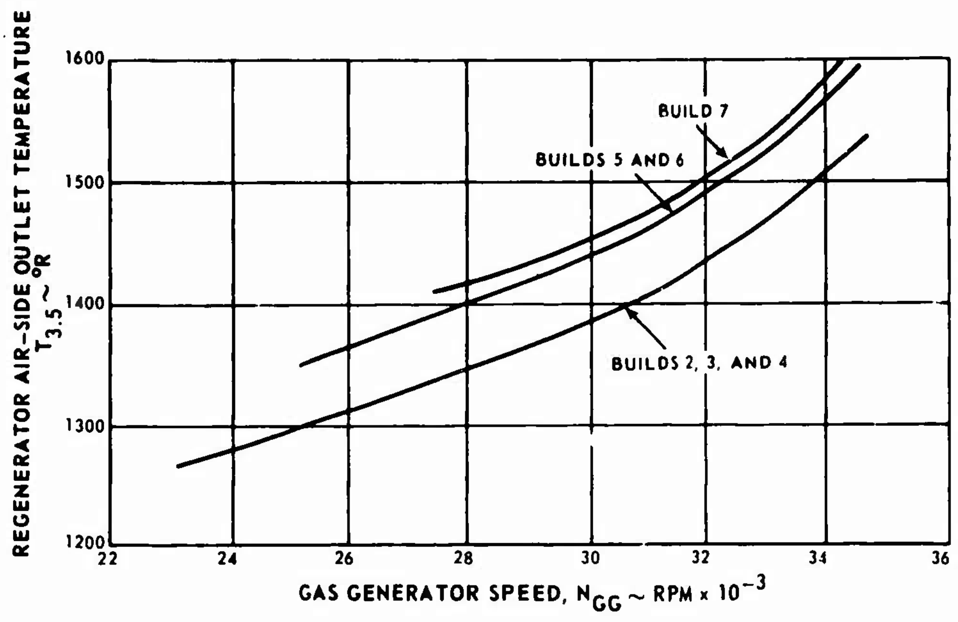

Figure 44. Temperature at the Regenerator Air-Side Outlet Vs. Gas Generator Speed.

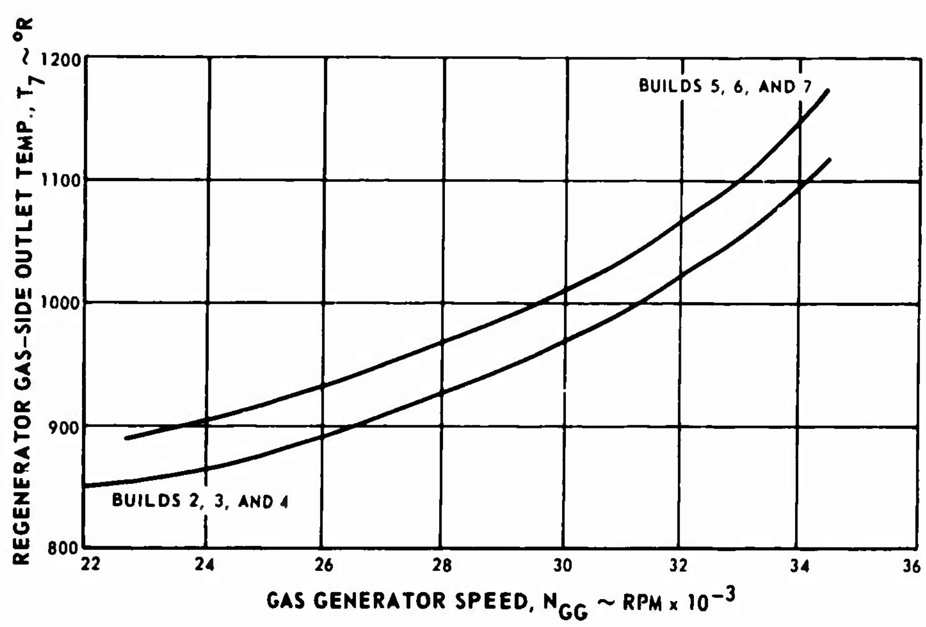

Figure 45. Temperature at the Regenerator Gas-Side Outlet Vs. Gas Generator Speed.

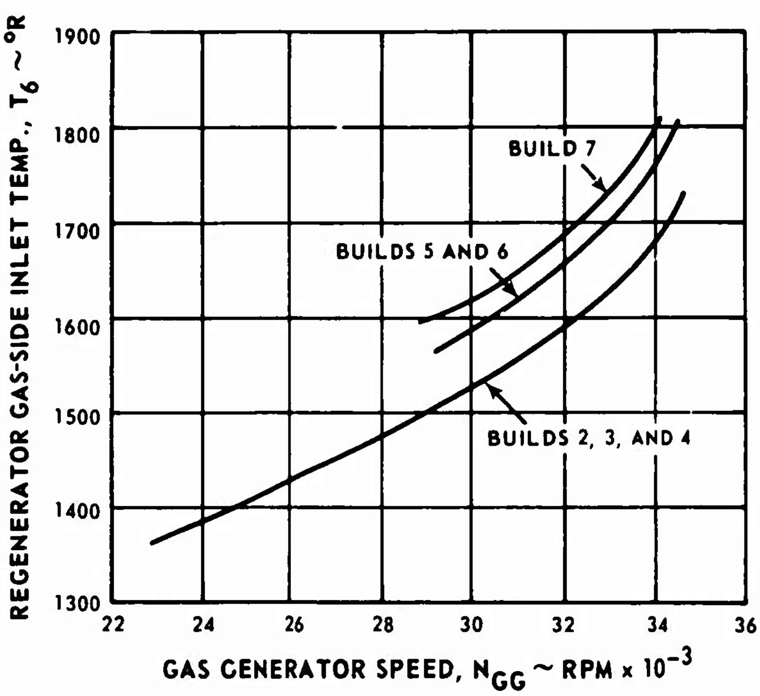

Figure 46. Temperature at the Regenerator Gas-Side Inlet Vs. Gas Generator Speed.

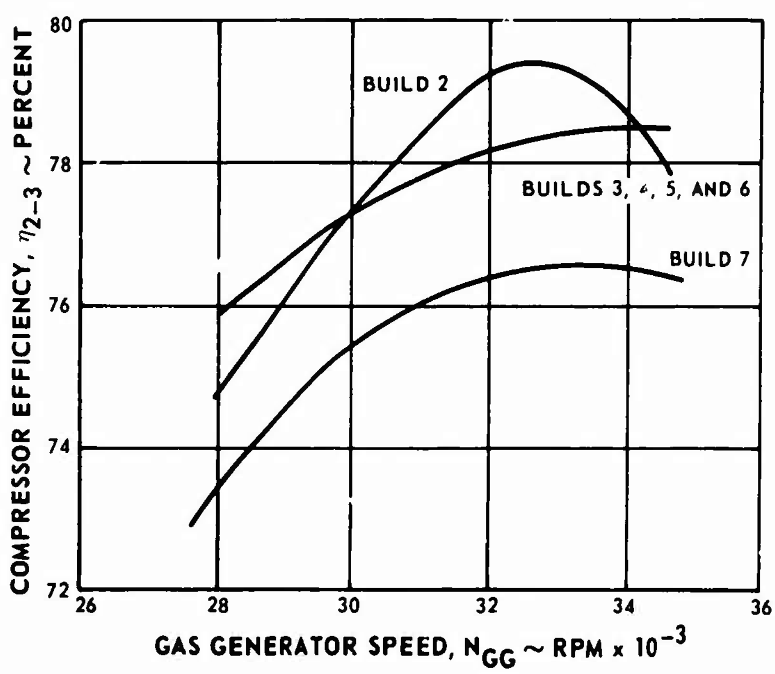

Figure 47. Compressor Efficiency Vs. Gas Generator Speed.

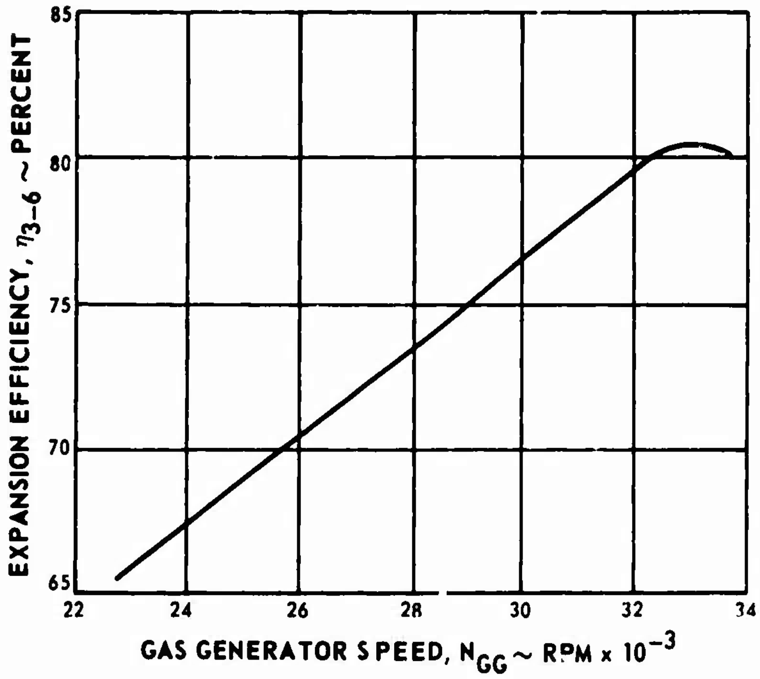

Figure 48. Expansion Efficiency Vs. Gas Generator Speed

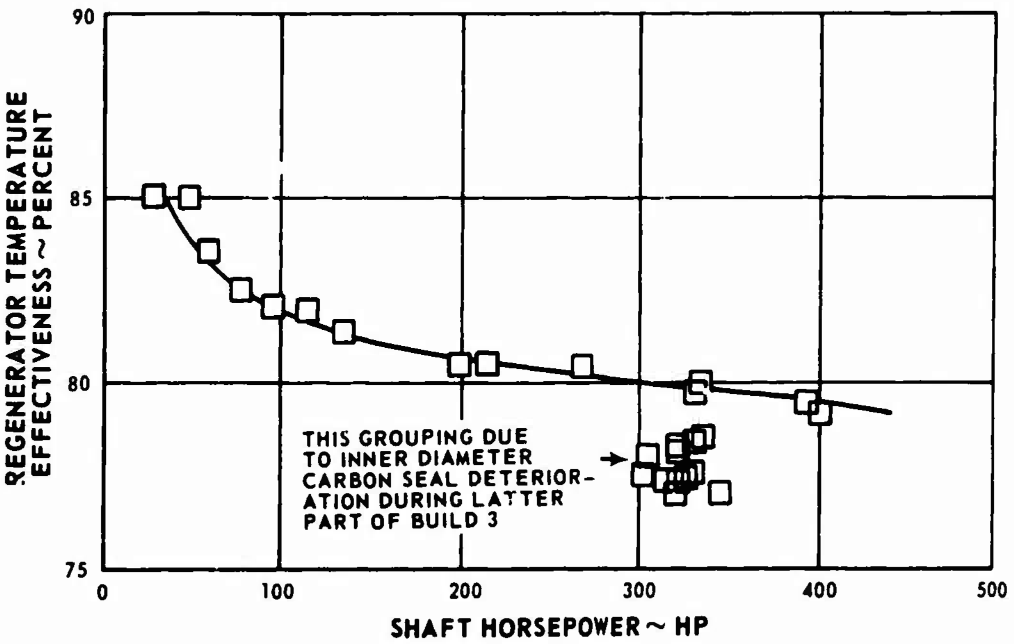

Figure 49. Regenerator Temperature Effectiveness Vs. Shaft Horsepower.

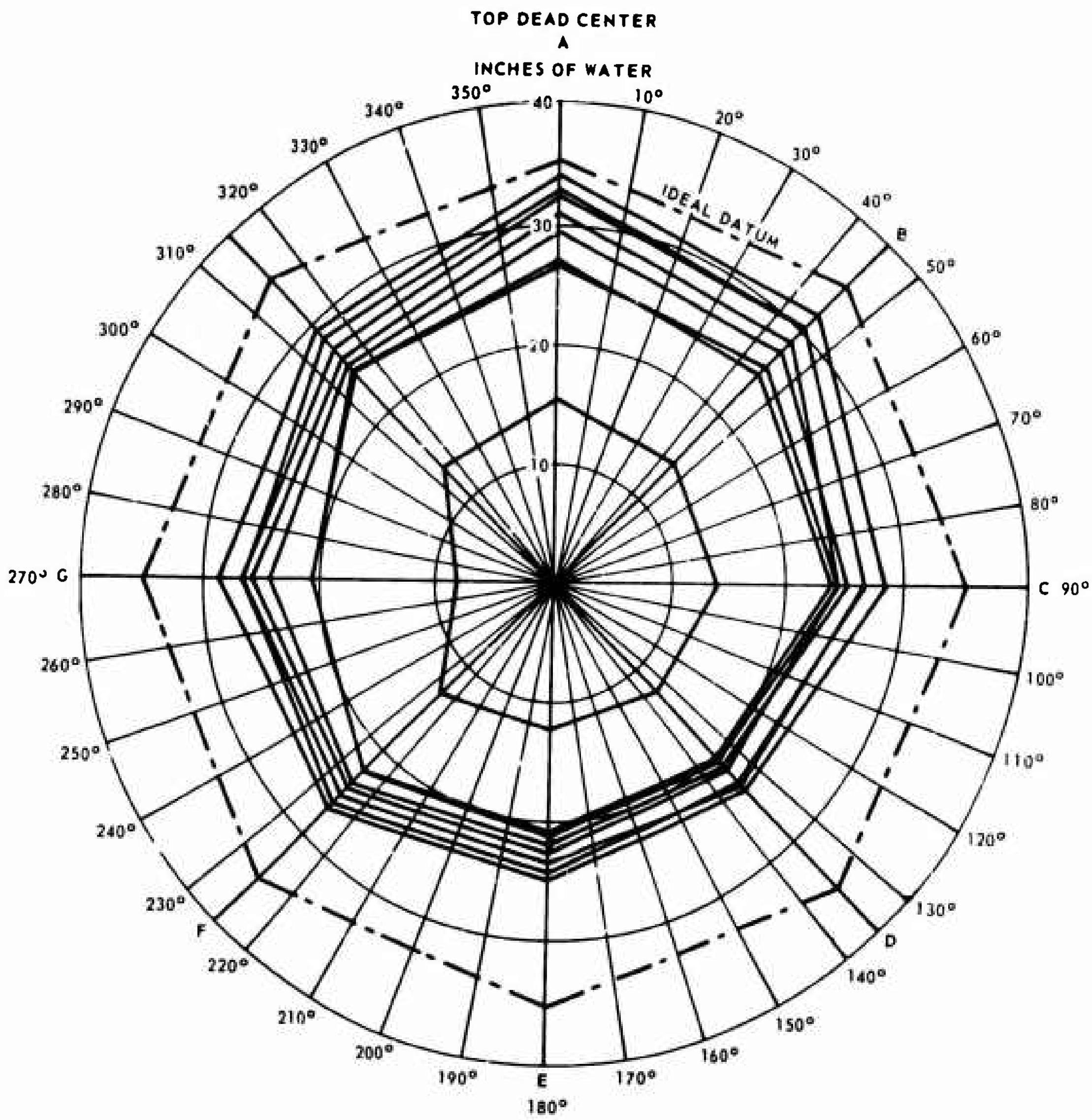

Figure 50. Static Pressure Distribution in Power Turbine Exhaust.

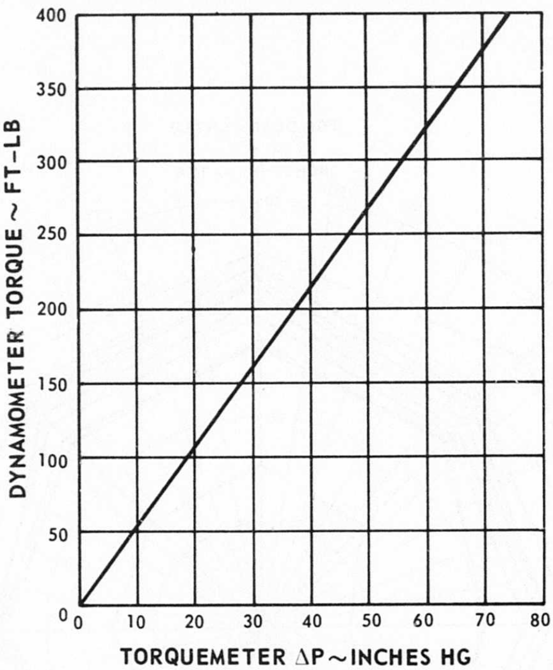

Figure 51. Dynamometer Calibration

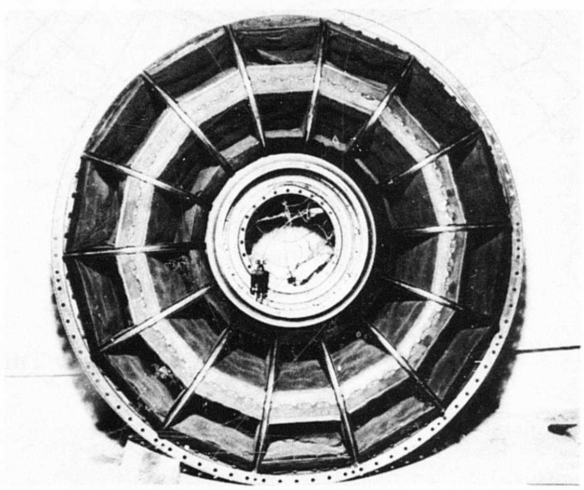

Figure 52. Deterioration of Outer Matrix Packages

TABLE VI
SUMMARY OF REGENERATOR ENGINE BUILDS AND TESTS

Build Number	Build Details	Running Time: Build (hr.:min.)	Running Time: Cumulative (hr.:min.)	Remarks
1	• Compressor: PT6A-6 standard • Burner: regenerative standard • Turbine, first stage: PT6A-20 standard • Turbine, second stage: PT6A-20 standard. • Regenerator: as shipped to subcontractor.	1:47	1:47	• Hot match. • N_1 was temperature and surge limited at 22,000 r.p.m. (N_2 taken to 36,000 r.p.m.).
2	Same as Build 1 except: • Turbine nozzle throat areas increased to give cooler match. • Screwed fittings on fuel manifold. • Gap closed in burner scroll.	8:03	9:50	• Partial carbon seal failure in regenerator. • Handling times were good (4 seconds from flight idle to maximum power).
3	Same as Build 2 except: • Impeller diameter reduced by 0.2 in.	14:44	24:34	• Locking pins between tie plates and bulkheads in regenerator failed (lockwire breakage initiated failure).
4	Same as Build 3 with: • Damaged tie plate and bulkhead replaced.	4:11	28:45	• Burned-out matrix package in regenerator due to oil loading caused by faulty stand-mounted scavenge pump.
5	Same as Build 4 except: • Power turbine nozzle throat area reduced. • Additional T_6 instrumentation	18:21	47:06	• Tie-plate pin and lug failure in regenerator.
6	Same as Build 5 except: • Compressor turbine blade opened 2°. • Compressor turbine nozzle vane closed. • Compressor turbine seals adjusted. • Instrumentation improved.	4:47	51:53	• Removed to flow-check turbine exhaust duct.
7	Same as Build 6 except: • Power turbine nozzle area increased. • Additional T_6 instrumentation. • Additional P_6 static probes.	4:33	56:26	• Tie-plate pin and lug failure in regenerator.

Mechanical Integrity During Test

The mechanical integrity of the regenerator-engine combination during test was very satisfactory, considering that is was a one-of-a-kind design involving major engine redesign. The following areas presented some problems:

Burner Can Primary Zone. The buckling of the primary zone skin was caused by incorrect spray pattern with some fuel nozzles. This was due to fuel coking in the nozzles, which in turn was due to insufficient nozzle cooling airflow at high power. This problem was eliminated when the pipe controlling the cooling airflow to the nozzle stem castings was increased in size to admit more cooling air.

Fuel Manifold O-Ring Leaks. The standard PT6 fuel manifold O-rings would not maintain a seal at the elevated temperatures of the regenerative engine. They were replaced by threaded connections which performed satisfactorily.

Regenerator Inner Diameter Carbon Seal Leakage. During Build 2, decay of regenerator performance suggested high leakage through the inner diameter carbon ring seal. At inspection, evidence of carbon erosion was found, and small chips were seen to be broken from the carbon. This seal had accumulated more than 134 hours of operating time and had been assembled and disassembled about six times.

Burned-Out Matrix Element. Figures 53 and 54 show the damage sustained by a matrix element during Build 4. The reason for the damage was the failure in the slave scavenge pump which allowed the oil level in the regenerator to rise and cause leakage. During one shutdown period this oil soaked onto the outer matrix element. On a subsequent start the element was heated to oil combustion temperature while exposed to the exhaust gases and then burned through when exposed to the high-pressure compressor air. It was a simple matter to replace the damaged element, and the unit was returned quickly to test.

Lock Pin and Tie Plate. During Build 3, regenerator rotation became erratic, then stopped. During teardown it was found that safety wire retaining three outer diameter lock (tie plate) pins had broken, permitting movement of the pins and damage to the tie plates and a bulkhead in the form of broken tie-pin lugs. An improved safety-wire procedure was established for the tie-plate pins, and no further safety wire failures occurred.

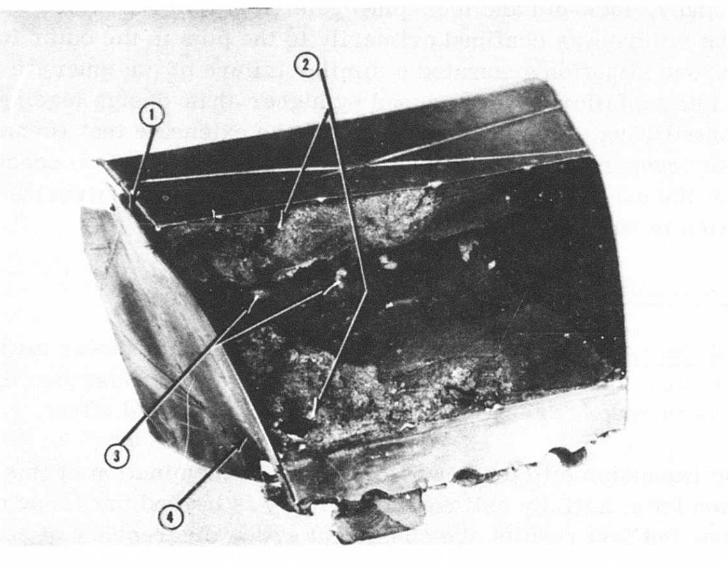

Figure 53. Front View of Burned Outer Matrix Package: (1) Broken Weld, (2) Burned Screen, (3) Fused Screening, (4) Buckled Side Plate.

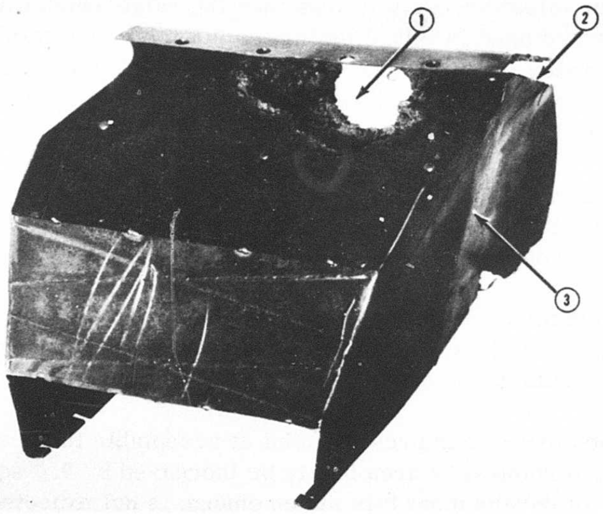

Figure 54. Rear View of Burned Outer Matrix Package: (1) Burned Screen, (2) Broken Weld, (3) Buckled Side Plate.

During Builds 5 and 7, lock-pin and lock-pin-eyelet (lug) failures halted testing. In both cases, the failure was confined primarily to the pins in the outer tie plate. However, one situation generated a similar failure of the inner tie plate and pin. These fatigue failures were caused by higher-than-design loading. Other factors contributing to pin failure were: (1) the extensive test running (130 hours) of the regenerator prior to mating with the engine and (2) concentration of most of the exhaust gas flow in the outer regenerator matrix package, a condition verified in subsequent testing.

Engine Test Performance Analysis

Summary of Test Data. Flow irregularities downstream of the power turbine existed, and it is clear that the turbine exhaust annulus and exhaust passages did not function as intended. These irregularities had a fourfold effect:

1. Turbine expansion efficiency was reduced. Determination of this reduction from initially estimated efficiency is beyond the scope of this program, but test results are consistent with a discrepancy of approximately 6 percentage points in turbine expansion efficiency (η_{4-6}).

2. Total pressure loss downstream of the power turbine was greater than estimated. Turbine exit circumferential static pressure maldistribution (Figure 50) makes the absolute value of this loss difficult to determine.

3. Regenerator effectiveness was less than the value which was indicated in rig tests and used in initial estimates. Engine test results indicated that regenerator effectiveness varied from about 70 percent up to 80 percent as a result of poor distribution of the gas entering the regenerator.

4. A T_6 reading which represents the true mean gas temperature (essential for the correct estimation of turbine inlet temperature and regenerator effectiveness) was difficult to measure.

In Build 7 a marked deterioration of compressor performance from that of Build 6 was evident. Examination indicated that cleaning techniques well established with the PT6 would have restored performance.

For operation on the correct compressor point at acceptable turbine inlet temperature, the power turbine vane area has to be increased by 0.6 square inch. In the present state of development this match change is not expected to improve significantly the relationship between power and specific fuel consumption.

Data Reduction. A modified PT6-engine test data reduction was used throughout these tests. On Builds 2, 3, and 4, the arithmetic mean of nine thermocouple readings in the outer turbine exhaust annulus was used for the calculation of burner exit temperature T_4 using shaft horsepower and compressor work. On Builds 5 and 6, nine additional thermocouples were placed in the inner exhaust annulus. The arithmetic mean of these readings and of the outer annulus readings was used to obtain a value for T_6.which, on the basis of rig test data, assumed 72-percent flow in the outer annulus and 28 percent in the inner annulus. In Builds 5 and 6, T_4 was calculated using this weighted mean T_6.

After Build 6, flow tests were conducted on the turbine exhaust duct (see Appendix IV). Test results indicated very low inner annulus flow with resulting doubt about the validity of these latest thermocouple readings. For Build 7, six additional thermocouples were arranged in the outer annulus, giving a total of 15 T_6 measurements. Arithmetic mean of these 15 outer annulus readings was the basis for calculation of T_4 on this build.

Table VII illustrates the demonstrated performance on Builds 6 and 7.

TABLE VII
ENGINE SEA LEVEL STANDARD DAY PERFORMANCE AT A BURNER EXIT TEMPERATURE OF 1900°F.

	Build 6	Build 7
Shaft power (hp.)	430	400
Fuel flow, W_f (lb./hr.)	230	210.5
Specific fuel consumption (lb./hp.-hr.)	0.535	0.527
Regenerator temperature effectiveness, ϵ (percent)	76.7	76.2
Compressor efficiency, η_{2-3} (percent)	77.8	76.2
Expansion efficiency, η_{3-6} (percent)	80.4	80.4
Gas generator speed, N_{GG} (r.p.m.)	34,200	33,700

General Performance. At derived T_4 values, measured shaft horsepower was consistently low despite good compressor performance and a fuel consumption approximately at the level anticipated. The series fuel meters were checked. The engine was closely examined for air or fuel leakage, and the combustion equipment never exhibited any evidence of poor fuel combustion.

In order to define the pressure losses from compressor exit to combustor inlet and across the regenerator hot side, differential pressures were carefully measured and total pressure loss from station to station was computed and compared with prior estimates based on rig test data. Throughout the engine and regenerator system it was apparent that there was a 3.2-percent total pressure loss in addition to original estimates. Total pressure loss in the inner and outer turbine exhaust annuli was not established on engine test, largely because of the turbine exhaust static pressure circumferential maldistribution (see Figure 50).

Using measured pressures, assuming 2.5-percent burner pressure loss and the previously estimated 4-percent turbine exhaust duct loss, the T_4-T_6 relationship obtained from reduced data indicates an apparent expansion efficiency (η_{4-6}) about 6 percent less than initially estimated. This is ascribed mainly to conditions downstream of the turbines. Rig tests of the turbine exhaust duct indicate extremely erratic flow patterns in both annuli with evidence of flow reversal taking place in the inner annulus.

In all of the data reduction, an internal leakage of 5.5 percent was assumed, comprising 3.1 percent due to the regenerator and 2.4 percent for engine requirements; this is slightly greater than that assumed in standard PT6 data reduction. Figures 32 through 48 show engine performance on this basis.

Turbine Inlet Temperature. T_6 measurements were not consistent. These measurements, which were used for T_4 estimation, show wide scatter in both ducts radially and circumferentially.

In all of the testing which was done, fuel flow was fairly consistent. Using this measured fuel flow, measured airflow, and estimated leakage, combustion temperature rise on Build 6 would be about 85°F. higher than analyzed results indicate. $T_{3.5}$ measurements were consistent: a deviation from arithmetic mean of no more than ±35°F. among all ten thermocouples was encountered.

Since rig and engine tests indicate that combustion efficiency is near 100 percent, the T_6 measurements are clearly not representative of mean gas temperature.

As a means of establishing truly representative T_6 value (and hence T_4), a free-shaft design point program was used as described in the following paragraphs.

Test results obtained at apparent turbine inlet temperatures of 1900°F. were used as input; turbine inlet temperature and expansion efficiency were varied, and test fuel flow was obtained by adjusting regenerator effectiveness.

Computed in the above manner, best agreement with Build 6 data was achieved at a T_6 corresponding to approximately 2445°R. turbine inlet temperature. It was concluded that at normalized gas generator speed of 34,200 r.p.m., Build 6 turbine inlet temperature is more truly represented by 2445°R. than by our initial T_6-based estimate of 2360°R. A similar analysis of Build 7 data at normalized gas generator speed of 33,700 r.p.m. was done, and the additional outer annulus T_6 thermocouples seemed to reduce the error in T_4 calculation. Here our T_6-based estimate of 2360°R. gives way to a calculated T_4 of approximately 2390°R. Adjusted for comparison purposes, this becomes 2439°R. at 34,200 r.p.m. On Build 7, T_5 measurements were successfully made and show good agreement with values derived from T_6 measurements. A differential, $T_{5A} - T_{5D} = -30°F.$, results from the calculated estimate of Build 7 turbine inlet temperature. Salient data from the initial performance estimate, from test data reduction, and from these latter design point calculations are presented in Table VIII.

Match Changes. Subsequent to test of Build 4, the power turbine vane area was reduced by 0.702 square inch. An increase of 0.33 square inch in this area was incorporated between Builds 6 and 7. For this reason, Build 4(T_4) is of interest and has been estimated in the same manner as Builds 6 and 7 and has also been tabulated.

In assessing the effects of these turbine vane area changes, the following factors were taken into consideration:

1. A reduction of 31°F. in average intake temperature between Builds 6 and 7.

2. A increase of 0.002 inch in compressor turbine tip clearance between Builds 4 and 5.

3. No change in configuration between Builds 5 and 6.

4. Reduction of compressor efficiency and mass flow between Builds 6 and 7.

TABLE VIII
COMPUTED AND DEMONSTRATED PERFORMANCE

	Initial Estimate	Build 4 Test Data	Build 4 Computed Data	Build 6 Test Data	Build 6 Computed Data	Build 7 Test Data	Build 7 Computed Data
$\Delta P/P$ Intake	0.0	0.0	0.0	0.0	0.0	0.0	0.0
$\Delta P/P$ Burner	0.025	-	0.0531	-	0.051*	-	0.0524
$\Delta P/P$ Exhaust	0.095	-	0.102	-	0.102**	-	0.098
$\Delta P/P$ Total	0.120	-	0.1531	-	0.152	-	0.1504
P_3/P_2	5.25	5.15	5.15	5.15	5.15	4.84	4.84
W_a (lb./sec.)	5.0	4.9	4.9	4.8	4.8	4.6	4.6
η_{2-3}	0.78	0.788	0.788	0.788	0.788	0.762	0.762
η_{4-5}	0.872	-	-	-	-	-	-
η_{5-6}	0.865	-	-	-	-	-	-
η_{4-6}	0.88	-	0.828	-	0.813	-	0.843
$\epsilon \; \dfrac{T_{3.5} - T_3}{T_6 - T_3}$	0.80	0.77	0.704	0.767	0.71	0.762	0.72
Parasitic loss (hp.)	10.3	10.4	10.4	10.4	10.4	10.0	10.0
Bypass leakage, W_{BL}/W_a	0.0521	0.055	0.055	0.055	0.055	0.055	0.055
T_3 (°R.)	922.2	912.4	912.4	917.4	917.4	906.7	906.7
$T_{3.5}$ (°R.)	1560.6	1513	1518	1575	1579	1569	1558
T_4 (°R.)	2360	2265	2350	2360	2445	2360	2390
T_5 (°R.)	1999.9	1915	2000	2006	2091	2013	2043
T_6 (°R.)	1720.2	1692	1772	1775	1852	1779	1810
Shaft power (hp.)	515.3	416	416	430	430	400	400
SFC (lb./hp.-hr.)	0.4284	0.539	0.539	0.535	0.535	0.527	0.527
W_f (lb./hr.)	221	224	224	230	230	210.5	210.5

*Comprises 0.026 measured regenerator pressure loss and 0.025 estimated burner pressure loss.

**Comprises 0.061 measured regenerator pressure loss and 0.041 assumed exhaust passage loss.

Upstream Effects of Turbine Exit Duct. Static pressure taps at the power turbine exit indicated that there was flow through only 80 percent of the annulus. This would produce the effect of an 80-percent partial-admission turbine wheel for impulse blading, which would cause a penalty of 4 percent on efficiency. Since the stage has about 20-percent reaction at the mean channel height, partial admission would cause about 5- or 6-percent loss in efficiency.

Transient Performance. Rapid acceleration and deceleration checks were made with the unit, moving the power lever from idle to maximum rating in less than 1 second. The engine response times were comparable to those of PT6 engines, with no stalling or hang-up observed. From a flight idle speed of 23, 300 r. p. m. (N_1), the unit accelerated to 96 percent of maximum power in 4. 5 seconds. Acceleration data for the regenerative engine are shown in Figure 55 and non-regenerative acceleration data are shown in Figure 56.

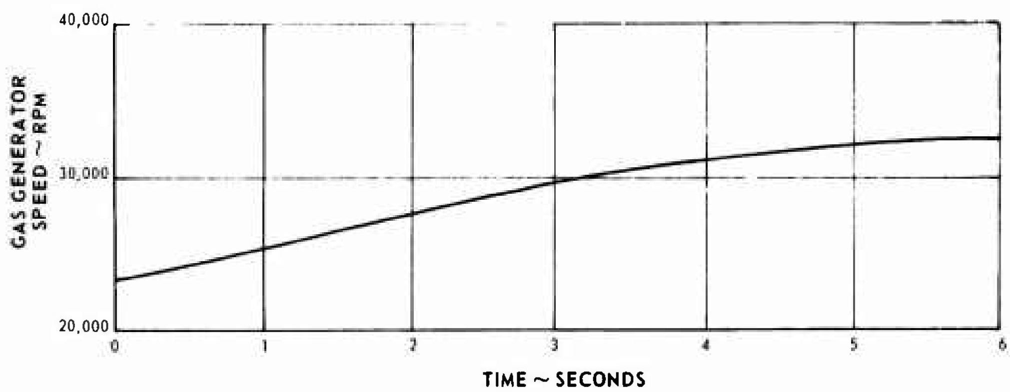

Figure 55 Typical Acceleration of Regenerative PT6 (T74) Engine

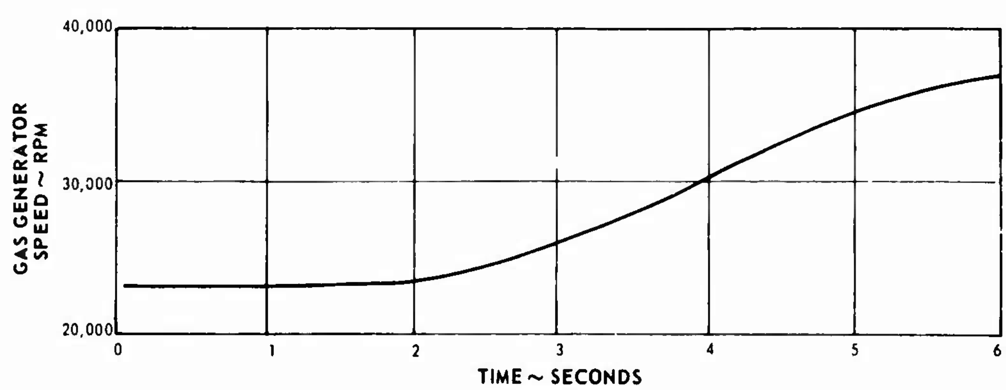

Figure 56 Normal Acceleration of Commercial PT6 (T74)

CONCLUSIONS

The following conclusions, based on analytical and experimental investigations conducted during the entire program, have been drawn. Conclusions 1 through 10 are based primarily on the results of work in Phase I of the program, as reported in USAAVLABS Technical Report 67 - 34 (PWA-2942).

1. The 60-mesh, 0.004-inch-wire-diameter matrix and the 80-mesh, 0.004-inch-wire-diameter matrix will not foul or clog from burner deposits during cyclic flow conditions which exist in the regenerator. (No matrix fouling was observed during the engine test program or performance loop tests.)

2. The heat transfer and friction factor characteristics determined experimentally for 16 matrix cores have extended the design information required for future lightweight regenerator designs.

3. The circumferentially folded matrix package has both performance and structural advantages over the radially folded matrix. The performance advantage was demonstrated by test.

4. The leakage goal of 10 standard cubic feet per minute at 100-p.s.i. pressure drop for the inner diameter torus seal was satisfied by three different types of carbon seal.

5. Inner diameter seal endurance tests at overspeed and overload conditions demonstrated long seal overhaul life and no performance deterioration.

6. The feasibility of three different types of all-metal inner diameter seals was demonstrated, but refinements are required before these configurations can be utilized.

7. Temperature effectiveness of 85-percent was demonstrated on a subscale regenerator (built with a circumferential vee package), which was operated at conditions comparable to those established for the PT6 (T74) regenerator designed under this contract.

8. The optimum matrix for the PT6 semiflightweight regenerator was a 60-mesh, 0.004-inch-wire-diameter or an 80-mesh, 0.004-inch-wire-diameter screen package.

9. The power required to motor the PT6 regenerator was less than one horsepower; this was provided by a small hydraulic motor.

10. Total regenerator mass loss of 3.2 percent, which includes 1.05-percent seal leakage, was demonstrated on two sets of full scale regenerators at a pressure ratio of 5.25.

11. Regenerator pressure loss of 6.1 percent was demonstrated at the design airflow of 5.0 pounds per second.

12. Regenerator tests in a loop which simulated engine conditions demonstrated 80.5-percent temperature effectiveness at the design point. This effectiveness is slightly above the minimum project goal.

13. Nonuniform matrix flow distribution was shown to be the cause of the effectiveness being lower than the predicted effectiveness of 85 percent.

14. Over 56 hours of regenerative engine testing and 110 hours of performance loop testing with essentially the same physical parts demonstrated the mechanical integrity of the toroidal rotary regenerator.

15. Acceleration and deceleration times for the PT6 regenerative engine were similar to the nonregenerative PT6 engine. No heat sink effect due to the regenerator could be detected.

16. The performance of the demonstrator model did not meet the design specific fuel consumption or shaft horsepower for the following reasons:

   - The regenerator maximum achievable effectiveness was lower than estimated because of matrix flow maldistribution.

   - The aerodynamic performance of the turbine exhaust duct caused higher-than-estimated losses in the power turbine, in the regenerator, and in the duct itself.

17. Based on actual regenerative PT6 engine weights and design weight reductions, an 85-percent-effectiveness regenerator system can be built for 55 pounds weight per pound of airflow. This would add 275 pounds to the weight of the basic PT6 engine.

18. The use of a regenerator on the PT6 or any engine can substantially reduce its specific fuel consumption.

19. The minimum effectiveness, pressure loss, and weight goals for the regenerator designed in this program (see tabulation below for minimum, target, and maximum as given in the original contract Statement of Work) were exceeded. The accomplished effectiveness was 80.5 percent; the accomplished pressure loss was 6.1 percent; and the accomplished weight (total weight in addition to the basic PT6 engine weight) was 275 pounds.

	Min.	Target	Max.
Effectiveness (%)	80	85	88
Pressure drop (%)	7	6	5
Regenerator weight (lb.)	300	250	240

20. While the minimum specific fuel consumption goal for the regenerative engine tests was not reached, the minimum goals and the targets for the number of engine starts and the number of test hours were exceeded. (See tabulation below for minimum, target, and maximum as given in the original contract Statement of Work.) The accomplished specific fuel consumption was 0.51 pound per horsepower-hour as demonstrated in Build No. 3, and the accomplished number of engine starts and test hours were 89 and 56, respectively.

	Min.	Target	Max.
Specific fuel consumption (lb./hp.-hr.)	0.44	0.40	0.38
Number of cycles or starts	24	48	60
Test hours	25	50	100

RECOMMENDATIONS

Two problem areas were encountered during the test evaluation of the full scale regenerator and the regenerative PT6 (T74) engine which are worthy of concentrated analytical and experimental investigation. These problems are discussed below, together with suggested methods of attack.

FLOW DISTRIBUTION OF A MATRIX WITH OBLIQUE FLOW

Test results of the full scale regenerator showed that the measured effectiveness was below predicted levels because of flow maldistribution within the matrix package. This problem had been anticipated, and a test program to evaluate the effects of inlet Mach number, matrix angle, relative matrix pressure loss, and entrance geometry on distribution was part of this program. This work was discussed in the Phase I final report. The matrix geometry which evolved from this work and which was used in the full scale regenerator was not refined enough to meet the regenerator requirements.

This problem is intrinsic not only to the toroidal rotary regenerator with a folded matrix package but also to compact fixed boundary heat exchangers with oblique flow. The work in this program showed that negligible maldistribution occurred over a wide range of oblique angles above a critical angle.

One suggested program would be to define this critical angle for selected matrix types over a range of pressure loss levels. A more general approach suggested is one which would determine what degree of flow distributors (e.g., turning vanes, contoured walls, etc.) is required for designs below this critical angle. With this information a designer could: (1) avoid maldistribution or (2) make trade-off studies of regenerator effectiveness, weight, and cost versus compactness.

Our work also showed that the three methods which were tried in mapping local distribution did not yield sufficient accuracy. These were: (1) streamline mapping, (2) static total pressure probing, and (3) hot wire anemometer probing. It is recommended that, in addition to refining techniques to measure flow distribution, this problem be attacked by measuring the temperature effectiveness in a single module rig such as described in Appendix V of this report.

FLOW MALDISTRIBUTION IN DUCTS

The ducting associated with any regenerator and regenerative engine is unique, and a generalized design program is not feasible for oddly shaped ducts. It is recommended that a duct distribution program be a contract demonstration item in any future regenerator development program. Model duct test results should be verified with performance tests of the finally developed duct.

It is recommended that, prior to any further testing of the regenerative PT6 engine, a development program for the turbine exhaust duct be conducted. It is further recommended that following satisfactory completion of this program, the operational characteristics of the regenerative engine be evaluated in a ground vehicle or helicopter installation, as it was for these applications (not for fixed-wing aircraft) that the demonstrator was designed.

APPENDIX I

DUCT FLOW DISTRIBUTION

Since the engine performance depends upon the duct pressure loss and the flow profile entering the regenerator, a test program was conducted to develop uniform flow in the exit plane of the compressor-discharge-to-regenerator duct and the turbine exhaust case with minimum pressure loss.

The airflow test rig shown in Figure 57 was constructed for flow tests of each duct configuration. The compressor discharge flow test model (Figure 58) and the turbine exhaust case flow test model (Figures 59 and 60) were used to develop the required flow distribution. Each duct was run at the engine design point Mach number, since the Fanning friction factor is approximately constant over the engine duct Reynolds numbers. The mass velocity at the duct exit was determined by measuring the velocity head with pitot-static pressure probes in small area increments by traversing circumferentially in 5° increments and radially in 0.25-inch increments. Since pitot-static pressure probes are sensitive to flow direction, honeycomb sections of a length-to-diameter ratio of 10 were installed at the duct exit, immediately upstream of the probes, to assure parallel flow at the probes. The duct pressure loss ratio ($\Delta P/P$) was determined by measuring the inlet pressure with pitot-static probes and subtracting the atmospheric pressure (the flow duct exhausted to atmosphere).

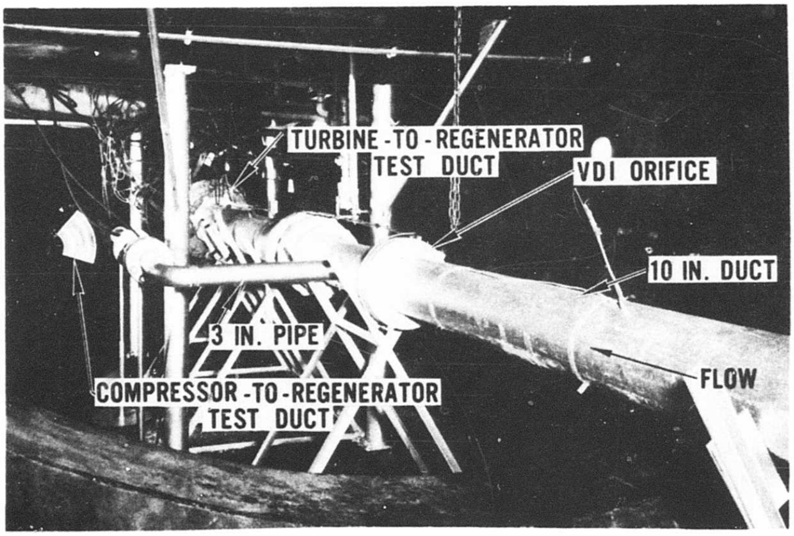

Figure 57. Regenerator Duct Airflow Test Rig.

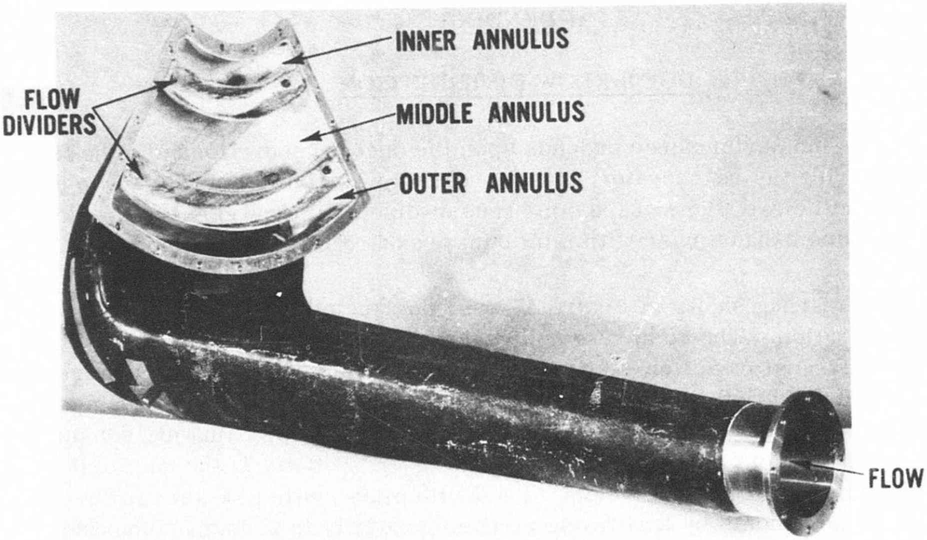

Figure 58. Model of Compressor Discharge Duct

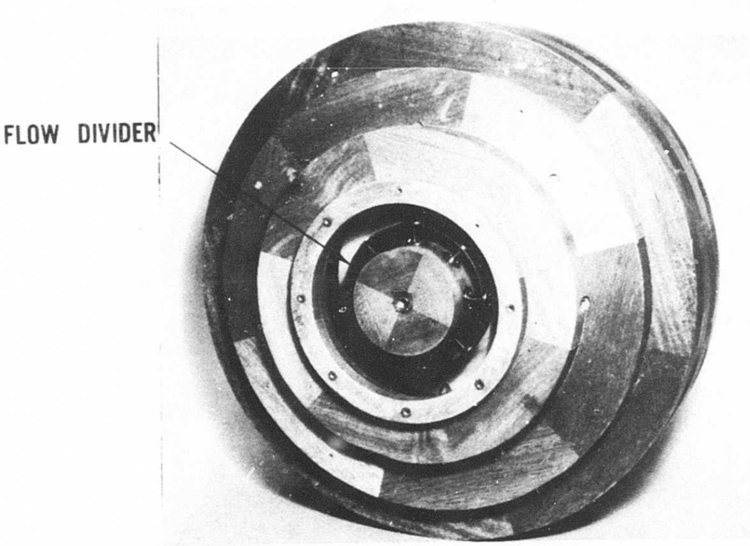

Figure 59. Turbine Exhaust Case Inlet

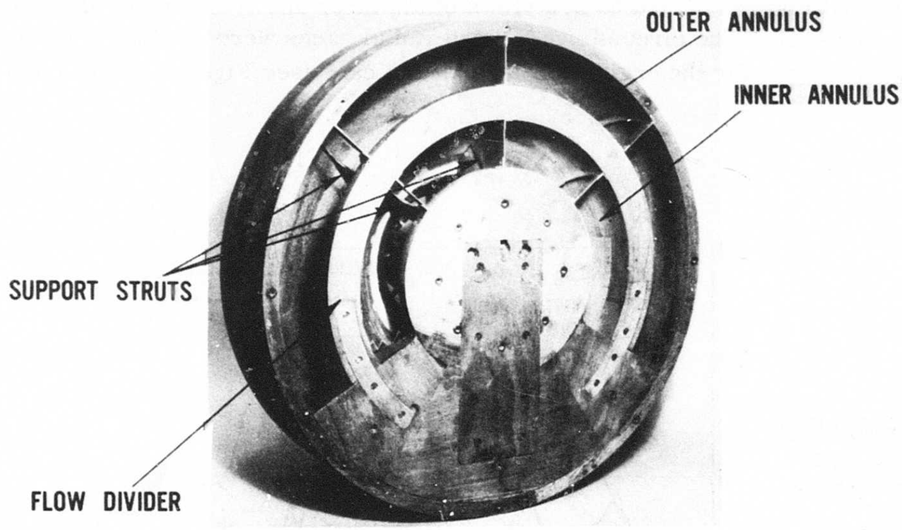

Figure 60. Turbine Exhaust Case Exit

The criterion for acceptable flow distribution from the ducts required both a uniform radial and circumferential flow distribution in each annulus and the required flow split between the annuli. These requirements were obtained with the minimum duct pressure loss.

TURBINE EXHAUST CASE

The initial flow distribution measured in this duct is represented by the light-shaded area in Figure 61 for the outer annulus and in Figure 60 for the inner annulus. This test revealed that higher flows occurred radially toward the inner walls of the annuli formed by the flow divider, and circumferentially in two regions from 30° to 90° and from 150° to 220°. The average mass velocities in both annuli were approximately equal, however. The pressure loss ratio was 4.5 percent, higher than the desired goal of 4.0 percent.

Analytical studies indicated the need for circumferential turning vanes approximately 4 inches from the inlet in each annuli to prevent flow separation in this area. After several tests, the optimum flow distribution was obtained by the use of two circumferential vanes and six radial vanes in each annulus. The final flow distribution is shown in Figures 61 and 62 in dark shade. The pressure loss ratio for this configuration was 1.86 percent, which is well below the design goal. Figures 63 and 64 show the inlet and exit view of the test duct assembly, and Figures 65 and 66 are views of the inner and outer annuli showing the vane contour. The circumferential and radial vanes were used as templates to form the vanes for the engine turbine exhaust case (see Figures 138 through 141 in Appendix VI).

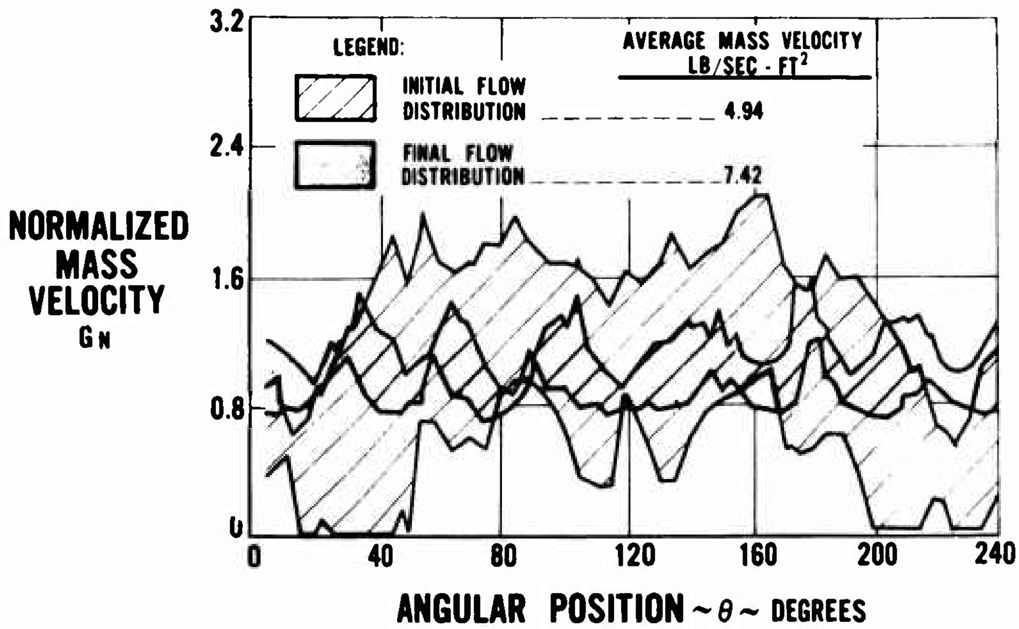

Figure 61. Flow Distribution in the Outer Annulus of the Turbine Exhaust Case.

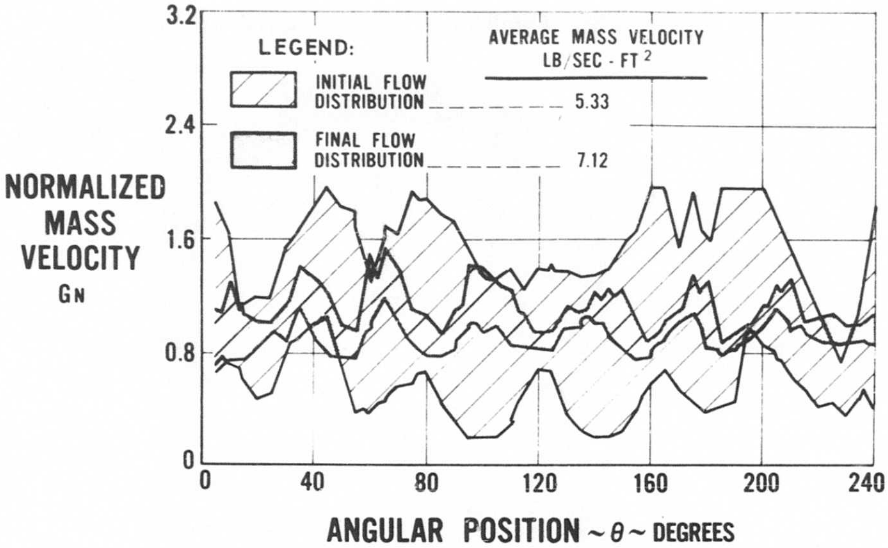

Figure 62. Flow Distribution in the Inner Annulus of the Turbine Exhaust Case.

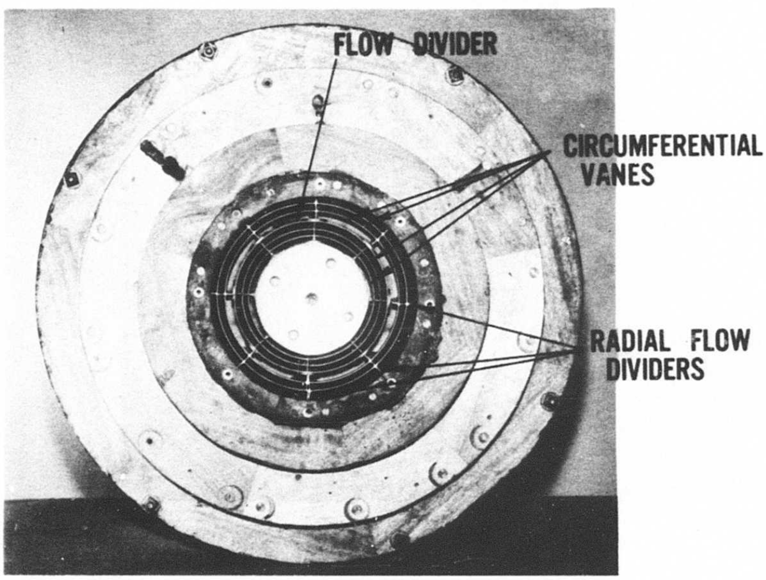

Figure 63. Turbine-to-Regenerator Test Duct Assembly Inlet

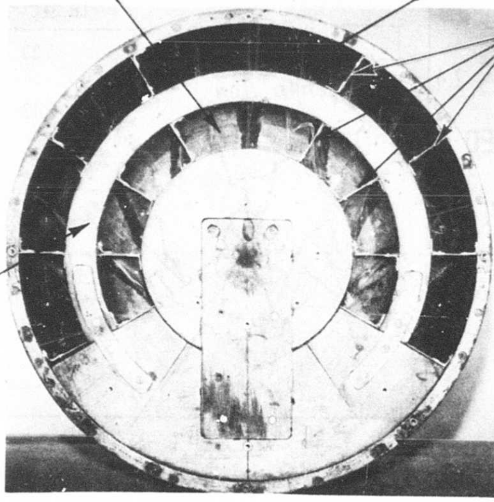

Figure 64. Turbine-to-Regenerator Test Duct Assembly Exit

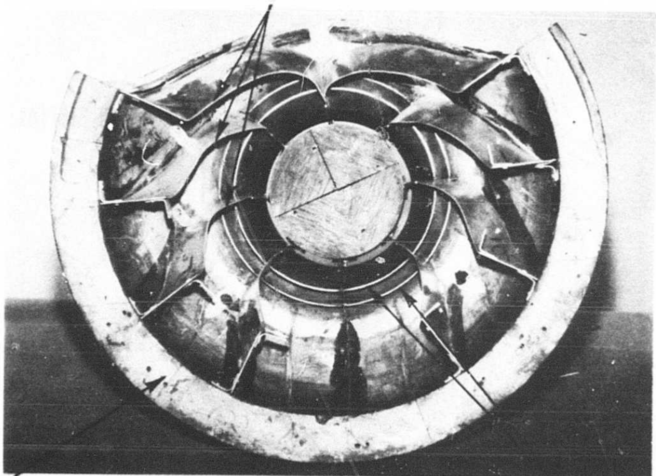

Figure 65. Turbine-to-Regenerator Test Duct Inner Annulus

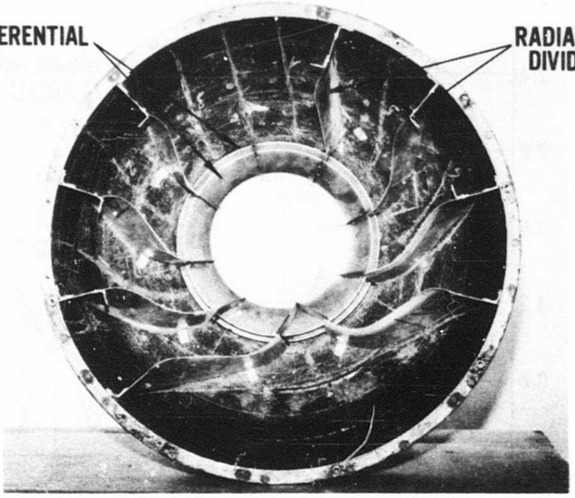

Figure 66. Turbine-to-Regenerator Test Duct Outer Annulus

COMPRESSOR-DISCHARGE-TO-REGENERATOR DUCT

The initial flow distribution measured in this duct is represented by the light-shaded area in Figures 67 through 69. The mass flow in the outer radius, where the flow path has the greatest turn, was only 27 percent of the required flow. Results of this test indicated that the annulus flow split would be the primary problem in this duct. The addition of another turning vane (see Figure 70) increased flow in the outer annulus slightly to 33 percent of required and increased the pressure loss from 1.9 percent to 3.3 percent; the design goal was 2.0 percent.

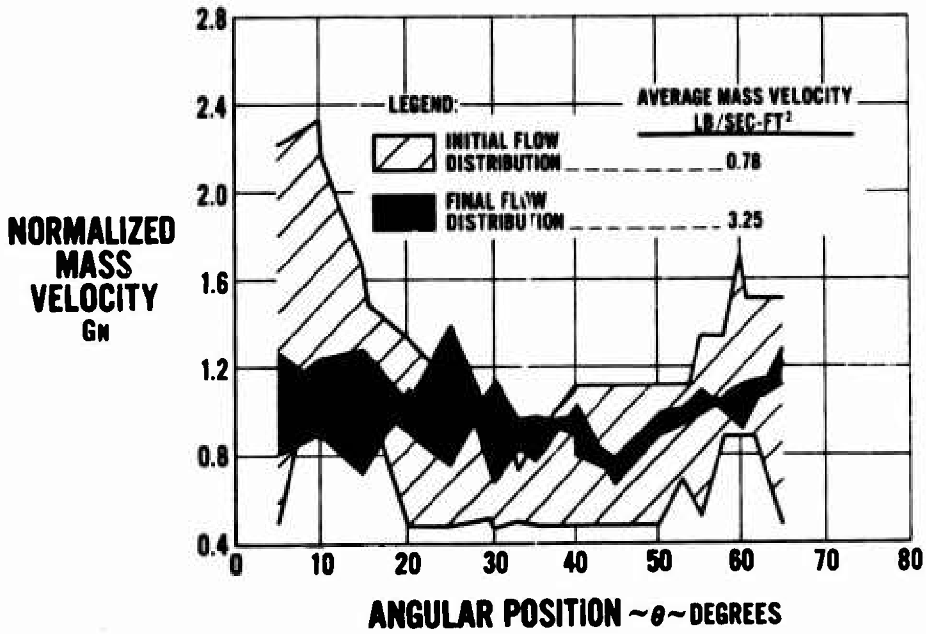

Figure 67. Flow Distribution in Outer Annulus of Compressor Discharge Duct.

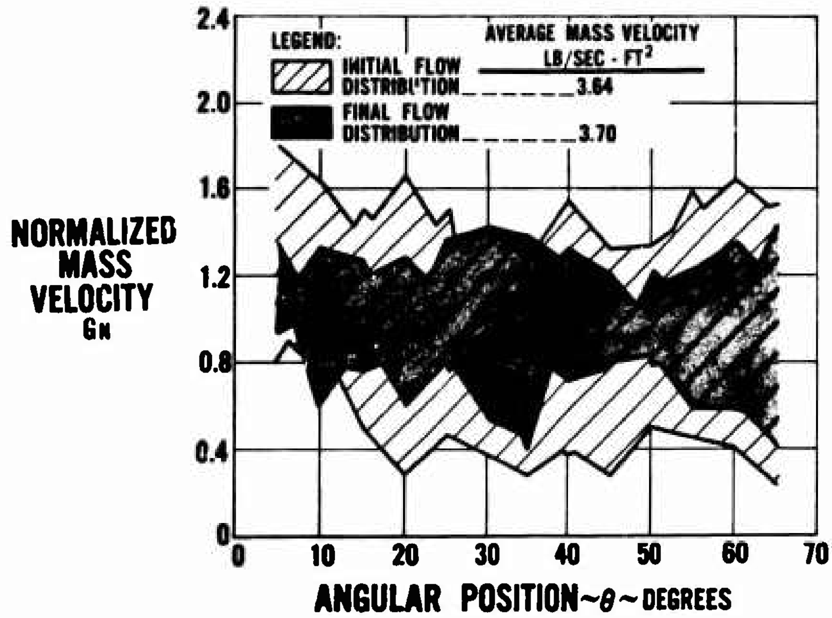

Figure 68. Flow Distribution in Middle Annulus of Compressor Discharge Duct.

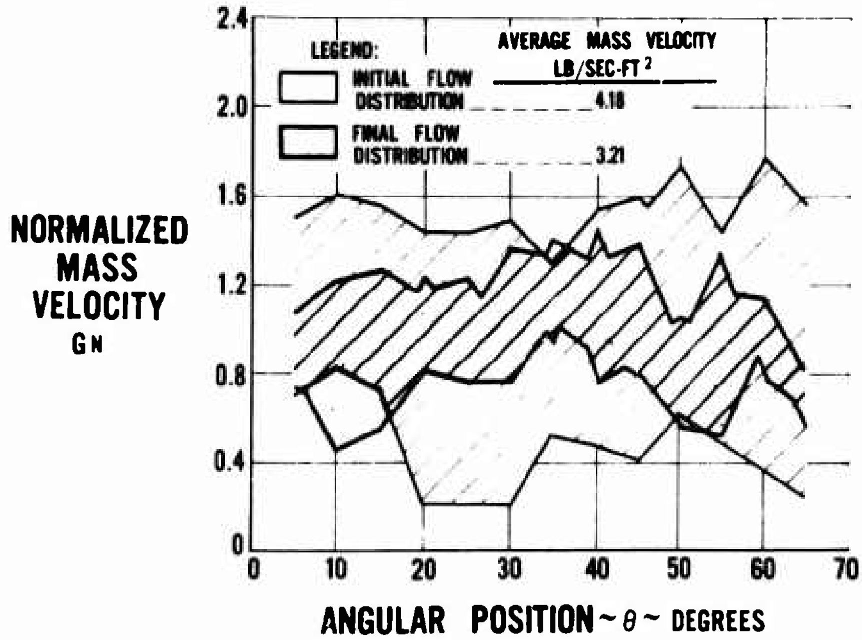

Figure 69. Flow Distribution in Inner Annulus of Compressor Discharge Duct.

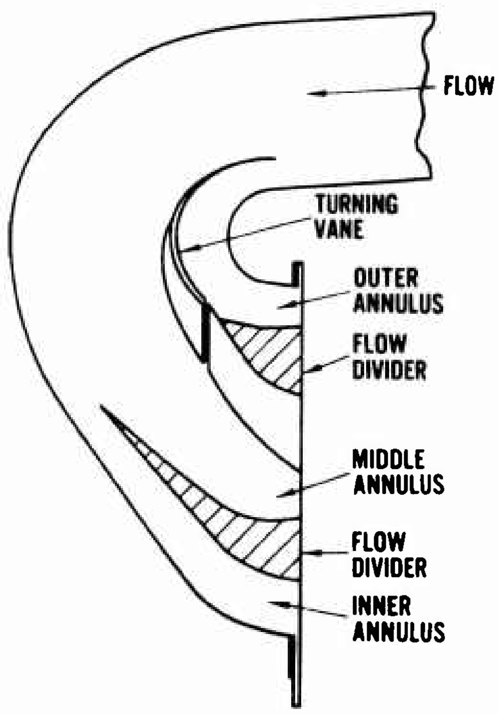

Figure 70. First Modification of the Internal Geometry of the Compressor Discharge Duct.

Using Frey's parameters*, a turning vane assembly with adjustable vane clearance was installed. This increased the outer annulus flow to 68 percent of the required flow. A measurement of the velocity profile at the vane assembly inlet indicated a warped profile which allowed the vane assembly to control only 40 percent of the flow (see Figure 71). To provide a uniform flow profile entering the vane assembly, one layer of 10-mesh, 0.035-inch-wire-diameter screen was installed in the upper half of the duct (Figure 72). After a series of tests varying the vane clearance, the required flow split in each annulus was obtained as follows:

Annulus	Required Flow(%)	Actual Flow (%)
Outer	29.5	28.0
Middle	57.1	58.4
Inner	13.4	13.6

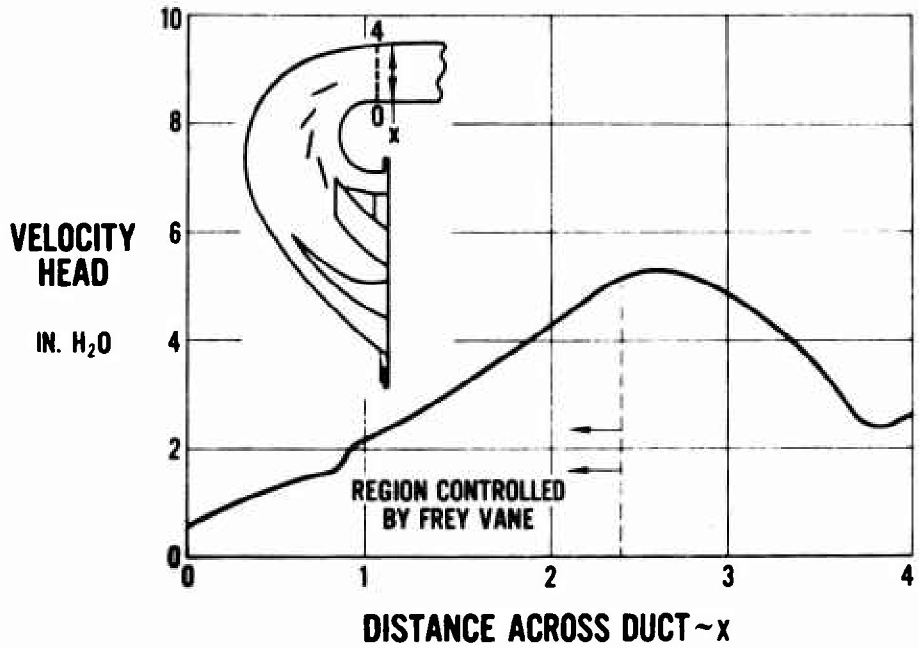

Figure 71. Velocity Profile in Compressor Discharge Duct at Inlet to Frey Vane Assembly.

*Kurt Frey, "Reduction of Flow Losses in Channels by Guide Vanes", Forshung, Volume 5, May-June 1934, pp. 105-117.

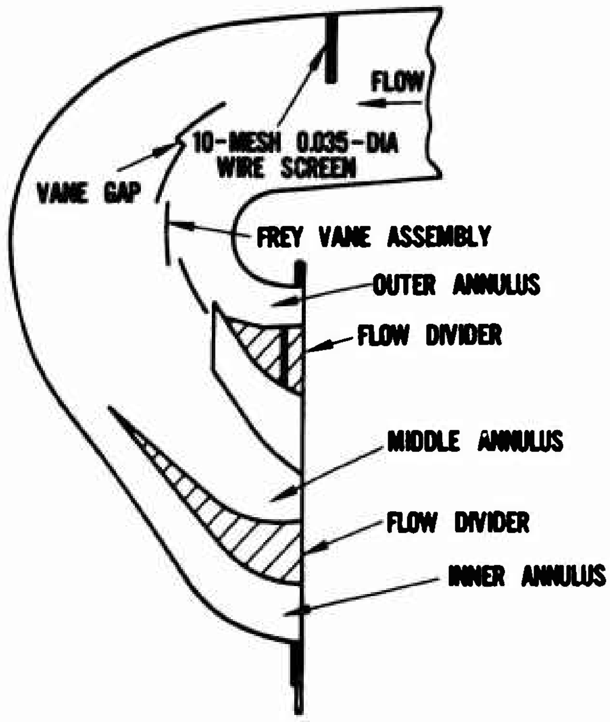

Figure 72. Final Modification of the Internal Geometry of the Compressor Discharge Duct.

The flow distribution shown in dark-shaded areas of Figures 67 through 69 indicates the improvement obtained with the redesigned duct. The duct pressure loss was 2.59 percent, which was above the 2.0-percent goal. The duct was tested at 50 percent of the design-point mass flow with no appreciable change in flow distribution. The turning vane assembly and screen were installed and tested in the actual engine duct with the same results as the flow model within experimental error. The total pressure loss ratio for both ducts was 4.45 percent as compared to the 6.0-percent goal.

TABLE IX
SUMMARY OF FLOW DISTRIBUTION TESTS
IN THE TURBINE EXIT-TO-REGENERATOR DUCT

Run No.	Configuration Description	Mass Velocity #/sec-ft^2	Range of Normalized Mass Velocity G/Gavg. Radial Max.	Radial Min.	Circumferential Max.	Circumferential Min.	Duct Pressure Drop Ratio $\Delta P/P$, %
1	Preliminary design with no back-pressure screen	5.34(a)	2.00+	0.66	2.00+	0.20	4.50
		4.94(b)	1.85	0.00	2.10	0.00	
2	Preliminary design with a back-pressure screen	5.10(a)	2.10	0.00	2.13	0.00	4.22
		6.34(b)	1.30	0.00	1.69	0.00	
3	Preliminary design with circular dowels in lieu of contoured struts	5.05(a)	1.45	0.00	1.98	0.00	3.75
		N.R.(b)	NR.	N.R.	N.R.	N.R.	
4	Replace strut at 120° and inserted axial dividers at 30° and 210° inlet and 60° and 180° discharge of both annuli. No back-pressure screen.	6.14(a)	2.28	0.62	2.34	0.20	N.R.
		5.50(b)	1.40	0.18	2.08	0.18	
5	Same as Run No. 4 with back pressure screen	7.07(a)	1.36	0.20	1.98	0.20	3.77
		5.12(b)	1.15	0.12	2.30	0.11	
6	Radial dividers in lieu of axial every 45° at the inlet and 30° at the discharge; two circumferential vanes in each annuli	7.42(a)	1.20	0.78	1.55	0.75	1.86
		7.12(b)	1.28	0.78	1.57	0.72	
7	Same as Run No. 6 with divider at 120° removed	5.75(a)	1.50	0.85	1.90	0.40	2.22
		9.98(b)	1.20	0.85	1.44	0.80	
8	Only circumferential vanes no radial dividers or support	5.22(a)	1.05	0.00	1.80	0.00	1.43
		5.56(b)	1.65	0.55	1.85	0.00	
9	Dividers every 15° from 30° to 210° at the inlet and every 15° at the discharge; two circumferential vanes	4.95(a)	2.03	0.33	2.25	0.14	3.37
		7.12(b)	1.50	0.51	1.95	0.41	

(a) Inner Annulus
(b) Outer Annulus
N.R. Means not recorded

TABLE X

SUMMARY OF FLOW DISTRIBUTION TESTS IN THE COMPRESSOR EXIT-TO-REGENERATOR DUCT

Run No.	Configuration Description	Total Duct Flow #/sec.	Percent of Total Duct Flow in Each Annulus, % Inner	Middle	Outer	Duct Pressure Drop Ratio $\Delta P/P$, %
			13.4*	57.1*	29.5*	
1	Preliminary Design	1.11	19.9	71.1	8.17	1.94
2	Preliminary design with divider added between middle and outer annulus	1.23	22.6	67.6	9.77	3.29
3	Frey vane assembly in lieu of two vanes from preliminary design	1.71	12.4	69.4	18.2	2.37
4	Frey vane assembly (5 vanes) with ΔX = 0.35" between all vanes	1.33	16.3	69.5	15.0	2.75
5	Same as Run No. 4 with ΔX = 0.20"	1.35	15.9	66.5	17.7	2.70
6	Same as Run No. 4 with ΔX = 0.10"	1.31	16.0	64.4	20.0	2.59
7	Frey vane assembly (4 vanes) with ΔX = 0.10"	1.31	19.1	62.8	17.9	2.51
8	Two (2) 10 x 10 x .035" screens covering upper 50% of flow area and located 1.0" from 180° flow turn. Frey vane assembly (5 vanes) with ΔX = 0.10"	1.57	6.74	60.0	33	2.25
9	Same as Run No. 8 with ΔX = 0.35	1.45	6.73	67.6	25.3	2.56
10	Same as Run No. 8 with ΔX = 0.50" for the 1st three (3) vanes and ΔX = 0.10" for the last two (2).	1.47	7.14	70.0	23.0	2.66
11	Same as Run No. 8 with a four (4) vane assembly	1.32	7.8	69.0	23.3	2.70
12	Same as Run No. 11 with ΔX = 0.5" for the 1st two (2) vanes and ΔX = 0.35" for the last two (2)	1.52	7.75	68.8	23.6	2.60

TABLE X (Cont'd)

SUMMARY OF FLOW DISTRIBUTION TESTS
IN THE COMPRESSOR EXIT-TO-REGENERATOR DUCT

Run No.	Configuration Description	Total Duct Flow #/sec.	Percent of Total Duct Flow in Each Annulus, % Inner	Middle	Outer	Duct Pressure Drop Ratio ΔP/P, %
13	One (1) 10 x 10 x .035" screen (located same as Run No. 8); Four (4) vane assembly with ΔX = 0.5" for the 1st two (2) vanes and ΔX = 0.35" for last two (2).	1.39	12.5	76.3	11.3	2.70
14	Same as Run No. 13 with ΔX = 0.25" for all vanes	1.35	12	71.5	16.4	2.50
15	Same as Run No. 13 with ΔX = 0.10" for all vanes	1.56	13.6	58.5	28.0	2.59
16	Same as Run No. 15 with 50% design test flow.	0.784	13.5	61.4	25.2	0.676

ΔX Clearance between individual vanes

*These are the area ratios for each annulus to the total duct exhaust area, e.g. $A_1 = A_1/(A_1 + A_2 + A_3)$. The mass flow ratios should equal these for each annulus to have the same mass velocity.

APPENDIX II

ENGINE-REGENERATOR ARRANGEMENTS

The purpose of this study is to determine whether other T74 regenerator-engine arrangements are potentially lighter, more compact, or offer other advantages over the test-bed arrangement. The regenerator and T74 test bed combination designed under Contract Item 5 of Phase I is estimated to weigh 400 pounds. This design reflects flightweight regenerator size, configuration, and performance, but the integration with the engine was limited to the most economical test-bed approach. The arrangements studied and reported below involve a more refined integration of regenerator and engine. These studies are all based on the use of the same aerodynamic components as the basic T74 with no allowance made for possible refinements and weight reduction in the basic engine. The designs discussed represent realistic design weight objectives which could be achieved as part of a development plan.

Six engine design studies were completed. Predicted total weight addition for each of these configurations is included in the tabulation below.

Configuration	Description	Total Additional Weight (lb.)
A	Test bed with regenerator weight reduction features (Figure 73)	339
B	Single rotor with integrated gearboxes (Figure 74)	291
C	Regenerator between turbine and compressor (Figure 75)	300
D	Regenerator over burner with separate gearboxes (Figure 76)	314
E	Regenerator over burner with integrated gearboxes (Figure 76)	275
F	Coaxial-shaft free turbine with integrated gearboxes (Figure 77)	287

DESCRIPTIONS OF CONFIGURATIONS STUDIED

Configuration A, Test Bed With Regenerator Weight-Reduction Features

The first design study was aimed at reducing regenerator system weight while retaining the basic arrangement of the test-bed installation. The main areas where weight can be reduced are the regenerator and the high-pressure ducting.

The configuration A (Figure 73) regenerator rotor has the same diameters as the regenerator constructed, but features piston ring inner diameter seals rather than conventional carbon ring and face seals. The feasibility of all-metal inner diameter seals was demonstrated during Phase I of the program, and, with development, this seal can be used in future designs. The advantage of this concept is that the regenerator inner housing can be shortened axially, since the seals require less space in the axial direction.

The two high-pressure ducts are integrated into a single pressure vessel of circular cross section, which is structurally more efficient. In addition, some duct flanges, which are part of the prototype design for test rig accessibility, are eliminated. The combined duct reduces the local protrusion of the currently designed cold duct.

Titanium has been substituted for steel in the compressor scroll case for a savings of 17 pounds.

The predicted weight savings of configuration A over the test-bed configuration are tabulated below:

Regenerator bearing and seal area	-34 lb.
Combined duct	-10
Titanium compressor scroll	-17
Total weight differential	-61 lb.

Configuration B, Single Rotor With Integrated Gearboxes

This design is a direct-coupled turbine configuration with basically the same lightweight regenerator as configuration A and an integrated main reduction accessory drive gearbox. Coupling the turbines is feasible, since both run at approximately the same shaft speed. The integrated duct of configuration A can be incorporated in this design.

This design eliminates the long power turbine shaft extension (critical speed is better) and permits unlimited access to the regenerator. In addition, it permits different-size regenerators for different installations or missions without major structural changes to the basic engine. Maximum engine diameter is approximately the same as that of configuration A, but this configuration is about 5 inches shorter.

The predicted weight savings of configuration B (Figure 74) over the test-bed configuration are tabulated below:

Regenerator bearing and seal area	-34 lb.
Combined duct	-10
Titanium compressor scroll	-17
Integrated gearbox system and shafting	-48
Total weight differential	-109 lb.

Configuration C, Regenerator Between Turbine and Compressor

The configuration C (Figure 75) design is a direct-coupled turbine arrangement with the same lightweight regenerator as that of configurations A and B located between the turbine and compressor. The turbine gas flow is opposite to that in the standard T74, but the blading is aerodynamically similar.

The advantages of this scheme include accessibility of the hot-section parts for rapid inspection and lower duct pressure losses due to the fewer duct turns. The disadvantages of this arrangement are the long shafting and the potentially high bearing thrust loads.

The predicted weight savings of this configuration over the test-bed arrangement are tabulated below:

Regenerator bearing and seal area	-34 lb.
Titanium compressor scroll and burner case	-28
High-pressure ducting	-21
Shorter regenerator drive shaft	-3
Integrated gearboxes	-14
Total weight differential	-100 lb.

Configuration D, Regenerator Over Burner With Separate Gearboxes

Configuration D (Figure 76) is a free-turbine version with the regenerator located outside of the burner case. This engine is the same length as the standard T74, since the free-turbine extension shaft used in the test-bed installation is not required. A unique duct-plenum arrangement, which is efficient structurally, is used for the regenerator flow system, and several duct turns are eliminated. The regenerator has the same lightweight configuration as that used in A, B, and C, but has a larger inner diameter. The bulkhead diameter is correspondingly smaller, resulting in an unchanged matrix frontal area. Due to the shorter axial length, the weight of the regenerator itself is the same as that of the regenerator with the smaller outside diameter. Accessibility of both the engine and regenerator components is excellent.

A weight-savings breakdown of this arrangement is tabulated below:

Regenerator bearing and seal area	-34 lb.
Removal of combined scroll and burner case	-57
Removal of high-pressure inlet duct	-20
Addition of new scroll and high-pressure duct	+18
Turbine exhaust case	+7
Total weight differential	-86 lb.

Configuration E, Regenerator Over Burner With Integrated Gearboxes

Configuration E (Figure 76) is similar to configuration D in regenerator arrangement, but is a direct-coupled turbine version with an integrated main reduction-accessory drive as in configuration B. This is the shortest engine studied; it is nearly a foot shorter than the basic T74 engine. Accessibility of this version is an improvement over that of configuration D, since the main reduction gearbox has been moved out of the way of the regenerator.

The weight savings of this scheme compared to the test bed is tabulated below:

Regenerator bearing and seal area	-34 lb.
Shorter shafting and integrated gearbox	-48
Longer regenerator drive shaft	+9
Removal of combined scroll and burner case	-57
Removal of high-pressure inlet duct	-20
Addition of new compressor scroll and high-pressure duct	+18
Turbine exhaust case	+7
Total weight differential	-125 lb.

Configuration F, Coaxial-Shaft Free Turbine With Integrated Gearboxes

A coaxial-shaft system was studied to determine whether the flexibility of the free turbine could be retained with the advantage of the integrated gearbox (see Figure 77). The lightweight regenerator configuration, together with the duct-plenum system of configurations D and E, can be used with this arrangement.

A weight-savings summary of this system compared to the test-bed arrangement is tabulated below:

Regenerator bearing and seal area	-34 lb.
Compressor disk and shaft modifications	+12
Integrated gearbox and shafting	-48
Longer regenerator drive shaft	+9
Configuration D ducting	-52
Total weight differential	-113 lb.

CONCLUSIONS

These design studies have shown that:

1. An 85-percent-effectiveness regenerator system can be integrated with the T74 engine with a total additional weight of 275 pounds. Configuration E is the shortest and lightest configuration studied using the standard T74 aerodynamic components.

2. Even greater weight savings could be obtained with the development of a more advanced seal system, which is feasible.

3. Each of the several configurations are attractive for possible use in different regenerative engine applications.

4. The toroidal rotary regenerator system itself is flexible, since it can be mounted in several engine locations, the choice depending on installation requirements.

5. The coaxial-shaft free turbine concept, which is desirable for its flexibility, is feasible, but it would require more development effort than the direct-coupled turbine arrangement and would still not obtain the weight savings of the direct-coupled turbine.

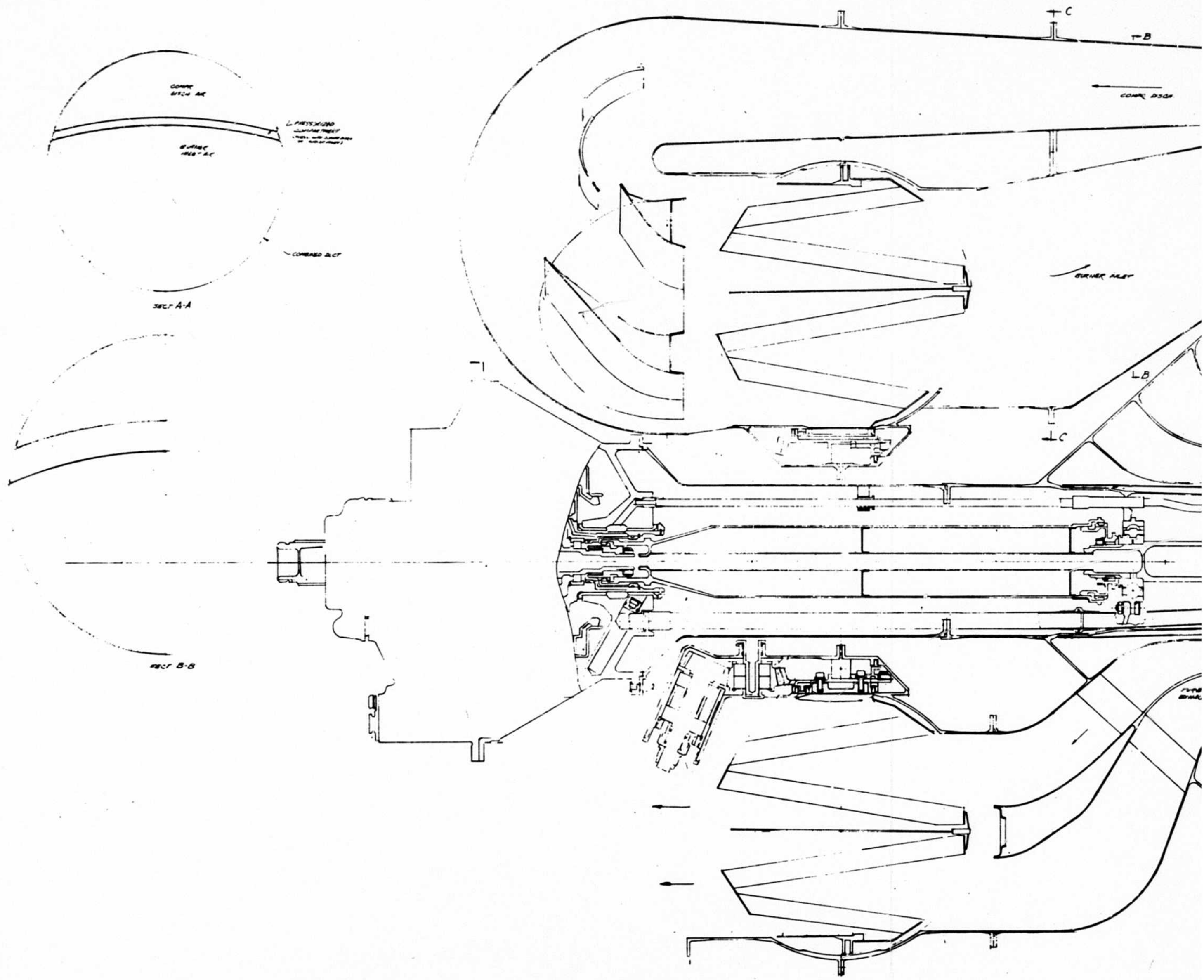

igure 73. Test Bed With Regenerator Weight Reduction Features

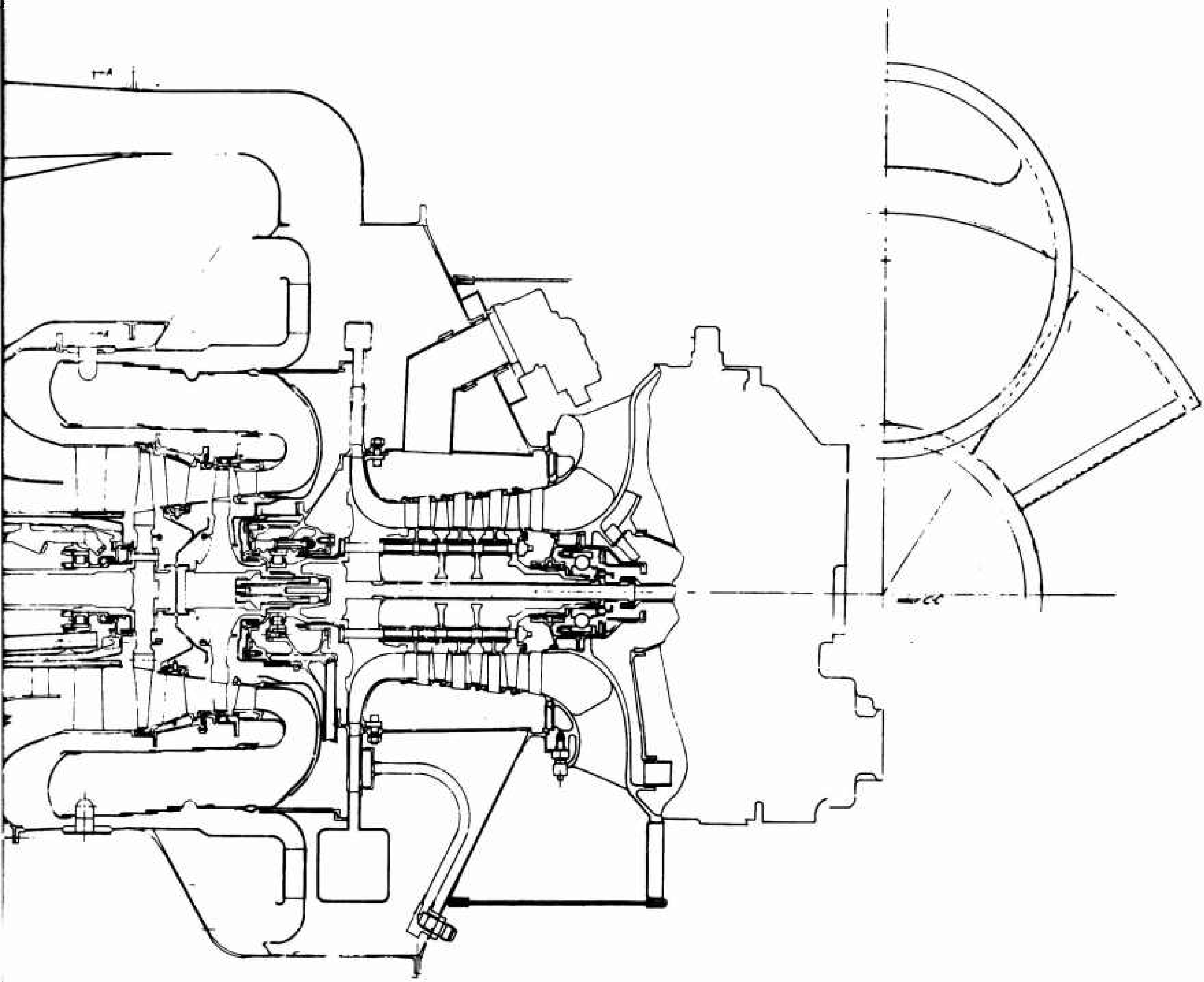

2

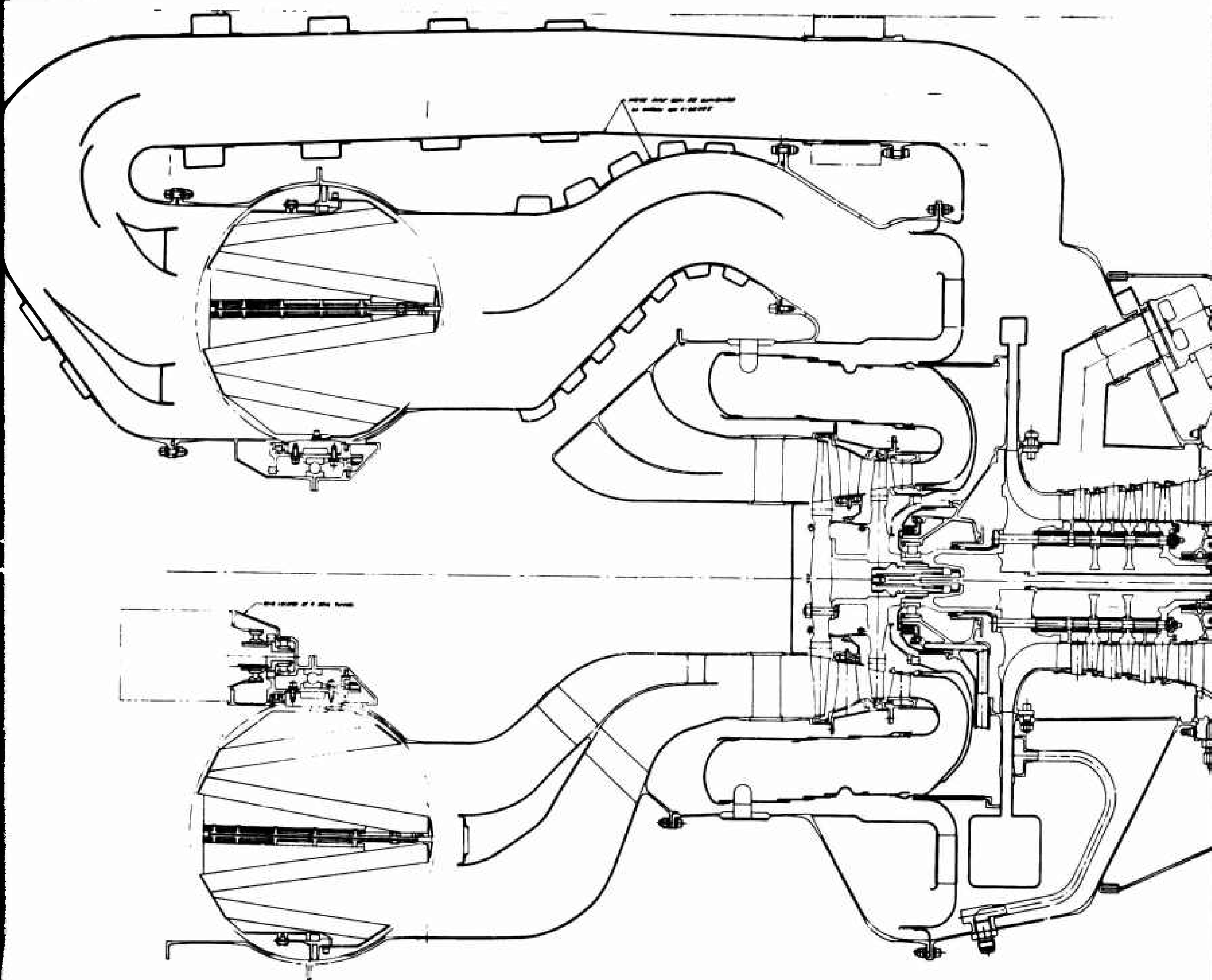

Figure 74. Single Rotor With Integrated Gearboxes.

2

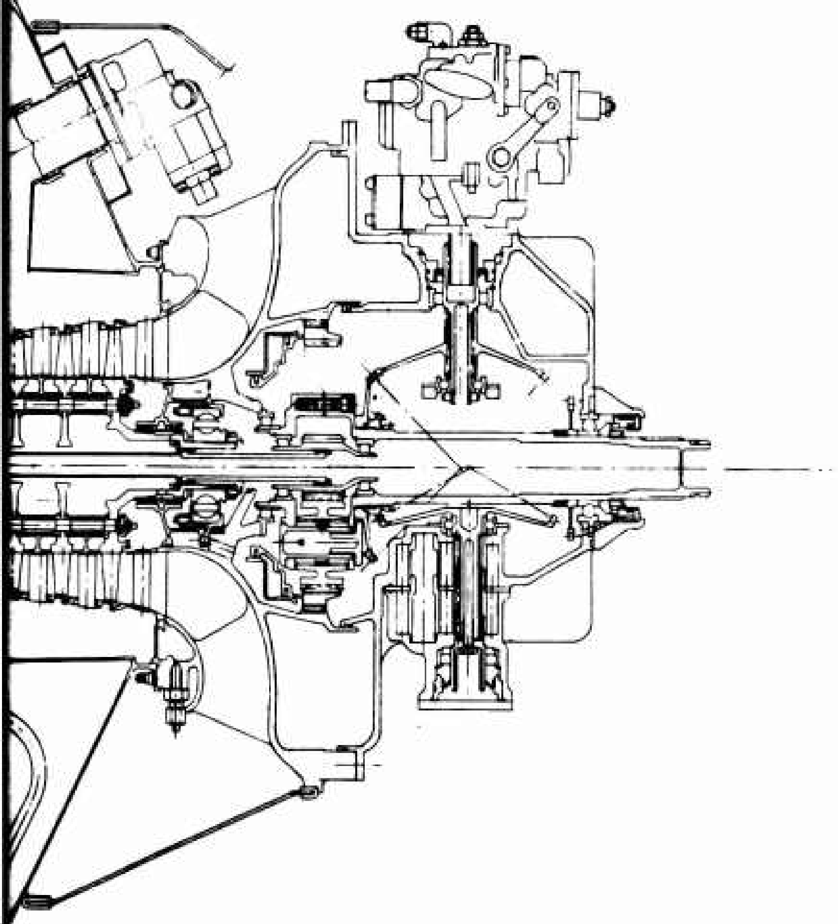

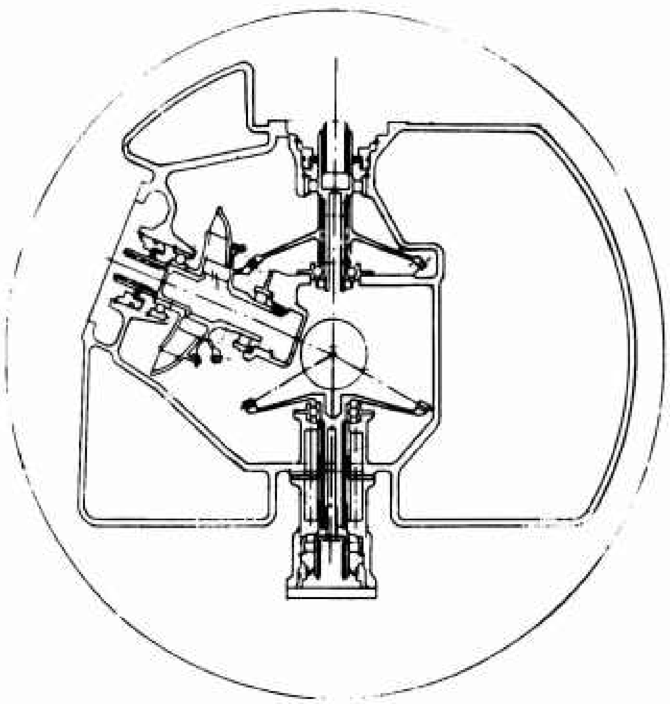

1

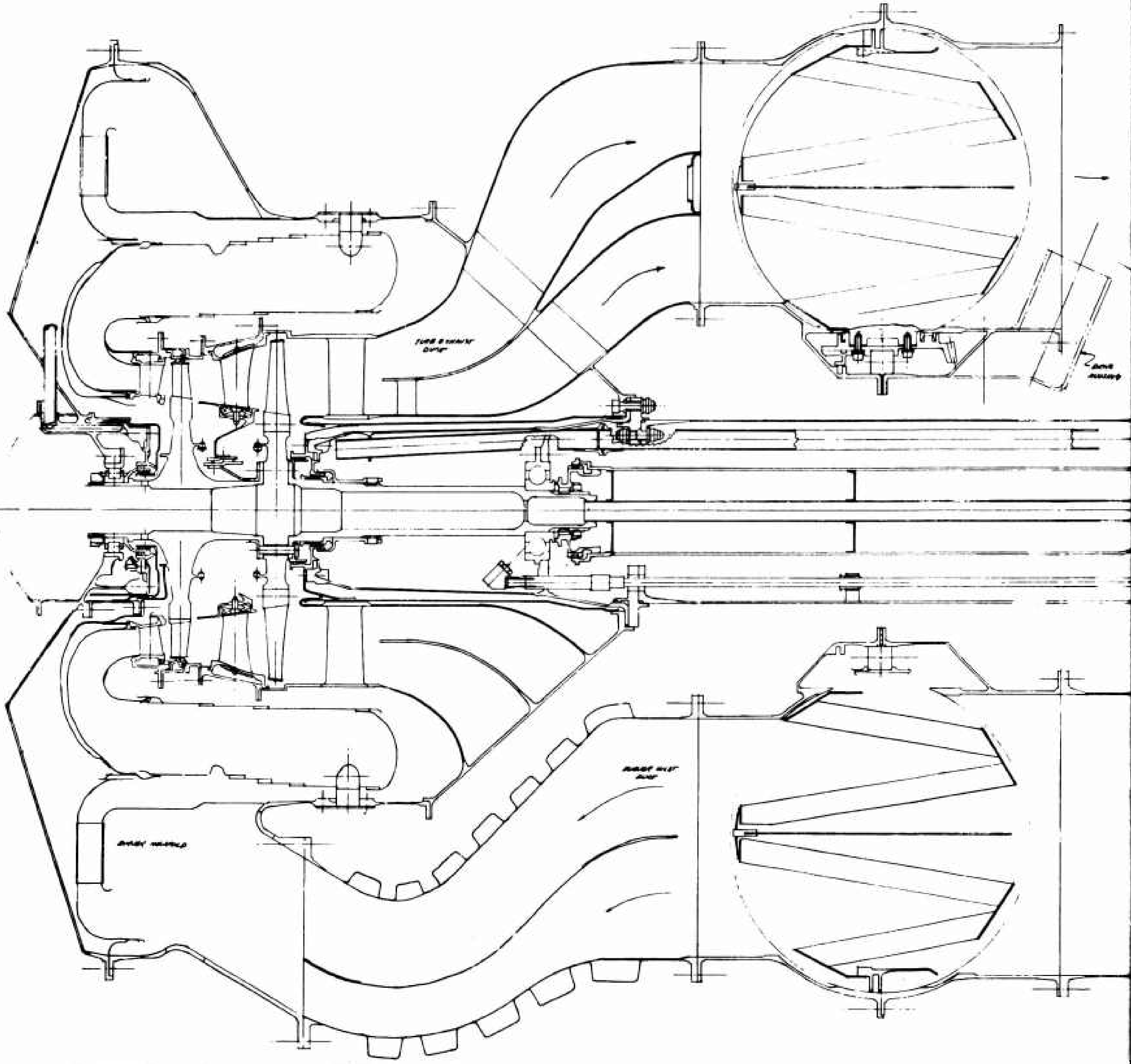

Figure 75. Regenerator With Integrated Gearboxes.

2

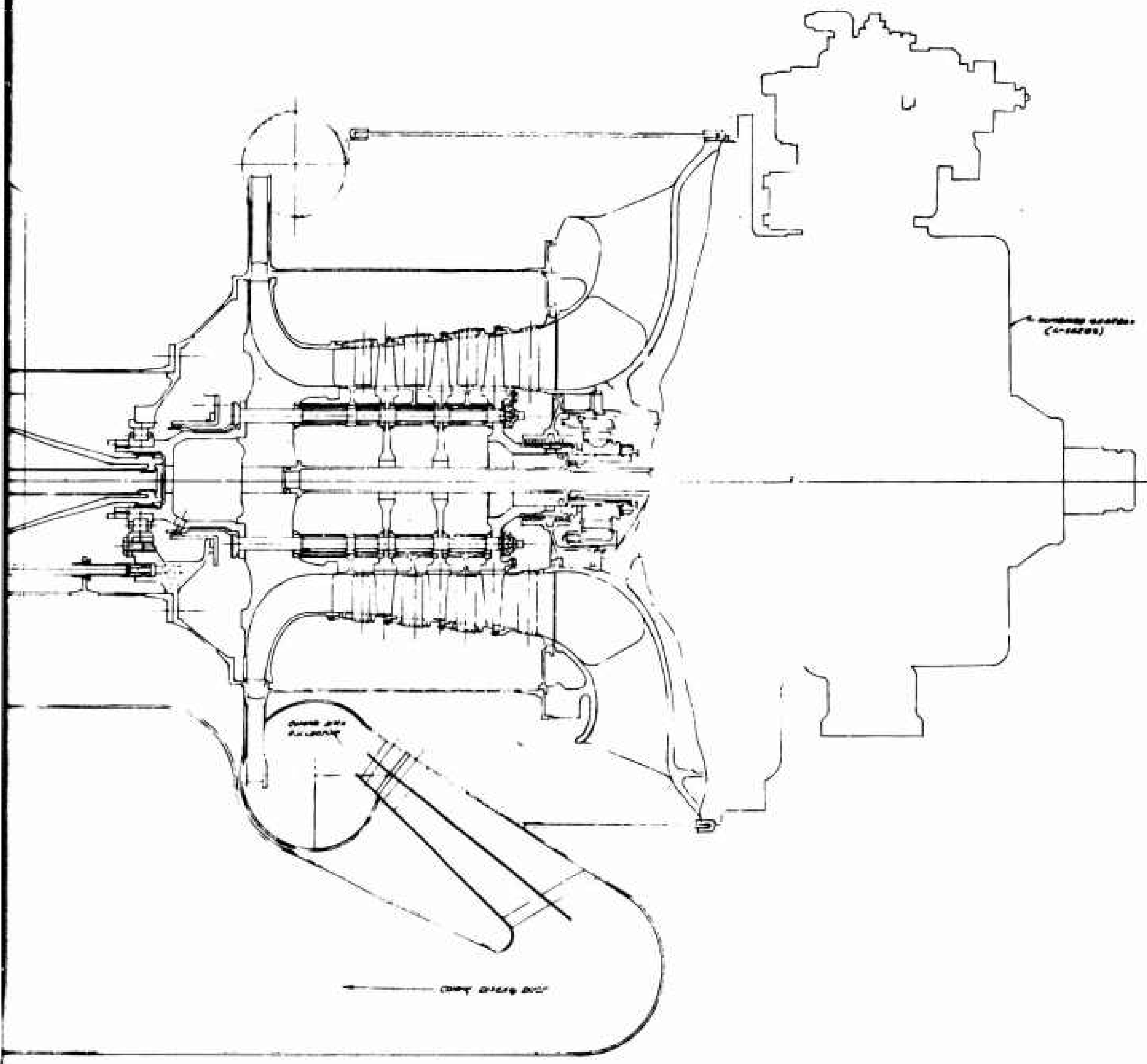

1

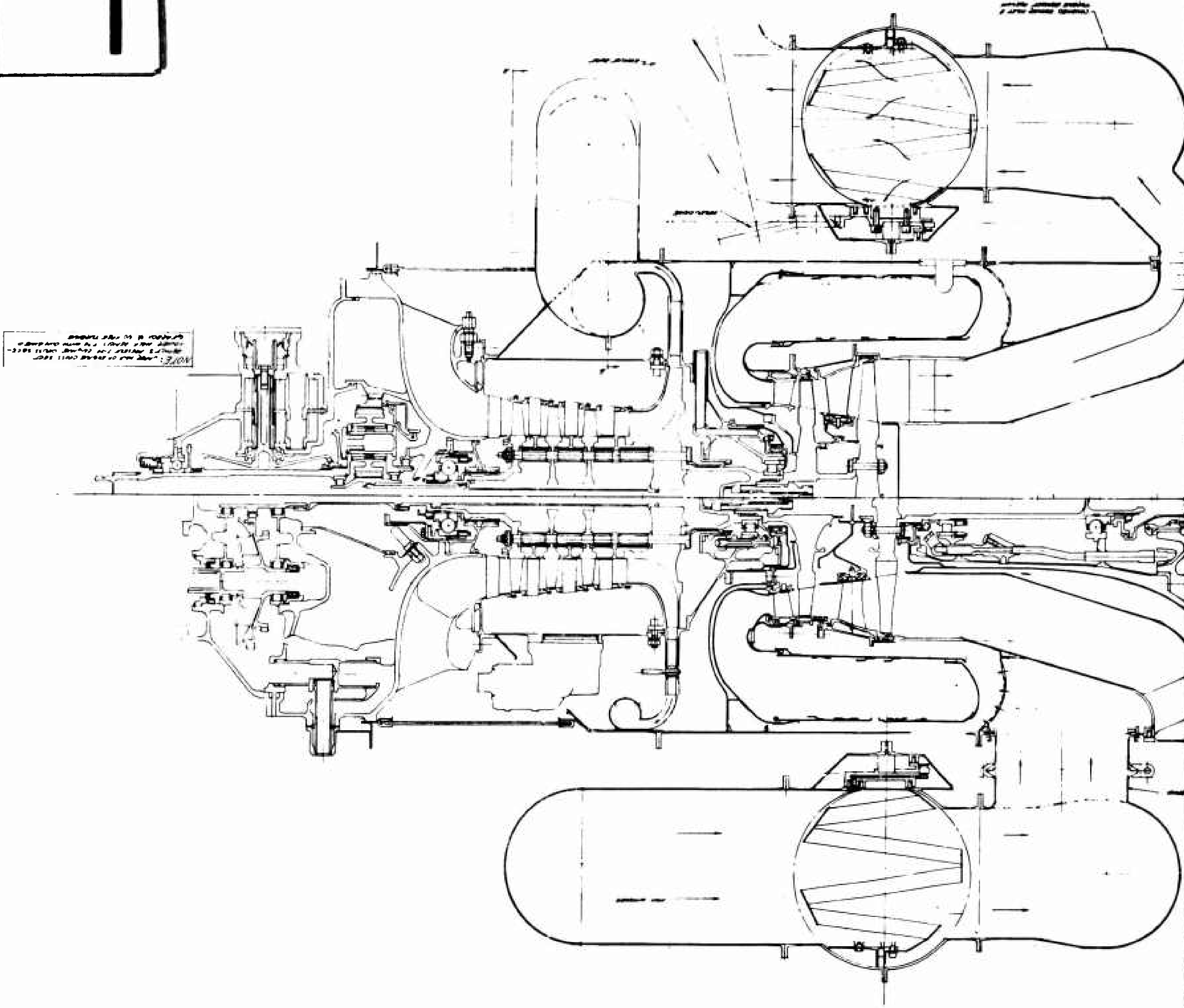

Figure 76. Regenerator Over Burner With Separate and Integrated Gearboxes

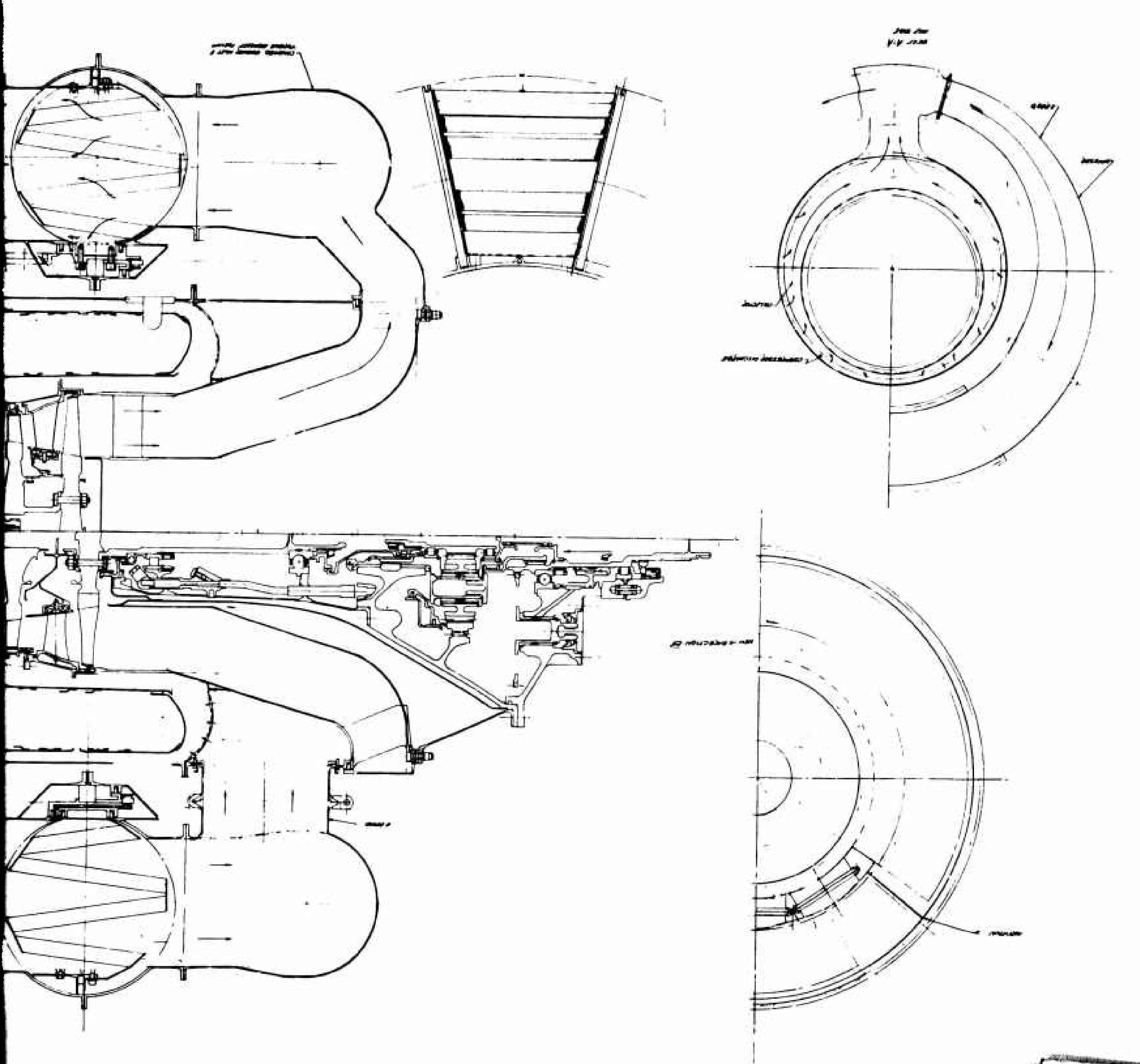

2

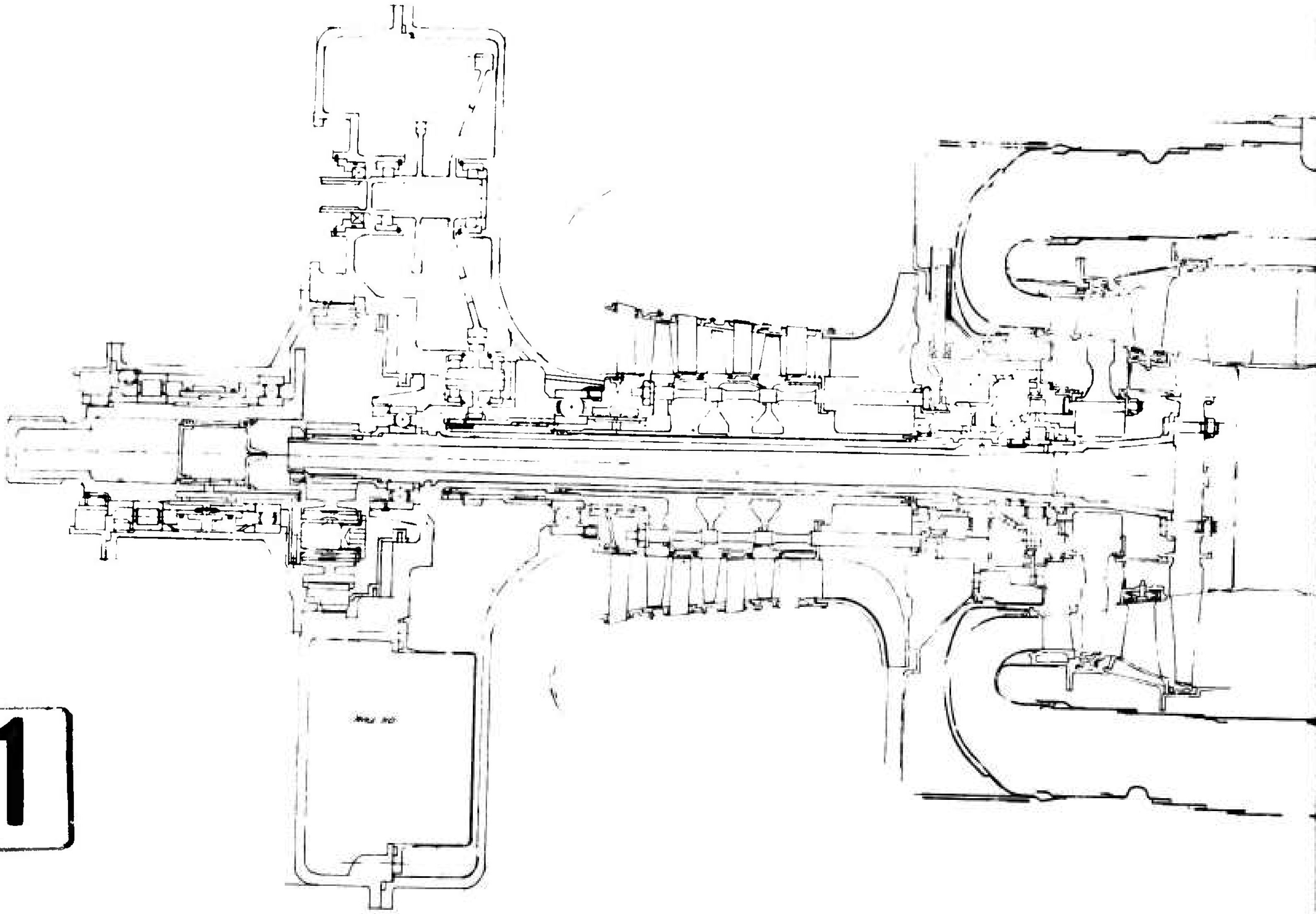

1

Figure 77. Coaxial-Shaft Free Turbine With Integrated Gearboxes

L

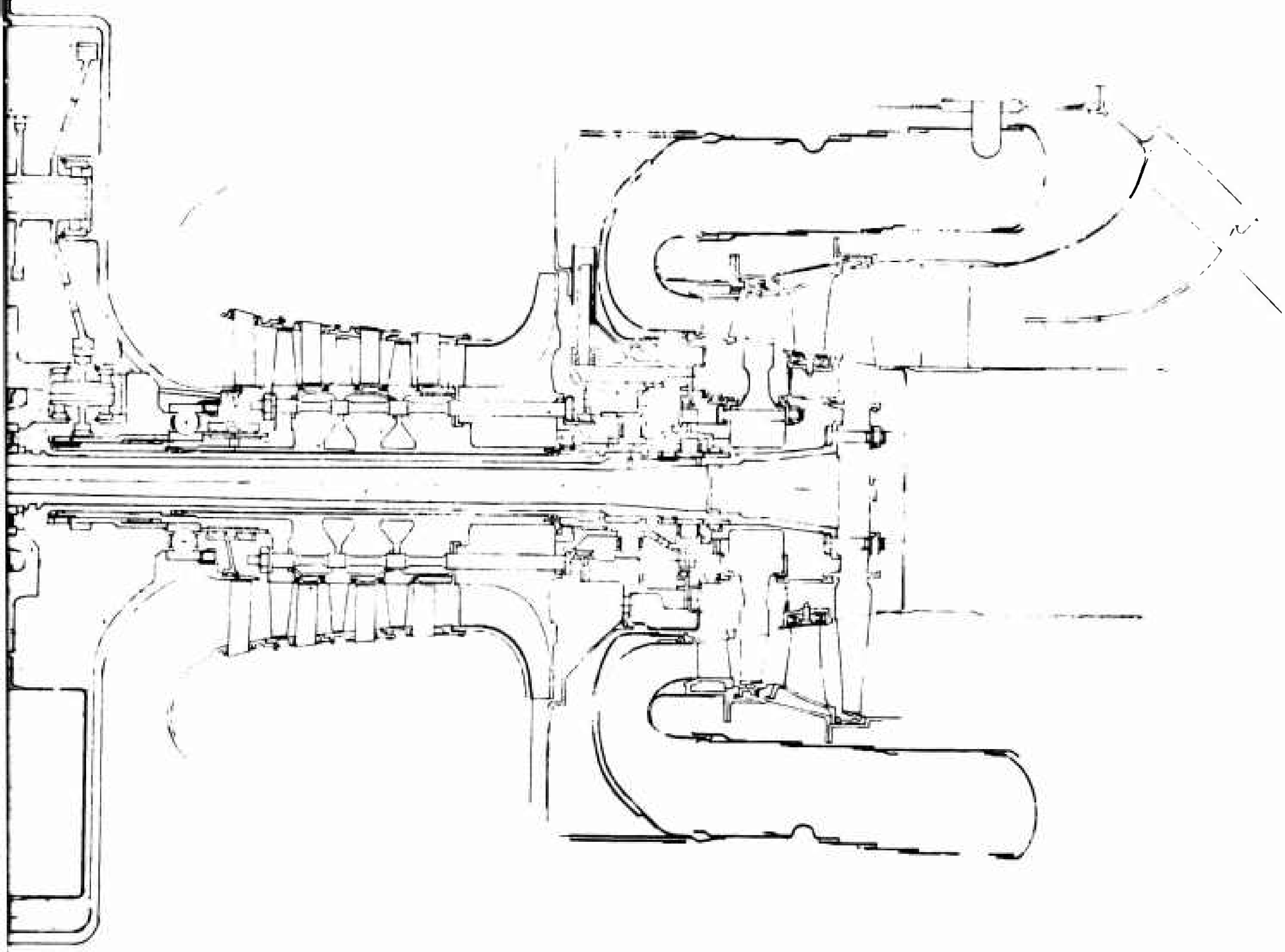

2

Vith Integrated Gearboxes

APPENDIX III

LIGHTWEIGHT REGENERATOR FLAME TUBE DEVELOPMENT

The object of this study was to design and develop a flame tube which would operate satisfactorily on a regenerative engine, with or without the regenerator. This study was conducted prior to fabrication of the flame tube used in the full scale regenerative engine testing.

The design-point conditions were specified as follows.

Burner inlet (regenerator discharge) temperature, $T_{3.5}$	1141°F.
Turbine inlet temperature	1900°F.
Temperature distribution factor, $\frac{T_{max} - T_{mean}}{T_{mean} - T_{3.5}}$	0.15 max.
Combustion efficiency	98% min.
Flame tube pressure loss	2% max.
Flame tube lean limit, W_f/W_a	0.004 max.

In addition, the flame tube should prove durable at the design-point conditions and should be carbon free.

All these conditions were met with the exception of the flame tube pressure loss, which was 2.5 percent. Efforts to reduce this appeared to require a redesign, which was likely to impair other, already acceptable aspects of combustion performance. It was therefore decided to accept a pressure loss of 2.5 percent.

Initial development was carried out on various water models in the water tunnel facility. The results of this development were incorporated into flame tube hardware.

Because of the high combustor inlet temperatures, the primary consideration in the flame tube design was skin cooling. Accordingly, a ram-air cooling system was incorporated in the flame tube walls, instead of the film cooling system employed on the PT6. It soon became apparent that the ram air would have to be closely controlled if it were not to seriously impair combustion performance.

Another important consideration was fuel nozzle and manifold cooling, manifested by fuel vaporization under high temperature inlet conditions.

Distortion of the rig inlet scroll components hampered flame tube performance evaluation by causing poor inlet air distribution. Various modifications to the rig scroll were carried out to eliminate this problem.

INITIAL WATER MODEL TESTING

Water model tests were carried out initially to establish a satisfactory gas path inside the flame tube. The first problem encountered was to establish a vigorous primary zone vortex. Because of the high velocities induced by the ram strips in the flame tube wall, the main flow would not detach itself from the walls, resulting in a stagnant zone in the center of the annulus over the whole length of the flame tube (Figure 78). To correct this situation, two of the ram strips in the primary zone were eliminated, slowing down the peripheral velocities. Due to this effect in conjunction with the presence of holes suitably placed in the inner wall of the primary zone, the flow detached from the inner wall and tended to form a vortex. Although the tendency was there, the recirculation was very weak, the detached flow traveling obliquely across the flame tube and the main body of it impinging on the ram air from the middle strip on the outer wall. This ram air was carried downstream, providing little cooling effect (Figure 79).

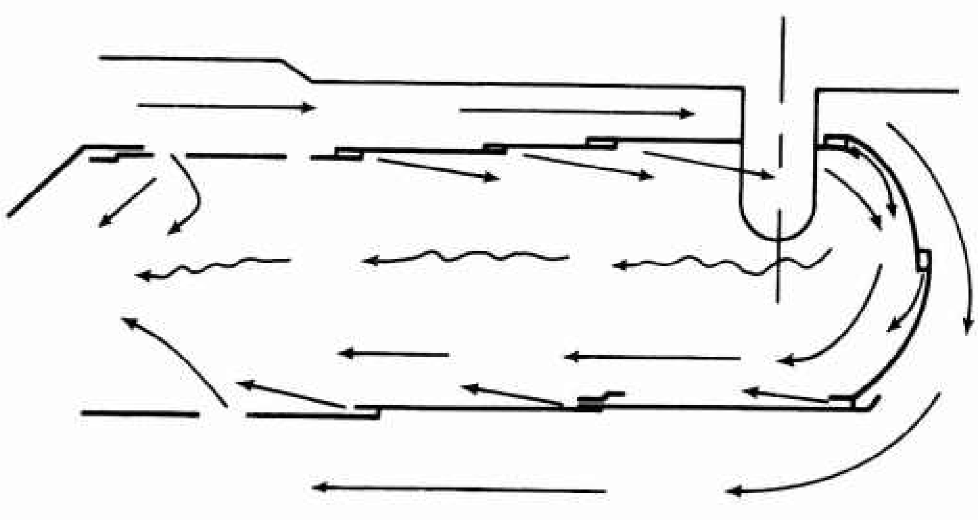

Figure 78. Effect of Peripheral Velocity in Flame Tube Water Model Tests.

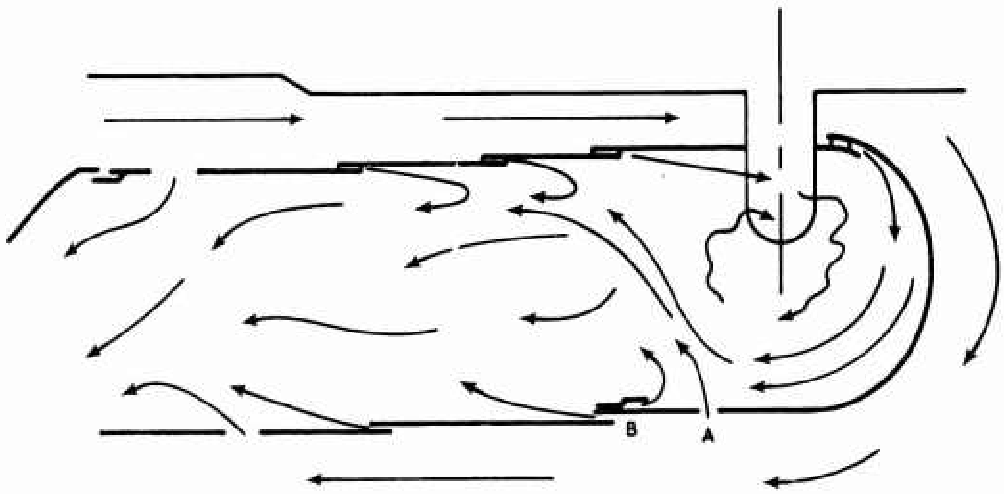

Figure 79. Reduced Velocities With Triggering Holes A and B

It was decided at this stage to use two ram strips instead of three on the outer wall to reduce further the velocities in the primary zone (Figure 80). This was effective in improving the primary zone vortex, and the outer wall cooling appeared to be satisfactory.

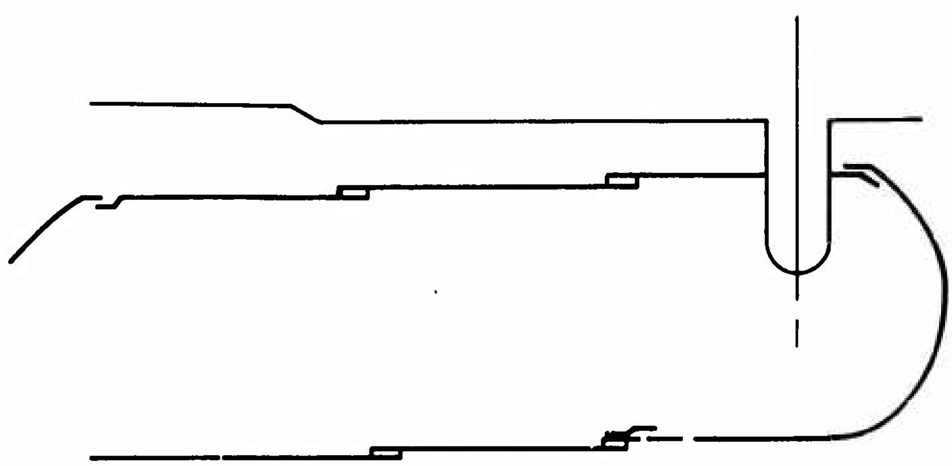

Figure 80. Reduced Ram Cooling

Attention was now turned to the mixing zone of the flame tube, since insufficient mixing appeared to be taking place and since it was judged that the radial profile at the turbine inlet would probably be reversed. Various positions of mixing holes were tried, but finally a device designated as an aerodynamic flow reverser was incorporated (Figure 81). This appeared to provide the necessary mixing and flow path to the turbine entry duct. This device permits air or gas flow reversing by means of a vortex created in a depression formed in the wall of an air passage. Holes are inserted in the wall of the depression at will, depending on the angle of discharge desired.

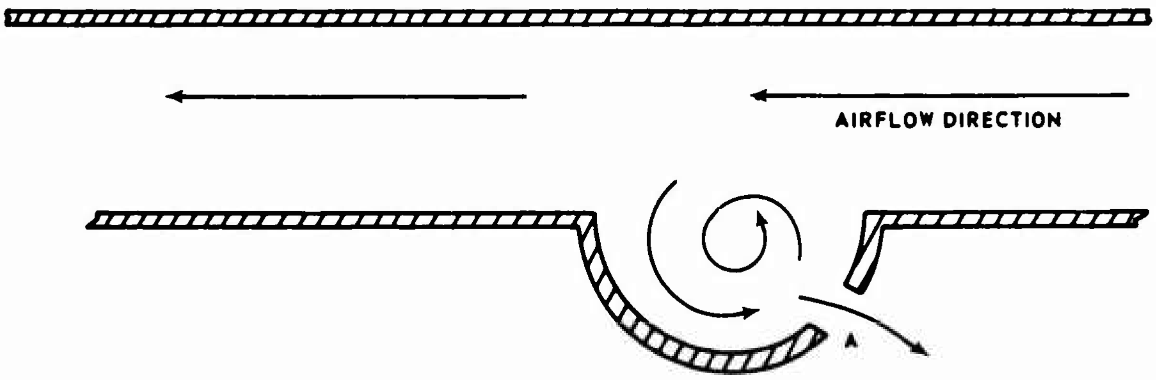

Figure 81. Aerodynamic Flow Reverser, Desired Angle of Discharge Selected by Positioning of Hole A.

COMBUSTION RIG TESTING

A flame tube incorporating most of the water model features but retaining the original cooling configuration was fabricated so that experiments with different combinations could be carried out.

The flame tube was tested on a modified PT6 combustion rig under cold inlet conditions. Apart from three hot spots on the outer wall, the skin temperatures were very low. The temperature distribution factor, however, was high (0.36), and there were some carbon deposits on the outer wall adjacent to the flow reverser ring.

Gap control on the ram-air cooling strips on the outer wall presented problems. Plans were made to modify these in a future configuration. Although large quantities of air were provided by the ram-air cooling strips, it was judged that most of this was flowing peripherally and that the primary zone vortex was feeble,

3

with overrich fuel-air ratio evidenced by flame visible at the turbine entry plane.

Cooling strips in the dome were blanked off to reduce velocities and to effect a tightening of the vortex. In conjunction with this, a cooling strip on the inner wall of the primary zone with a discharge contrary to the vortex direction was moved up closer to the dome. The action of this strip was to detach the vortex flow from the wall and direct it into the middle of the primary zone and thus increase residence time. Moving this strip closer to the dome appeared to have the desired effect, as performance generally improved.

Various combinations of holes and cooling arrangements were tried, but primary zone control was difficult due to the flexing of the ram-air cooling slots on the outer wall, a condition which became worse as testing proceeded.

Thought was given at this time to modifying the primary zone to the PT6 configuration, as this had a proven satisfactory performance and could easily be mated to a dilution zone designed especially for regenerative operation. Experiments were carried out on a water model, and the validity of this approach became evident. Primary zone requirements were satisfactory. These water model experiments were put into practice on a new flame tube (Figure 82).

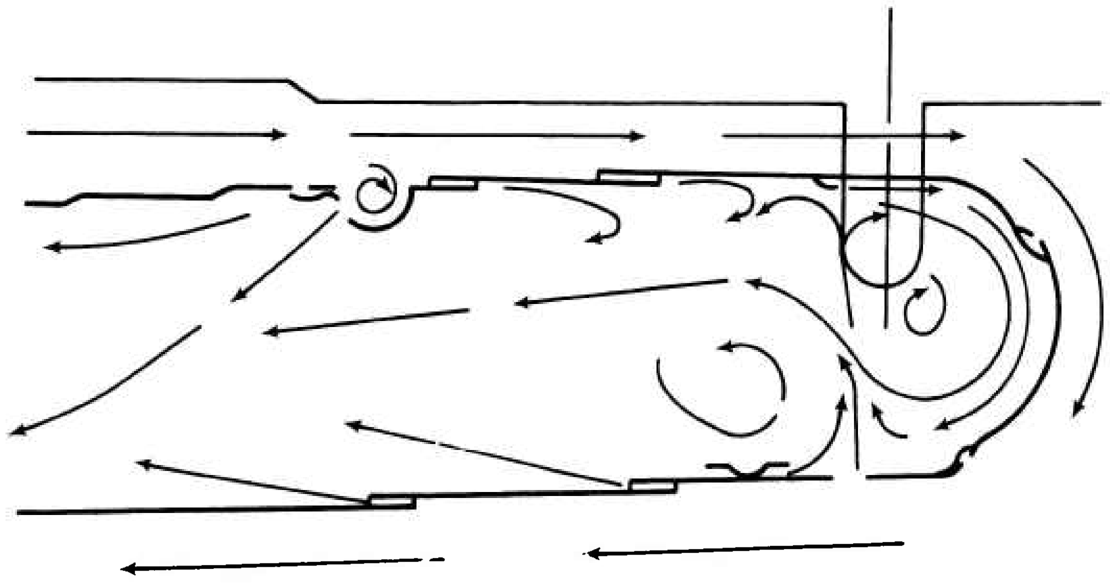

Figure 82. Regenerator Flame Tube With PT6 Primary Zone.

Initial tests with the new flame tube were encouraging, and attention was now paid to the effect of increasing the inlet temperature to the combustor. The increased inlet temperature was supplied by a slave PT6 combustor exhausting into the scroll of the regenerator section. Two problems became evident. First, the straightening vane section of the scroll became distorted at the entry, and secondly, vaporization was experienced in the fuel manifold and nozzles.

After investigation, a remedy for the distortion was found to be a rearrangement of the vanes in the entry section and insulation of the vanes from the backplate of the scroll. Fuel vaporization was eliminated by bathing the fuel manifold and nozzles in air from a shop supply. On an engine this could be achieved by compressor bleed air supplied to shrouded hardware.

Performance of the new flame tube showed that the ram-air cooling strips in the existing form were difficult to control and resulted in uneven cooling air distribution and some instability. To improve this situation, a perforated skirt was incorporated over both cooling strips on the outer wall (Figure 83). The purpose of this was to meter the cooling air through the perforations and also to stiffen the flame tube wall to eliminate distortion. The beneficial effects were immediately apparent. For the remainder of the program, flame tube distortion was never a problem, and stability was satisfactory.

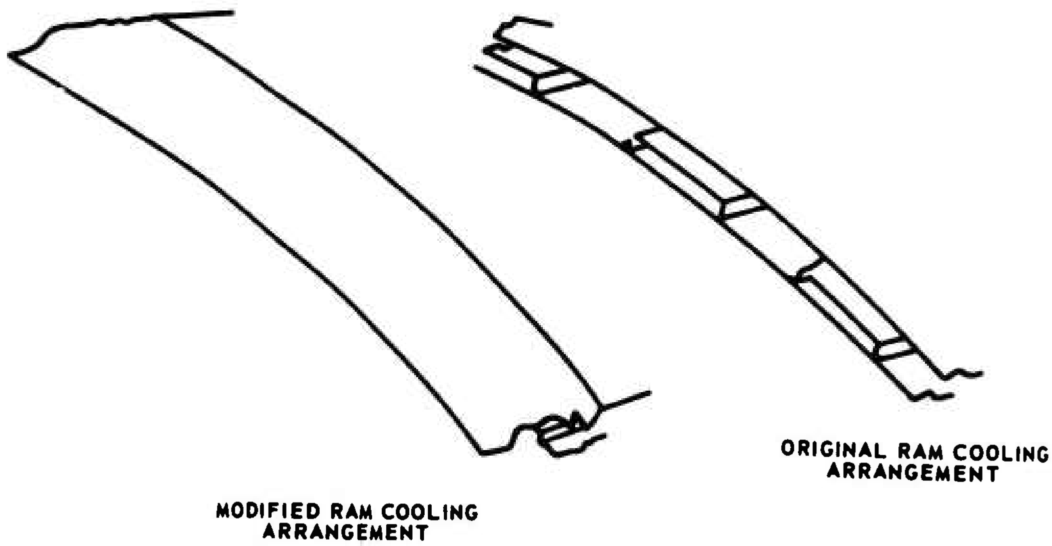

Figure 83. Original and Modified Ram Cooling Arrangements.

Operation with high inlet temperatures up to 1160°F. provided by the slave combustor produced a problem in assessing regenerator combustion efficiency, due to the interference of slave combustor exhaust products with the inlet air. It was decided to use the high inlet temperatures for durability evaluation and cold inlet conditions for performance.

Performance curves drawn from the results of tests on the completed flame tube are in Figures 84 through 89. Ignition and stability characteristics were very satisfactory over a wide range of operation. Mechanical durability at design-point conditions for 5 hours of continuous operation was good, as demonstrated by the performance values in the figures.

A view of the finished flame tube is shown in Figure 90.

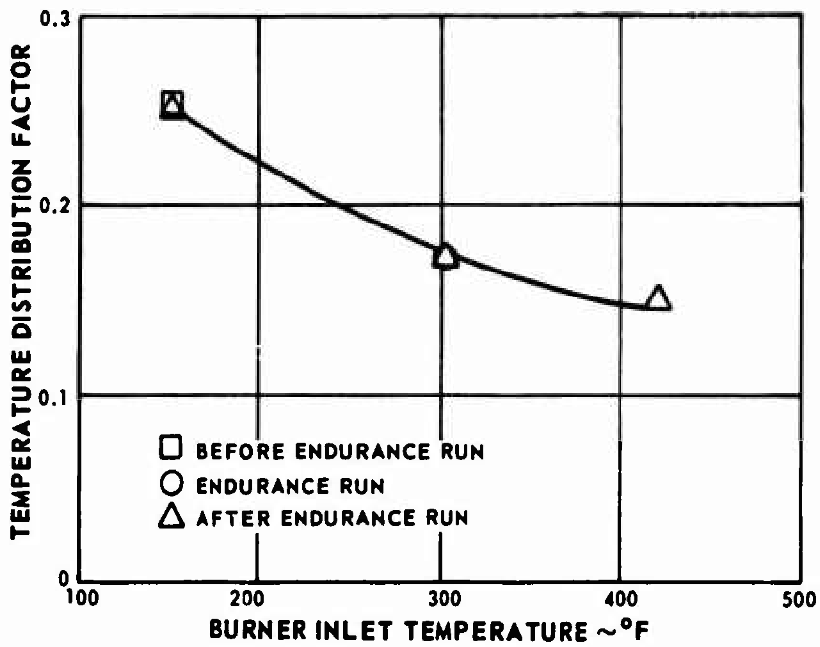

Figure 84. Temperature Distribution Factor Vs. Burner Inlet Temperature.

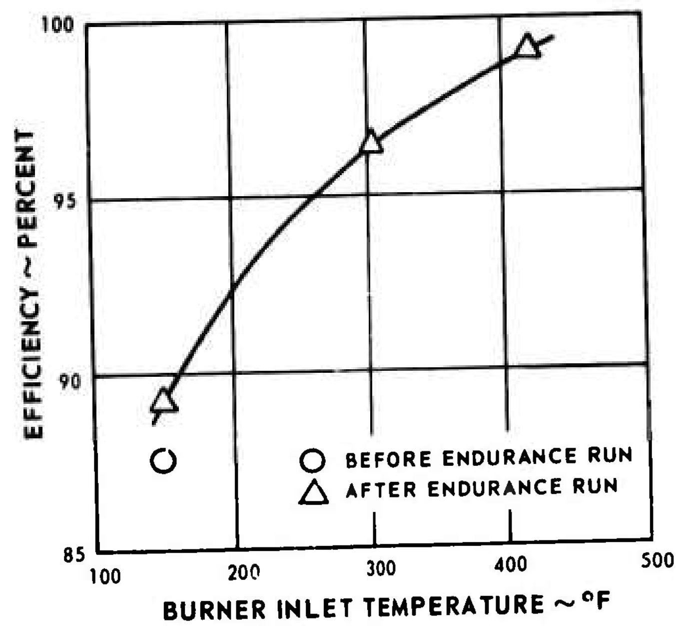

Figure 85. Burner Efficiency Vs. Inlet Temperature.

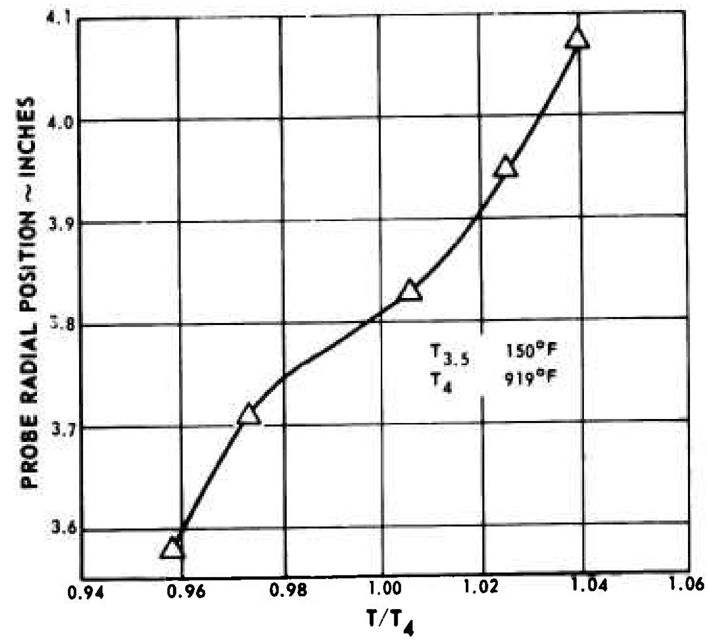

Figure 86. Radial Temperature Profile at the Turbine Inlet Plane Before Endurance Run.

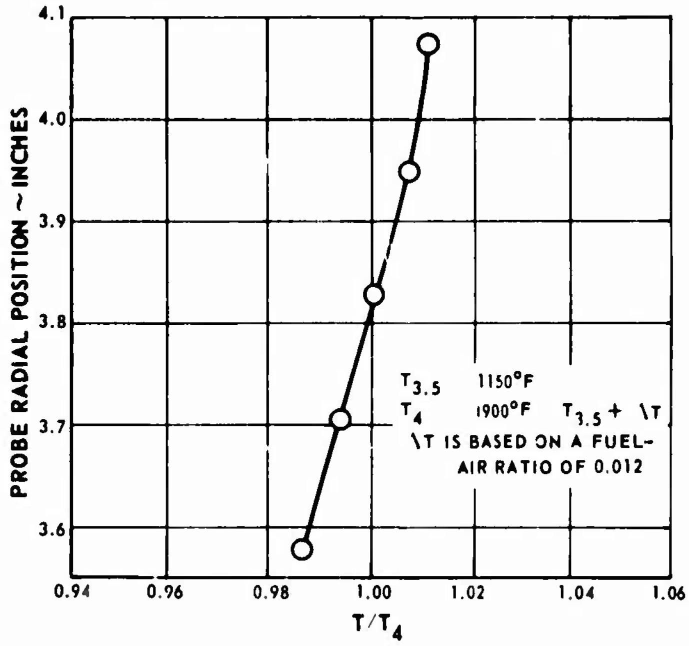

Figure 87. Radial Temperature Profile at the Turbine Inlet Plane in Endurance Run.

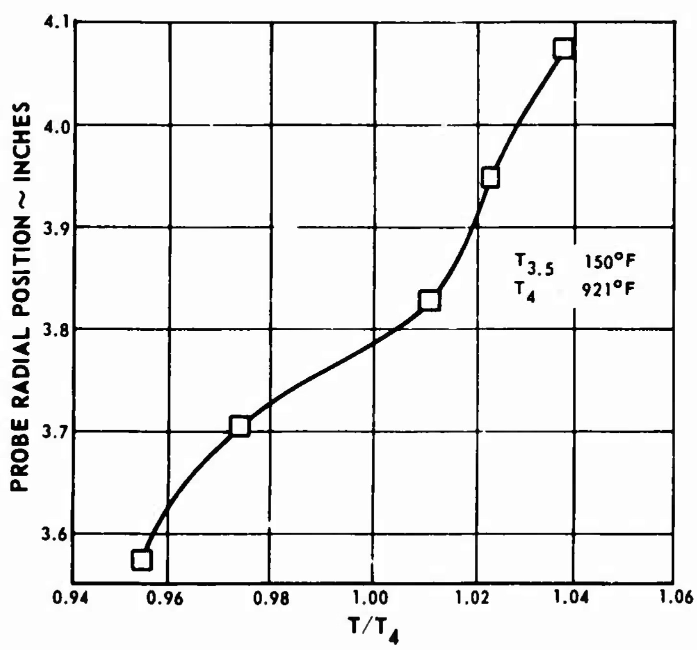

Figure 88. Radial Temperature Profile at the Turbine Inlet Plane After Endurance Run.

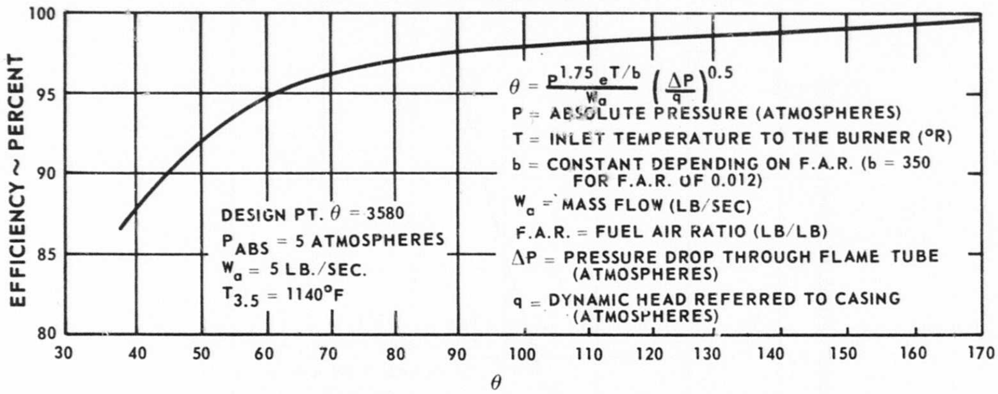

Figure 89. Anticipated Efficiency of Lightweight Regenerator Burner Installed in Engine Based on Rig Performance.

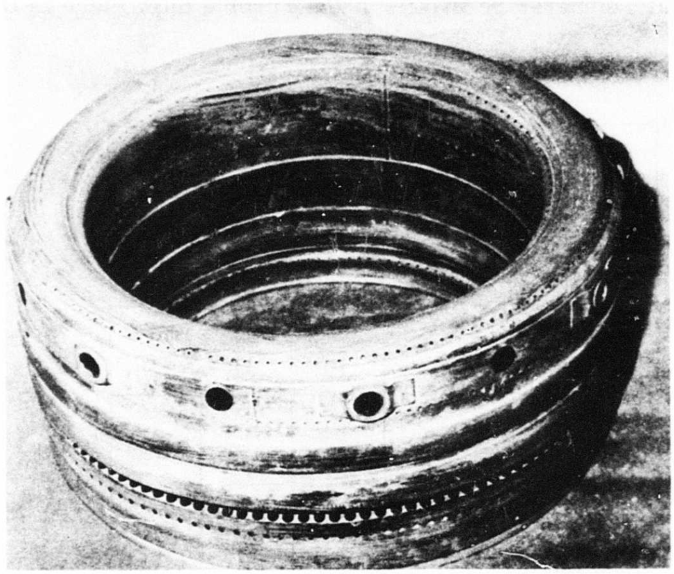

Figure 90. Flame Tube for the Regenerative Engine.

APPENDIX IV

TURBINE EXHAUST DUCT FLOW DISTRIBUTION INVESTIGATION

Development testing of the PT6 regenerative engine indicated serious deficiencies in performance of the engine-regenerator combination. Data obtained from these tests indicated a possible deficiency in performance of the turbine exhaust duct. The exhaust duct was therefore installed on the exhaust rig and tested with various inlet swirl vane settings.

TEST PROCEDURE

The exhaust duct was installed on the exhaust rig and instrumented as shown in Figure 91. The corrected flow into the exhaust duct was set at 7.0 pounds per second (maximum flow capability of the rig) and the swirl vane setting was varied from 0° (axial) to 45°. For each swirl vane setting the static pressures, total pressures, and flow angles were recorded for the duct inlet and exit. This was achieved by radially traversing wedge probes at three circumferential positions at the inlet and every 10° circumferentially at the exit.

The corrected mass flow was reduced to 5.8 pounds per second for the swirl vane setting of 45° because of exhaust duct vibration and noise.

Tufts were placed on the honeycomb exit to allow visual examination of exhaust duct exit flow.

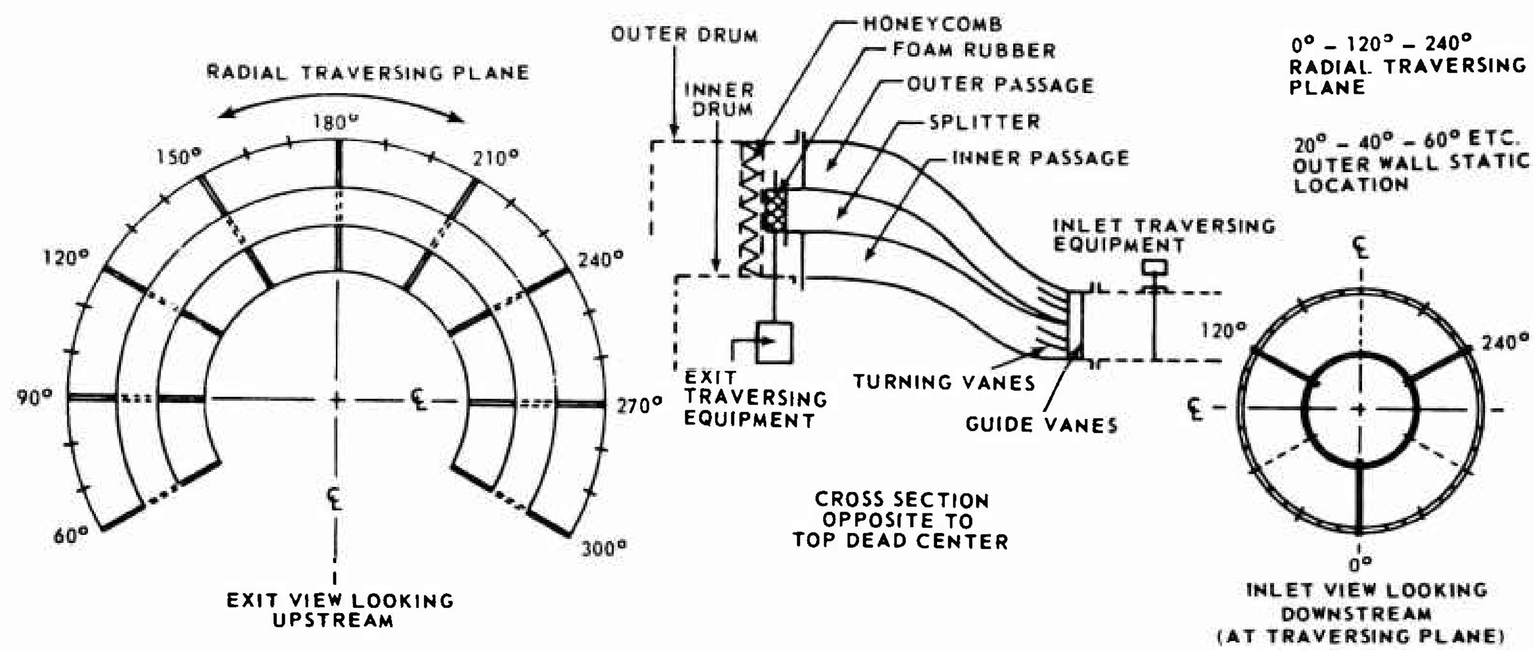

Figure 91. Schematic of Turbine Exhaust Duct for Cold Flow Test.

RESULTS

Figures 92 through 95 give an isobaric presentation of the exhaust duct exit total pressure (inches of water above ambient) upstream of the honeycomb for inlet swirl vane settings of 0°, 15°, 30°, and 45°, respectively.

Figures 96 through 99 give a constant flow angle (yaw angle from axial) presentation of the flow at the exit of the exhaust duct for swirl vane settings of 0°, 15°, 30°, and 45°, respectively.

Figure 100 shows the radial distribution of flow angle at the inlet traversing plane (6 inches upstream of the exhaust duct inlet) for various swirl vane settings.

Figure 101 shows the radial distribution of velocity at the inlet traversing plane for various swirl vane settings.

Figure 102 shows the radial distribution of total pressure at the inlet traversing plane for various swirl vane settings.

Figure 103 shows the circumferential distribution of wall static pressure at the inlet traversing plane for various swirl vane settings.

Figure 104 shows the total pressure loss through the outer channel of the exhaust duct. The dynamic pressure is based on conditions at the inlet traversing plane.

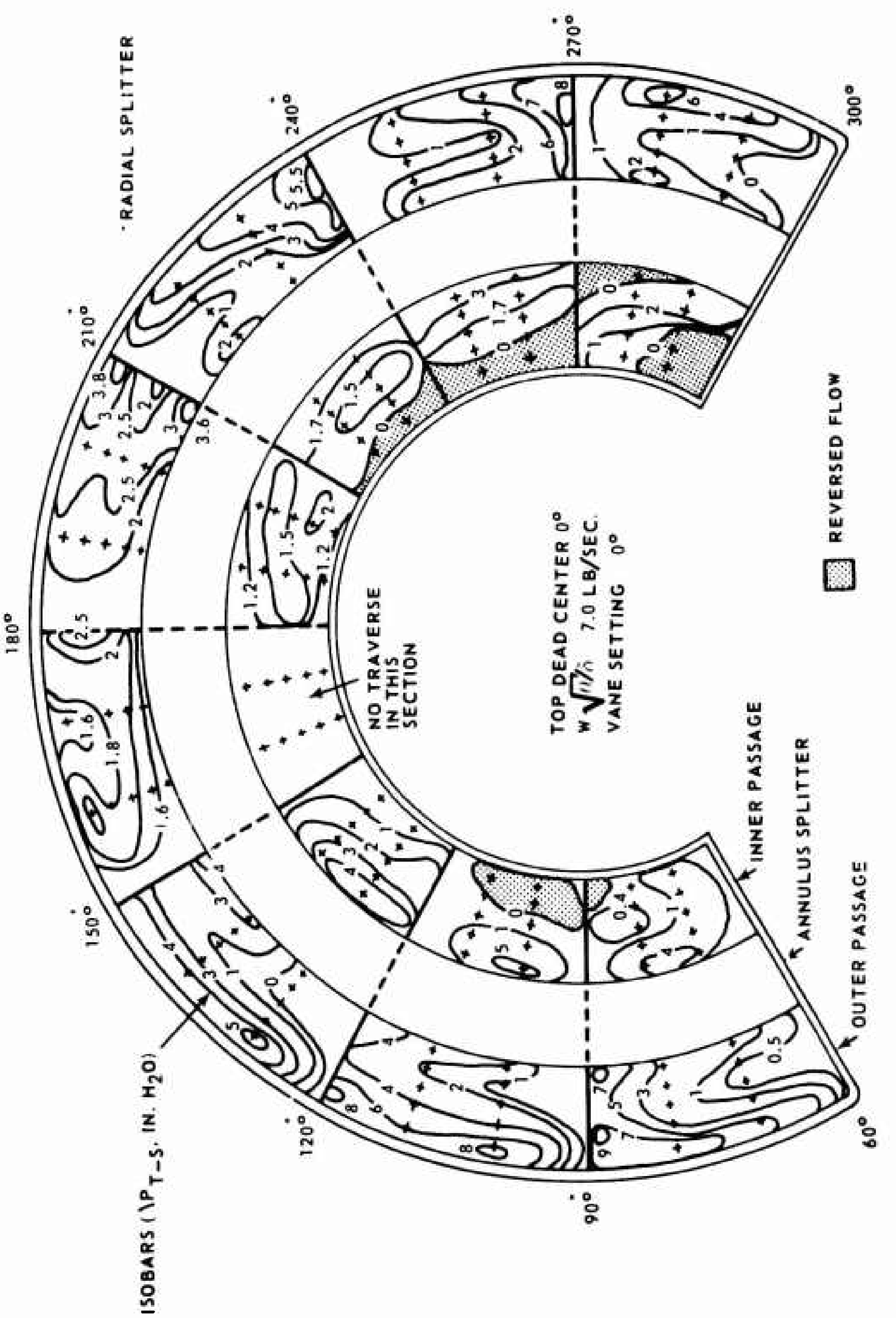

Figure 92. Exhaust Duct Exit Total Pressure With Inlet Swirl Vanes Set at 0°.

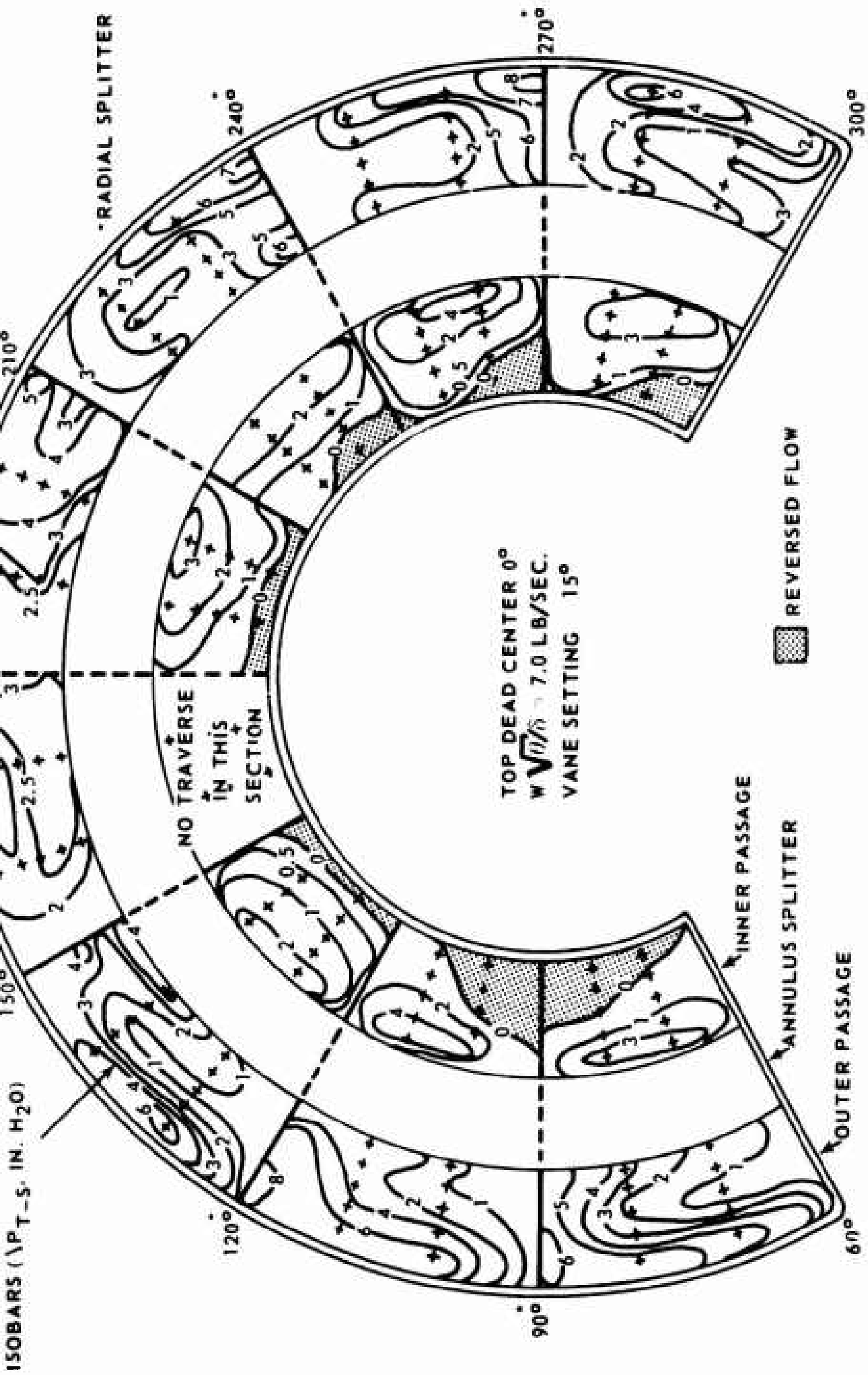

Figure 93. Exhaust Duct Exit Total Pressure With Inlet Swirl Vanes Set at 15°.

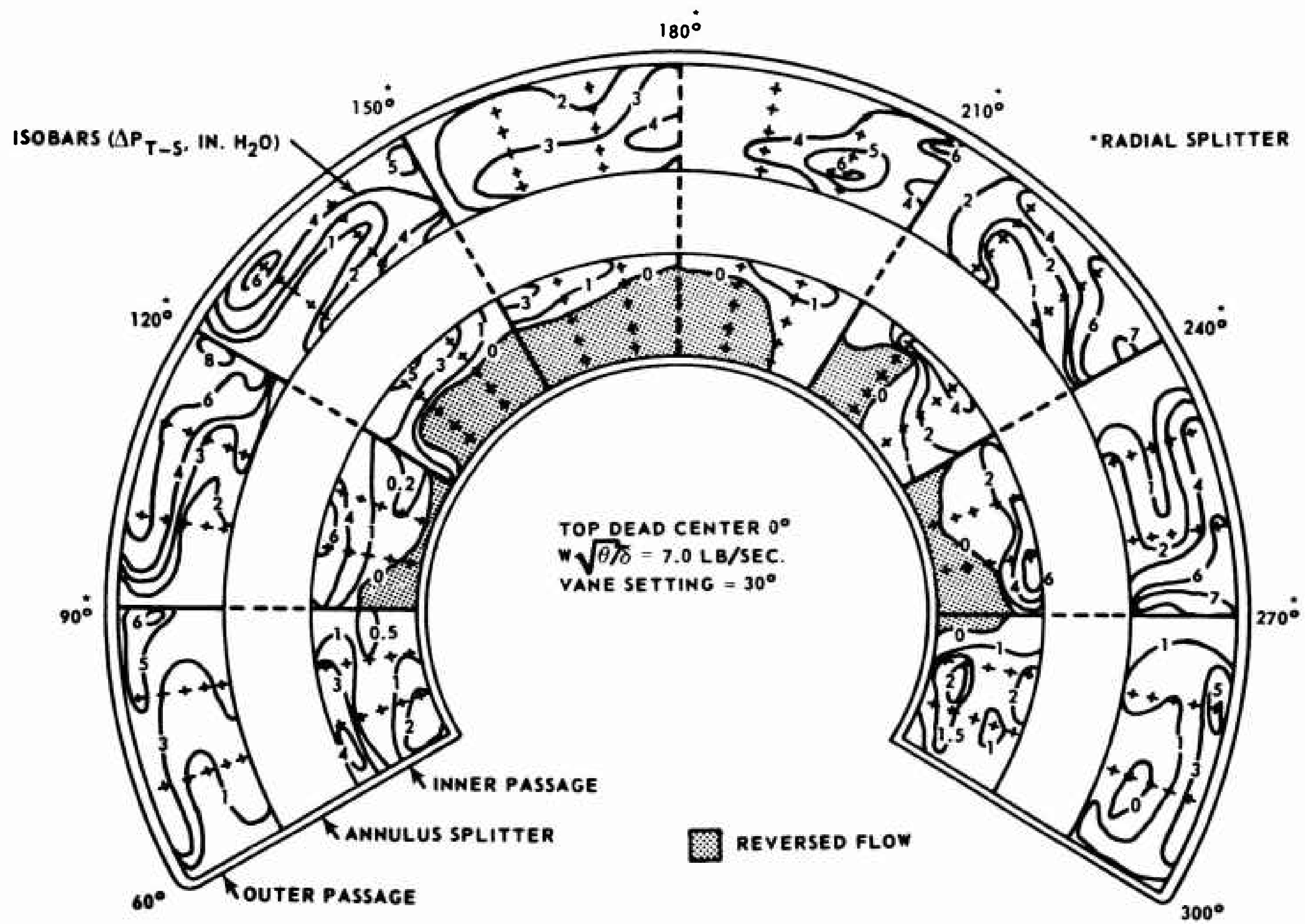

Figure 94. Exhaust Duct Exit Total Pressure With Inlet Swirl Vanes Set at 30°.

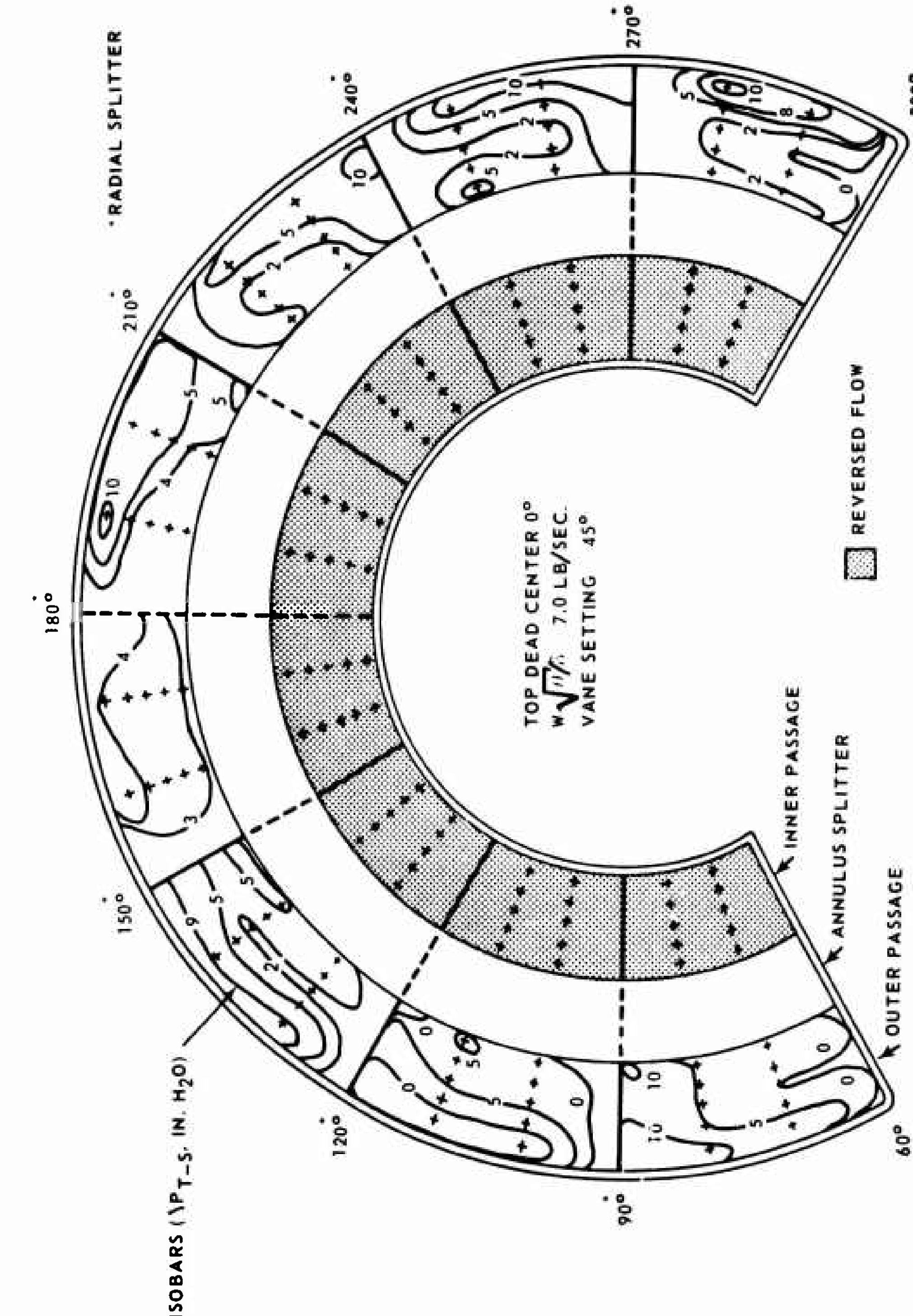

Figure 95. Exhaust Duct Exit Total Pressure With Inlet Swirl Vanes Set at 45°.

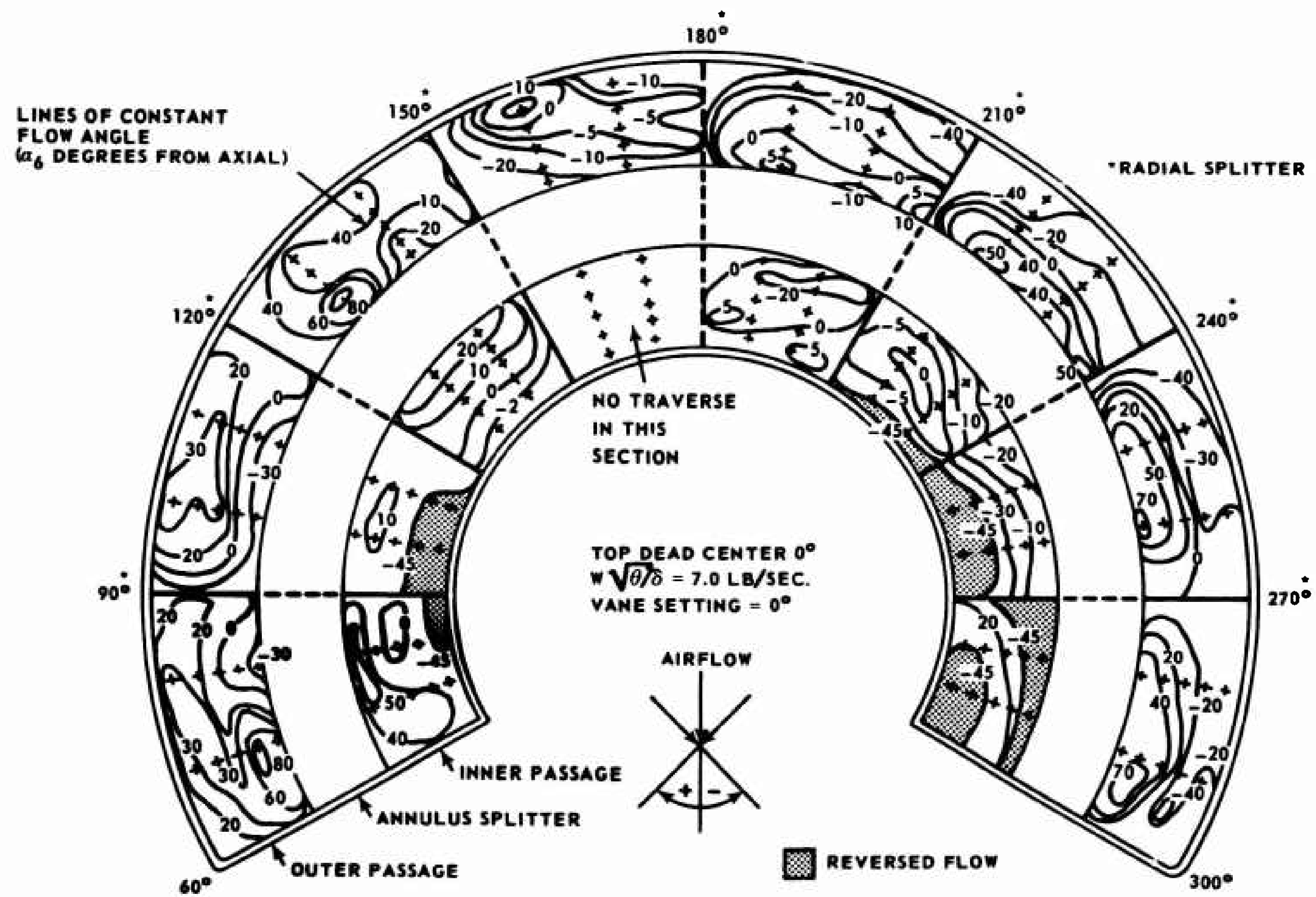

Figure 96. Flow Angles in Exhaust Duct Exit With Inlet Swirl Vanes Set at 0°.

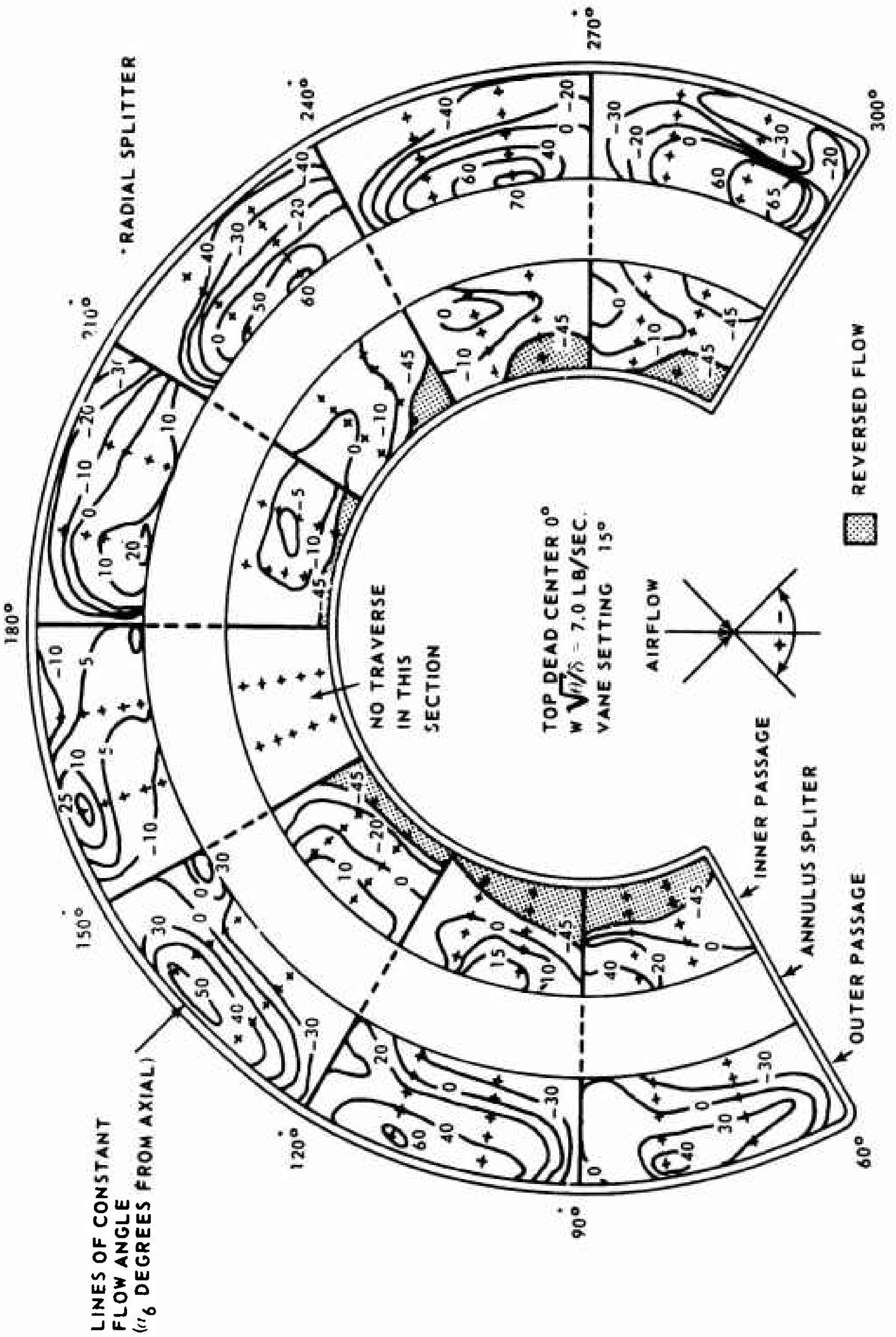

Figure 97. Flow Angles in Exhaust Duct Exit With Inlet Swirl Vanes Set at 15°.

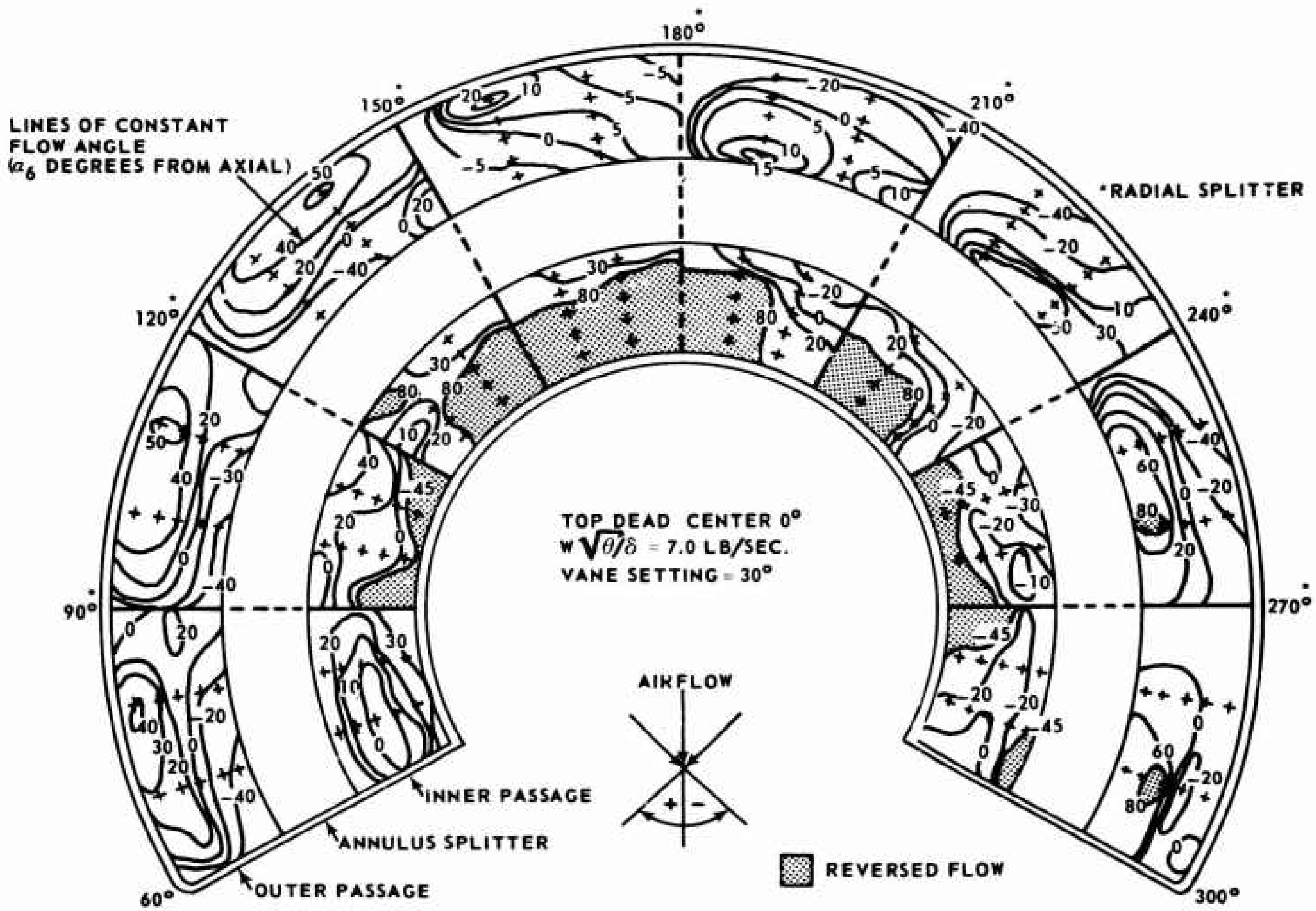

Figure 98. Flow Angles in Exhaust Duct Exit With Inlet Swirl Vanes Set at 30°.

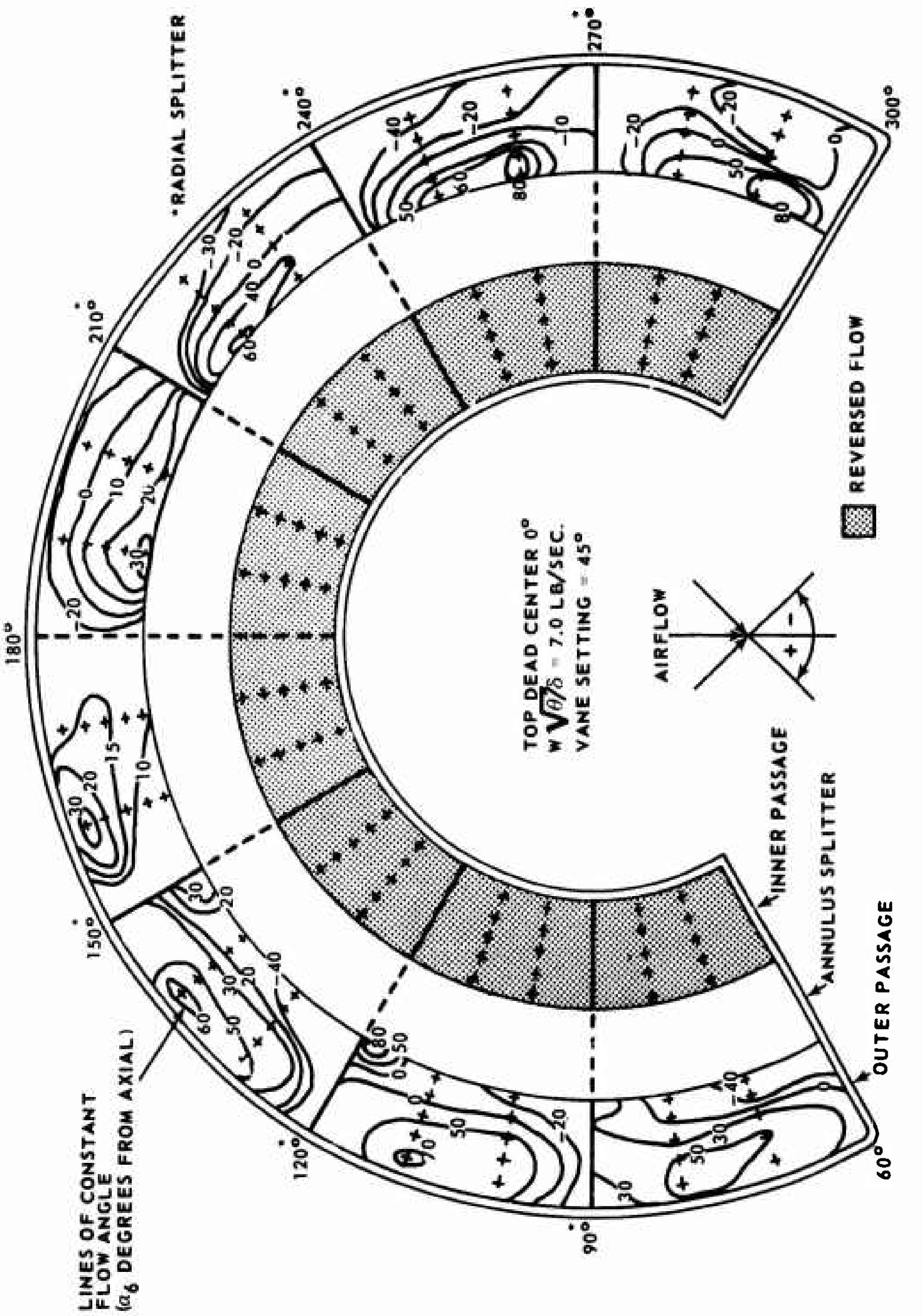

Figure 99. Flow Angles in Exhaust Duct Exit With Inlet Swirl Vanes Set at 45°.

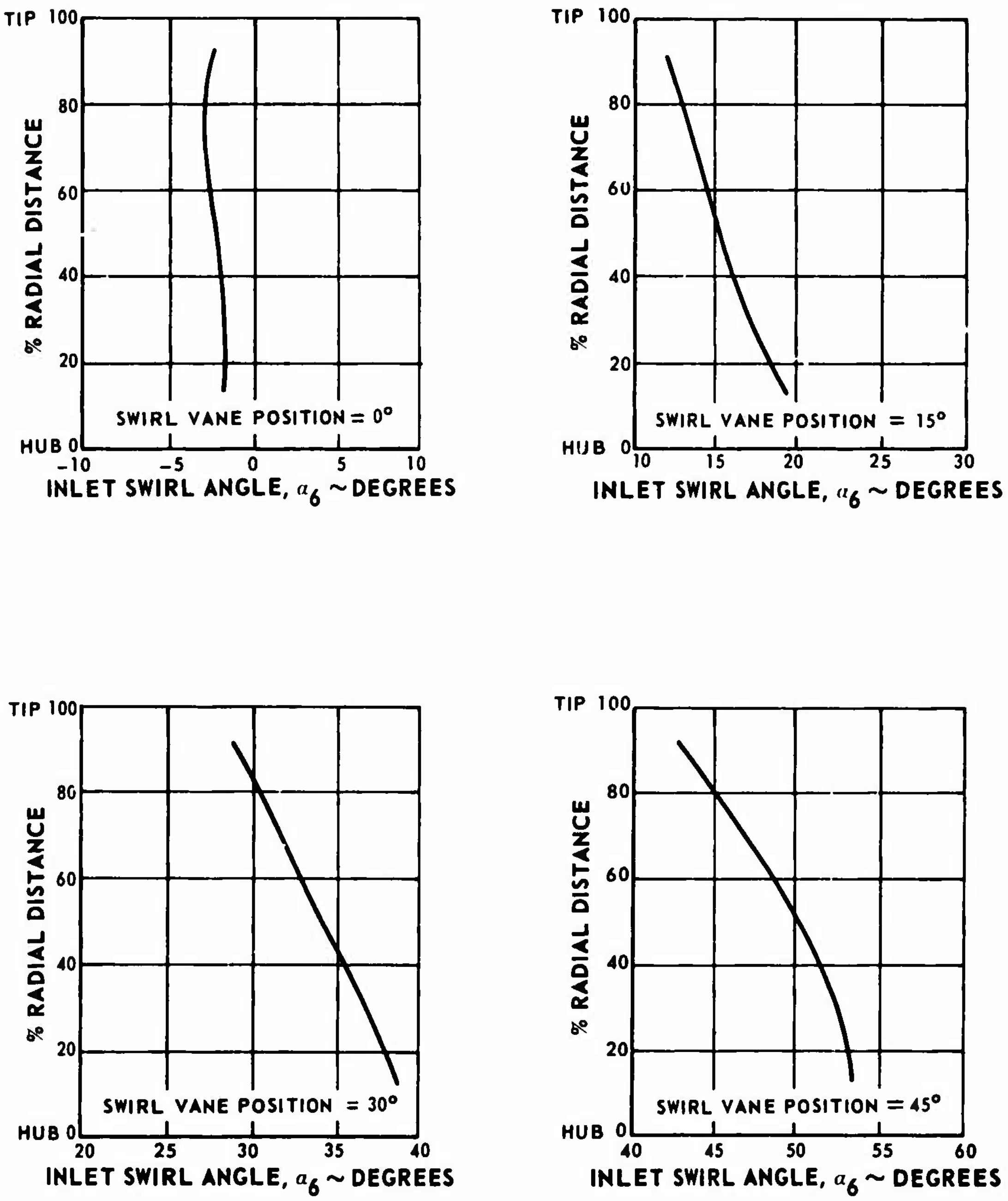

Figure 100. Radial Distribution of Inlet Swirl Angle in the Turbine Exhaust Duct.

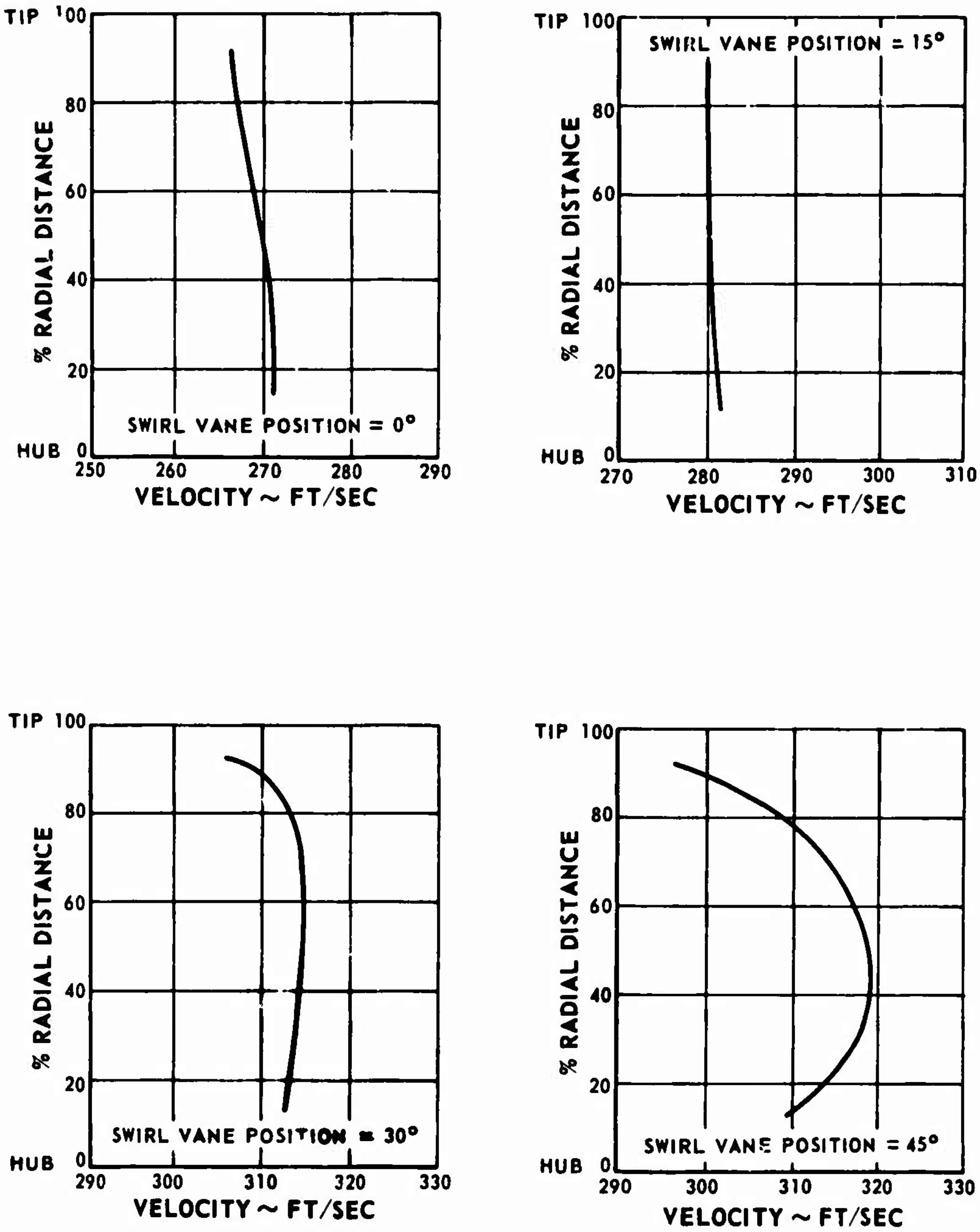

Figure 101. Radial Distribution of Inlet Velocity in the Turbine Exhaust Duct.

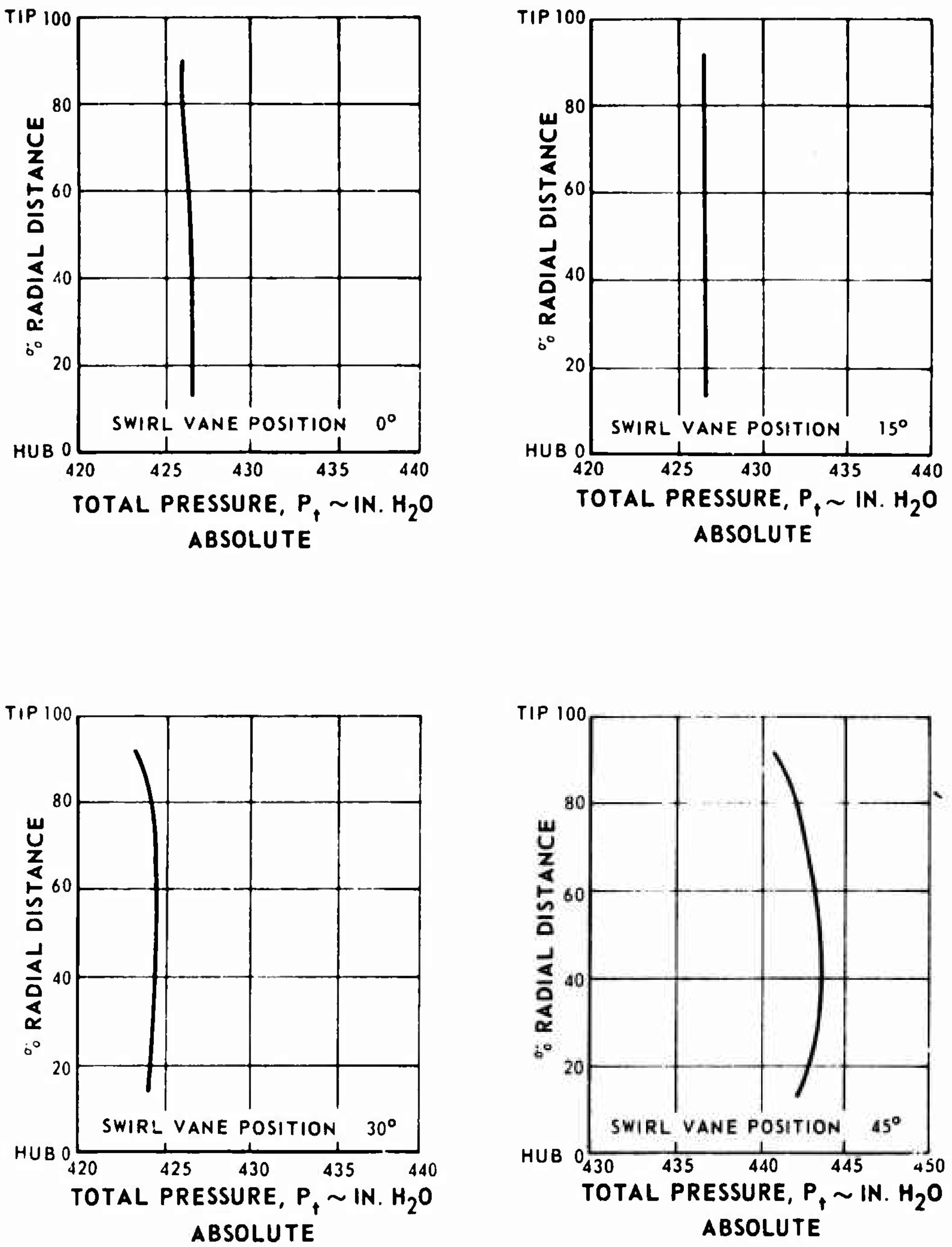

Figure 102. Radial Distribution of Inlet Total Pressure in the Turbine Exhaust Duct.

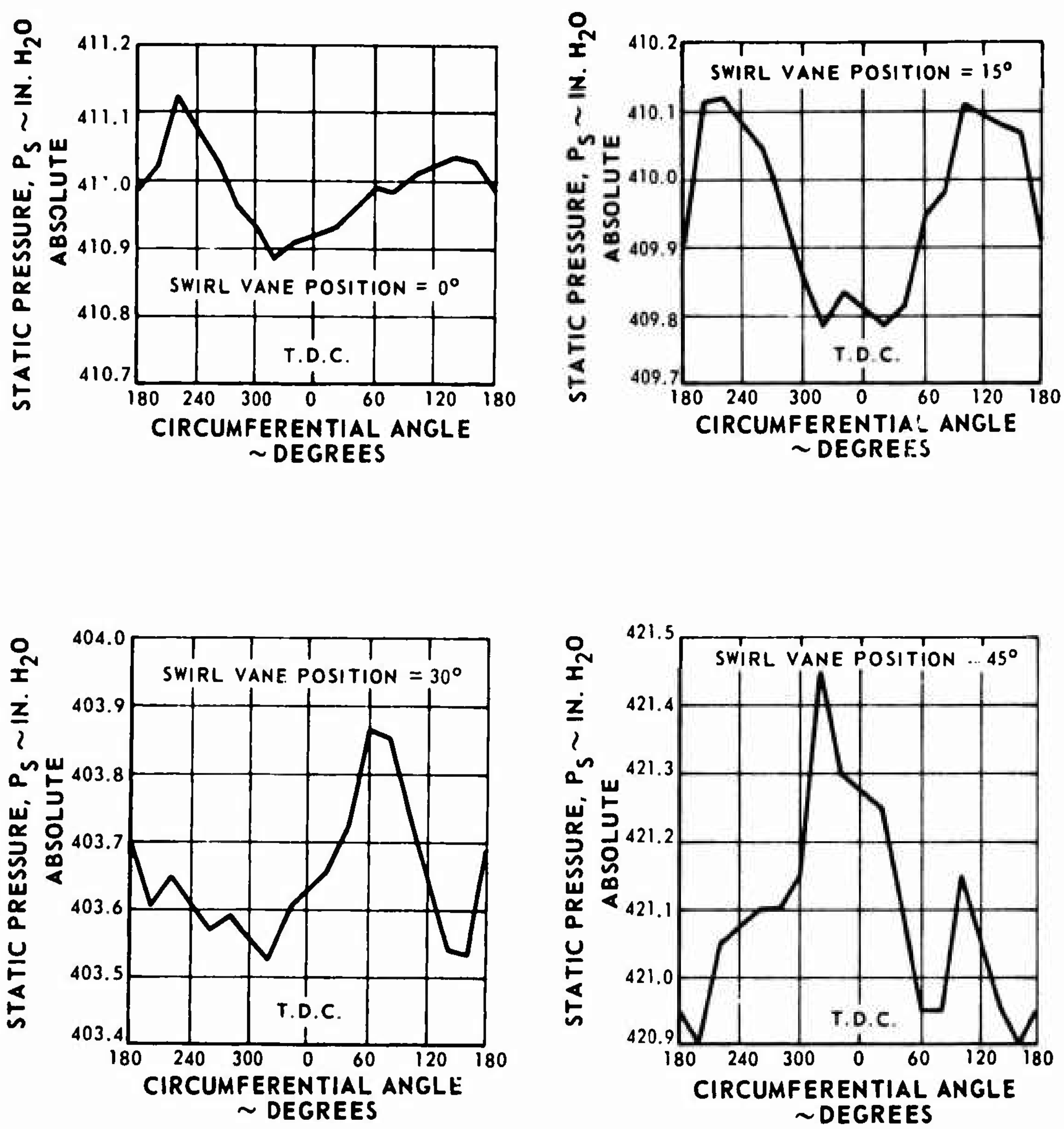

Figure 103. Circumferential Distribution of Inlet Wall Static Pressure in the Turbine Exhaust Duct.

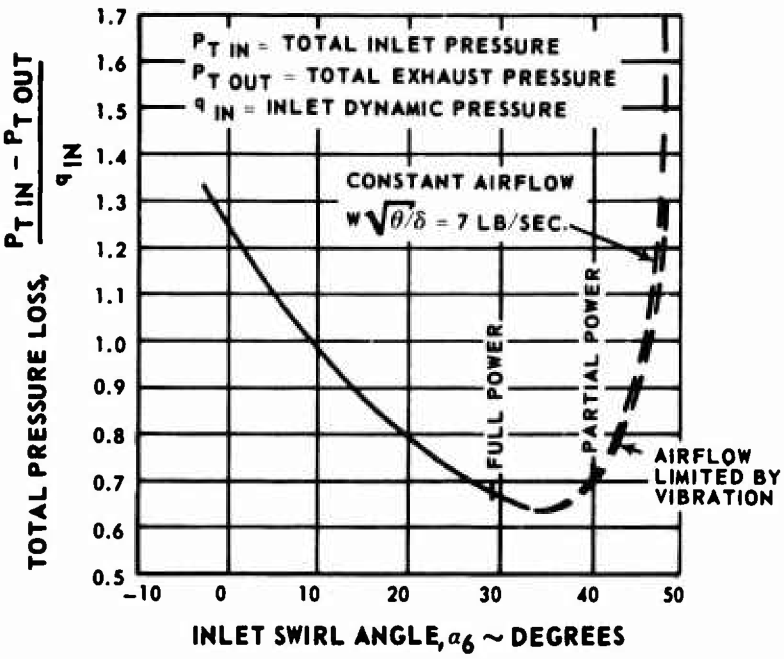

Figure 104. Total Pressure Loss Through the Turbine Exhaust Duct as a Function of Inlet Swirl Angle.

DISCUSSION OF RESULTS

Figures 92 through 99 indicate increasing flow separation in the inner annulus of the exhaust duct for increasing swirl vane settings. For all conditions, most of the flow goes through the outer annulus. This is to be expected. For a swirl vane setting of zero, the outer annulus offers a path of lower pressure loss because of lower annulus curvatures. As the inlet flow angle is increased, the static pressure at the hub decreases most rapidly, causing an increase in the adverse static pressure drop through the inner annulus; this results in even more unfavorable flow conditions, leading to complete flow reversal at a swirl vane setting of 45°. The reduction in flow through the inner annulus; for increasing swirl vane settings, reduces the axial velocity at the inlet, resulting in an increase in the flow angle onto the straightening vanes. This explains the tremendous noise and vibration encountered for swirl vane settings above 30° for mass flows of 7.0 pounds per second.

Figure 98 shows that flow angle at the exit of the outer annulus varies from +60° to -45°, while the flow angle at the exit of the inner channel varies from +80° to -20° with about 50 percent of the area in reverse flow.

Figures 100 through 103 show no consistent influence circumferentially due to the shape of the exhaust duct. The measuring plane, though, is 6 inches upstream of the straightening vanes. This measuring plane was chosen to expedite testing of the duct because of the availability of hardware.

CONCLUSIONS

The flow from the exhaust duct will adversely affect the performance of the regenerator.

Under engine conditions, the pressure loss $\Delta P/P$ through the outer duct is 0.062. This value is optimistic based on engine data, which show that the annulus at the power turbine exit is not flowing full. This would result in a higher local dynamic pressure than that of a standard PT6 engine and hence lead to a higher $\Delta P/P$ through the exhaust duct.

The diffusion from inlet to exit of the exhaust duct is equivalent to a 30° (total included angle) conical diffuser. The splitter reduces greatly the equivalent diffusion in each passage but unfortunately does little to reduce the highly unfavorable pressure gradient through the inner duct for swirling flows.

Patterns made by the tufts at the exit of the honeycomb verified the areas of reversed flow that were found by the exit traverse.

The inlet traversing plane was too far upstream to show the effects of exhaust duct shape.

Assessment of a total pressure loss for the inner annulus would be tedious and inaccurate due to the presence of reversed flow.

APPENDIX V

SINGLE-MODULE ROTARY REGENERATOR TEST RIG

An oscillating single rotary regenerator package or module test rig was designed and constructed to evaluate toroidal rotary regenerator module designs. The rig was used in conjunction with the matrix airflow distribution test rig, wherein the flow distribution through the matrix was determined and then heat transfer tests were performed to evaluate the effects of any flow maldistribution on performance. The operation of the rig is similar to that of the regenerator, where each module is subjected to the regenerator time-temperature cycles and mass velocities. This is accomplished by periodic cycling of the module between two countercurrent streams at different temperatures and by controlling the dwell time in each stream. The upstream and downstream temperatures are recorded continuously for each stream. The thermal effectiveness of the module is determined from the integrated average exit stream temperature and the inlet temperatures of the streams.

The rig has the following advantages: (1) Only one regenerator module is required for test; (2) costs to evaluate module designs are substantially lower than those of a rotary regenerator; (3) modules may be readily installed and tested; (4) the regenerator Reynolds numbers and rotational speed can be simulated by controlling the airflow in each duct and the module dwell time in each stream; (5) the sealing problems are alleviated by operating both streams at approximately the same pressure; and (6) requirements for the air supply are substantially less than for a full rotary regenerator.

The rig has the following possible disadvantages: (1) The flow is temporarily interrupted when the piston is shuttled into and out of the stream. Analysis of data thus far has shown that the flow perturbation has an insignificant effect on mass-averaged downstream temperature. This could be a problem, however, if the dwell time is short, corresponding to high regenerator speed. (2) If the flow leaving the matrix is nonuniform, then either transient downstream temperature and flow over the face must be recorded or mixers must be used to allow direct measurement of mass-averaged temperature.

DESCRIPTION OF TEST RIG

The test rig is shown schematically in Figure 105. The rig basically consists of: (1) two countercurrent air streams, one of which contains a heater burner; (2) valves for controlling airflow; (3) an orifice in each stream for measuring flow, (4) a test section which is comprised of a cylinder containing two ports on each side to allow passage of air and a piston within the cylinder which houses the module; (5) a pneumatic actuator to shuttle the module between streams; and (6) instrumentation for measuring temperature and pressure. A photograph of the rig is in Figure 106.

Air is supplied countercurrently to the test section at different temperatures through two ducts of lengths equivalent to 20 hydraulic diameters. The air in one duct is 90°F. and in the other 350°F. The cross-sectional area and geometry of the ducts are the same as the area between the bulkheads of the T74 rotary regenerator. To ensure uniform flow entering the test section, flow straighteners consisting of three perforated plates having a porosity of 0.5 and spaced one diameter apart are employed in each duct. A pressure regulating valve in the air supply line is used to control air pressure to the test rig. Control of the airflow rates in each duct is accomplished with flow control valves. So that the periodic variation in flow resistance caused by shuttling the module in and out of the stream would not result in cyclic flow, the flow is choked across valves located between the flow control valves and the test ducts. Flow in each stream is measured with standard VDI orifices. An alcohol heater burner is employed in one stream to heat the air to the test temperature of 350°F.

The test section consists of a 10-inch-inside-diameter cylinder, approximately 50 inches in length, through which a piston assembly containing a regenerator module package is periodically cycled between streams. Pie-shaped ports through the sides of the cylinder, which mate to the test ducts, allow air to flow through the module. Seal shoes, consisting of semicircular cylinders attached to each end of the piston, are used to divert the flow through the ports located at each end of the cylinder when the module leaves each stream. Incorporation of a resistance in the ports equal to the module resistance maintains constant resistance in each stream while periodically cycling the module. Figure 107 depicts the design features of the seal shoes.

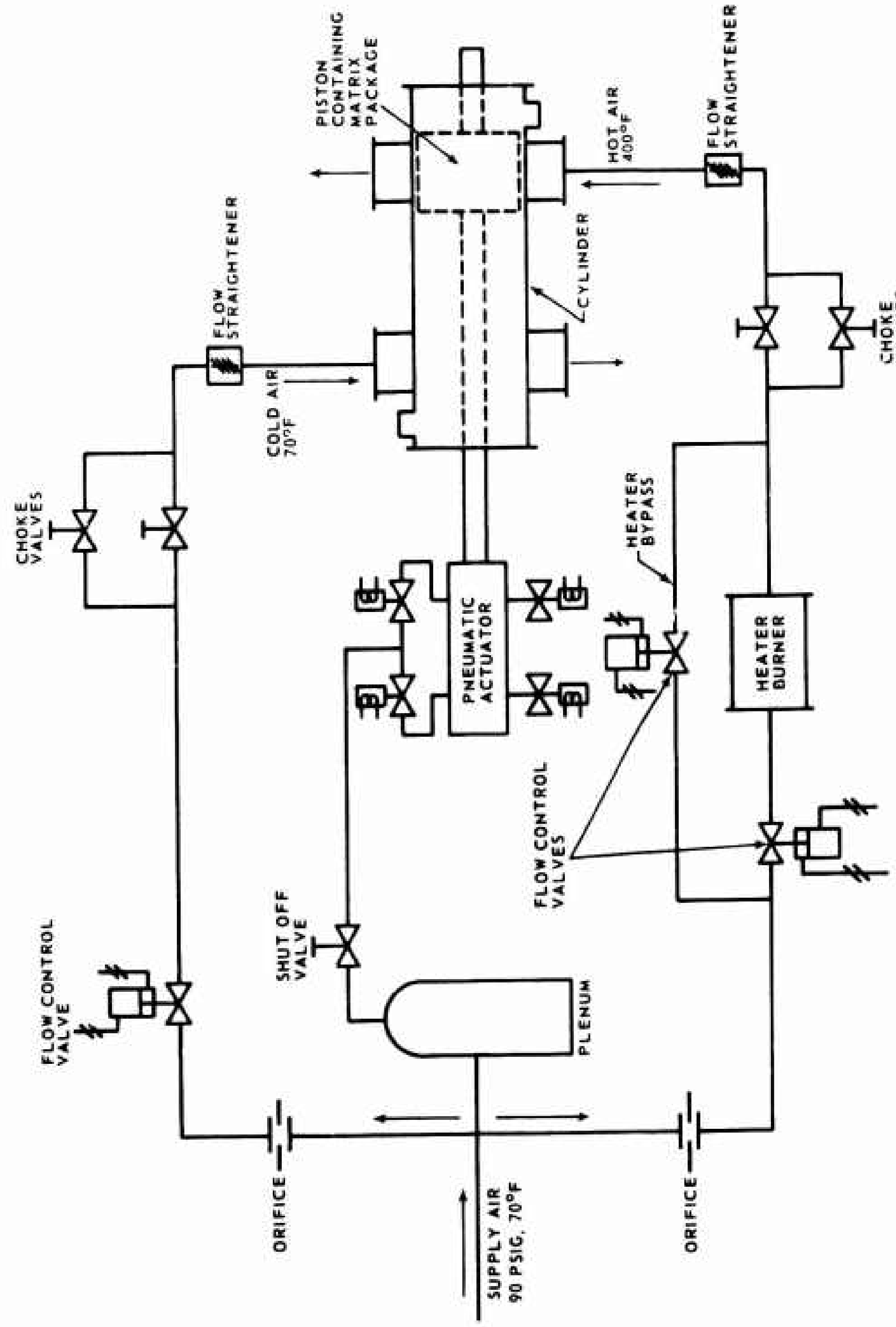

Figure 105. Schematic of Regenerator Module Heat Transfer Test Rig.

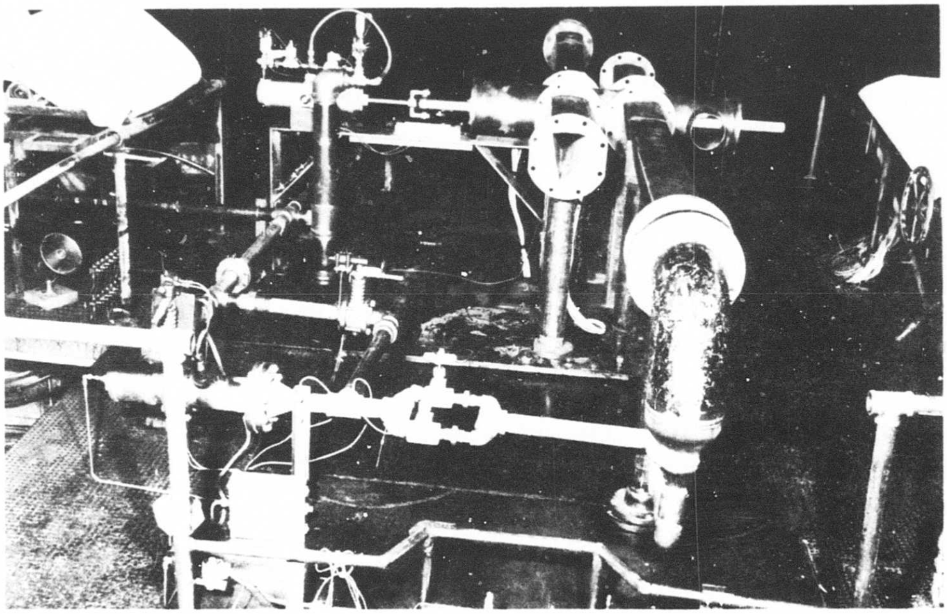

Figure 106. Regenerator Module Heat Transfer Test Rig.

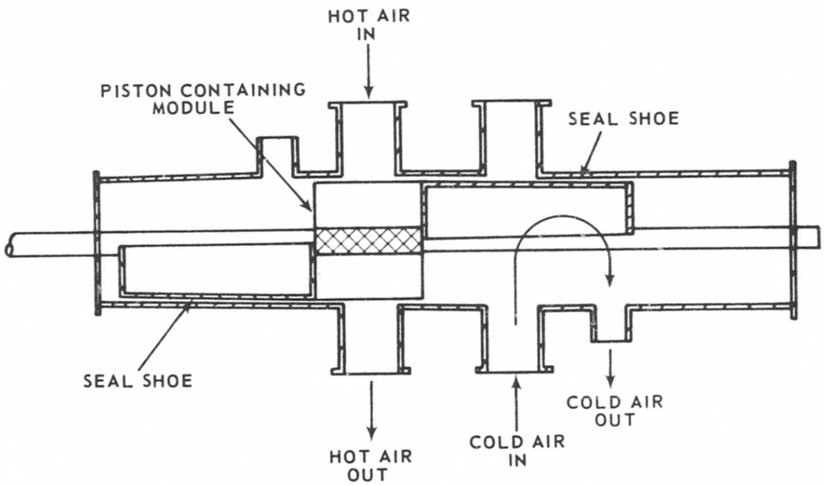

Figure 107. Diagram Showing Location of Seal Shoes in Regenerator Module Heat Transfer Test Rig.

The module is housed in the piston, which is shuttled between the two streams by a pneumatic actuator. Sealing is accomplished by piston rings on each end of the piston and rub seals on the top and bottom of the piston as in the regenerator. The piston rings prevent interstrean leakage, while the rub seals prevent short-circuiting of the flow through the module. The piston is approximately 10 inches in diameter, and the physical arrangement of the module within the piston was kept the same as in the regenerator. The piston is supported on shafts which in turn are supported by carbon bushings at each end of the cylinder. To prevent piston rotation, one of the shafts contains an axial keyway which mates with the guide key of one of the bushing retainers. Figure 108 is a photograph showing the piston assembly shafts, seals, bushings, and cylinder end plates.

Control of the module dwell time within the streams is accomplished with timers and microswitches. Instrumentation used on this rig is identical to the instrumentation employed in the tests described in the Phase I report under Matrix Experimental Investigation, Periodic-Flow Heat Transfer Tests.

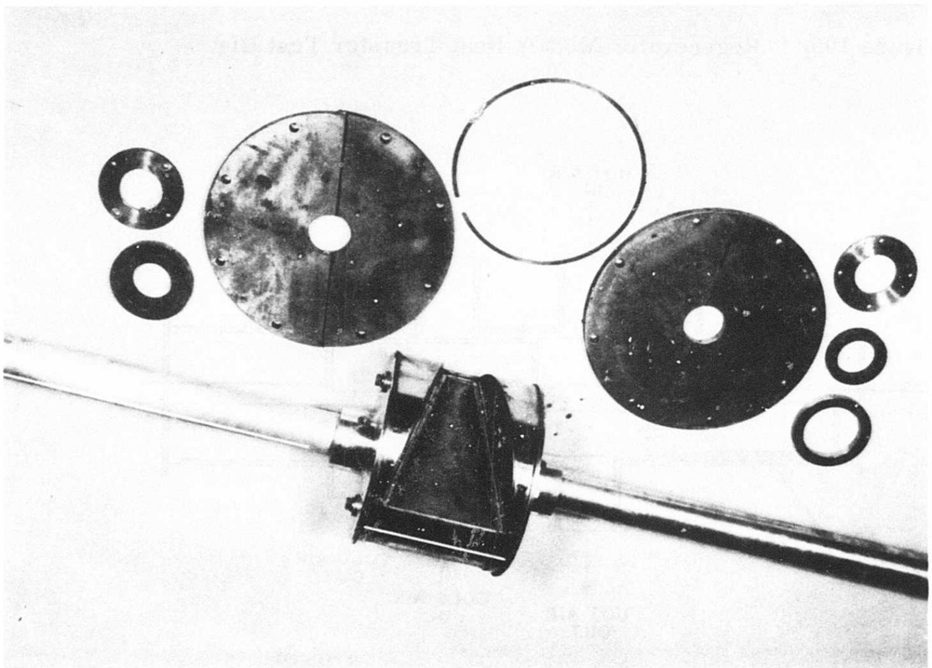

Figure 108. Piston and Support Assembly.

SHAKEDOWN TESTS

A flat module (i.e., frontal area normal to flow) was fabricated for shakedown tests on the rig. The module was composed of 80 layers of 24-mesh, 0.0145-inch-wire-diameter screens sintered so that the resultant thickness was 2.0 inches. To provide a basis for determining the validity of test results, the heat transfer characteristic of the matrix was first determined in the periodic-flow heat transfer rig, and a module theoretical effectiveness was computed. This was accomplished using the same method outlined for the periodic-flow tests in the Phase I report.

The heat transfer characteristics are shown in Figure 109 in the form of the product of the Stanton and the Prandtl numbers plotted versus the Reynolds number.

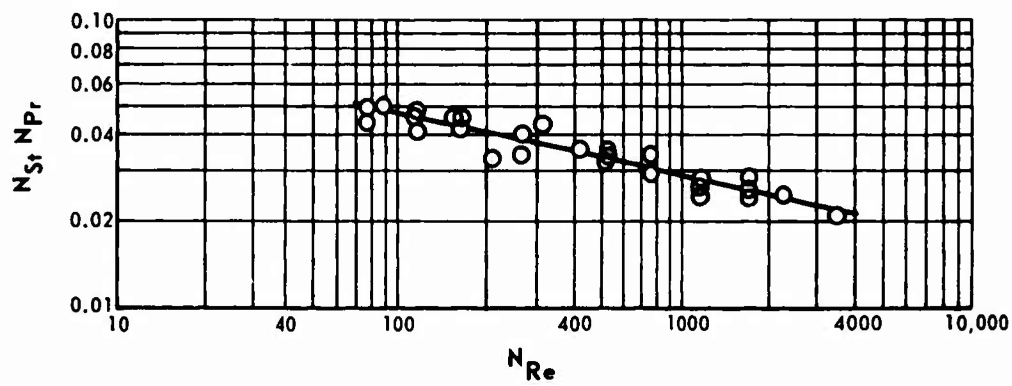

Frontal area	0.8726 ft.^{2}
Package thickness	2.118 in.
Mass of matrix	1.845 lb.
Number of screens	60
Screen material	type 304 stainless steel
Porosity of matrix	0.7555
Surface area/total volume	782.33 ft.^{2}/ft.^{3}
Layer thickness	0.0353 in.
Density of screen material	490 lb./ft.^{3}
Screen specific heat	0.12 B.t.u./lb.-°F.
Hydraulic diameter	0.00376 ft.

Figure 109. Heat Transfer Characteristics of 24-Mesh, 0.0145-Inch-Diameter Wire Screen Sintered Matrix.

Performance tests were conducted on the module at a Reynolds number of 1200 and at dwell times of 1.2 seconds in each stream. Tests were conducted both with and without the seal shoes. The tests conducted without the seal shoes resulted in an effectiveness of 0.69 on the hot and cold sides. Tests conducted with the seal shoes resulted in effectivenesses of 0.71 and 0.72 on the cold and hot sides, respectively. During these tests a hot wire anemometer in the upstream duct was used to measure the time required for flow establishment. Results showed that a time of 0.25 second was required with the use of seal shoes and 0.35 second without. The computed theoretical effectiveness was 0.73, indicating that the rig was performing satisfactorily.

ROTARY REGENERATOR MODULE TESTS

Since the design performance of the T74 rotary regenerator 60-mesh, 0.004-inch-wire-diameter screen W-package was not attained in the performance loop tests, a spare package was installed in the module rig for testing. Tests were conducted to obtain a more detailed experimental picture of the low-effectiveness problem and develop a suitable change to improve performance.

The first test was conducted at the T74 regenerator design Reynolds numbers and dwell times in each stream corresponding to 20 r.p.m. Since the duct fairings which mate to the matrix blunt ends were not employed in the regenerator tests, they were omitted in this test. The tie plate which contains the rub seal was also omitted, since a spare tie plate was not available. The test results showed a large variation in local effectiveness, indicating that the flow distribution through the matrix was not uniform. Therefore, to determine the true overall effectiveness, it was necessary to determine the flow profile as well as the temperature effectiveness profile on the downstream face of the module. The temperature effectiveness was then flow averaged.

A pitot-static probe was used to determine the downstream velocity profile and hence the corresponding mass flow rate of air downstream of the module. Separate profiles were obtained for flow into the W-package and flow over the W-package and are shown in Figures 110 and 111, respectively. Traversing was done in the radial direction in 0.25-inch increments for a total of 32 readings in each duct. Circumferential probing yielded essentially flat profiles.

A thermocouple traverse was also made downstream of the module, radially in the same incremental areas as the pitot-static probe. The transient response of the thermocouple was recorded on an oscillograph. The recordings were made as the module was shuttled alternately between the cold- and hot-air streams until the quasi-steady-state responses were obtained in both ducts. Integration was used to determine the average temperature of the downstream air response curve. The temperatures of the hot and cold air entering the package are steady with time.

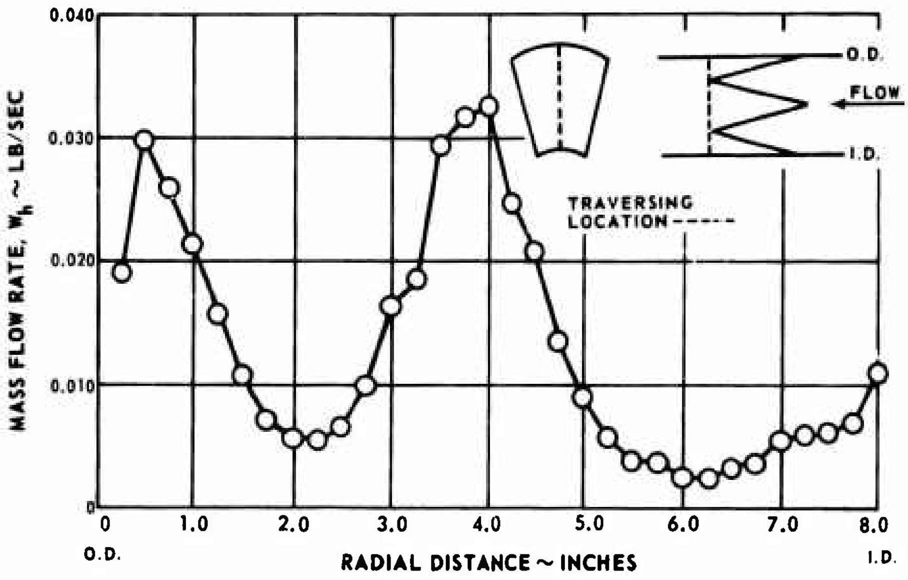

Figure 110. Mass Flow Profile on the Hot Side of the Matrix Package.

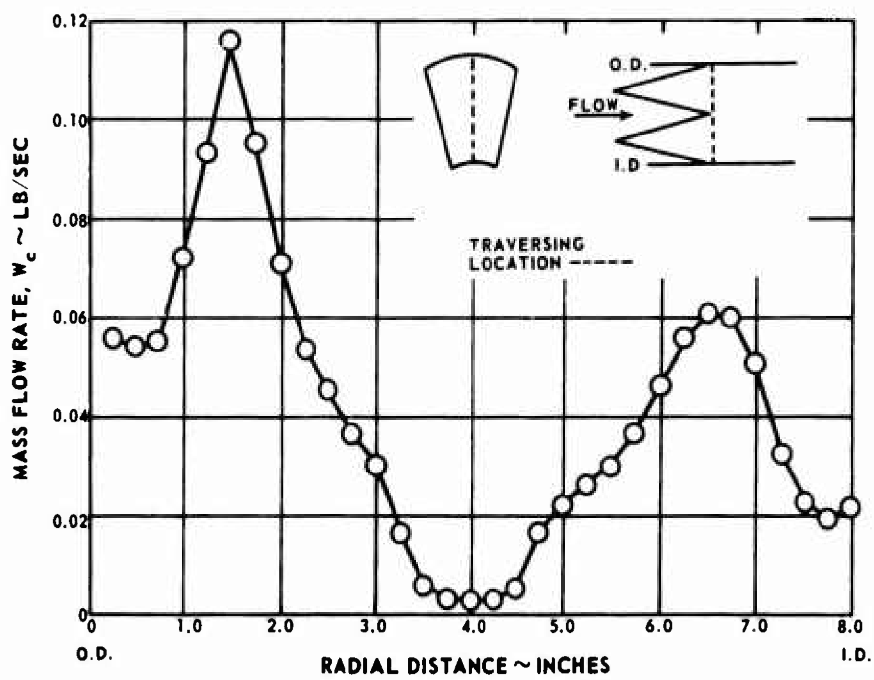

Figure 111. Mass Flow Profile on the Cold Side of the Matrix Package.

The local effectiveness measured radially across the package is shown in Figure 112 for the hot side and in Figure 113 for the cold side. The flow-weighted effectiveness for both the hot side and the cold side was lower than predicted. Testing was continued to resolve the discrepancies. These tests were performed with the intention of matching various parametric properties of the module with the corresponding ones of the rotary regenerator. The parameters which were matched are as follows: (1) Reynolds numbers of both streams; (2) the ratio of matrix to stream capacities, overall number of transfer units, and flow parameter ($W\sqrt{T}/P$), and (3) the ratio of the module dwell times in each stream. It is physically impossible to match all parameters simultaneously, because the frontal area ratios are different in the module and in the rotary regenerator. None of the tests succeeded in giving an indication of the reason for the discrepancy in effectiveness between the predicted values and the results of the module tests. Tests were also conducted to determine flow profiles on the downstream faces of the module with the effectiveness level remaining essentially unchanged. At this point, it was felt that if the discrepancies could not be resolved readily, the lower effectiveness values could be used as a baseline for evaluating flow distribution fixes to improve the regenerator performance. The planned fixes included turning vanes, as well as honeycomb sections in place of turning vanes, on each face of the matrix to assure uniform flow entering and leaving the matrix.

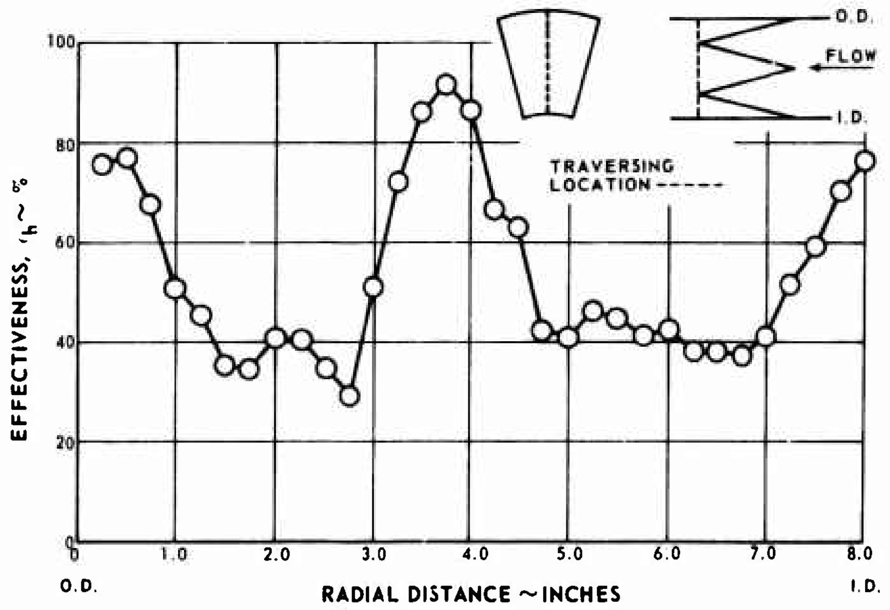

Figure 112. Effectiveness Profile on the Hot Side of the Matrix Package.

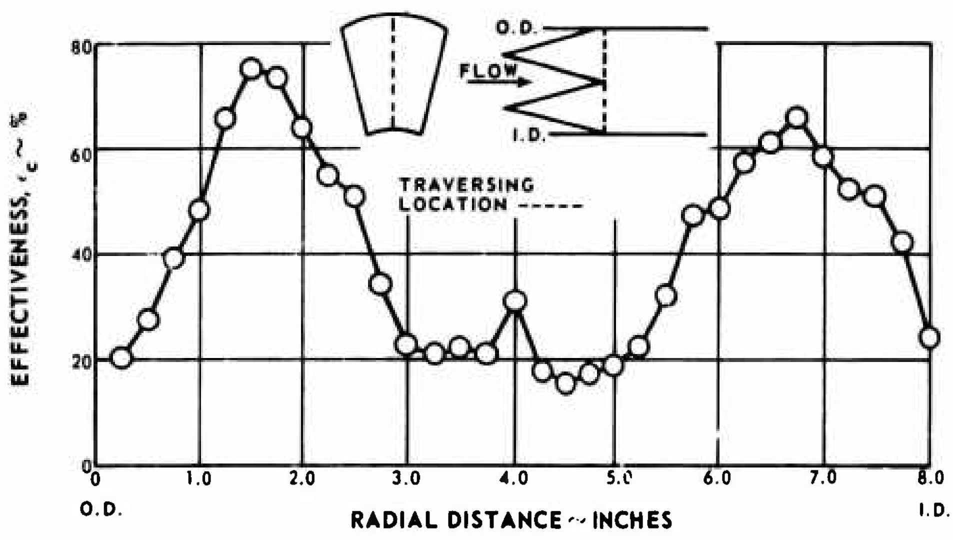

Figure 113. Effectiveness Profile on the Cold Side of the Matrix Package.

Honeycomb sections were enclosed in a 10-mesh, 0.35-inch-wire-diameter screen capsule and tack-welded to the matrix. Although a small improvement in performance was realized, it was difficult to determine whether the improvement was due to the honeycomb sections or to the added mass of the screens. Examination of the module after test showed that some of the honeycomb sections were crushed. This may have occurred during installation into the module.

Turning vanes were fabricated but were not tested, because the one available spare module was required as a replacement for the T74 rotary regenerator module which was damaged during engine test.

CONCLUSIONS

1. This rig shows much promise of being an intermediate step between heat transfer tests of core candidates and full scale regenerator tests, but requires further development.

2. Good agreement between predicted performance and measured effectiveness was obtained for a single module in normal (uniform) flow.

3. Poor agreement between predicted and integrated locally determined effectiveness was obtained for a single module with oblique flow. It

is felt that the largest single contributor to this problem is in the area of associating the correct local flow with the correct local temperature response. This again points out the degree of difficulty of local measurements in nonuniform flow.

RECOMMENDATIONS

It is recommended that further development of this rig and technique be pursued, with particular emphasis on instrumentation improvements and the addition ot flow mixers of low heat capacity on the downstream side of each duct.

APPENDIX VI

PHOTOGRAPHS OF MAJOR REGENERATOR AND ENGINE COMPONENTS

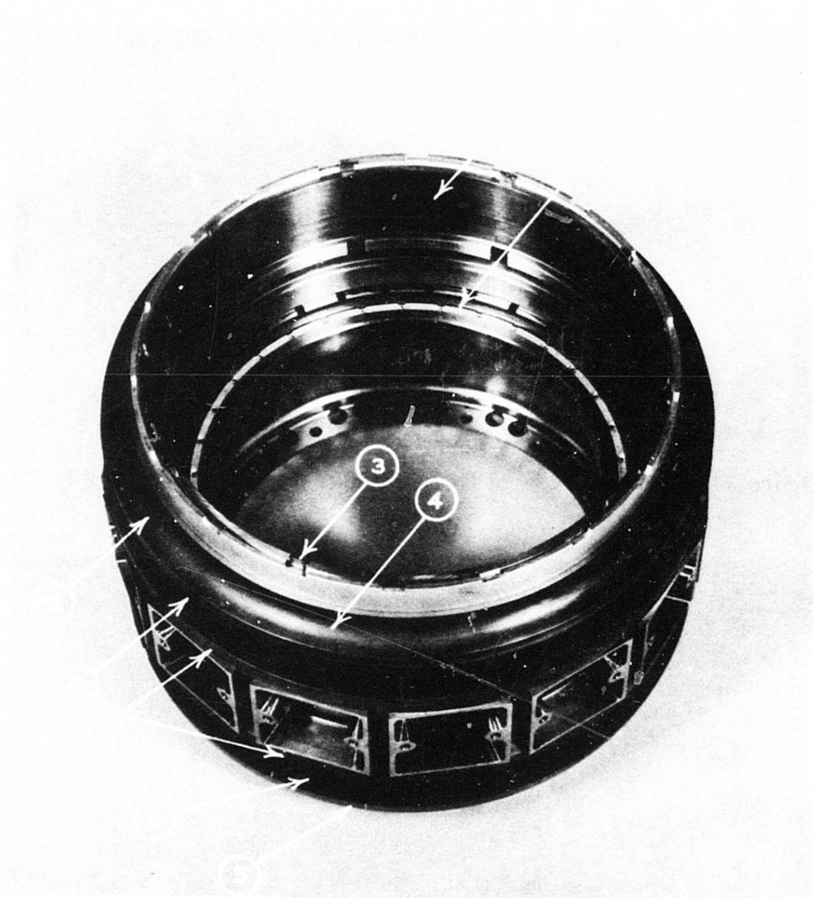

Figure 114. Rear View of Bearing and Seal Area Showing Inner Ring Seal on Hub: (1) Hub, (2) Bearing, (3) Tab Lock Washer, (4) Nut, (5) Seal Plate, (6) Carbon Ring Seal, (7) Seal Plate.

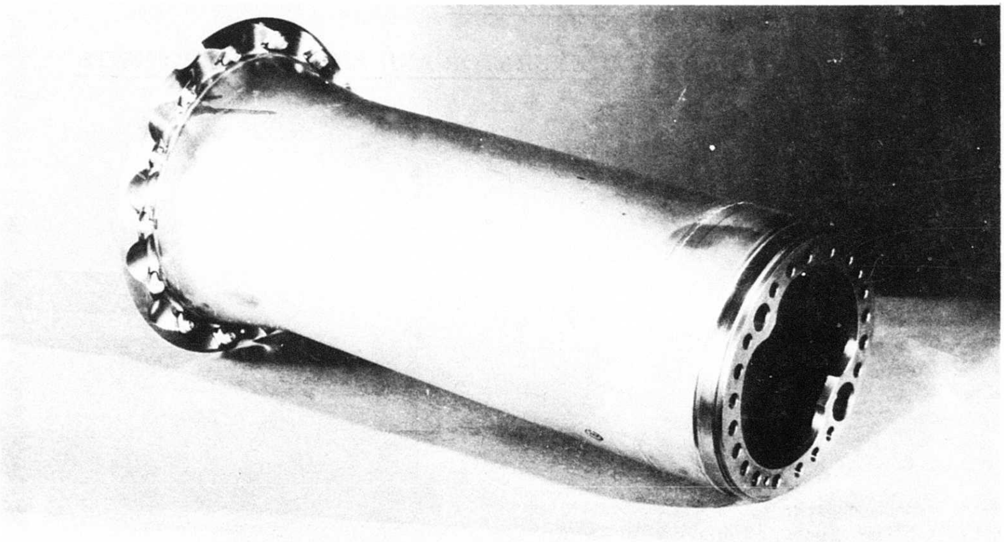

Figure 115. Rear View of Gearbox Extension Case Assembly.

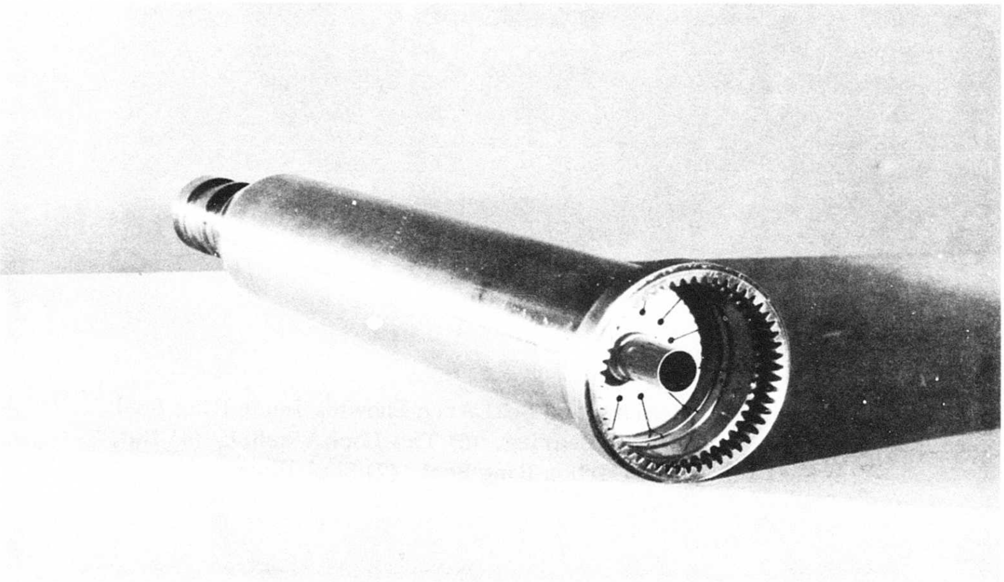

Figure 116. Rear View of Gearbox Extension Shaft.

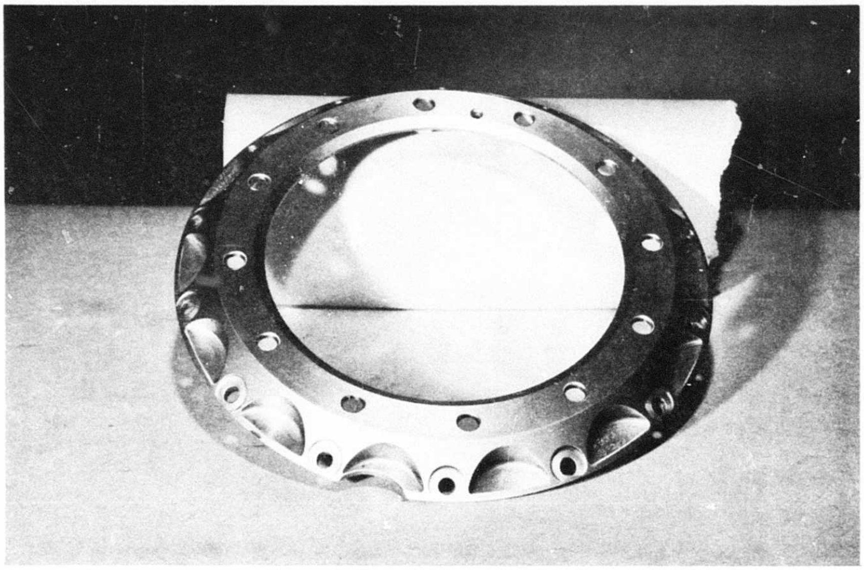

Figure 117. Front View of Gearbox Adapter Assembly Which Fits on Front of Gearbox Extension Case.

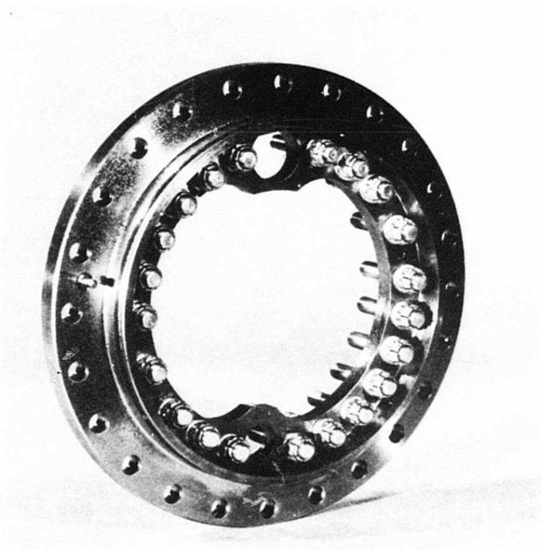

Figure 118. Rear View of Turbine Exhaust Case Adapter Assembly.

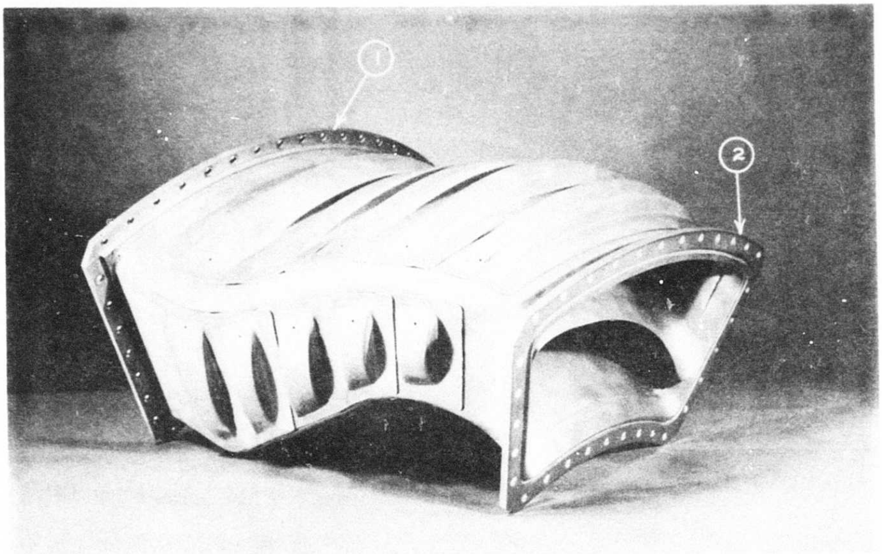

Figure 119. Duct Leading From Regenerator to Burner Inlet: (1) Regenerator End, (2) Burner End.

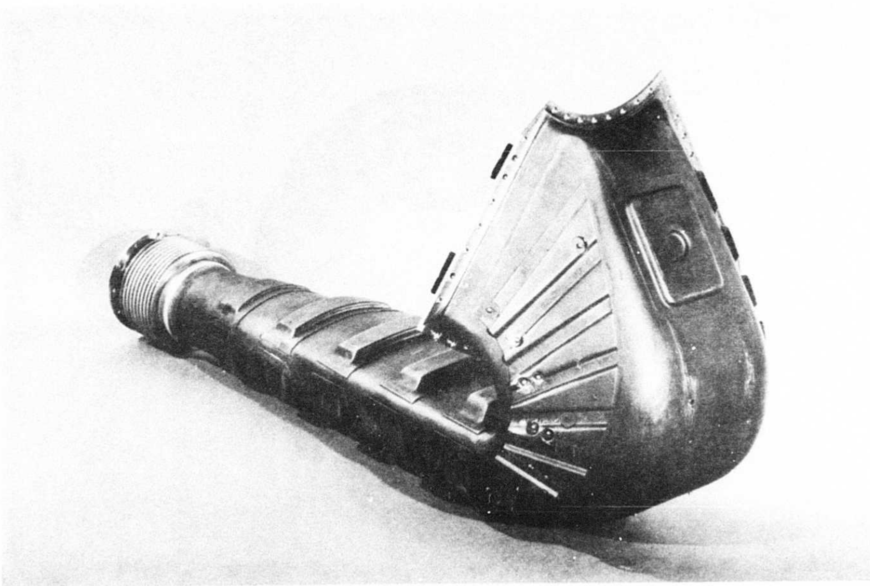

Figure 120. Front View of Compressor Discharge Duct.

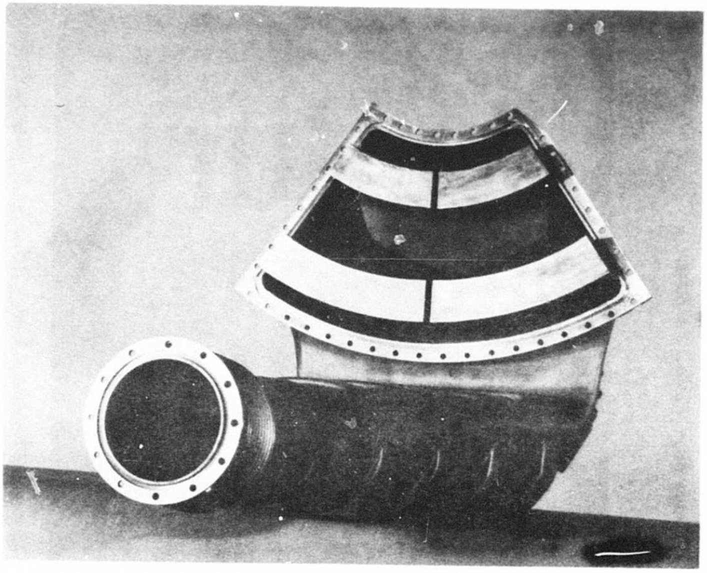

Figure 121. Rear View of Compressor Discharge Duct.

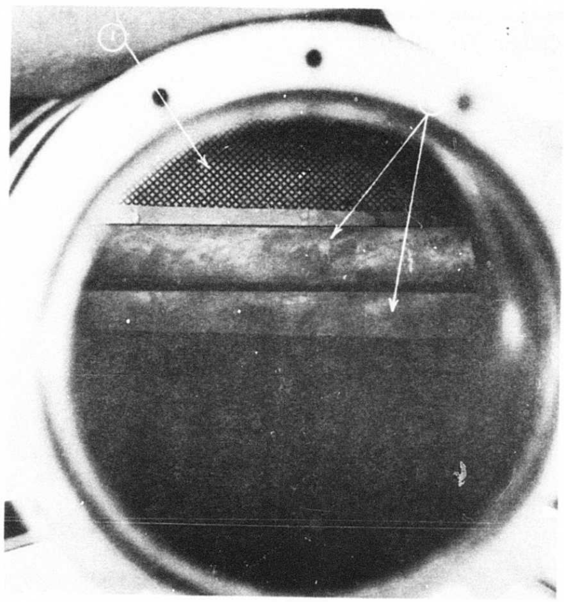

Figure 122. Interior View of Compressor Discharge Duct: (1) Screening, (2) Frey Vanes.

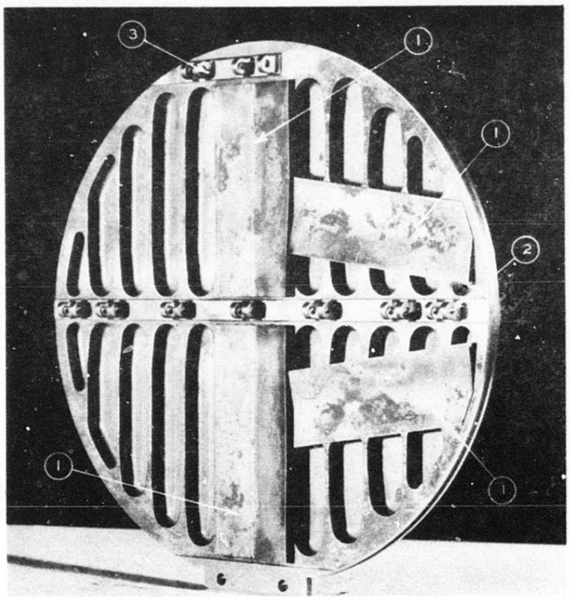

Figure 123. Bulkhead Assembly: (1) Four Strips Which Act as Seals Against the Screening Package, (2 & 3) Lugs Which Hold Pins for Inner and Outer Tie Plates.

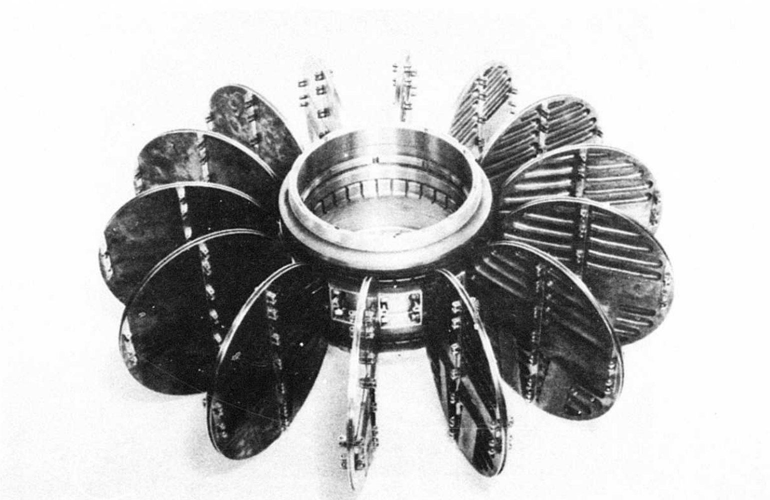

Figure 124. Hub With Ring Seals and Bulkheads Bolted in Place.

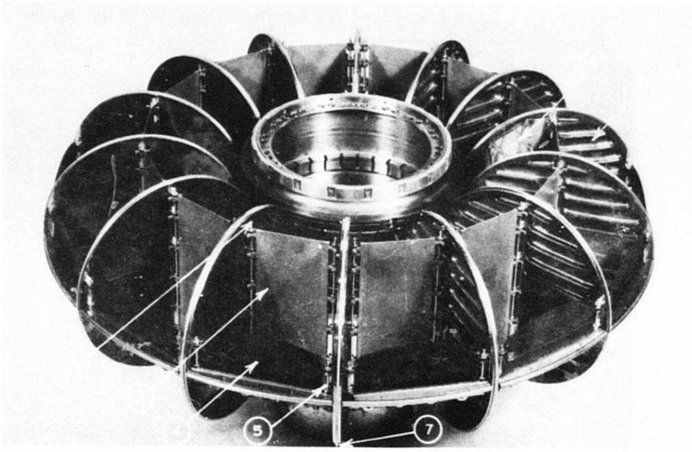

Figure 125. Partially Built-Up Hub: (1) Bulkhead Assembly, (2) Tie-Plate Pin, (3) Inner Tie Plate, (4) Outer Tie Plate and Seal Assembly, (5) Tie-Plate Pin, (6) Inner Matrix Package, (7) Piston Ring.

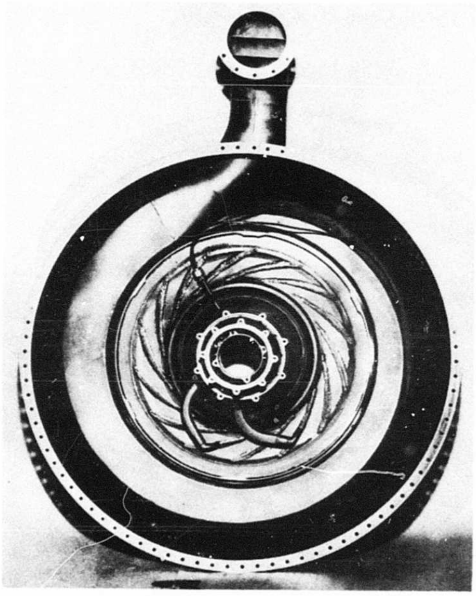

Figure 126. Compressor Scroll Case.

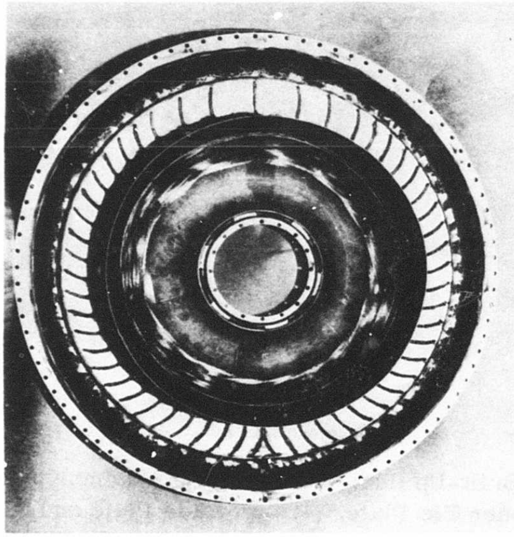

Figure 127. Burner Outer Entry Duct and Radial Deswirl Vane Assembly.

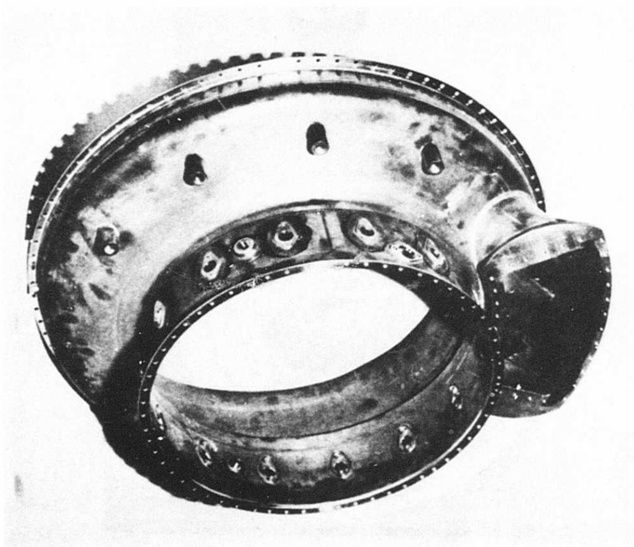

Figure 128. Burner Scroll Case.

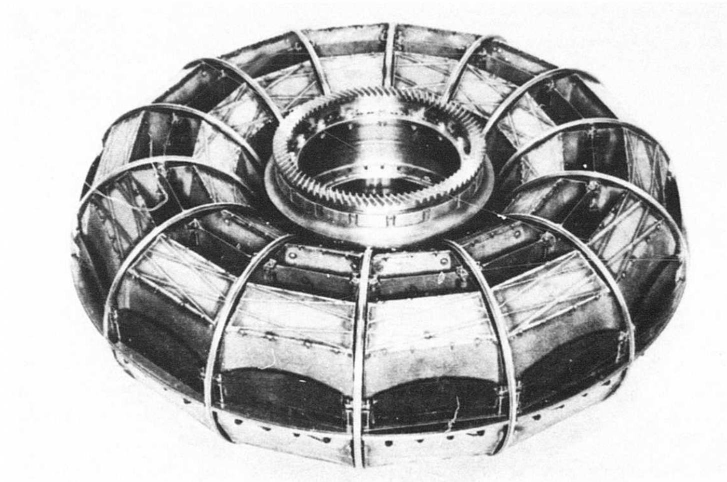

Figure 129. Side View of the Cold Side of the Rotor Assembly.

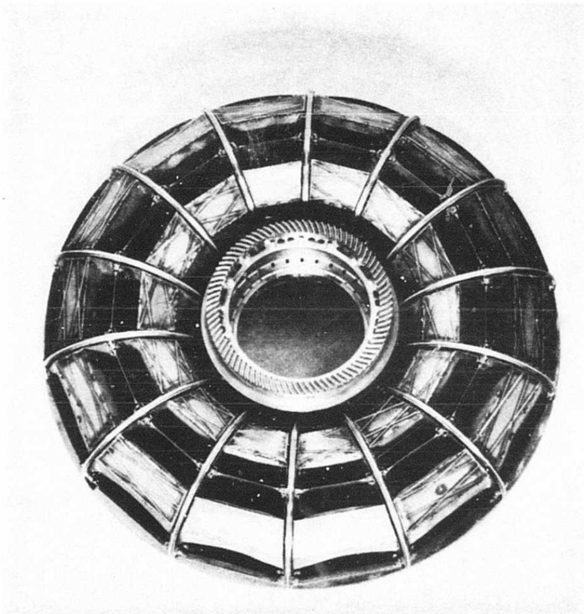

Figure 130. Front View of the Cold Side of the Rotor Assembly.

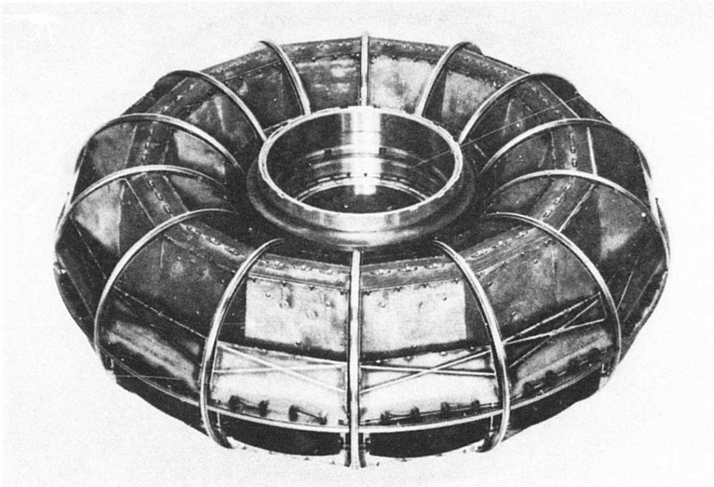

Figure 131. Side View of the Hot Side of the Rotor Assembly.

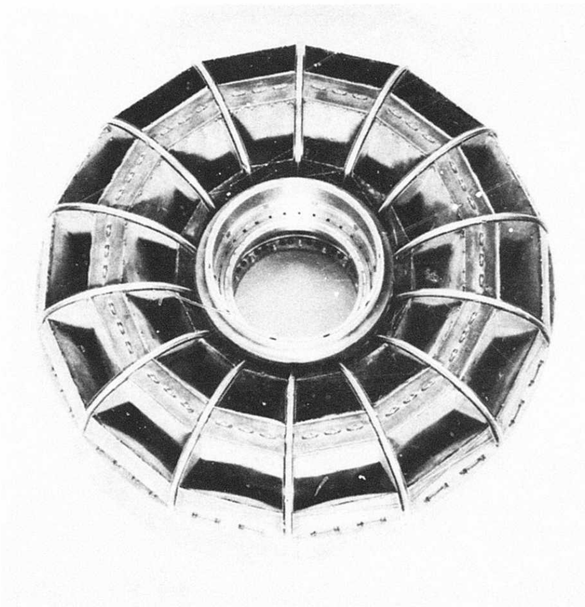

Figure 132. Front View of the Hot Side of the Rotor Assembly.

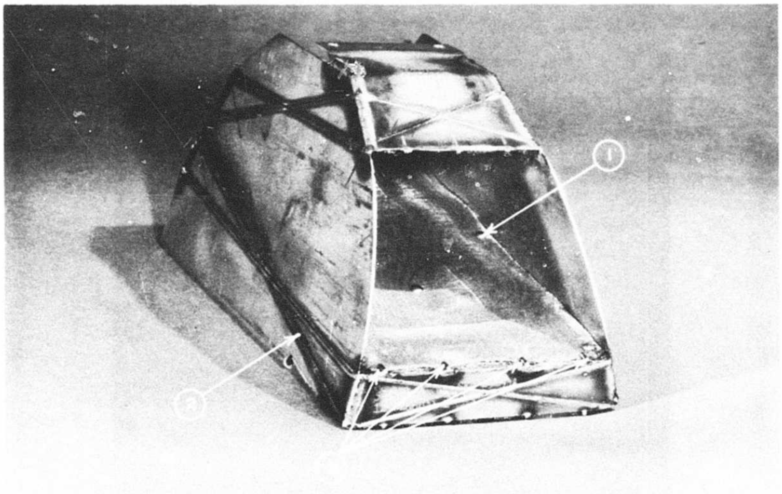

Figure 133. Hot Side of the Inner Matrix Package: (1) Rivets Holding Screens Together, (2) Welds Holding Screen Packs in Position, (3) Fingers Preventing Lifting of Screen Ends Into Airstream.

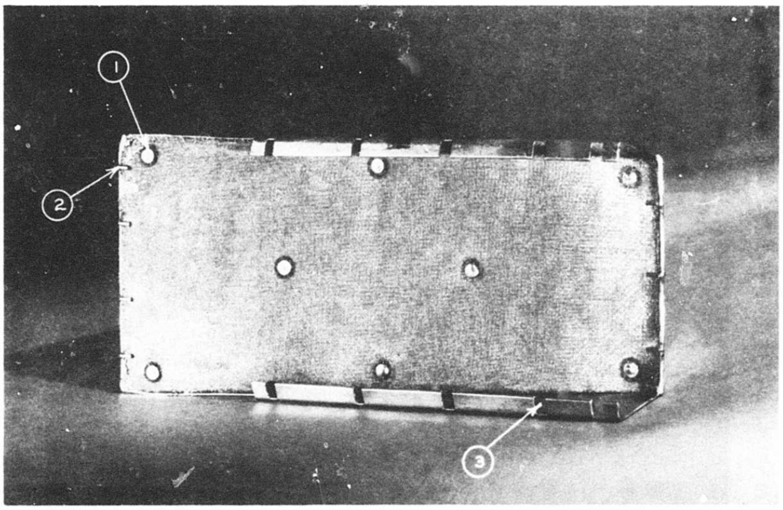

Figure 134. Radial View of the Inner Matrix Package: (1) Screen Rivets, (2) Screen Restraining Fingers, (3) Slots for Lugs From Inner Tie Plate.

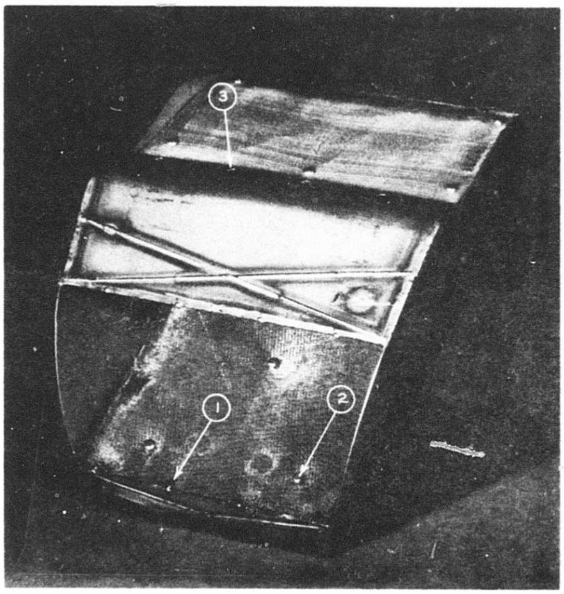

Figure 135. Hot Side of the Outer Matrix Package: (1) Screen Restraining Fingers, (2) Screen Rivets, (3) Bolt Holes for Bolts From Outer Tie Plate.

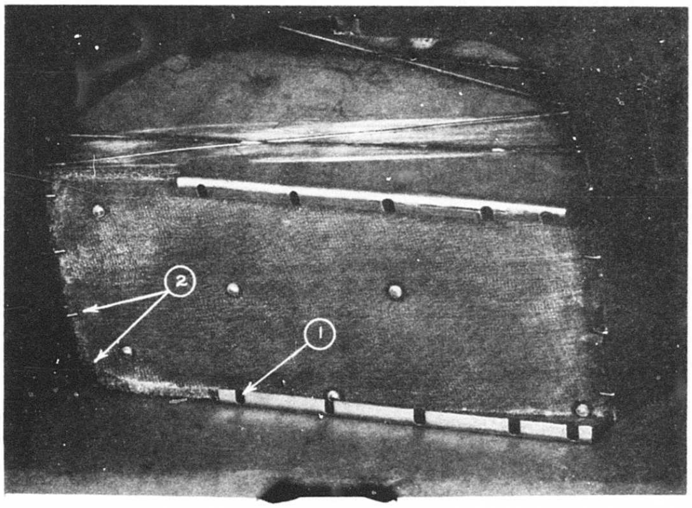

Figure 136. Radial View of Outer Matrix Package: (1) Slots for Lugs From Inner Tie Plate, (2) Screen Restraining Fingers.

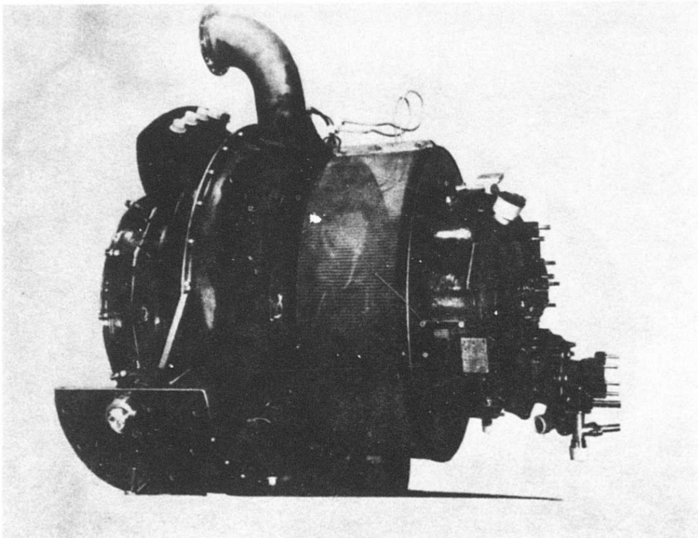

Figure 137. Gas Generator Assembly.

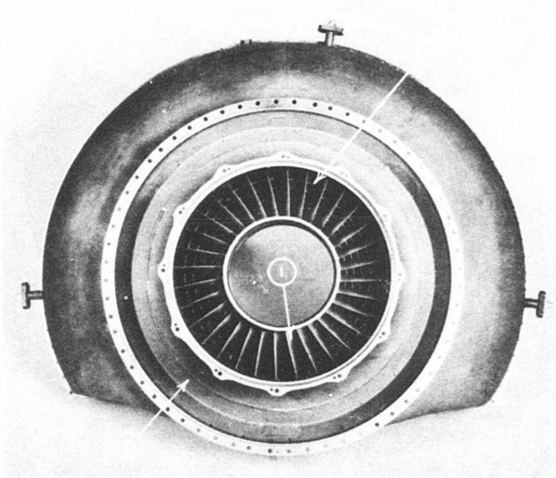

Figure 138. Front View of Turbine Exhaust Duct Inlet: (1) Antiswirl Vanes, (2) Circumferential Vanes, (3) Instrumentation Bosses, (4) Drain Boss, (5) Burner Annulus Space.

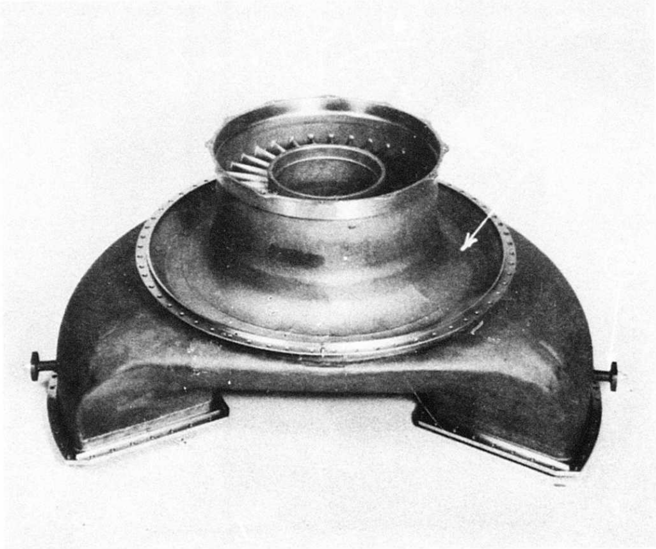

Figure 139. Side View of Turbine Exhaust Duct Inlet: (A) Direction of Flow, (1) Burner Chamber, (2) Instrumentation Bosses.

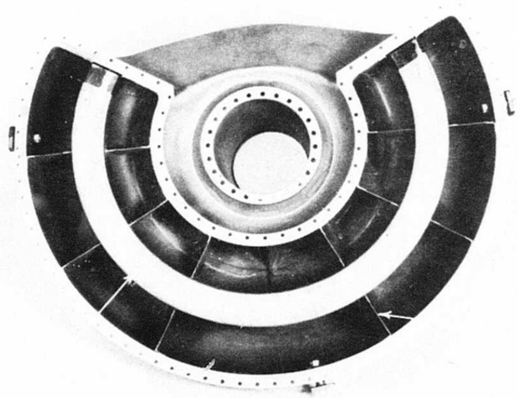

Figure 140. Rear View of the Turbine Exhaust Duct Exit: (1) Radial Vanes, (2) Circumferential Splitter, (3) Instrumentation Bosses.

Figure 141. Side View of the Turbine Exhaust Duct Exit: (1) Radial Vanes, (2) Circumferential Splitter, (3) Instrumentation Bosses.

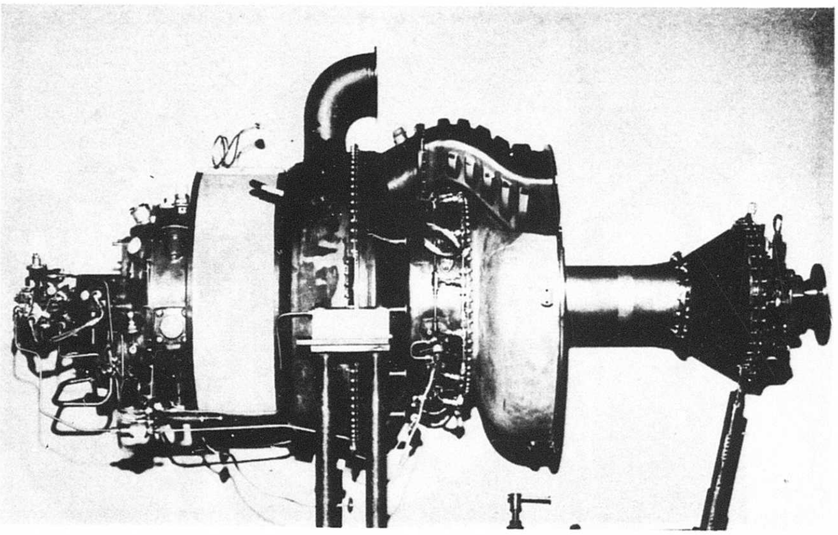

Figure 142. Side View of Partially Assembled Regenerative Engine.

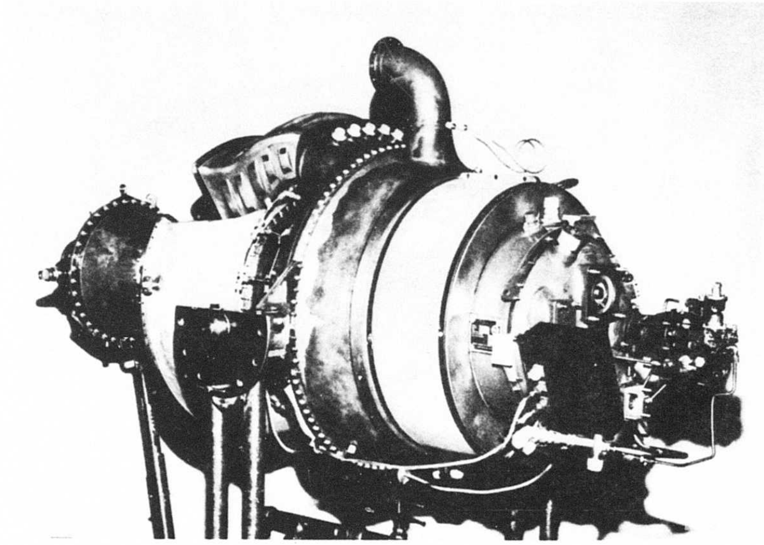

Figure 143. Partially Assembled Engine; Accessory Gearbox at Right.

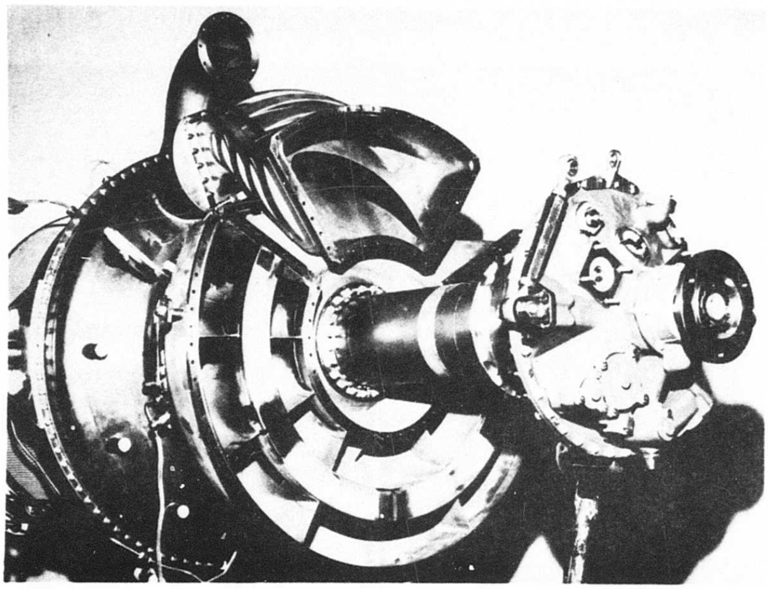

Figure 144. Partially Assembled Engine; Reduction Gearbox at Right.

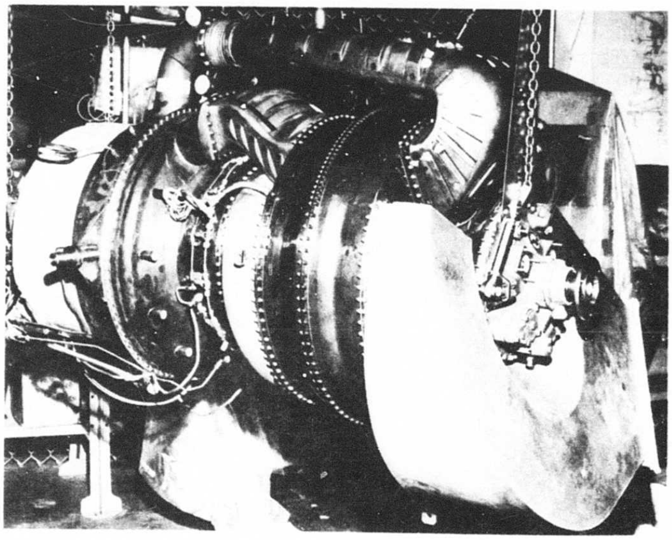

Figure 145. Complete Engine Assembly With Test Exhaust Duct Attached; Reduction Gearbox at Right.

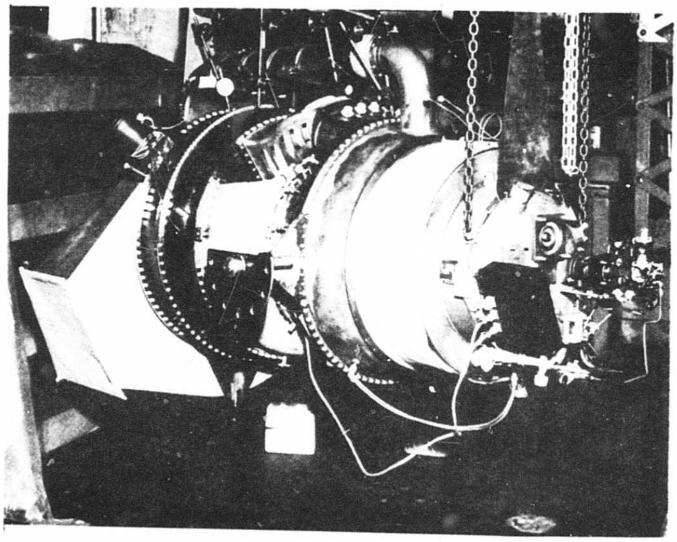

Figure 146. Complete Engine Assembly With Test Exhaust Duct Attached; Accessory Gearbox at Right.

APPENDIX VII

LAYOUTS OF THE HIGH-EFFECTIVENESS REGENERATOR AND T74 TEST BED INTEGRATION

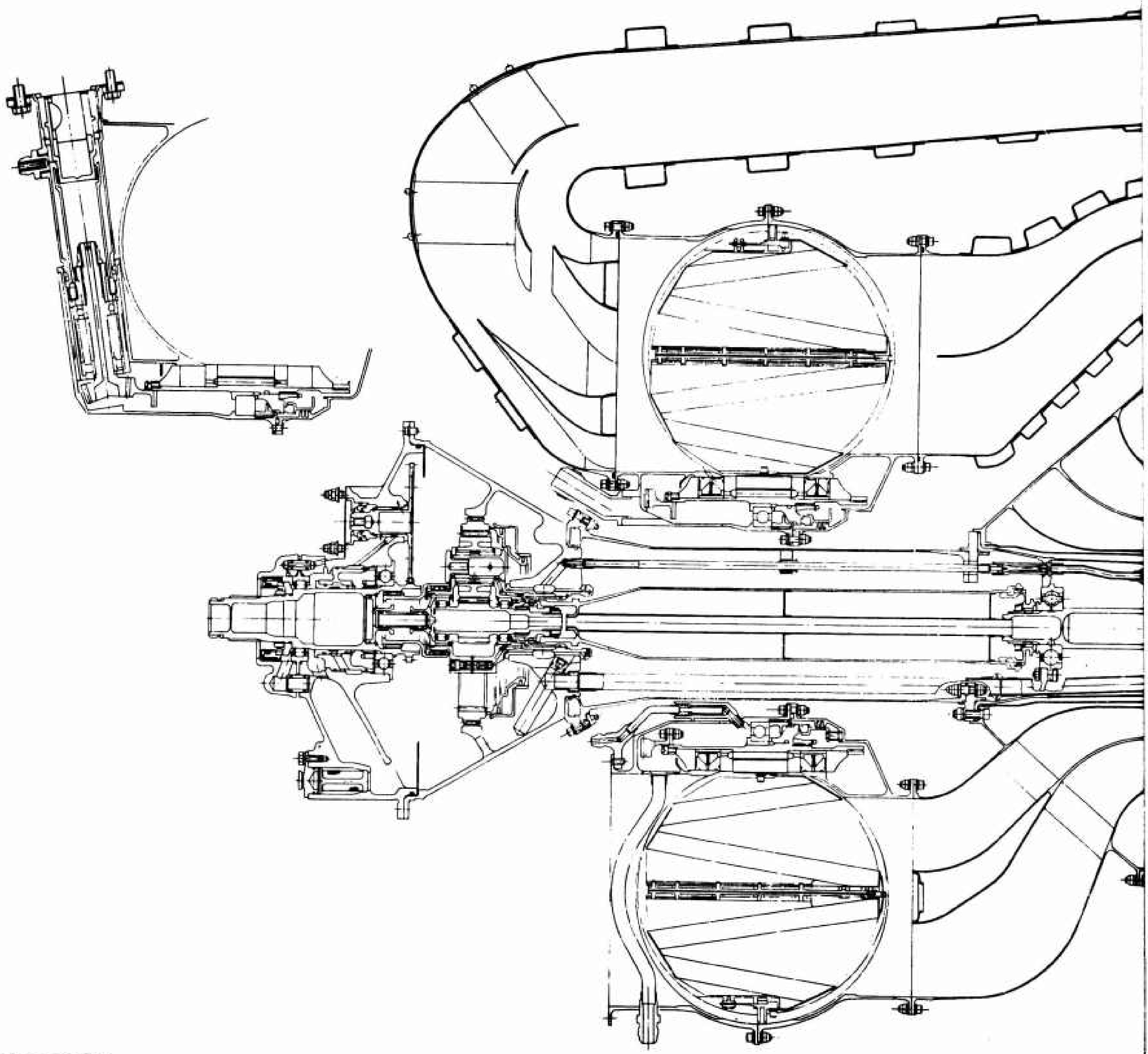

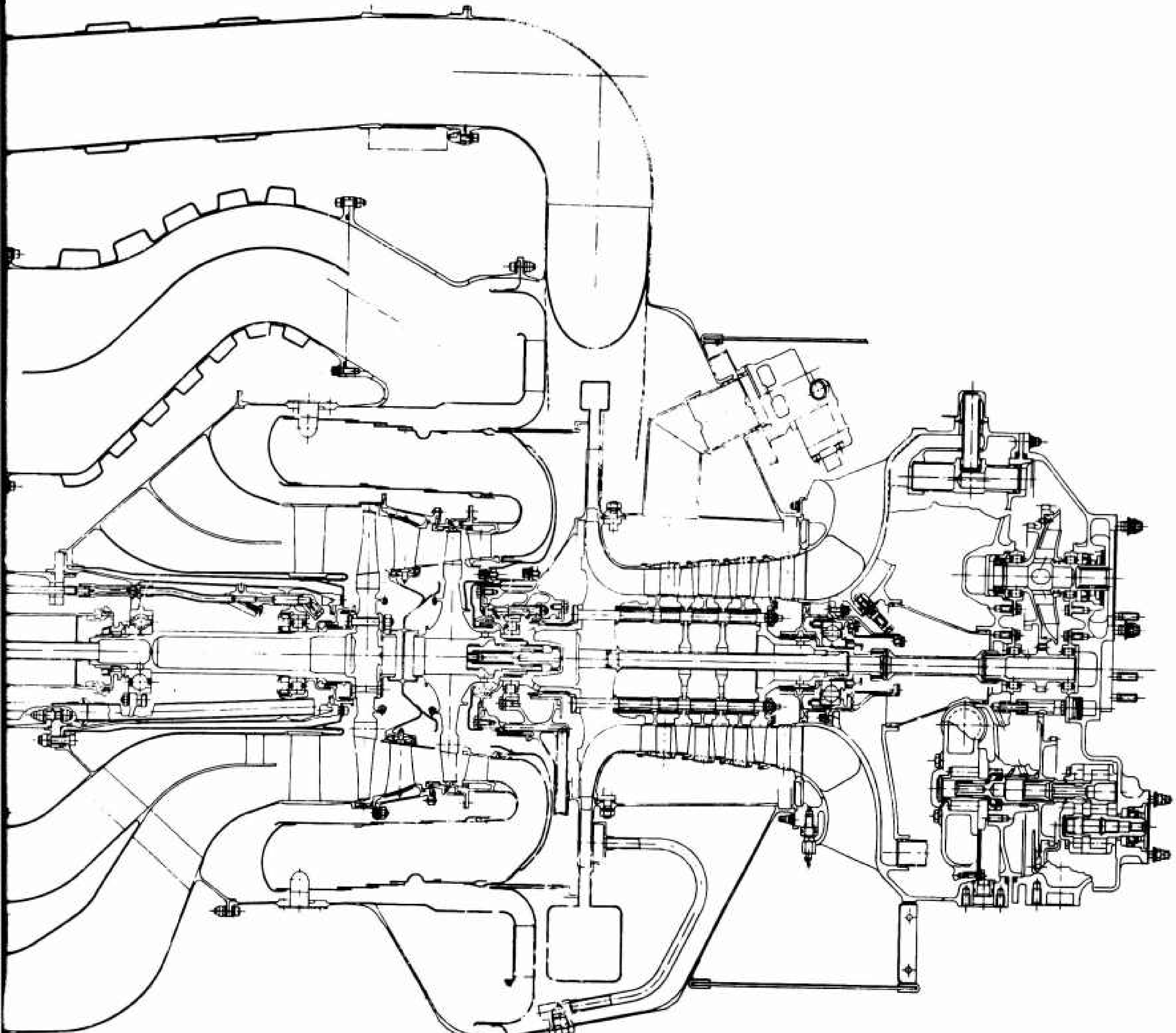

2

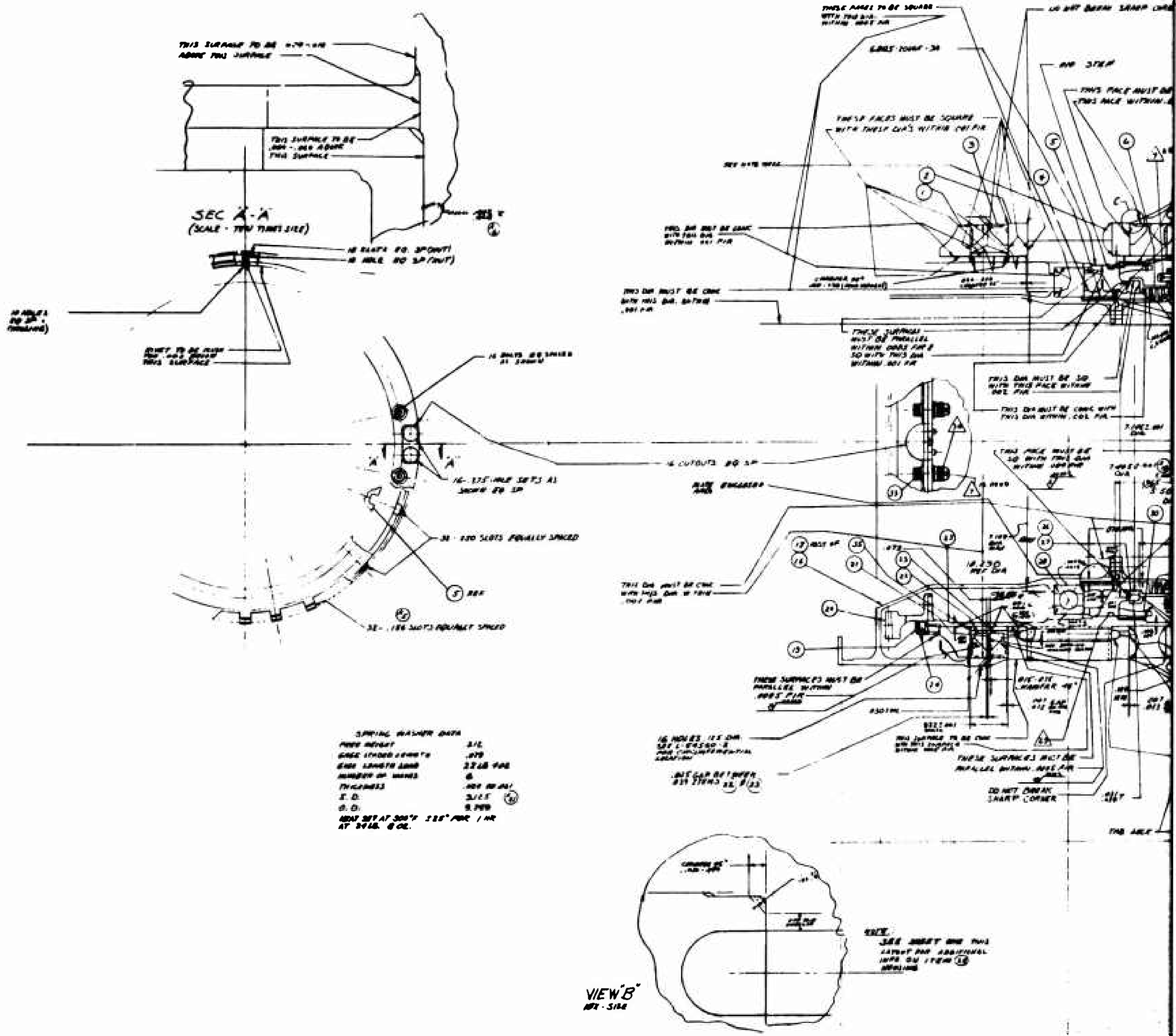

1

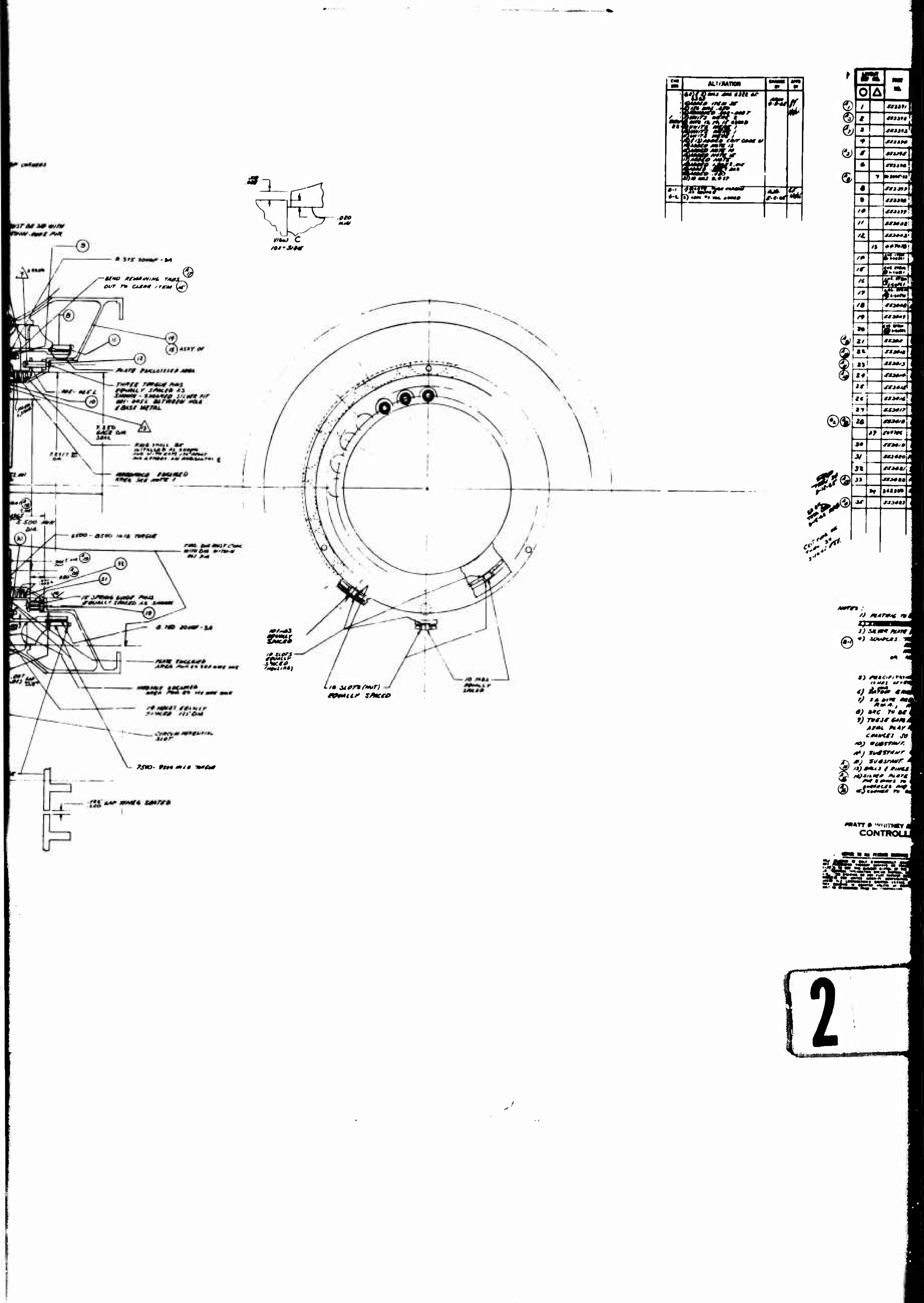
ALTERATION
VIEW C
10 SLOTS (NUT) EQUALLY SPACED
NOTES:
2

3

CHG SYM	ALTERATION	CHANGE BY	APPD BY
[illegible]	[illegible]	[illegible]	[illegible]
B-1	[illegible]	[illegible]	[illegible]
B-2	[illegible]	[illegible]	[illegible]

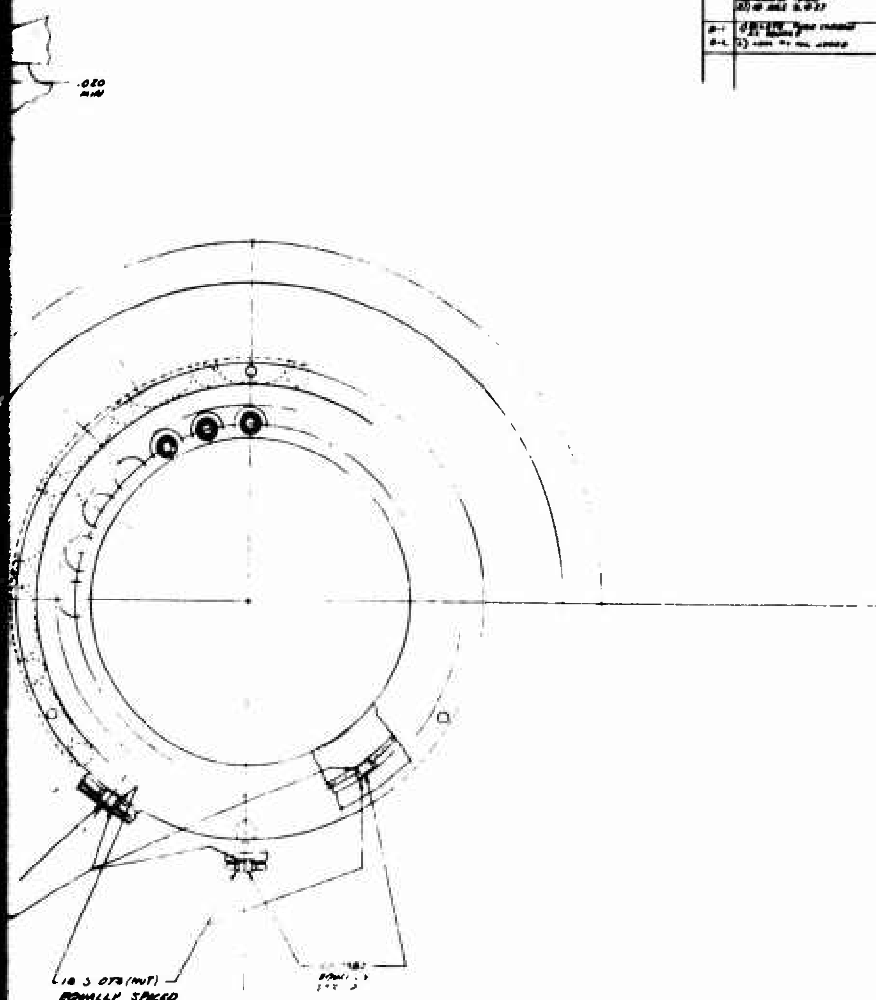

LAYOUT REF NO. ○	LAYOUT REF NO. △	PART NO.	QTY	PART NAME	REF PART NO.	MATERIAL	HEAT TREATMENT OR REMARKS					
1		553391	2	SEAT	[illegible]	[illegible]	[illegible]	[illegible]	[illegible]			
2		553392	2	SEAT		AMS 5613	[illegible]	[illegible]	[illegible]			
3		553393	4	SEAL	[illegible]	[illegible]	[illegible]		[illegible]			
4		553394	1	NUT		[illegible]	[illegible]	[illegible]	U			
5		553395	1	SEAT	[illegible]	AMS 5613	[illegible]	[illegible]	[illegible]			
6		553396	1	HOUSING	[illegible]	AMS 5613	[illegible]	[illegible]	[illegible]			
	7	[illegible]	19	PIN, COTTER		AMS 7210			—			
8		553397	1	NUT	[illegible]	AMS 5613	[illegible]	[illegible]	U			
9		553398	1	WASHER [illegible] .003 THK		AMS 5510			U			
10		553399	1	WASHER [illegible] .003 THK		AMS 5510			U			
11		553002	1	WASHER [illegible] THK		AMS [illegible]			U			
12		553003	3	PIN	[illegible]	AMS 5613	[illegible]		U			
	13	447078	1	PACKING PREFORMED		AMS 7270			U			
14		[illegible]	1	HOUSING RB INNER	[illegible]	[illegible]	[illegible]		-			
15		[illegible]	1	HOUSING RB ASSY	[illegible]	—	[illegible]	[illegible]	-			
16		[illegible]	1	HOUSING RB INNER	[illegible]	[illegible]	[illegible]		—			
17		[illegible]	1	HOUSING RB ASSY	[illegible]	—	[illegible]	[illegible]	—			
18		553008	15	GUIDE-BRG [illegible]	[illegible]	AMS 5613			U			
19		553009	1	NUT	[illegible]	AMS 6322	[illegible]	[illegible]	U			
20		[illegible]	1	GEAR	[illegible]	AMS [illegible]	[illegible]		—			
21		55301[illegible]	2	WASHER SPRING	[illegible]	AMS [illegible]	[illegible]	[illegible]	U			
22		553012	2	RING	[illegible]	AMS 5613	[illegible]	[illegible]	U			
23		553013	2	RING	[illegible]	AMS [illegible]	[illegible]	[illegible]	✓			
24		553014	2	RIVET-TUBULAR [illegible]	[illegible]	AMS [illegible]	SAME AS [illegible]		U			
25		553015	1	HOUSING		AMS 5613	[illegible]	[illegible]	[illegible]			
26		553016	1	SEAL RING	[illegible]	[illegible]	[illegible]		[illegible]			
27		553017	1	SEAL ASSY	[illegible]	—	[illegible]		[illegible]			
28		553018	1	BRG		[illegible]	[illegible]		[illegible]			
	29	507706	1	PACKING PREFORMED		AMS 7270			—			
30		553019	1	NUT		AMS 5613	[illegible]	[illegible]	U			
31		553020	15	SPRING	[illegible]	AMS [illegible]	[illegible]	[illegible]	U			
32		553021	2	SEAL - PISTON RING	[illegible]	AMS 7311	[illegible]		[illegible]			
33		553022	16	BOLT [illegible]	[illegible]	AMS 6322	[illegible]		U			
	34	[illegible]	16	NUT		AMS 6322	[illegible]	[illegible]	—			
35		553023	2	SPACER		AMS 5613	[illegible]	[illegible]	[illegible]			

NOTES:

1) PLATING TO BE .003-.005 AFTER [illegible]

[redacted]

3) SILVER PLATE, PER AMS 2410 OR 2412 .0003-.0005 THICK [illegible] AFTER PLATING

4) SOURCES [redacted] - DATA LIST [illegible] B

OR NATIONAL CARBON CO.

CDJ 83 , IMPREGNATION PER [illegible] SPEC.

5) PRECIPITATION HEAT TREAT AT 1400°F ± 25° FOR 16 HRS AFTER FORMING

6) EATON ENGINEERING CORP. - MUSKEGON, MICHIGAN - [illegible] DATA LIST [illegible]

7) SA BIVE PROD. DATA LIST [illegible] B, R.W.A., KOPPERS CO. INC.

8) BRG TO BE DOUBLE [illegible] GROUND & WITH A NARROW INNER RACE

9) THESE GAPS ARE WITH BRG RACES IN NORMAL POSITION. TOTAL AXIAL PLAY FOR BRG ASSUMED TO BE .004. IF AXIAL PLAY CHANGES SO SHOULD GAPS CHANGE ACCORDINGLY

10) SUBSTANT. NOTE FOR CRIT. CODE [illegible]

11) SUBSTANT. NOTE FOR CRIT. CODE 1A - [illegible]

12) SUBSTANT. NOTE FOR CRIT CODE - [illegible]

13) BALLS & RINGS MUST BE STABILIZED FOR NO DISTORTION AT 600°F

14) SILVER PLATE PER AMS 2412 NO STRIKE METAL REQUIRED. BAKE AT 425° TO 500°F FOR 2 HOURS TO CHECK FOR BOND. PLATE .0005-.0015 THICK ON LAND RIDING SURFACES AND BALL POCKETS. OTHER SURFACES OPTIONAL.

15) CORNER TO CLEAR .035 MAX FILLET R, I.D. & OD MAX CORNER BREAKOUT .010 MAX I.D. & O.D.

L-64560

PRATT & WHITNEY AIRCRAFT
CONTROLLED

LAYOUT
T-39
LAYOUT No. L-64560

PRECEDING PAGE BLANK-NOT FILMED

CONFIDENTIAL

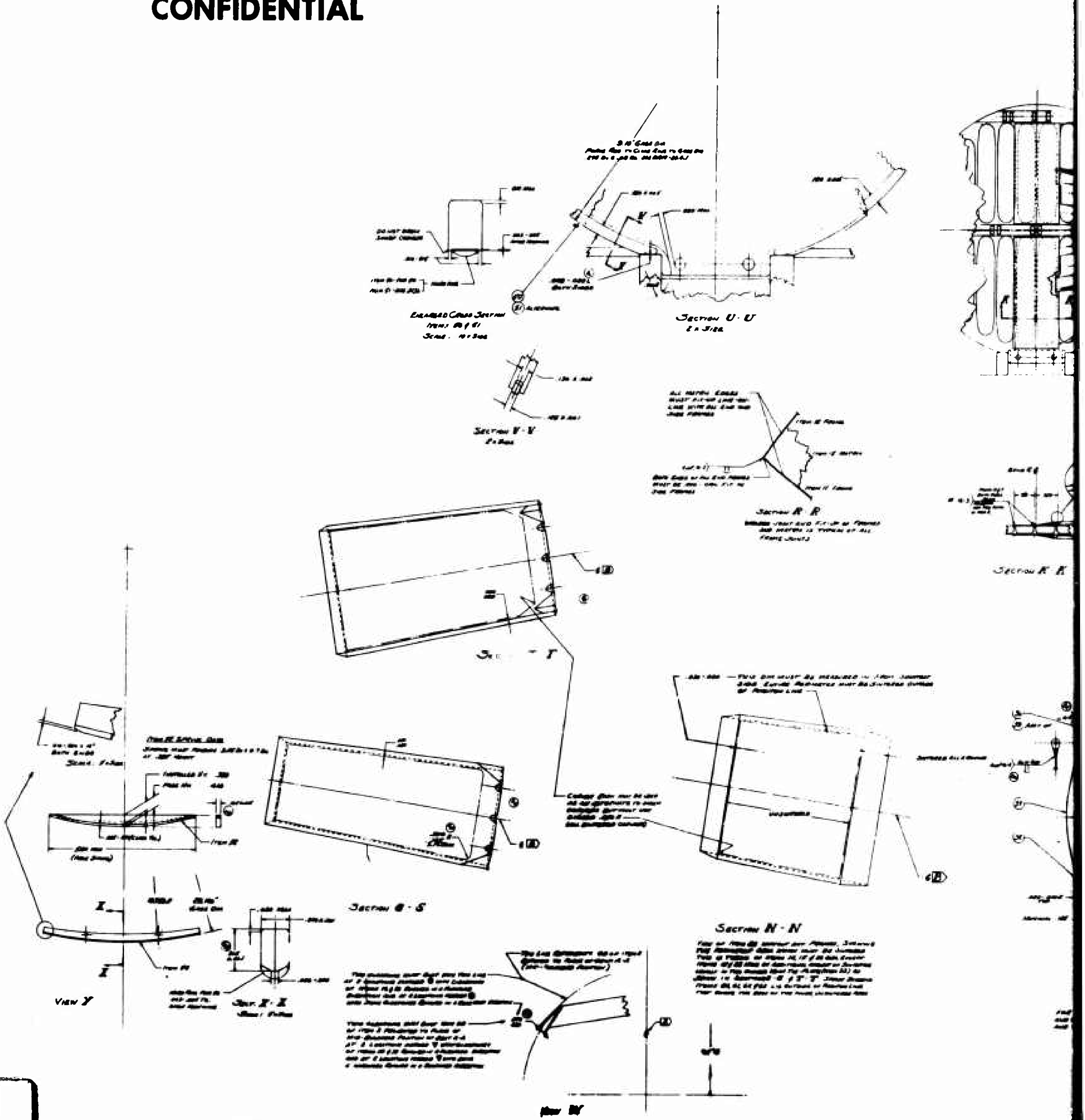

1

CONFIDENTIAL

2

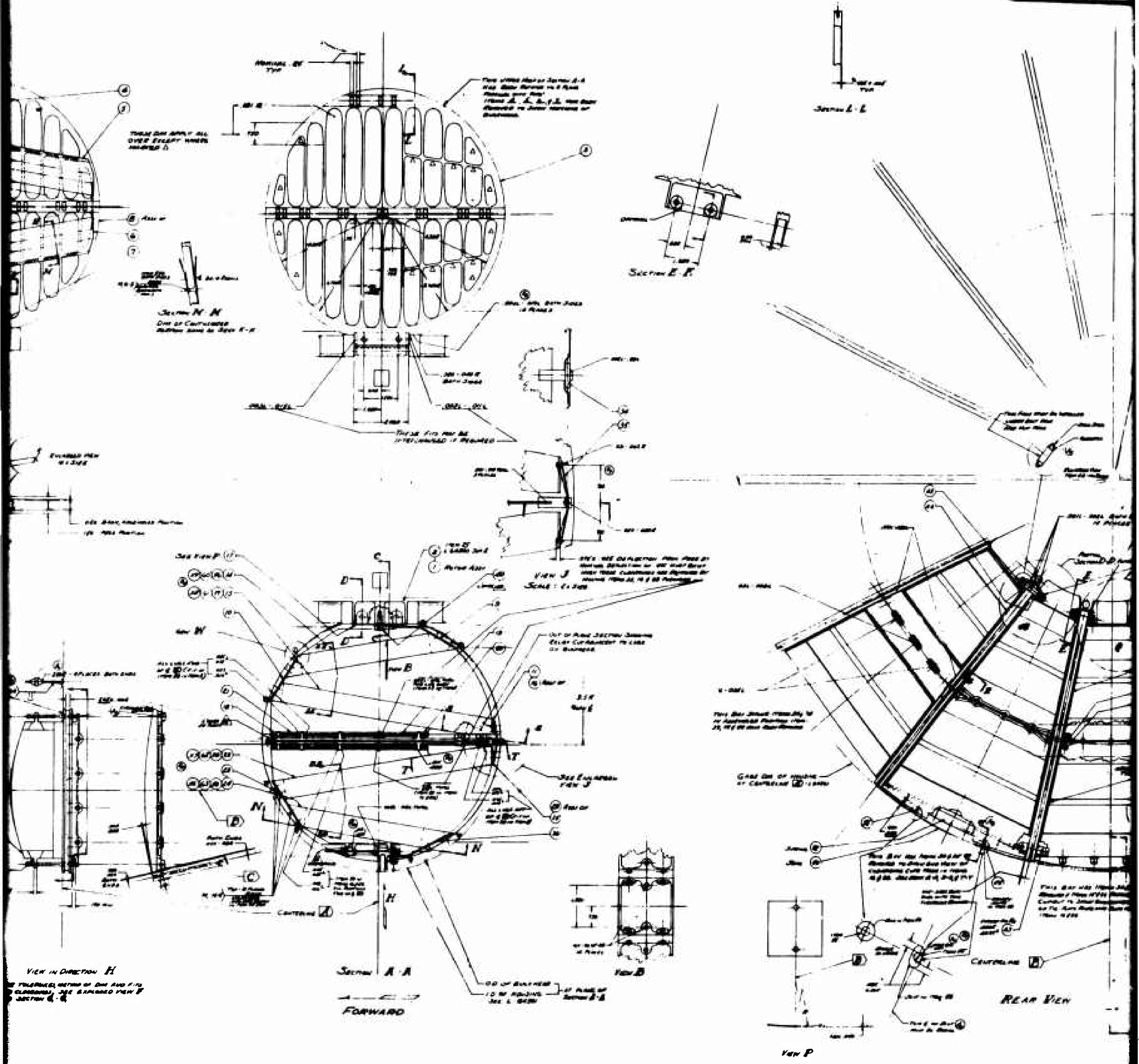
Section L-L
Section E-E
Section N-N
View J
Scale: 2x Size
View in Direction H
Section A-A
Forward
View B
Rear View
View P

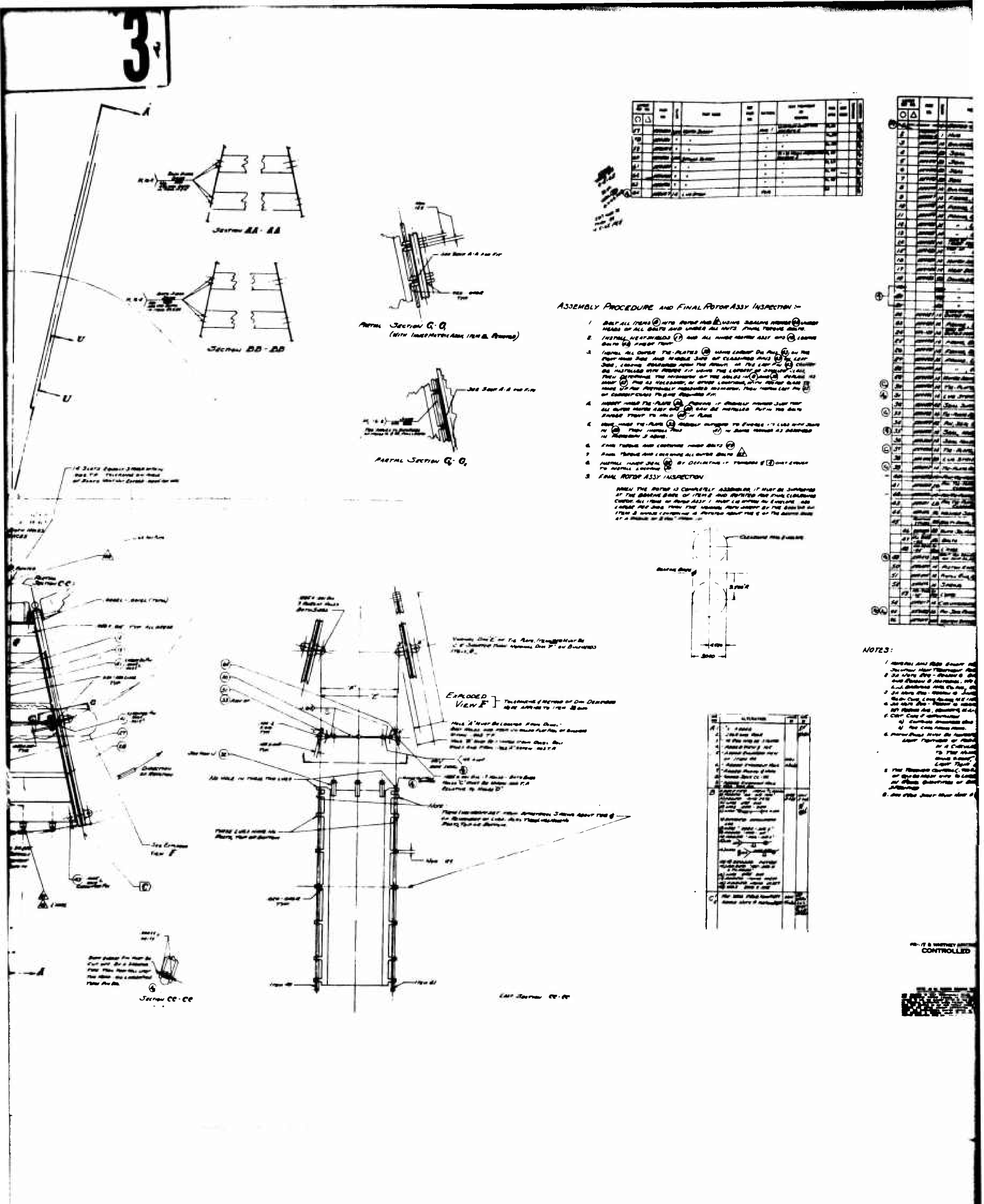
3
Section AA - AA
Section BB - BB
Partial Section G - G
Partial Section G - G
Assembly Procedure and Final Rotor Assy Inspection :-
Final Rotor Assy Inspection
Exploded View F
Section CC - CC
Notes:
CONTROLLED

4

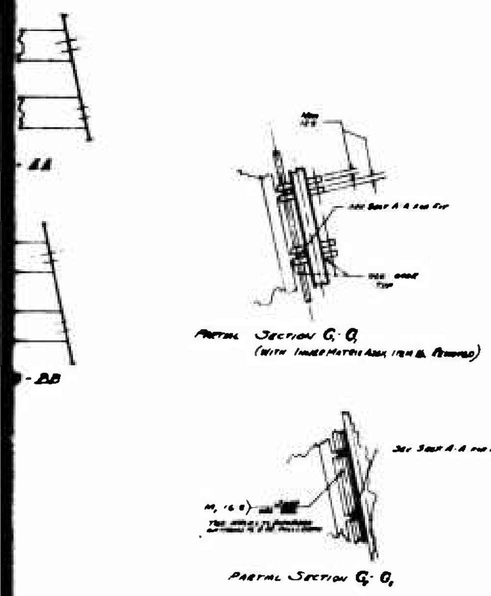

PARTIAL SECTION G-G (WITH INNER ROTOR ASSY ITEM B REMOVED)

PARTIAL SECTION G-G

ASSEMBLY PROCEDURE AND FINAL ROTOR ASSY INSPECTION :-

1. [illegible]
2. INSTALL HEAT SHIELDS [illegible]
3. INSTALL ALL OUTER TIE-PLATES [illegible]
4. [illegible]
5. [illegible]
6. [illegible]
7. [illegible]
8. INSTALL INNER SEAL [illegible]
9. FINAL ROTOR ASSY INSPECTION

[illegible]

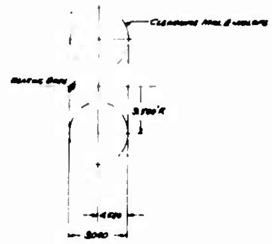

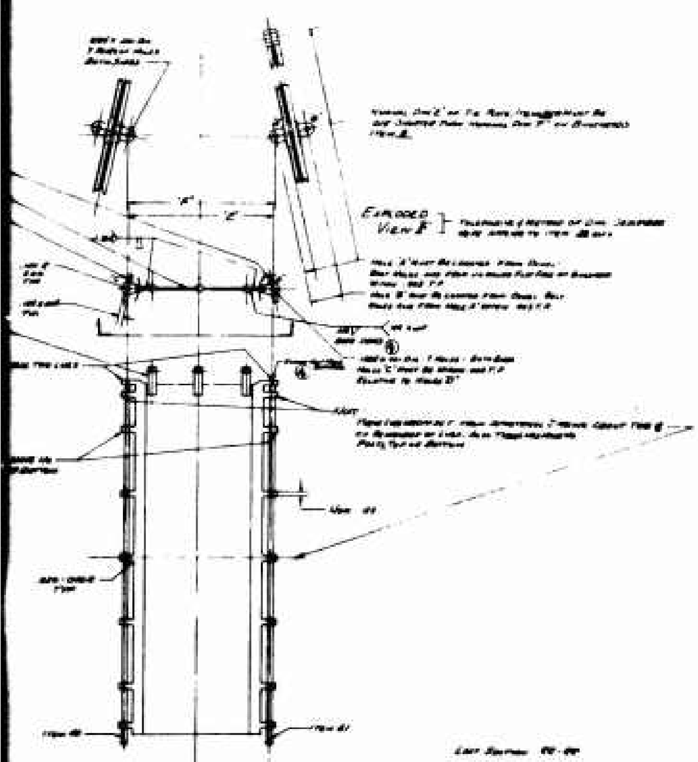

EXPLODED VIEW F

NOTES:

1. [illegible]
2. [illegible]
3. [illegible]
4. [illegible]
5. [illegible]
6. [illegible]
7. [illegible]
8. [illegible]

L 64960-1

PRATT & WHITNEY AIRCRAFT CONTROLLED

LAYOUT

L 64560

1

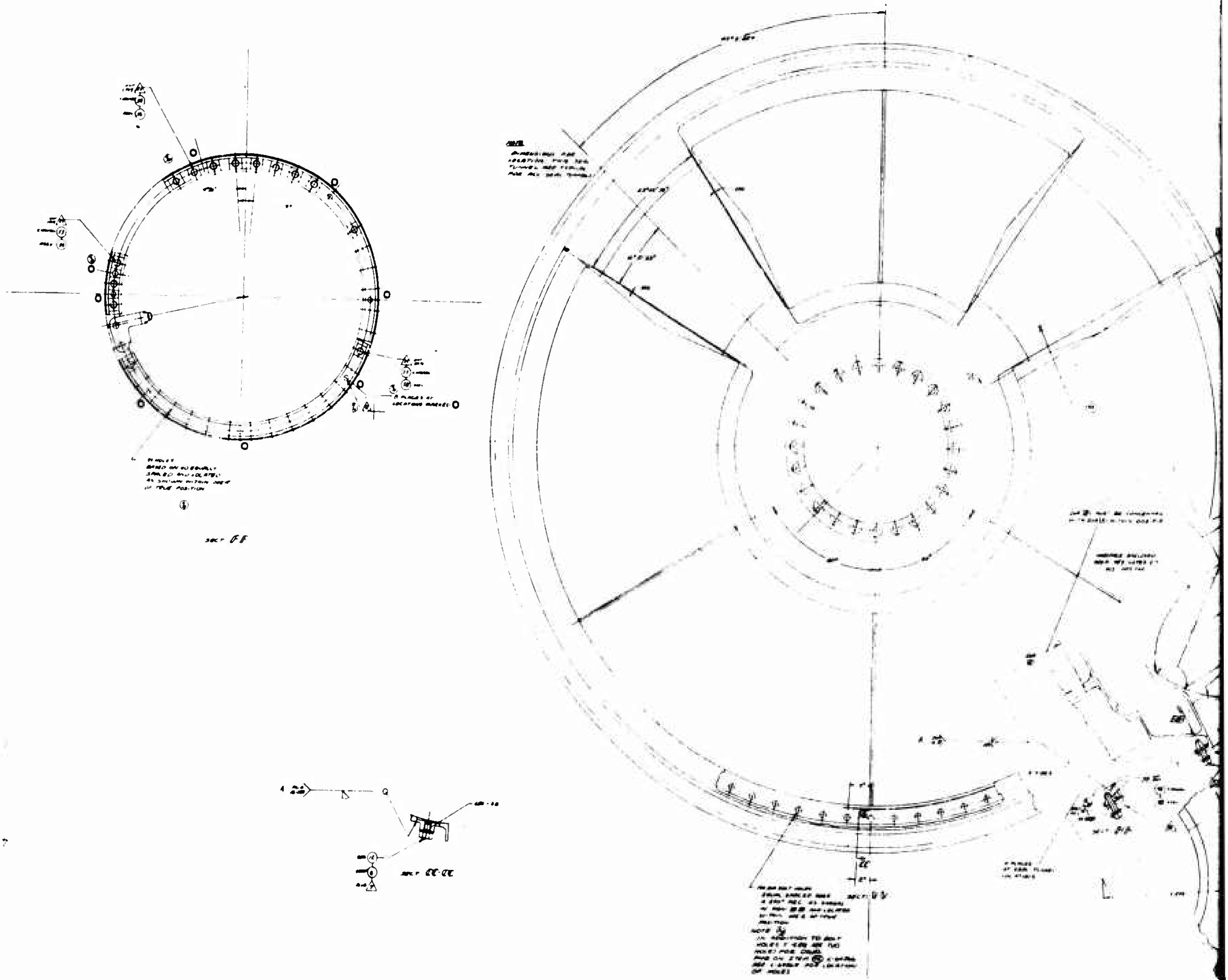

2

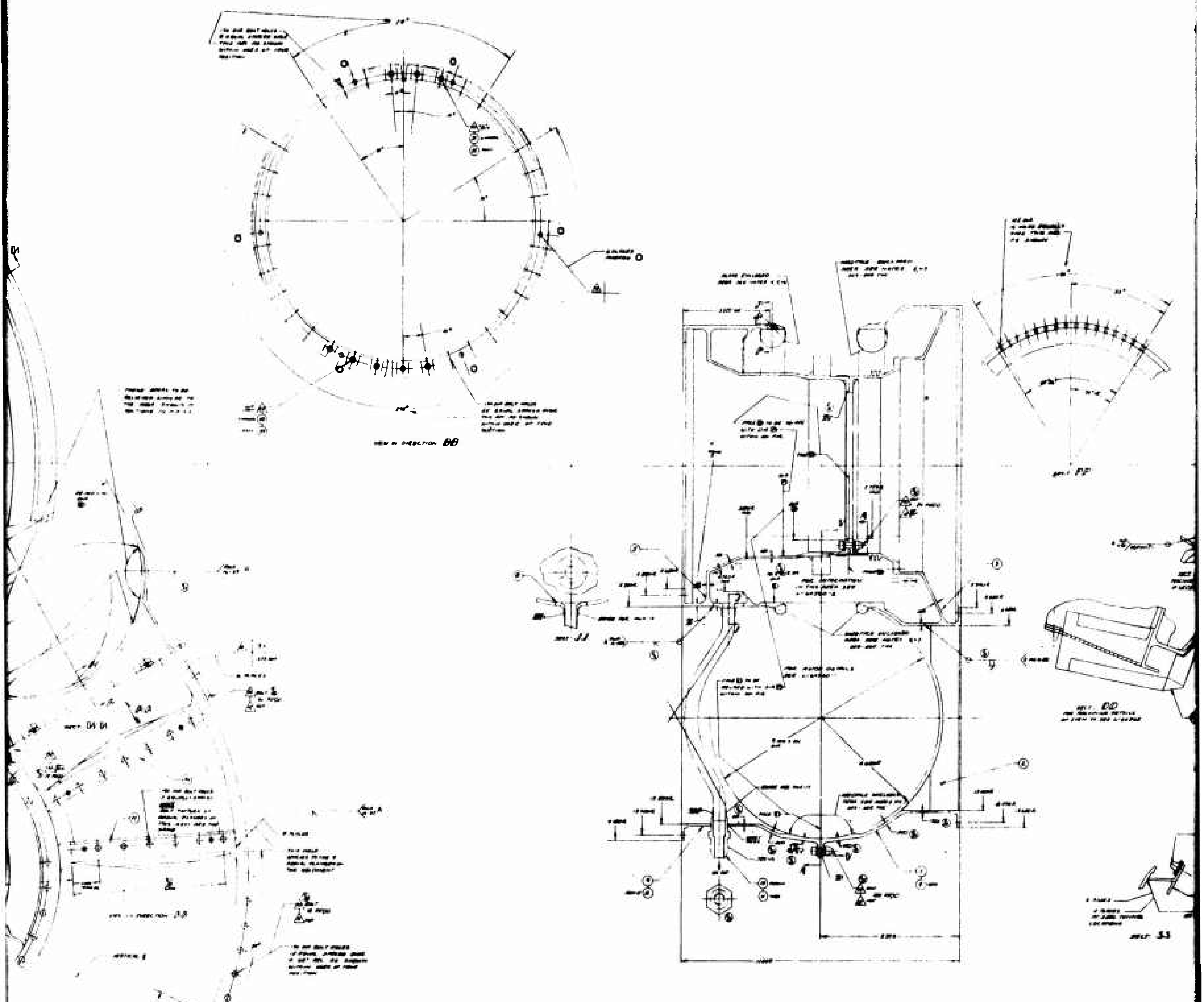

3

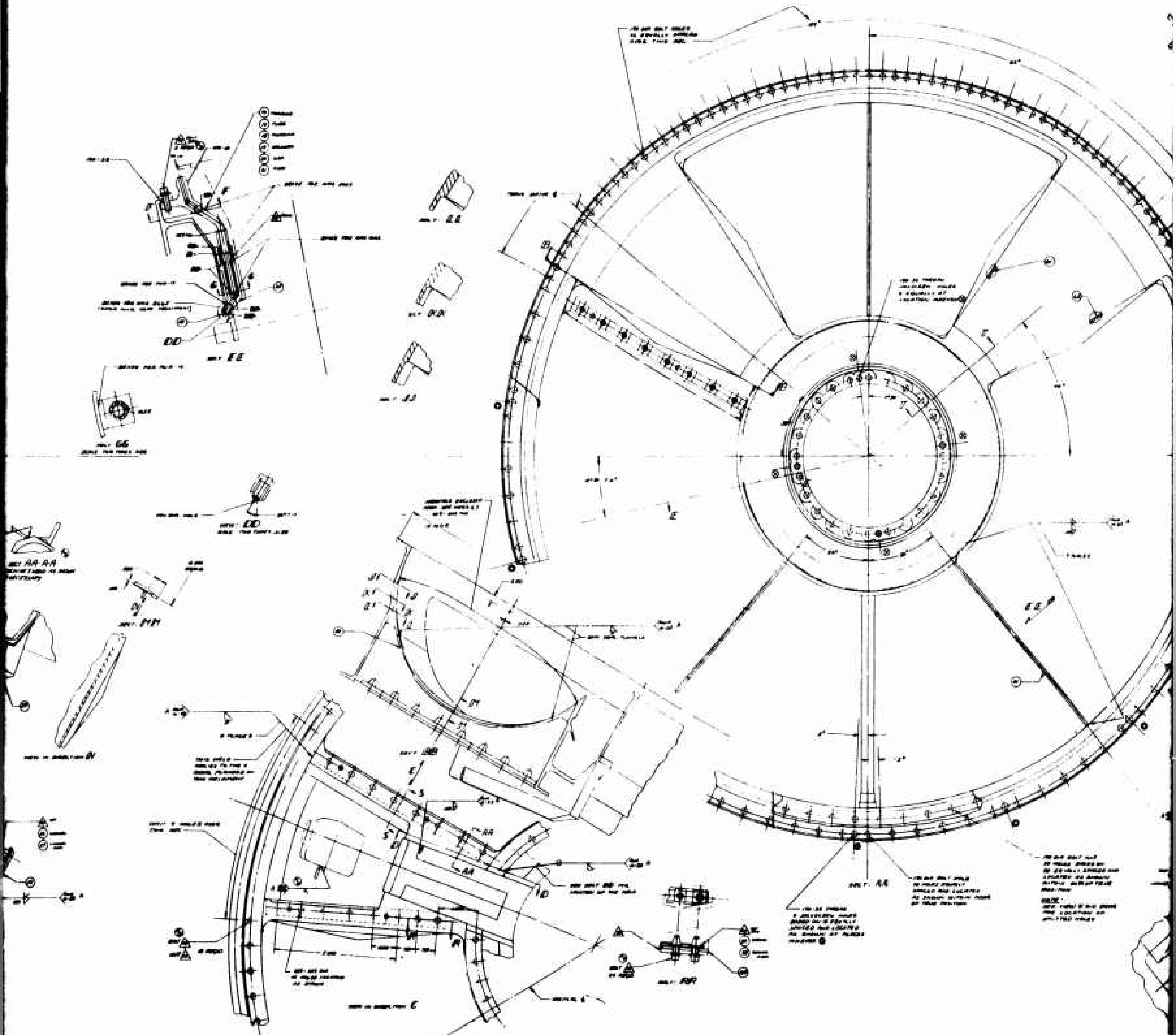

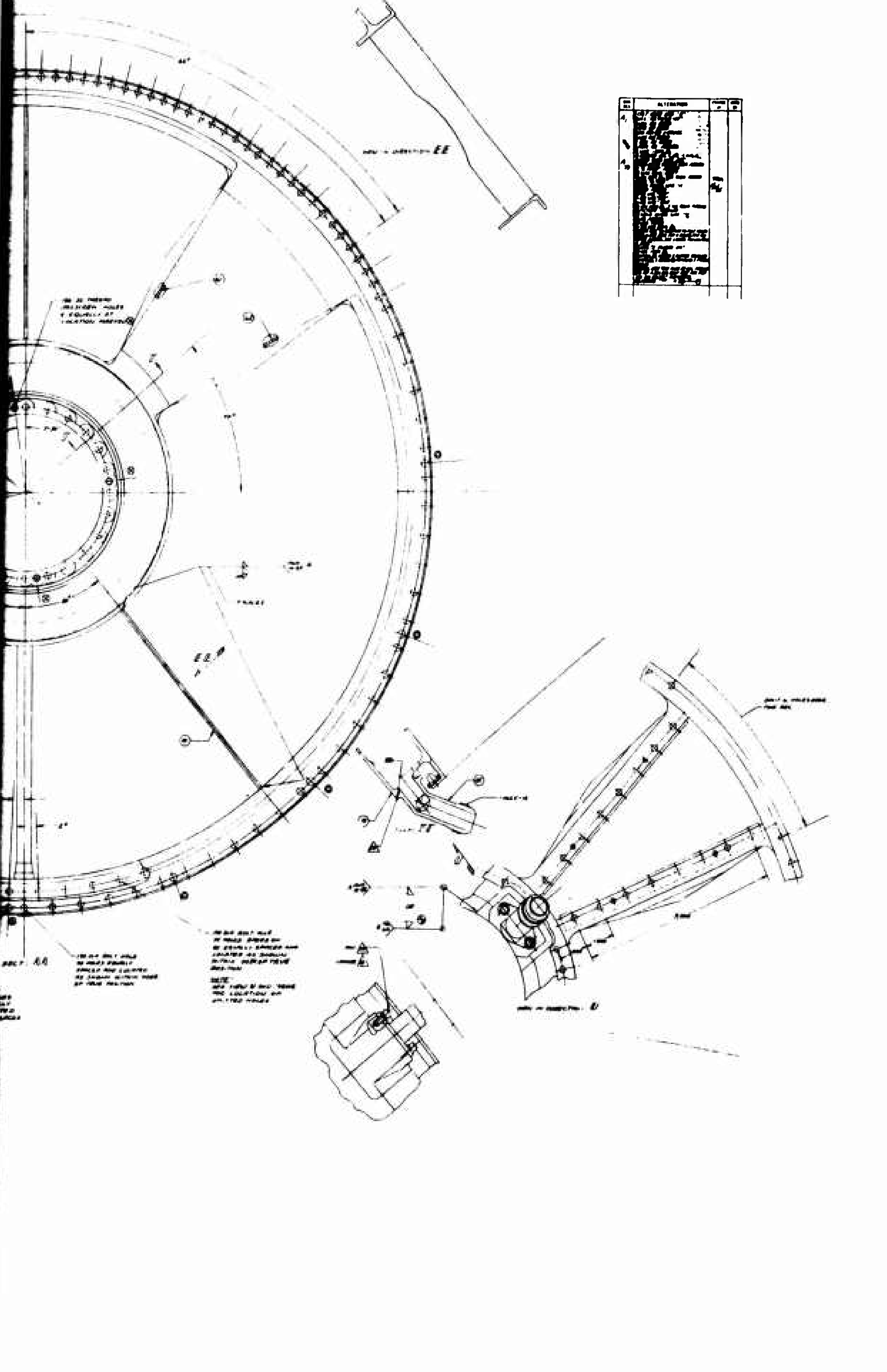

NOTES:

1. SCALE FULL SIZE
3. REFERENCE LAYOUTS

L-69361

PRATT & WHITNEY CONTROLLED

LAYOUT

L-69361

1

PRECEDING PAGE BLANK-NOT FILMED

CONFIDENTIAL

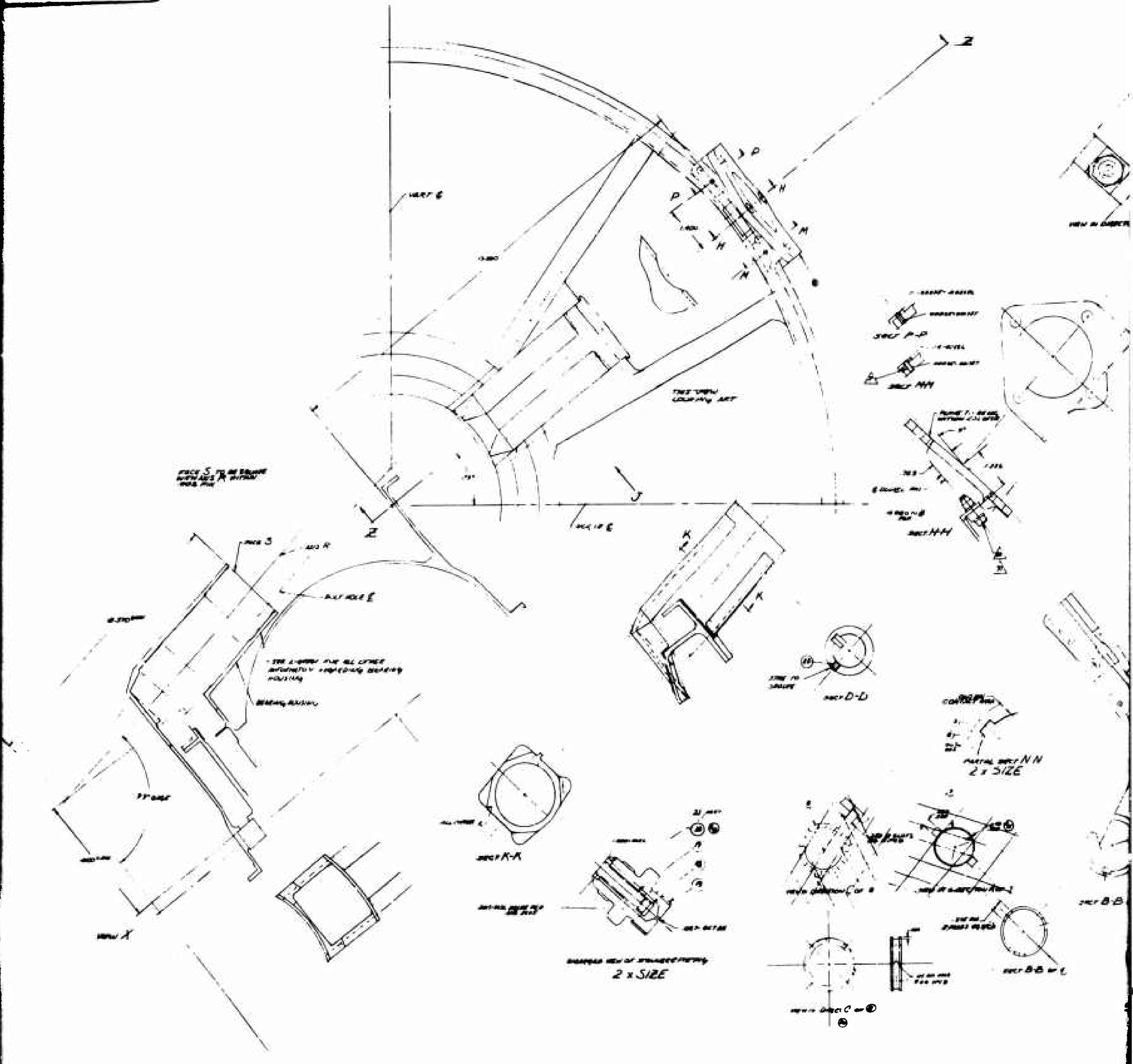

CONFIDENTIAL

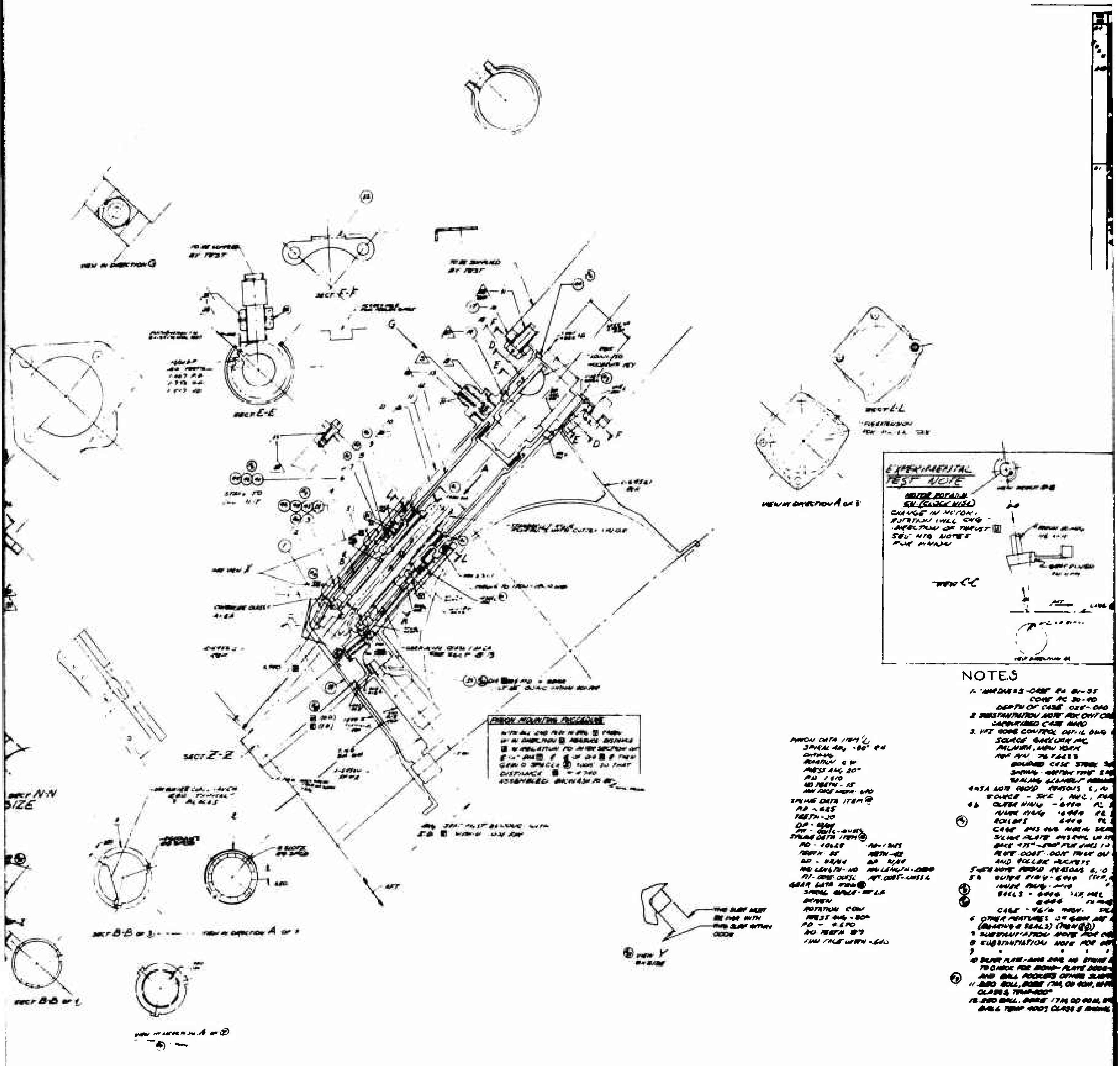

EXPERIMENTAL TEST NOTE
NOTES
SECT E-E
SECT F-F
SECT L-L
SECT Z-Z
SECT N-N
SECT B-B
VIEW C-C
VIEW Y
PINION MOUNTING PROCEDURE
2

3

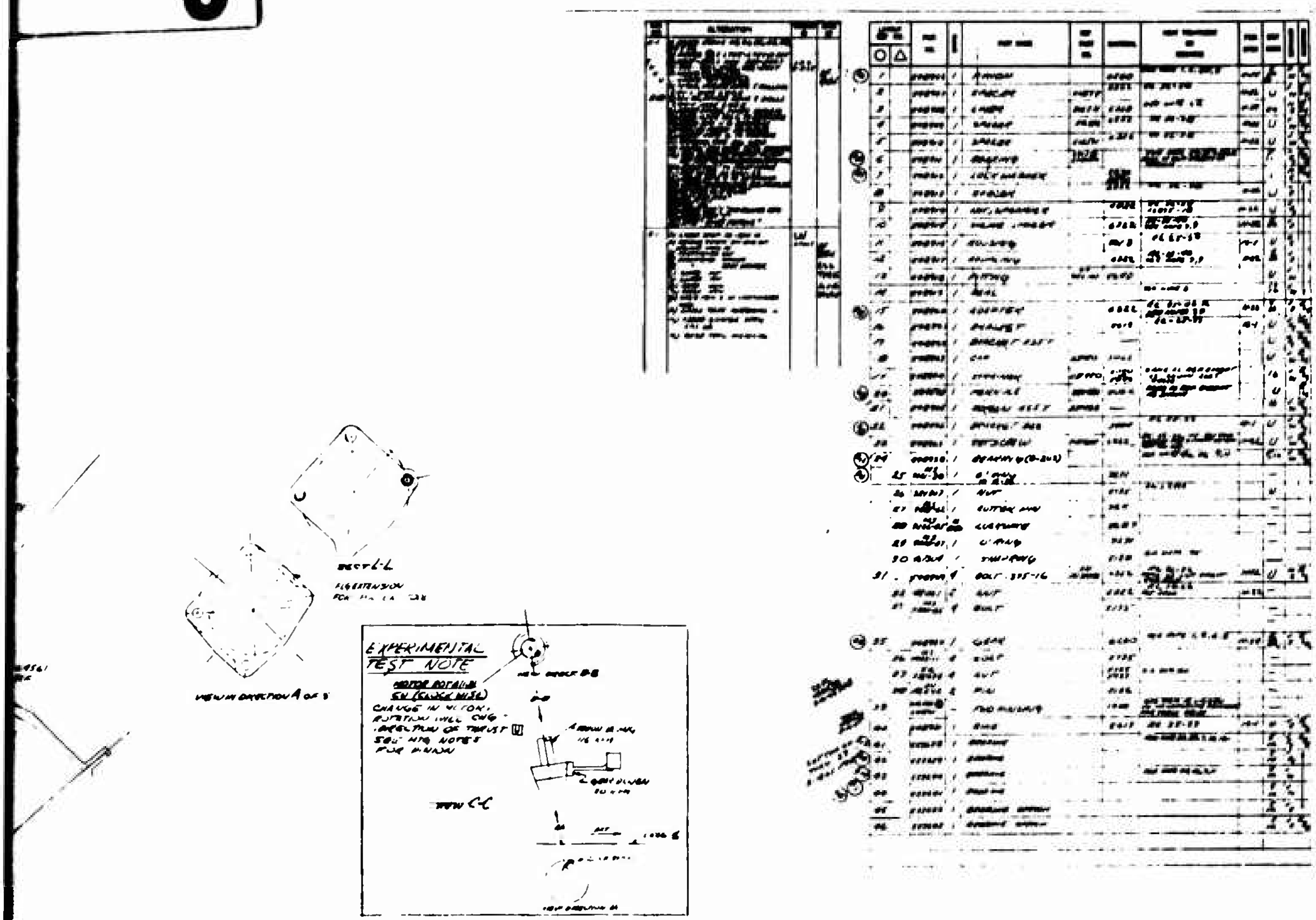

NOTES

1. HARDNESS - CASE RA 81-85
CORE RC 30-40
DEPTH OF CASE .025-.040
2. SUBSTANTIATION NOTE FOR CRIT CODE 3A
CARBURIZED CASE HARD
3. VFZ CODE CONTROL DETAIL DWG REQ'D [illegible]
SOURCE GARLOCK INC
PALMYRA, NEW YORK
REF P/N [illegible]
BONDED CASE STEEL [illegible]
SHAFT [illegible] STAINLESS STEEL [illegible]
SEALING ELEMENT [redacted] SILICONE [illegible]
4. 4A SUBST NOTE REQ'D REASONS 6, 10 VFZ CODE CONTROL DWG
SOURCE - SKF, MRC, FAFNIR
4b OUTER RING [illegible] RC 58 MIN OR EQUIV
INNER RING [illegible] RC 58 MIN OR EQUIV
ROLLERS [illegible] RC 58 MIN OR EQUIV
CAGE AMS [illegible] BRONZE
SILVER PLATE AMS [illegible] STRIKE METAL REQ'D
BAKE 475°-500° FOR [illegible] TO CHECK FOR BOND
PLATE .0005-.001 THICK ON LAND RIDING SURFACES
AND ROLLER POCKETS
5. 5A SUBST NOTE REQ'D REASONS 6, 10 SKF, FAFNIR, MRC VFZ CODE CONTROL DWG
5b OUTER RING - [illegible] (SKF, MRC, FAFNIR) RC 58 MIN OR EQUIV
INNER RING - [illegible] RC 58 MIN OR EQUIV
BALLS - [illegible] SKF, MRC RC 58 MIN OR EQUIV
[illegible] FAFNIR
CAGE - [illegible] SILICON BRONZE
6. OTHER FEATURES OF GEAR ARE INCORPORATED ON L-69450 (BEARING & SEALS) (ITEM 10)
7. SUBSTANTIATION NOTE FOR CRIT CODE 5 [illegible]
8. SUBSTANTIATION NOTE FOR CRIT CODE 8A - TEST GEARS
9. " " " " " " - SPECIAL GAGE
10. SILVER PLATE - AMS [illegible] STRIKE METAL REQ'D - BAKE 475°-500° FOR 2 HRS TO CHECK FOR BOND - PLATE .0005-.001 THICK ON LAND RIDING SURFACES AND BALL POCKETS OTHER SURFACES OPTIONAL
11. [illegible] ROLL, BORE 17M, OD 40M, WIDTH 12M [illegible] CLASS 5, TEMP 400°
12. [illegible] BALL, BORE 17M, OD 40M, WIDTH 12M, [illegible] CLASS 5, BALL TEMP 400° CLASS 5 RADIAL CLEAR [illegible]

L-64562

PRATT & WHITNEY AIRCRAFT
CONTROLLED

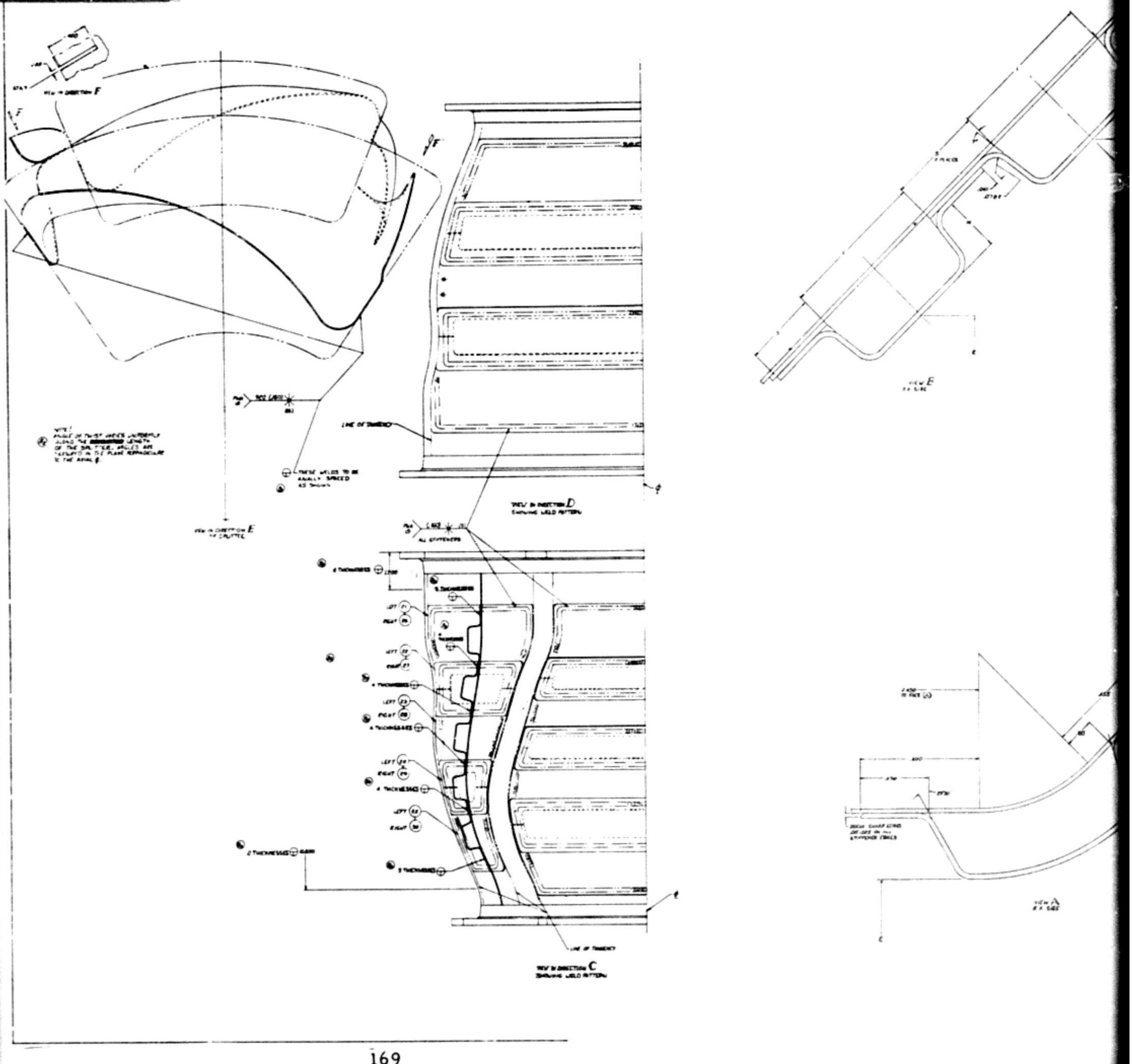

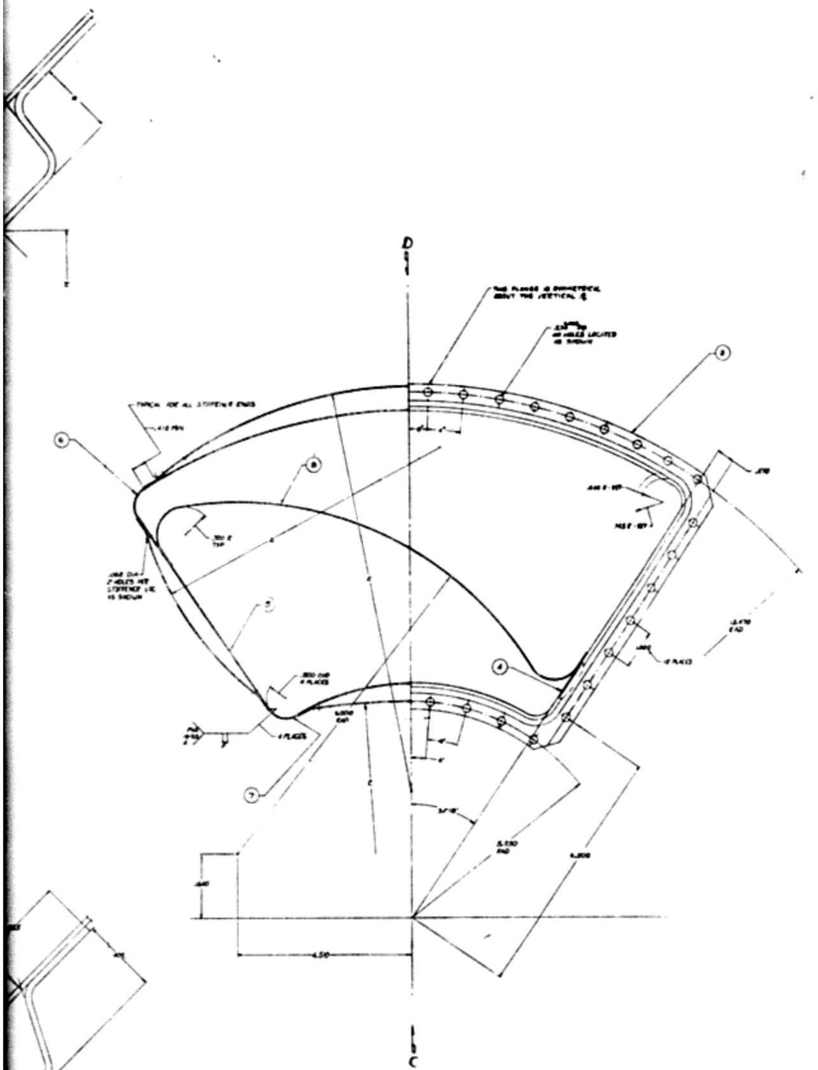

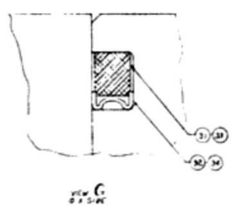

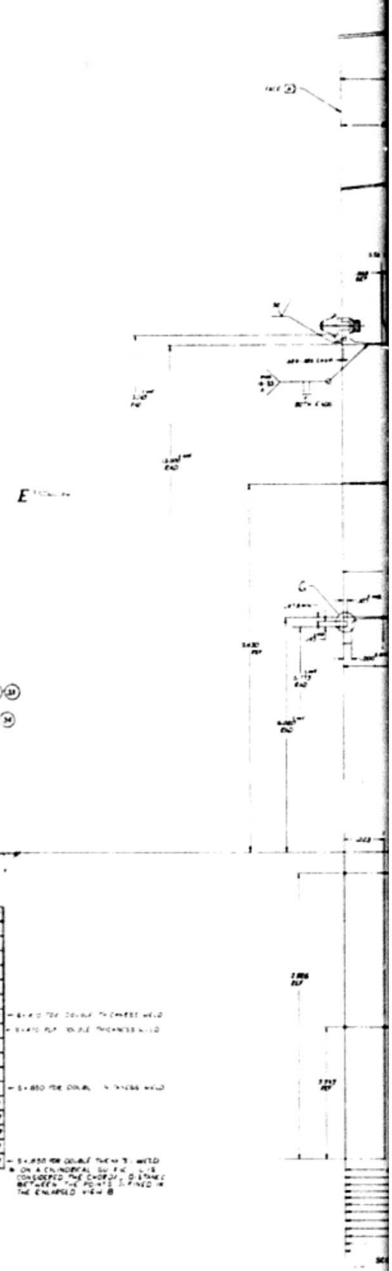

ITEM	H	*L	S	E	BEND RADIUS	T
9	.468		.470	—	.078	.120
10	.370	.910	.470	—	.078	.037
[illegible]	.405	.970	.630	—	.078	.037
12	.370	.370	.470	—	.078	.037
13	.405	.970	.620	—	.078	.037
14	.370	.960	.470	—	.078	.037
15	.405	.370	.630	—	.078	.037
16	.580	1.450	.650	—	.094	.045
17	.540	1.260	.330	—	.094	.045
18	.580	1.290	.650	—	.094	.045
19	.540	1.050	.550	—	.094	.045
20	.680	1.680	.600	—	.094	.045
21,26	.405	.970	.620	—	.078	.037
22,27	.370	.850	.620	—	.078	.037
23,28	.405	.930	.620	—	.078	.037
24,29	.370	.810	.600	—	.078	.037
25,30	.405	.960	.630	—	.078	.037

← S = .470 FOR DOUBLE THICKNESS WELD (item 15)
← S = .470 FOR DOUBLE THICKNESS WELD (item 16)
← S = .650 FOR DOUBLE THICKNESS WELD (item 20)
← S = .650 FOR DOUBLE THICKNESS WELD (items 25,30)

* ON A CYLINDRICAL SURFACE L IS CONSIDERED THE CHORDAL DISTANCE BETWEEN THE POINTS DEFINED IN THE ENLARGED VIEW B

3

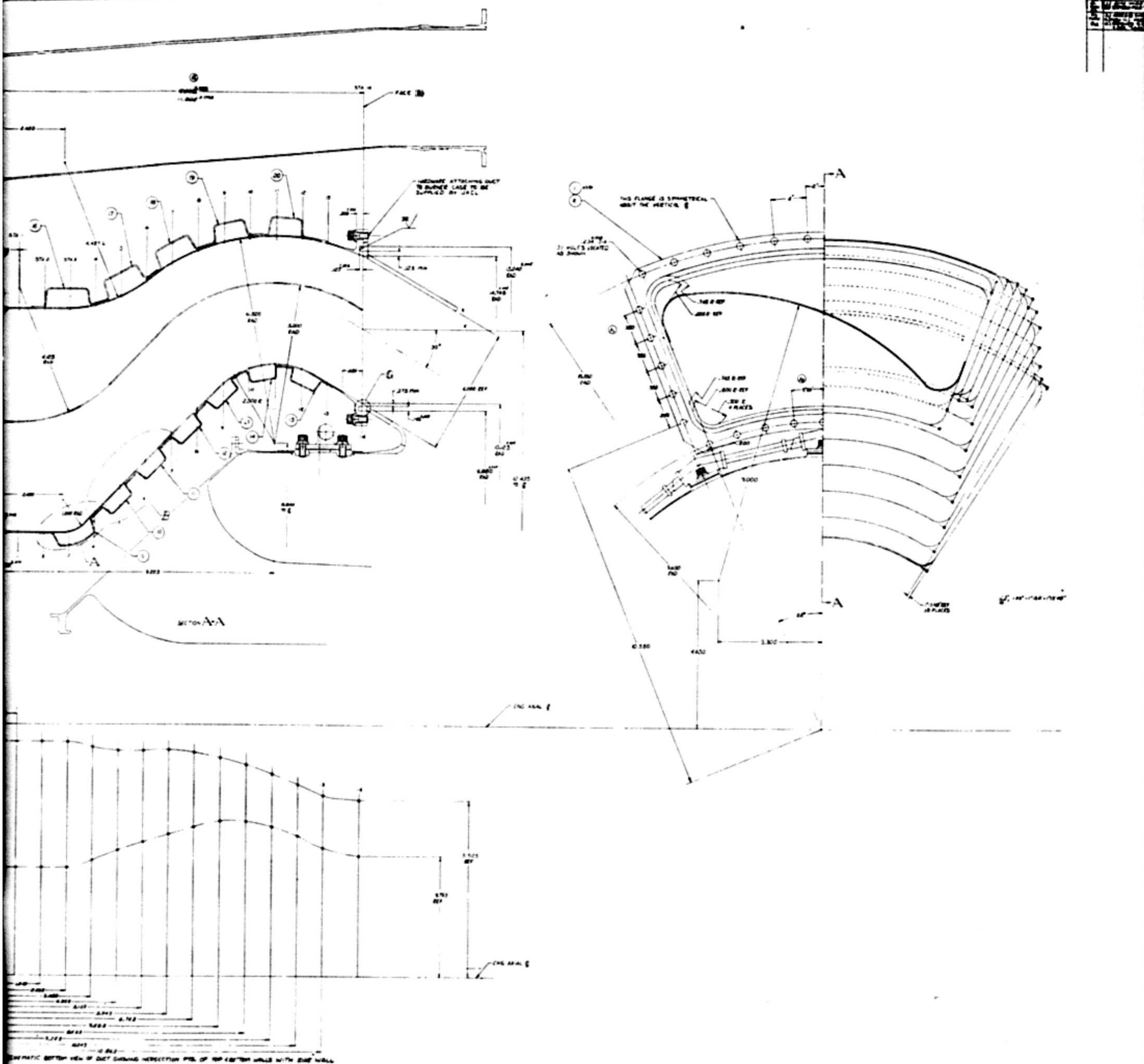

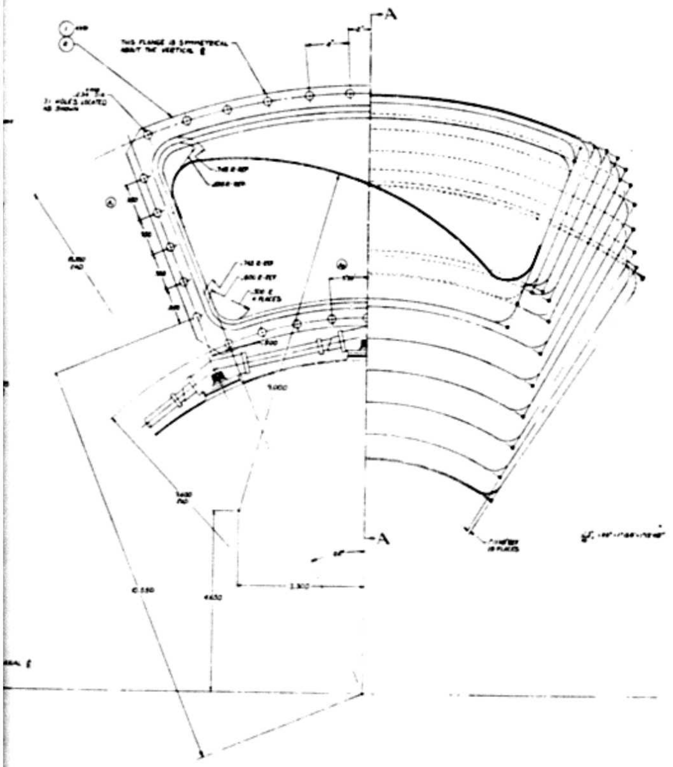

Item	Part No.	Part Name	Material	Stock	Code
1	559653	DUCT ASSY	—	NOTE 3, 4	
2	559651	FLANGE-REAR			
3	559652	FLANGE-FRONT			
4	559653	SIDE-RIGHT	493	[illegible] THK	
5	559654	SIDE-LEFT	493	[illegible] THK	
6	557655	TOP	493	[illegible] THK	
7	559656	BOTTOM	493	[illegible] THK	
8	559657	SPLITTER	493	[illegible] THK	
9	559658	STIFFENER	493	[illegible] THK	
10	559659				
11	559663				
12	557661				
13	559662				
14	559664				
15	559665				
16	559666			[illegible] THK	
17	559667				
18	559668				
19	559669				
20	559670				
21	559671			[illegible] THK	
22	559672				
23	559673				
24	559674				
25	559675				
26	559676				
27	559677				
28	559678				
29	559679				
30	559680				
31		MESH TO FLANGE		NOTE 2	
32		℄ SEAL TO FLANGE		NOTE 2	
33		[illegible] REAR FLANGE		NOTE 2	
34		℄ SEAL [illegible] FLANGE		NOTE 2	

DO NOT DETAIL UNTIL NECESSARY INFORMATION IS RECEIVED FROM VENDOR

NOTES
1. FACE [illegible] TO BE PARALLEL TO FACE [illegible] WITHIN .001 FIR
2. [illegible] REQUIRED [illegible]
   [illegible] CODED CONT DETAIL
   SOURCE [illegible]
3. AFTER WELDING SOLUTION & PRECIPITATION HEATTREAT PER SPEC 493 HARDNESS [illegible]
4. [illegible] WELD
   5 [illegible]

FOR MATING PARTS SEE THE FOLLOWING LAYOUTS: [illegible] - REGENERATOR HOUSING
[illegible] - TURBINE EXHAUST DUCT
[illegible] - COMPRESSOR EXIT DUCT

L-64564

PRATT & WHITNEY AIRCRAFT
CONTROLLED

[redacted]
LAYOUT
[illegible] ROTARY REGENERATOR
TITLE: DUCT - REGENERATOR TO BURNER INLET
LAYOUT No. L-64564

1

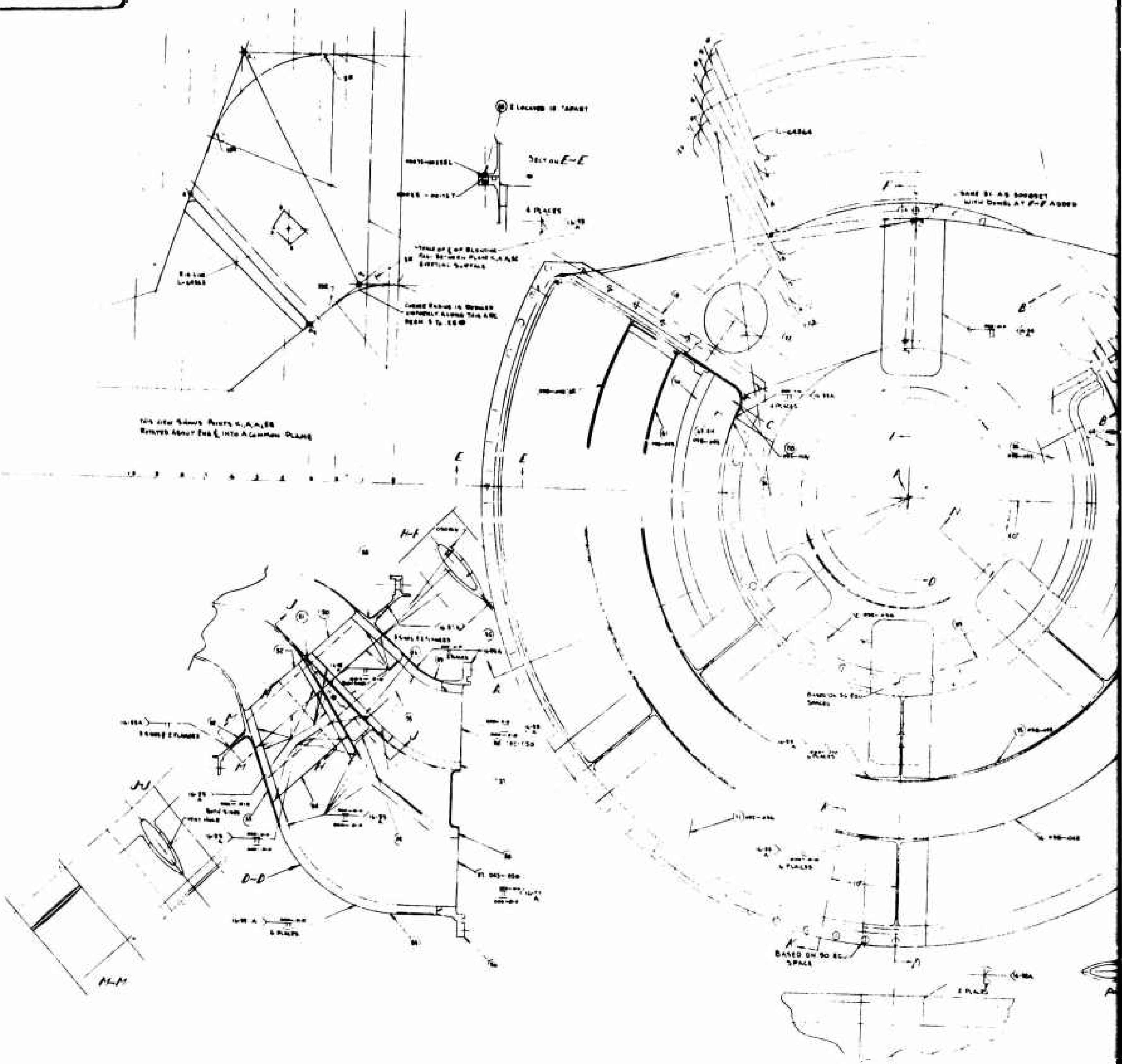

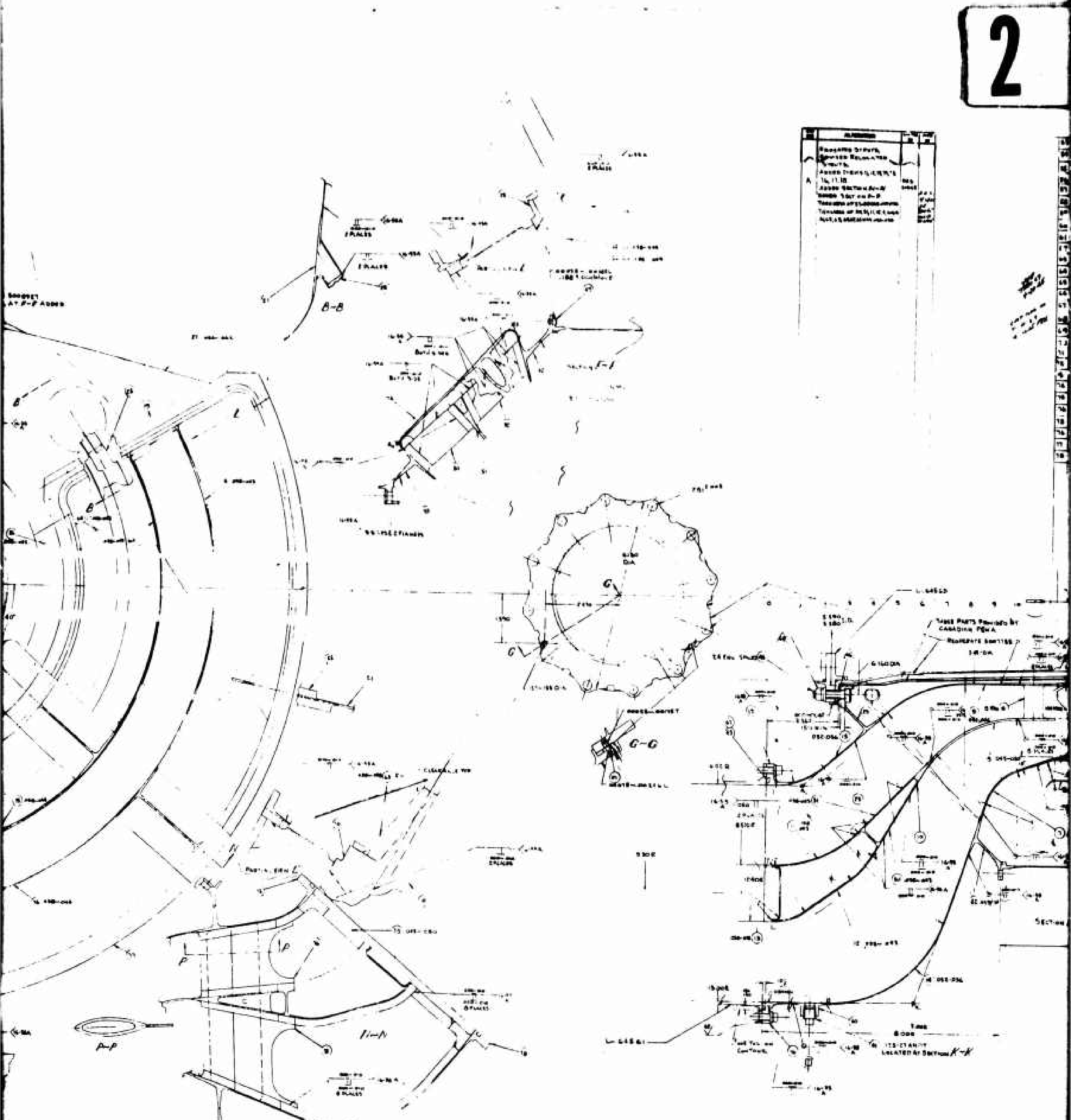

2
B-B
G-G
P-P
N-N

3

Sym	Alterations		
A	Relocated Struts, Revised Relocated Struts, Added Items 11, 12, 13, 14, 15, 16, 17, 18, Added Section N–N, Added Section P–P, [illegible]		

Item	Part No.	Qty	Part Name	Material	Heat Treat / Remarks	Code
53	[illegible]	2	STRUT	1009		5b
54	[illegible]	2	STRUT	1009		5b
55	[illegible]	2	BOSS	1009		5b
56		2	BOSS	1009		5b
57		2	STRIP	1009		5b
58		2	STRIP	1009		5b
59	[illegible]	32	VANE	1009		[illegible]
60	[illegible]	1	SPLITTER	1055		5b
61		1	SPLITTER	1055		5b
62		1	SPLITTER	1055		5b
63		1	SPLITTER	1055		5b
64		1	SPLITTER	1055		5b
65	[illegible]	1	SPLITTER	1055		5b
66		1	SPLITTER	1055		5b
67		1	[illegible]		SEE NOTE 5	[illegible]
68		2	FLANGE	1009		5b
69		2	FLANGE	1009		5b
70		1	RING	1009		5b
71		2	DUCT	1055		5b
72		2	DUCT	1055		5b
73		2	STRUT	1009		5b
74		1	ADAPTER	1009		5b
75		2	FLANGE	1009		5b
76		2	STRUT	1009		5b
77		2	SPLITTER	1055		5b
78		2	SPLITTER	1055		5b
79		5	FLANGE	1009		5b
80		2	STRIP	1055		5b

Item	Part No.	Qty	Part Name	Material	Heat Treat or Remarks	Code
1	[illegible]	1	FLANGE	1009		5b
2		1	SHROUD	1009		5b
3		1	DUCT	1009	[illegible]	5b
4		1	SPLITTER	1055		5b
5		1	SHROUD	1009		5b
6		6	SUPPORT	1009		[illegible]
7		1	DUCT	1055	SEE NOTE 1	5b
8		1	DUCT	1055	SEE NOTE 1	5b
9		1	DUCT	1055	SEE NOTE 1	5b
10	[illegible]	4	RING	1009		5b
11		1	SPLITTER	1055		5b
12		1	SPLITTER	1055		5b
13		1	RING	1055		5b
14		1	DUCT	1055		5b
15		1	DUCT	1055		5b
16		2	FLANGE	1009		5b
17		2	FLANGE	1009		5b
18		1	FLANGE	1009		5b
19		1	FLANGE	1009		5b
20	[illegible]	1	SHROUD	1055	SEE NOTE 1	5b
21		1	ADAPTER	1009		5b
22		1	ADAPTER	1009		5b
23		2	RING	1009		5b
24		2	RING	1009		5b
25		1	RING	1009		5b
26		2	DUCT	1055		5b
27		1	DUCT	1055		5b
28		1	DUCT	1055		5b
29		1	FLANGE	1009		5b
30	[illegible]	2	SPLITTER	1055		5b
31		2	SPLITTER	1055		5b
32		6	ADAPTER	1009		5b
33		6	ADAPTER	1009		5b
34		3	STRIP	1009		5b
35		5	FLANGE	1009		5b
36		3	FLANGE	1009		5b
37		1	PLATE	1055		5b
38		1	PLATE	1055		5b
39		3	STRIP	1009		5b
40	[illegible]	1	BOSS	1009		5b
41	[illegible]	1	PLUG	510		U
42	[illegible]	1	ASSY OF		SEE NOTE 5	[illegible]
43	[illegible]	1	E SEAL		SEE NOTE 5	[illegible]
44		24	BOLT	AMS [illegible]		U
45	[illegible]	24	NUT	AMS [illegible]	SACK	
46	[illegible]	24	SNAP RING	AMS [illegible]	SACK	
47		1	DOWEL	AMS 5613	[illegible]	U
48	[illegible]	2	DOWEL	AMS 5613	[illegible]	U
49		1	DOWEL	AMS 5613		U
50		4	STRUT	1009		5b
51		4	RING	1009		5b
52		4	STRUT	1009		5b

4. CRIT CODE SUBSTANTIATION
5b CONT ATM WELDING
52 X-RAY
56 GUILLOTINE GAGE
6 PER CHAS FEAKES MEMO

5. SA REDUCE
VF CAGED CONT DET
SOURCE – JOHNS MANVILLE (DETAILS W/ [illegible])

2. AFTER WELDING SOLUTION & PRECIPITATION HEAT TREAT PER SPEC PWA 1055 HARDNESS [illegible]

1. LONGITUDINAL WELD

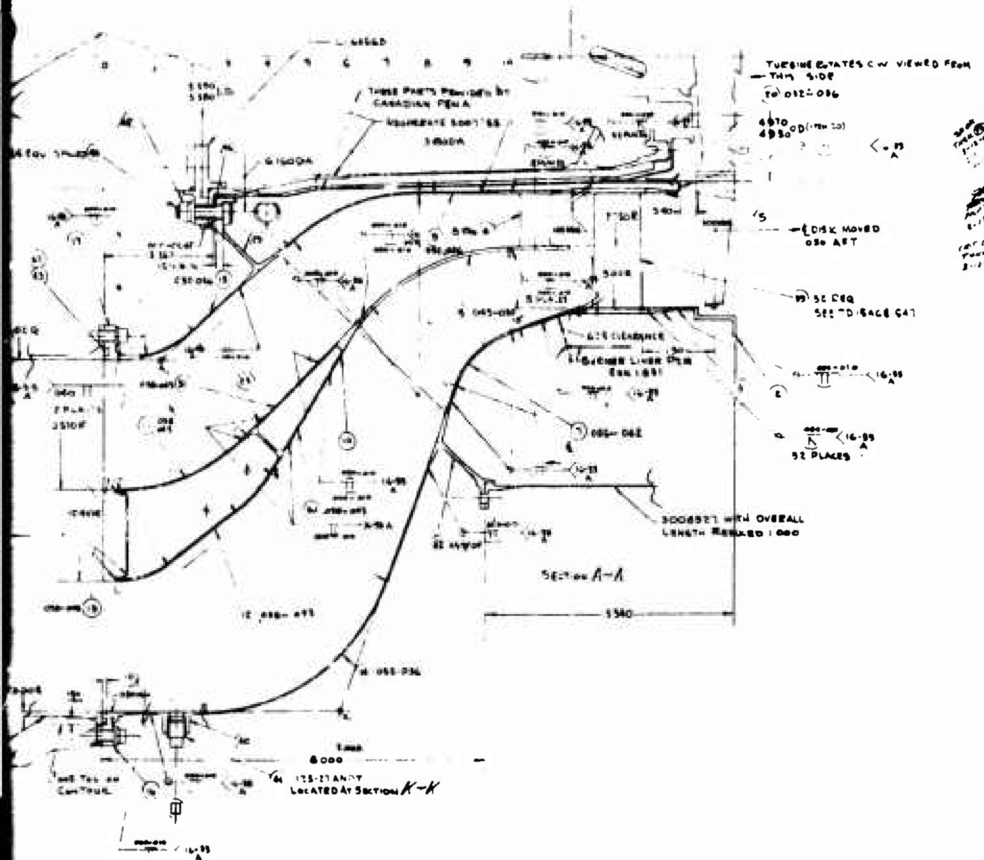

PRATT & WHITNEY AIRCRAFT
CONTROLLED
TURBINE STAGE TO REGENERATOR
L-64565

PRECEDING PAGE BLANK-NOT FILMED

CONFIDENTIAL

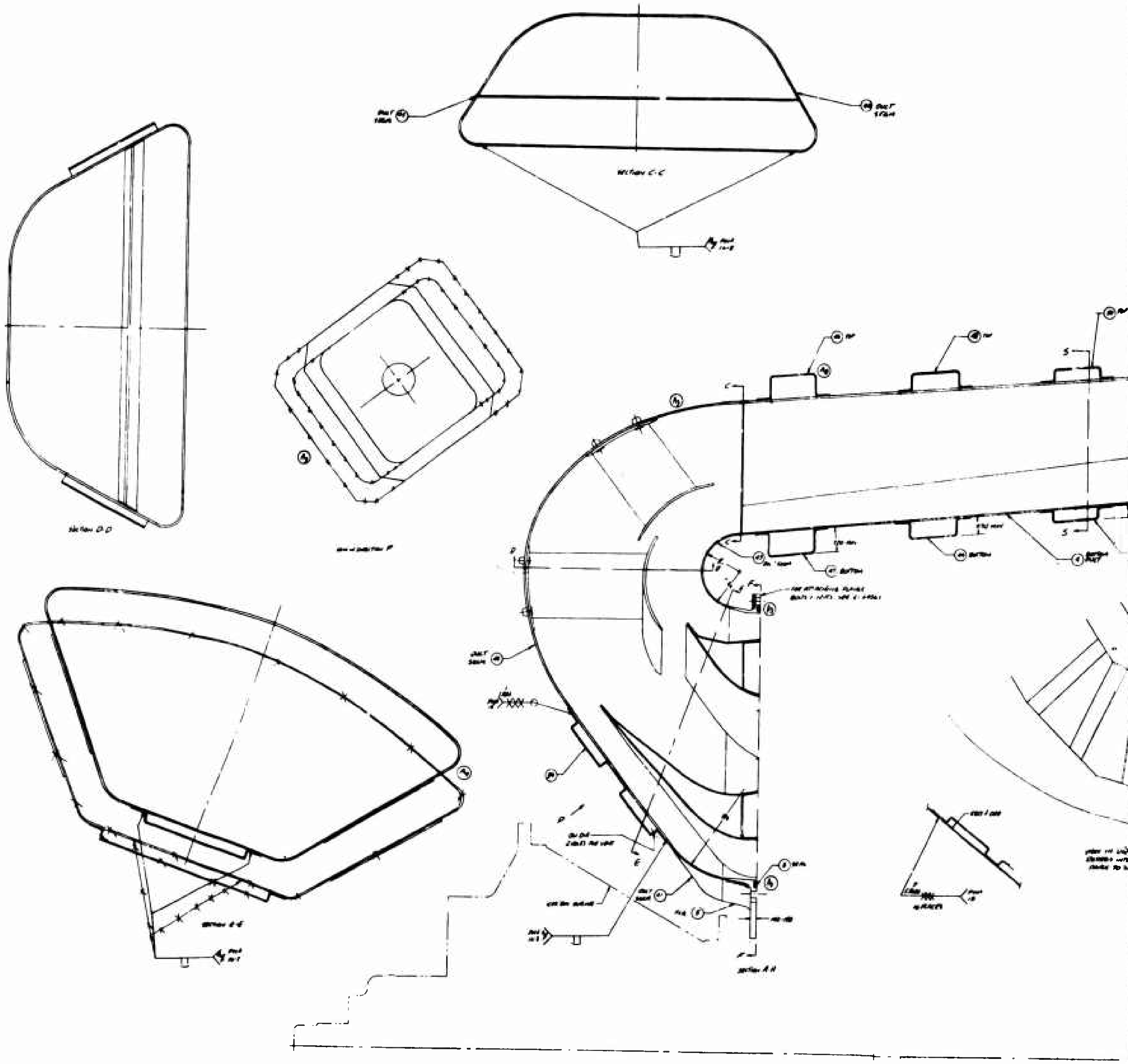

CONFIDENTIAL

2

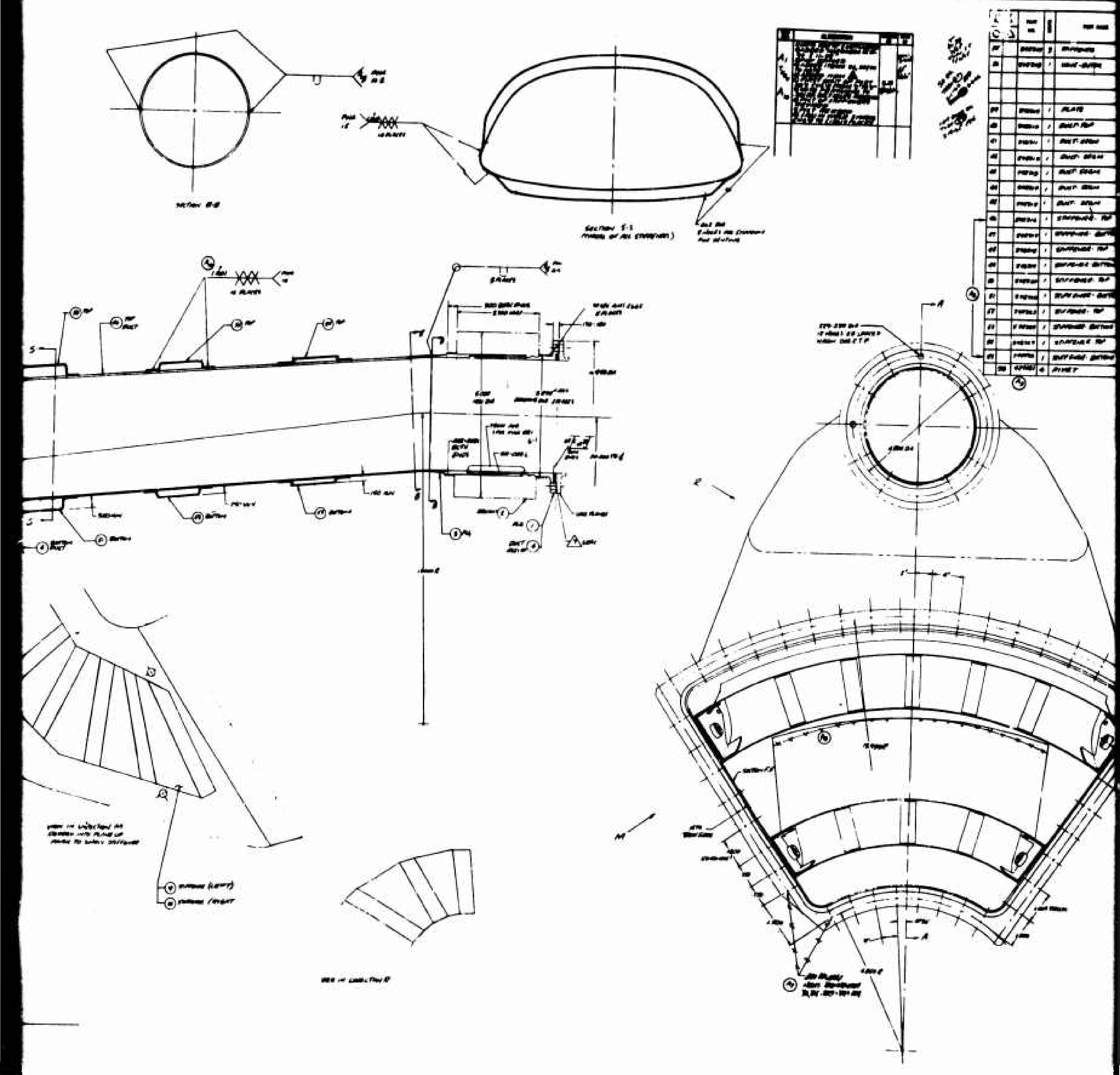

3

34		[illegible]	3	STIFFENER	AMS 5510	.033-.037TH	30
35		[illegible]	1	VANE-OUTER	AMS 5510	.033-.037TH	30
39		[illegible]	1	PLATE	AMS 5510	.033-.037TH	30
40		[illegible]	1	DUCT-TOP	AMS 5510	.033-.037TH	30
41		[illegible]	1	DUCT-SEAM	AMS 5510	.033-.037TH	30
42		[illegible]	1	DUCT-SEAM	AMS 5510	.033-.037TH	30
43		[illegible]	1	DUCT SEAM	AMS 5510	.033-.037TH	30
44		[illegible]	1	DUCT-SEAM	AMS 5510	.033-.037TH	30
45		[illegible]	1	DUCT SEAM	AMS 5510	.033-.037TH	30
46		[illegible]	1	STIFFENER-TOP	AMS 5510	.033-.037TH	30
47		[illegible]		STIFFENER-BOTTOM	AMS 5510	.033-.037TH	30
48		[illegible]	1	STIFFENER-TOP	AMS 5510	.033-.037TH	30
49		[illegible]	1	STIFFENER BOTTOM	AMS 5510	.033-.037TH	30
50		[illegible]	1	STIFFENER TOP	AMS 5510	.033-.037TH	30
51		[illegible]	1	STIFFENER-BOTTOM	AMS 5510	.033-.037TH	30
52		[illegible]	1	STIFFENER-TOP	AMS 5510	.033-.037TH	30
53		[illegible]	1	STIFFENER BOTTOM	AMS 5510	.033-.037TH	30
54		[illegible]	1	STIFFENER TOP	AMS 5510	.033-.037TH	30
55		[illegible]	1	STIFFENER-BOTTOM	AMS 5510	.033-.037TH	30
	51	[illegible]	4	RIVET	[illegible]	SA OK	—

1		[illegible]	1	FLANGE-FRONT	AMS [illegible]	[illegible]	30
2		[illegible]	1	BELLOWS	AMS 5510	SEE NOTE 4	[illegible]
3		[illegible]	1	FLANGE-INTERMEDIATE	AMS [illegible]		30
4		[illegible]	1	DUCT, BOTTOM	AMS 5510	.033-.037TH	30
5		[illegible]	1	FLANGE, FRONT	AMS [illegible]		30
6		[illegible]	1	DUCT ASSY OF		[illegible]	[illegible]
	7	[illegible]	1	SEAL [illegible]	AMS 7676		—
8		[illegible]	1	SEAL [illegible]	AMS 7676	[illegible]	[illegible]
9		[illegible]	1	STIFFENER	AMS 5510	.033-.037TH	30
10		[illegible]	1	STIFFENER	AMS 5510	.033-.037TH	30
	11	[illegible]	[illegible]	RIVET	[illegible]	SA OK	—
	12	[illegible]	16	COLLAR		SA OK	—
13		[illegible]	1	PLATE	AMS 5510	.062TH	30
14		[illegible]	2	SUPPORT	AMS 5510	.062 TH	30
15		[illegible]	1	VANE	AMS 5510	.062 TH	30
17		[illegible]	1	PLATE	AMS 5510	.062TH	30
18		[illegible]	2	SUPPORT	AMS 5510	.062 TH	30
19		[illegible]	1	VANE	AMS 5510	.062 TH	30
21		[illegible]	5	STIFFENER	AMS 5510	.033-.037TH	30
22		[illegible]	1	PLATE	AMS 5510	.033-.037TH	30
23		[illegible]	1	VANE INNER	AMS 5510		30
25		[illegible]	4	BUSHING	AMS [illegible]		30
26		[illegible]	4	PIN	AMS [illegible]	HARDNESS [illegible]	[illegible]
27		[illegible]	1	PLATE	AMS 5510	.033-.037TH	30
28		[illegible]	1	VANE-OUTER	AMS 5510	.033-.037TH	30
	29	XC	4	RIVET	AMS 7268		—
30		[illegible]	4	GUIDE	AMS [illegible]	HARDNESS [illegible]	[illegible]
31		[illegible]	2	PLATE	AMS 5510	.033-.037TH	30
32		[illegible]	1	PLATE	AMS 5510	.033-.037TH	30
33		[illegible]	1	PLATE	AMS 5510	.033-.037TH	30
34		[illegible]	1	VANE-INNER	AMS 5510	.033-.037TH	30

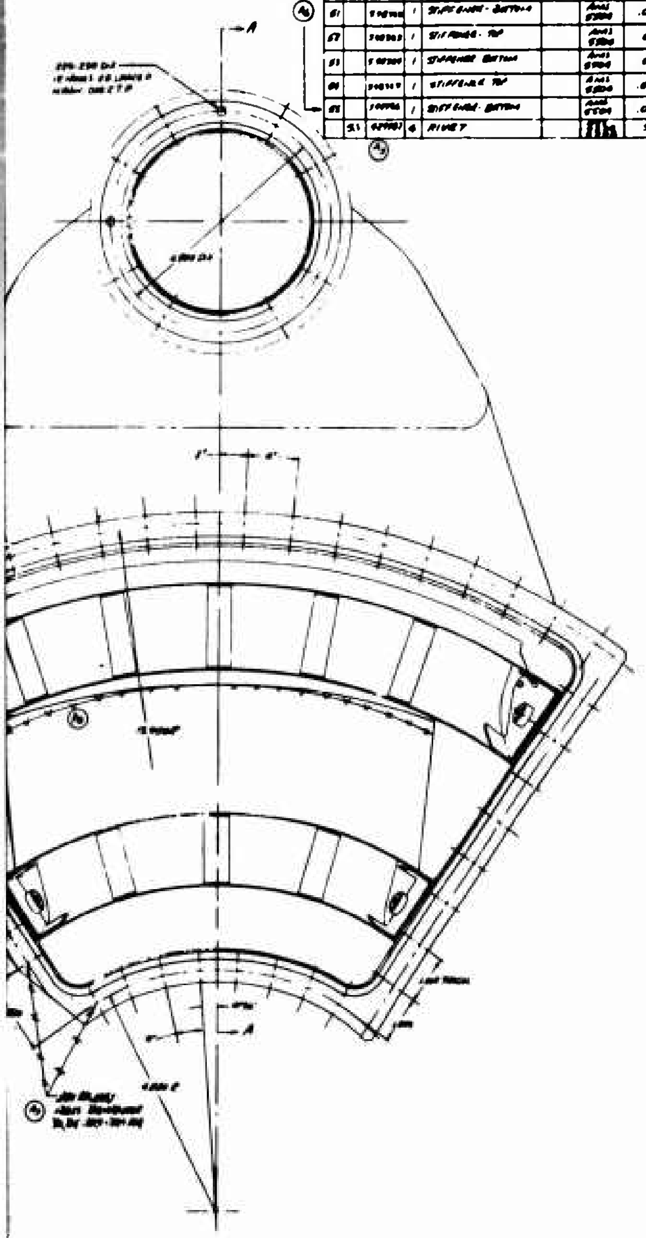

NOTES
1. DUCT CONTOUR IS DEFINED AS FOLLOWS:
SECTIONS B-B, C-C, D-D, E-E, F-F DESCRIBE THE DUCT AT THEIR RESPECTIVE LOCATIONS BETWEEN SECTION B-B & C-C THE DUCT IS STRAIGHT LINE FAIRED AT PROPORTIONATE STATIONS OF [illegible] BETWEEN C-C & D-D THE OUTER (UPPER) WALL CONTOUR IS DEFINED IN SECTION [illegible]
[illegible]
2. [illegible]
3. [illegible]
4. [illegible] NOTE [illegible]
BELLOWS MUST BE CAPABLE OF EXTENDING .400 WITHOUT YIELDING [illegible]
SOURCES
STEIN SEAL CO PHILA PA.
[illegible] FLEXON CONTROL CO. MILFORD CONN.
5. [illegible] HARDNESS [illegible]
6. RIVET PER SPEC PWA 357
7. SURF ROUGHNESS PER SPEC PWA 351
CRF SUBSTANTION
[illegible] INSPECTION
[illegible]
[illegible] WELD

C-64566

PRATT & WHITNEY AIRCRAFT
CONTROLLED

PRATT & WHITNEY AIRCRAFT [illegible]
LAYOUT
TITLE [illegible]
LAYOUT NO.
C-64566

PRECEDING PAGE BLANK-NOT FILMED

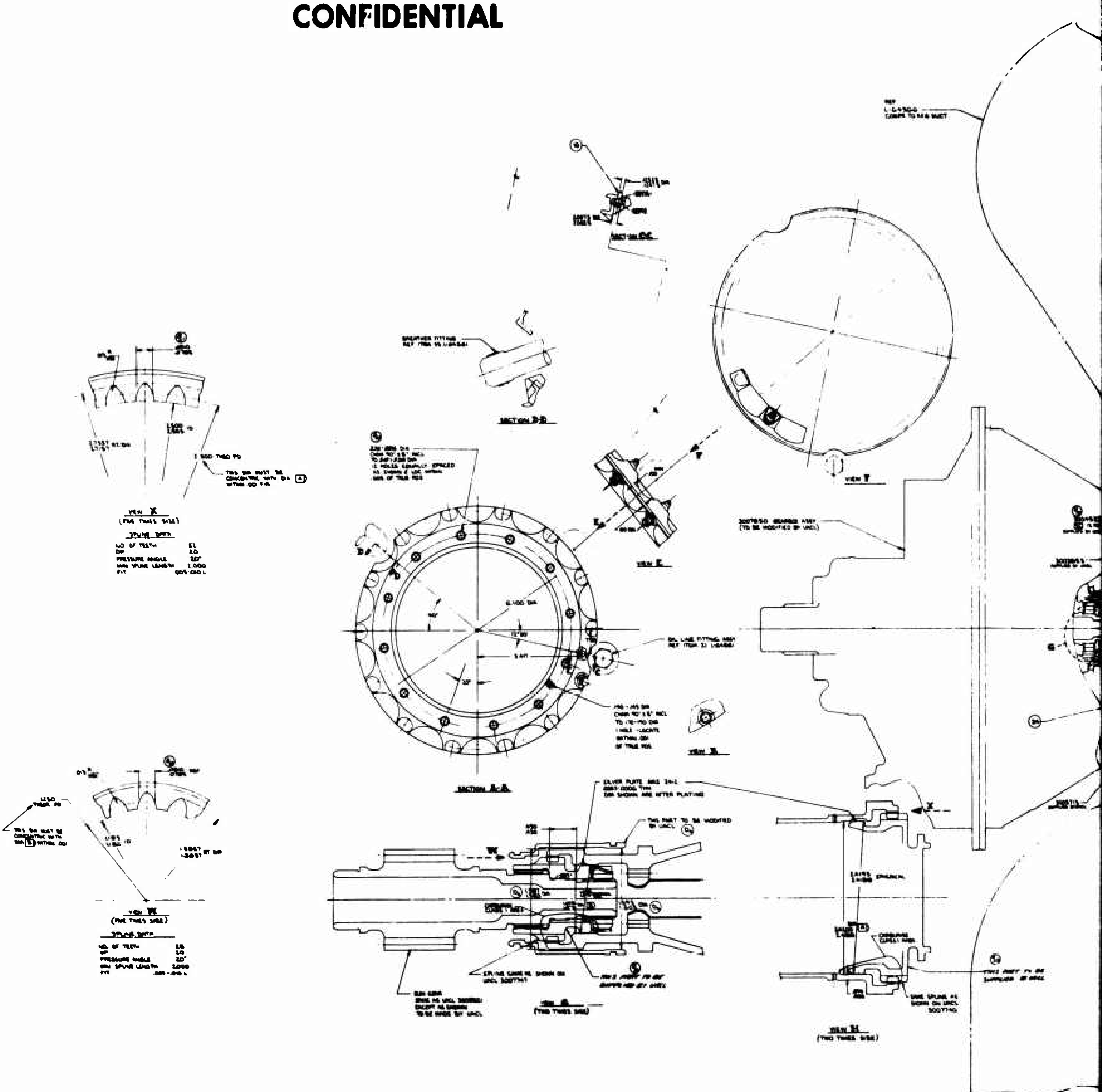

1

2

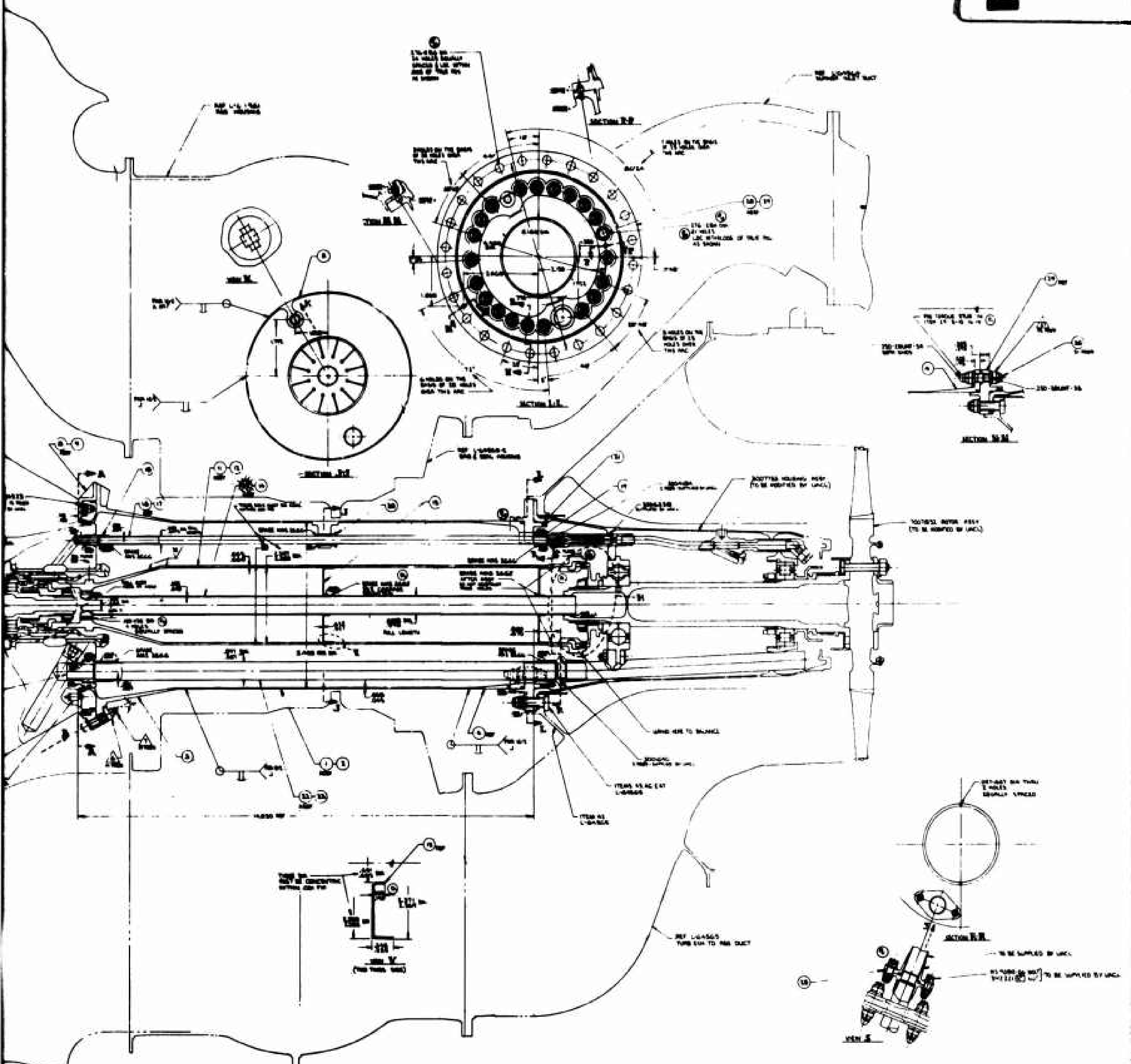

3

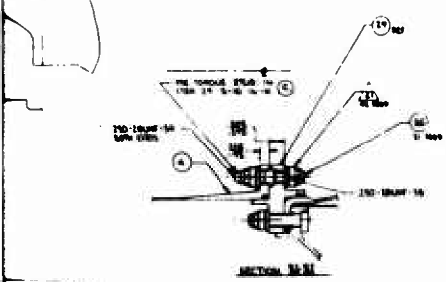

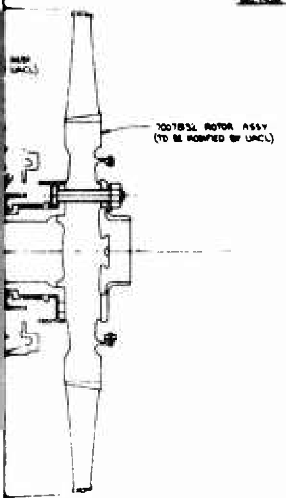

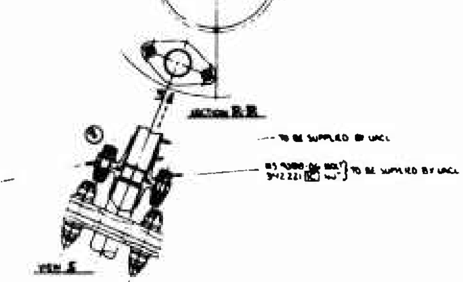

7. [illegible]
6. CASE FLANGE FACES MUST BE PARALLEL WITHIN .001 FIR
5. ALL BRGS MUST BE CONC WITHIN .001 FIR
4. ALL SHAFT BRGS MUST BE CONC WITHIN .001 FIR
3. CRIT CODE SUBS - PER (THICKNESS MEMO
2. CRIT CODE SUBS - SPLINE GAGE
1. [illegible] CORRECT BY REMOVING MATERIAL IN PLANES [illegible] (REF.UACL 300785L)

L-G4563

PRATT & WHITNEY AIRCRAFT
CONTROLLED

[redacted]

E-2090

LAYOUT

T-74

DRIVE & CASE

L-G4563

UNCLASSIFIED
Security Classification

DOCUMENT CONTROL DATA - R & D

(Security classification of title, body of abstract and indexing annotation must be entered when the overall report is classified)

1. ORIGINATING ACTIVITY *(Corporate author)* Pratt & Whitney Aircraft Division United Aircraft Corporation East Hartford, Connecticut 06108	2a. REPORT SECURITY CLASSIFICATION Confidential 2b. GROUP 4

3. REPORT TITLE
SMALL GAS TURBINE ENGINE COMPONENT TECHNOLOGY, REGENERATOR DEVELOPMENT, PHASE II, FULL SCALE REGENERATOR FABRICATION AND ENGINE-REGENERATOR TESTING (U)

4. DESCRIPTIVE NOTES *(Type of report and inclusive dates)*
Final report, May 1965 to January 1967

5. AUTHOR(S) *(First name, middle initial, last name)*

Lucas, Barrett R., and Selfors, Henry J.

6. REPORT DATE	7a. TOTAL NO. OF PAGES	7b. NO. OF REFS
October 1967	197	1

8a. CONTRACT OR GRANT NO. DA 44-177-AMC-181(T) b. PROJECT NO. Task 1M121401D14413 c. d.	9a. ORIGINATOR'S REPORT NUMBER(S) USAAVLABS Technical Report 67-35 9b. OTHER REPORT NO(S) *(Any other numbers that may be assigned this report)* PWA-3008

10. DISTRIBUTION STATEMENT
Each transmittal of this document outside the Department of Defense must have prior approval of U.S. Army Aviation Materiel Laboratories, Fort Eustis, Virginia 23604.

11. SUPPLEMENTARY NOTES	12. SPONSORING MILITARY ACTIVITY
	U.S. Army Aviation Materiel Laboratories Fort Eustis, Virginia 23604

13. ABSTRACT

This report describes the work accomplished during the 20-month Phase II portion of a 32-month program devoted to the advancement of toroidal rotary regenerator technology for small gas turbine engines. As a result of component investigations conducted in Phase I, major improvements in regenerator technology were made and were incorporated into the design of a flightweight high-effectiveness toroidal rotary regenerator which was fabricated and performance tested on a PT6 (T74) engine. The work described herein includes experimental determination of regenerator duct flow distribution; experimental evaluation of regenerator mass losses, system pressure losses, and overall performance in an ideal test loop, and finally the results of performance testing on the PT6 (T74) engine conducted by the subcontractor, United Aircraft of Canada, Ltd. (U)

DD FORM 1 NOV 65 1473 REPLACES DD FORM 1473, 1 JAN 64, WHICH IS OBSOLETE FOR ARMY USE.

UNCLASSIFIED
Security Classification

14. KEY WORDS	LINK A		LINK B		LINK C	
	ROLE	WT	ROLE	WT	ROLE	WT
Toroidal Rotary Regenerator						
Lightweight Regenerator						
Regenerative Gas Turbine Engine						
PT6 (T74) Gas Turbine Engine						
High Performance Engine						
Heat Exchanger						
Wire-Screen Matrix Heat Transfer						

SUPPLEMENTARY

INFORMATION

AD-387292

ERRATA

USAAVLABS Technical Report 67-35

"Small Gas Turbine Engine Component Technology
Regenerator Development" (U)

"Phase II, Full Scale Regenerator Fabrication
and Engine-Regenerator Testing" (U)

October 1967

The distribution statement on the cover, on the title page, and in block 10 of DD Form 1473 should be changed to read:

> In addition to security requirements which apply to this document and must be met, each transmittal outside the Department of Defense must have prior approval of US Army Aviation Materiel Laboratories, Fort Eustis, Virginia 23604.